The Petrology and Geochemistry of the Marginal and Lower Zones in the Clapham Trough, Eastern Bushveld Complex.

By

Masibulele P. Zintwana

Submitted in fulfilment of the requirements for a Master of Science degree in Geology, in the Department of Geosciences, University of the Witwatersrand, Johannesburg, South Africa.

2015

Declaration

I, *Masibulele P. Zintwana*, hereby state that all work contained in this thesis is my own, unaided work, except where it is explicitly stated otherwise and the work of others is acknowledged accordingly. I further declare that no part of this thesis has been, or is currently being submitted for a degree or other qualification at any other institution of higher education.

Signed: 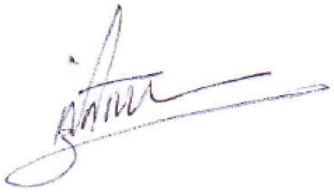

Masibulele P. Zintwana

School of Geosciences

University of the Witwatersrand

Johannesburg

September 2015

Acknowledgements

The National Research Foundation, School of Geosciences (Wits University) and Anglo Platinum are acknowledged for the generous financial support to this project. Furthermore, Anglo Platinum is thanked for allowing access to use core the company drilled for research purposes.

I am deeply indebted to my supervisor, Professor Allan H. Wilson, for all the patience in reviewing my work, assistance and support through the most challenging times of this work. Mr Gordon Chunnett is gratefully thanked for his dependable morale support and organising access to some of the core that was held in Anglo Platinum premises in Germiston. I am genuinely indebted to the staff of the Earth Labs for the geochemical analyses done in this work. I mention Mr Joe Aphane in particular for the dependable support during the logging and transportation of the relevant drill cores from storage and the logging place. Many thanks to the Dr C. Reinke and the staff of Spectrau are thanked for all the support and help during the EMPA at University of Johannesburg. Sable Data works (www.sable.co.za) is thanked for allowing and providing of Sable database to capture the lithological logs of the data used in this work. Last, but not least, I thank Mr THC Pegram for his support during the latter stages of the writing of this work.

Dedications

This work is dedicated to my mother who has been my source of strength and the absolute reason for my perseverance through my studies and putting this work to completion, even during her ill health.

Abstract

This study undertook to re-evaluate the conventional historic interpretation that accepted the Marginal Zone as representative of the chill phase to the earliest emplacement of Lower Zone magmas. The Clapham Trough preserves a thick sequence of the Marginal Zone rocks, at least 220 m thick. Poor exposures and incomplete stratigraphy of the rock succession that occurs between the floor and the Marginal Zone rocks presented great limitations to earlier studies, and led earlier workers to accepting that the base of the Bushveld Complex is the Marginal Zone norite. This study presents results from the 692 m CH6 drilled core, which intersects the Marginal-Lower Zone boundary in the Clapham Trough.

The base of the CH6 drill core consists of melanorite (with less than 40 % cumulus plagioclase), which is conformable with the underlying, thick Basal Ultramafic Sequence (BUS, described in Wilson and Chunnett, 2010; and Wilson, 2012) separating the Marginal Zone rocks with the floor rocks of the Magaliesberg Formation. The amount of cumulus plagioclase in the Marginal Zone increases with increasing stratigraphic height such that the top units of the Marginal Zone are norite-leuconorites (typically 45-65 % cumulus plagioclase), bordering on anorthosite. The progressive changes in the modal variations led to the subdivision of the Marginal Zone norite to a basal Mafic Norite and a xenolith-bearing Shelter Norite. The latter is deemed a correlative of the Xenolithic Norite described at Olifants River Trough.

Coupled with the increasing amount of cumulus plagioclase, the An# increases with stratigraphic height. The An# fractionation trend is reversed from that of the co-existing orthopyroxene observed in the same interval (An_{63-74} vs. En_{81-70}). The reversed An# compositions are an abnormal differentiation trend. The compositional disequilibrium

between co-existing orthopyroxene and plagioclase formed from in-situ crystallization with floatation of plagioclase, through convection, separating the cotectic phases.

All the data in the Marginal Zone show that these rocks have continuous fractionation trends with no interruptions. The Marginal Zone rocks are cumulus rocks that formed through fractional crystallization in a temporarily closed magma chamber. The present work showed unequivocally that the Marginal Zone is a product of differentiation of earlier emplacement of B1-magma, and cannot be representative of either a chill zone or composite sills. The appropriate (parental) liquid composition of the Marginal Zone formed after 30 % crystallization of the B1-magma. The postulated liquid composition is 6 wt. % MgO and 56.7 wt. % SiO_2. The entire Marginal Zone succession would have formed from about 30-54 % crystallization of the B1-magma. The crystallization of the Marginal Zone was ended abruptly by the emplacement of a new batch of B1-magma, which must have mixed with the residual magma that must have ponded atop Marginal Zone cumulates after 54 % crystallization.

The mixing of the evolved residual magma and the primitive B1-magma formed the liquid postulated to be parental to the Lower Zone A (10.59 wt. % MgO and 57.10 wt. % SiO_2). The Transitional Pyroxenite bears all the evidence of mixing between magmas of contrasting compositions, forming the 10-30 m gradational boundary unit between the Marginal Zone and Lower Zone A (correlative of the Lower Orthopyroxenite Subzone described at Olifants River Trough). The Lower Orthopyroxenite Subzone at the Clapham Trough is almost a mono-mineralic rock succession with generally constant orthopyroxene composition (En_{87-86}), with the exceptions at marker norite horizons (En_{84-82}; An_{83-81}). The constant compositions observed in Lower Zone A are attributed to contemporaneous emplacement of new magma and differentiation, which maintained the composition of the parental magma.

Table of Contents **Page Numbers**

List of Figures **Page Numbers**

List of Tables **Page Numbers**

Chapter 1

Introduction

The Bushveld Complex is a large igneous province in the Kaapvaal Craton, which is the underlying basement to most of the geology of the Republic of South Africa. It is mostly known for the layered intrusion phase of the magmatic event (the Rustenburg Layered Suite) that discordantly intrudes the Late Archaean to Paleoproterozoic Transvaal Supergroup. For this reason, many scholars use the term 'Bushveld Complex' interchangeably with the 'Rustenburg Layered Suite'. In the present work, Bushveld Complex refers to the layered mafic phase of the 2.06 Ga emplacement event.

The Bushveld Complex is traditionally subdivided into the eastern, western (including the far western), the northern and the hidden southern limbs (Fig. 1.1). The inter-connectivity of these limbs is debated but there is substantial evidence that suggests there is connectivity at least between the western and eastern limbs (Cawthorn and Webb, 2001; Webb *et al*, 2011). These two limbs (i.e. western and eastern limbs) dip gently towards the centre, showing remarkably similar lithological sequences and thicknesses. The absence of a gravity anomaly at the centre to indicate the presence of denser mafic rocks is one of the key arguments against the connectivity of the limbs of the Bushveld Complex. It has been shown, however, that crustal flexure beneath the intrusion due to the density and temperature of the intrusion would not create a density anomaly in the centre of the Bushveld Complex, as observed (Cawthorn and Webb, 2001). Whether rocks of the Bushveld Complex occur at depth remains to be demonstrated because of the depth of drilling required. However, a younger kimberlite pipe located at the centre of the structure contains xenolithic fragments of

pyroxenite that are most likely of Bushveld Complex origin brought to the surface during the emplacement of the Cretaceous Palmietgat pipe (Webb *et al.*, 2011).

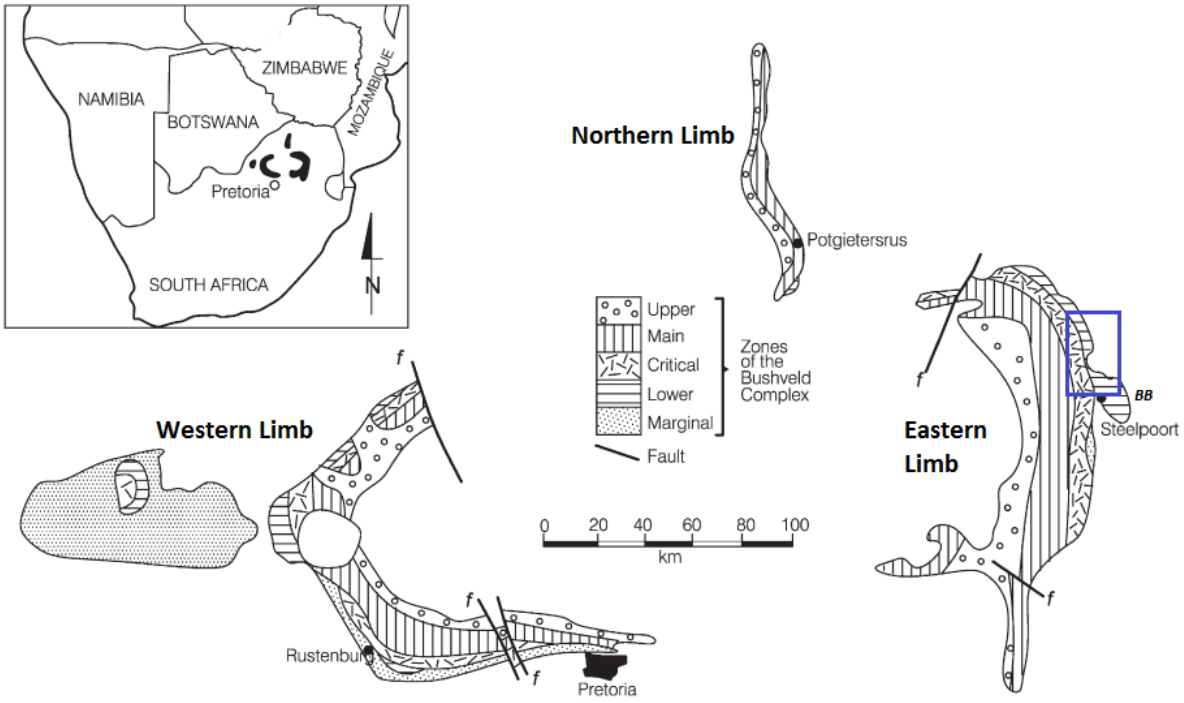

Fig. 1.1: Simplified map of the locality and geology of the Bushveld Complex, the main limbs and the location of the study area (shown as the blue box). BB represents the Burgersfort Bulge. Map modified after Cawthorn (2007).

The floor of the Bushveld Complex is mainly the Magaliesberg quartzite but in the eastern limb, the stratigraphically lowest rocks of the Bushveld Complex transgress the stratigraphy of the Transvaal Supergroup. To the north of the Burgersfort bulge (including the entire study area of the present work), the Magaliesberg quartzite is the floor to the mafic intrusion. Further south progressively younger sediments are cut by the Bushveld Complex, which comes to rest atop of the Dullstroom volcanic rocks near Stoffberg (Eales and Cawthorn, 1996). Discordance between the Bushveld Complex and the floor is also observed in the northern limb where the intrusion cuts into progressively older sequences northwards and comes to rest on the Archaean granite basement (Ashwal *et al.*, 2005; and Kinnaird *et al.*,

2005). The discordances have been explained by the existence of a regional unconformity that occurs between the Pretoria Group and the Rooiberg Group (Cheney and Twist, 1991). It has been argued, however, that there is no need of a regional unconformity if the Bushveld Complex transgresses the sediments of the Transvaal Supergroup and has preserved some of the apparently missing sequences beneath the main intrusion (Cawthorn, 1998).

The stratigraphy, though informal, of the Bushveld Complex (SACS, 1980) is divided into the Marginal Zone (whose relationship to the main body of the layered intrusion is still an issue of contention), the Lower, Critical, Main and Upper Zones. The generalised stratigraphic column of the Bushveld Complex is shown in Fig. 1.2 as observed in the eastern limb. The Marginal Zone forms the lowest (earliest formed) exposed units of the Bushveld Complex and it is assumed to be in contact with the Magaliesberg Quartzite. Nowhere in the Bushveld Complex is the contact of the Marginal Zone rocks with the floor observed. The work of Wilson (2012) shows the existence of at least 1000 m of a non-exposed ultramafic sequence (in contact with the floor, and referred to in that work as the Basal Ultramafic Sequence, abbreviated to BUS) separating the Marginal Zone rocks from the quartzite floor.

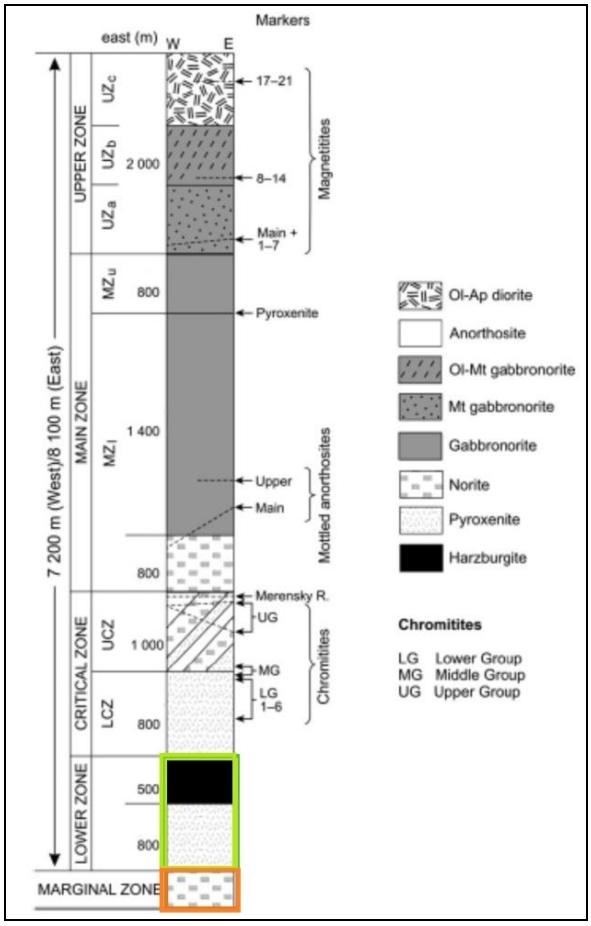

Fig. 1.2: Generalized stratigraphic column of the Bushveld Complex showing the common lithologies of each zone and the thicknesses in the eastern limb, modified after Clarke et al. (2009). Green and orange rectangles show the Lower Zone and the Marginal Zone successions, respectively.

It is important that the nature and the position of the Marginal Zone within the Bushveld Complex stratigraphy and its relationship with the BUS and the Lower Zone be re-examined. The study area for the present work is located in the eastern limb of the Bushveld Complex, some 20-25 km north of Burgersfort (Fig. 1.3). The eastern limb of the Bushveld Complex is exposed at the Olifants River Trough in the north, to the south of Stoffberg where it disappears below younger sedimentary cover. The geology of the Lower and Marginal Zones of the Bushveld Complex is discussed below, with particular emphasis on the geology of the eastern limb.

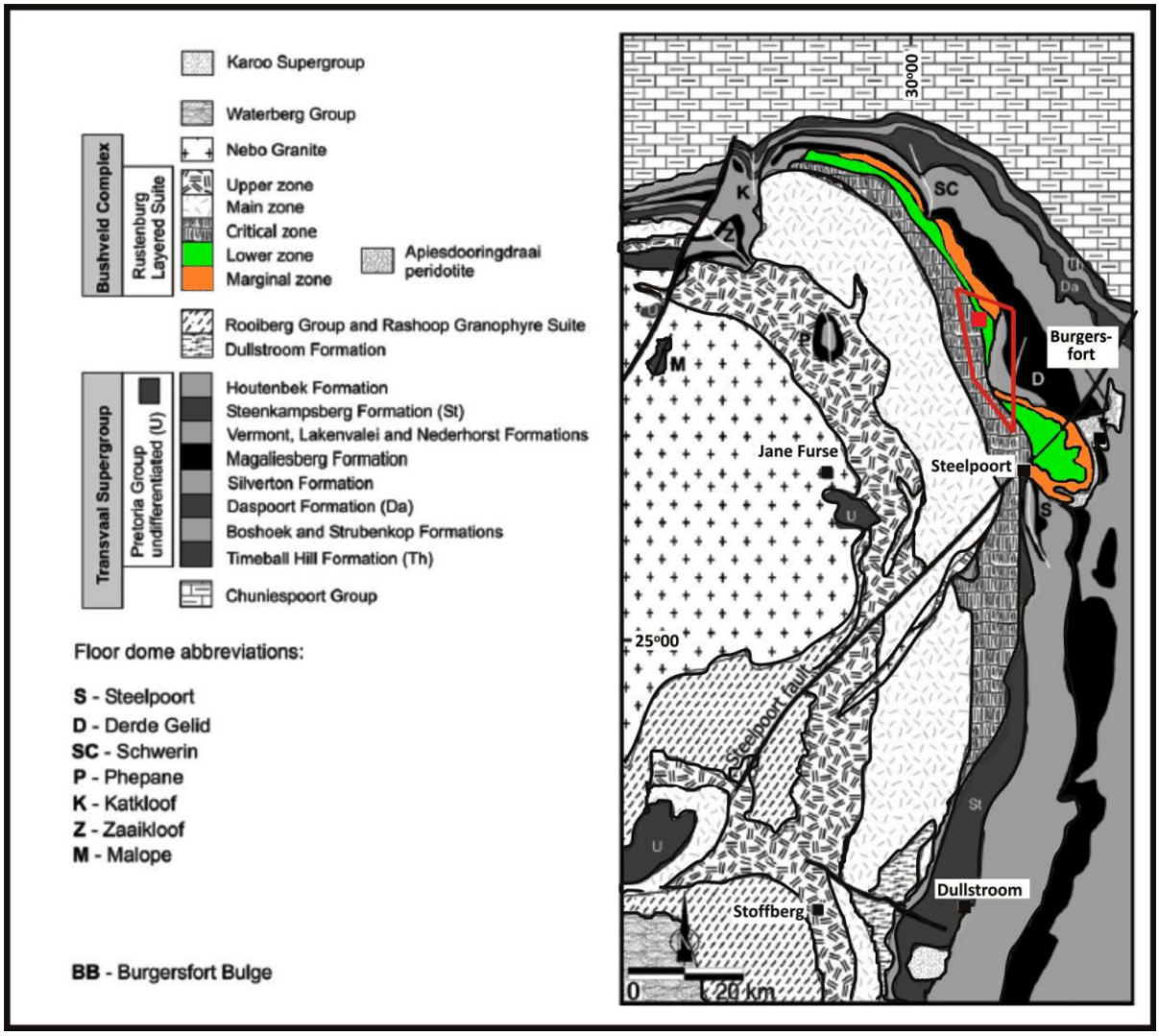

Fig. 1.3: Simplified geology of the Eastern limb of the Bushveld Complex showing the study area (red borders) and the location of the CH6 borehole (red square). Map, modified after Clarke et al., (2009).

1.1. The Marginal Zone

The Marginal Zone of the Eastern limb consists of two broad groups of rocks as described by Harmer and Sharpe (1985). These groups are the pyroxenitic group which borders the Lower and Lower Critical Zones and a gabbroic group which borders the Upper Critical and Main Zone. The pyroxenitic group is interpreted as a chill phase, and it was originally suggested to be associated with the initial magma injection(s) into the Bushveld Complex

chamber. The liquid composition whose chill zone is associated to the Marginal Zone rocks, and gave rise to the Lower and Lower Critical Zones is referred to as the B1-type magma. The composition of marginal sills supposedly related to the gabbroic group rocks associated with the Upper Critical and the Main Zones are designated B2 and B3 magma, respectively. These two groups (B2 and B3) have similar petrography but their grain sizes (in the marginal sills), initial Sr isotopic compositions and the REE geochemistry differ from the B1 rocks (Sharpe and Hulbert, 1985). The sills of these corresponding compositions intrude into the country rocks as the wall and floor rocks of the RLS (Sharpe and Hulbert, 1985; Barnes *et al.*, 2010).

The pyroxenite group is predominantly made of quench-textured orthopyroxenites with interstitial plagioclase. The modal proportion of the orthopyroxenes (2-10 mm grains) varies from about 50 to 90 % with the reported composition of En_{84-90}. The matrix in these orthopyroxenite mainly consists of orthopyroxene (En_{66}), plagioclase (An_{65-70}) and devitrified glass. The so-called pyroxenite group also includes norite, quartz norite, and xenolithic fragments (up to 70 % floor rock inclusions) and ultramafic rocks. The norite generally contains relatively evolved orthopyroxene compositions (En_{67-78}) with quartz and biotite as essential minerals and clinopyroxene and oxides as accessory minerals. The xenoliths (derived from the Pretoria Group sediments) are mainly quartzite and hornfels (Cameron 1978, Harmer and Sharpe, 1985). The ultramafic rocks of the 'chill phase' do not seem to be developed in all areas where the Marginal Zone rocks are present. They are interpreted as either occurring as sill-like bodies or discontinuous pods between the floor and the norite-pyroxenite group, or within the floor rocks of the Bushveld Complex. Some of the ultramafic (peridotites) rocks have been described in the Burgersfort Bulge and the Olifants River Trough (Cameron, 1978, Harmer and Sharpe, 1985). These peridotites contain cumulus olivine compositions of Fo_{83-90} and orthopyroxene of

compositions of En_{84-90}. The orthopyroxene exhibits a poikilitic textural relationship with the olivine crystals (Harmer and Sharpe, 1985). Plagioclase compositions are more evolved and have been reported to be An_{59-76}.

The gabbroic group of the Marginal Zone sills is found adjacent the Upper Critical (B2) and Main zone (B3) – type sills. These groups have similar petrology in some aspects except that the B3 gabbroic group is coarser-grained, marginally higher amount of clinopyroxene and magnetite, and has lower REE content (Harmer and Sharpe, 1985). The B2 group is thought to be a result of magma mixing between residual liquid from B1 magma with B3 magma. The B2 and B3 groups will not be discussed further in this work since they are not related to the work at hand. The Marginal Zone, as mentioned above, is associated with a number of ultramafic sills but the exact relationship remains unclear.

1.2. Ultramafic Sills in the eastern Bushveld Complex

There are two generations of sills that penetrate the floor of the Bushveld Complex, namely, the pre-Bushveld and the syn-Bushveld sills as described by Willemse (1959). Pre-Bushveld sills are generally metamorphosed to amphibolite facies with a large total volume, about 150 000 km^3 (Willemse, 1959; Sharpe, 1981). The syn-Bushveld sills are considered to be genetically related to the Marginal Zone. It is thought that this generation of sills intruded the country rock as offshoots from the main Bushveld Complex chamber during the emplacement stages (Sharpe and Hulbert, 1985; Barnes *et al.*, 2010).

The sill compositions vary according to the adjacent rocks of the Bushveld Complex, i.e. the sills that are adjacent to the Lower and Lower Critical Zone vary from harzburgitic to pyroxenitic compositions (Ultramafic, B1-UM sills) whereas those that intrude rocks that are adjacent to the Upper Critical and Main Zones are generally gabbroic in nature

(Sharpe, 1981; Sharpe and Hulbert, 1985 and Barnes *et al*, 2010). More focus here is given to the B1-UM sills because they can provide insight to the earliest processes and some ideas about the possible parental magma(s) during the emplacement of the earliest stage of the Bushveld Complex.

The work that has been done on ultramafic sills around the study area is inadequate but the mapping by Willemse (1959, his Fig. 4) revealed the occurrence of sills similar to the Aapiesdoorndraai peridotite (ADP) body and described by Sharpe and Hulbert (1985). Most of the ultramafic sills are emplaced above the Magaliesberg quartzite and are most abundant around the Burgersfort bulge but the exposure is poor in this area. In the study area, this relationship is apparently consistent with the BUS as described by Wilson (2012). These sills might be continuous with each other but poor exposures make it hard to positively confirm if that is the case or not. Many of these sills intrude the floor rocks in close proximity to the pyroxenitic group of the Marginal Zone. Important examples of these sills are discussed below.

1.2.1. The Wimbledon Peridotite Body

The Wimbledon peridotite sill crops out some 40 km north of Burgersfort for a strike length of 1 km. It intrudes the Magaliesberg quartzite some 10 km from the nearest Bushveld Complex contact and similar sills intrude the Lower Zone further north (Sharpe and Hulbert, 1985). This peridotite sill has 5-15 mm fine-grained chill margin of harzburgite composition. The basal part of the sill consists of olivine (Fo_{89}) and poikilitic orthopyroxene (En_{90}). There is layering higher up in the sill indicated by varying amounts of plagioclase (not more than 5 % modal proportion). The amount of olivine is also variable, resulting in lithologies that range from harzburgite to dunite (53-97 % modal abundance and compositions Fo_{86-89} (Sharpe and Hulbert, 1985). Clinopyroxene,

biotite and chromite are other important minerals present in small proportions. The petrography and field relations of the Wimbledon sill are similar to many other sills along the floor contact of the Bushveld Complex, both north and south of Burgersfort (Sharpe and Hulbert, 1985).

1.2.2. The Wildebeestkraal Peridotite Body

The Wildebeestkraal body crops out in a relatively small area south of Burgersfort (Willemse, 1959; and Sharpe and Hulbert, 1985) and it is harzburgitic in composition. Like many other ultramafic bodies around the Burgersfort bulge, the Wildebeestkraal body is coarse-grained with somewhat vague layering indicated by variable plagioclase content (Sharpe and Hulbert, 1985). The olivine (Fo_{84-89}) grains are subhedral and are poikilitically surrounded by orthopyroxene grains (En_{87-91}) with interstitial plagioclase (0-6 % modal abundance). Chromite, biotite and clinopyroxene are accessory minerals. The petrography of this sill is also similar to many other bodies of ultramafic sills in the area around the Burgersfort Bulge.

1.2.3. The Aapiesdoorndraai Peridotite Body

The Aapiesdoorndraai peridotite (ADP) body is arguably the most important occurrence of ultramafic sills in the Eastern limb of the Bushveld Complex. This sill is harzburgitic in composition, with subhedral olivine grains with the composition Fo_{88-85} (Sharpe and Hulbert, 1985). These olivine crystals are poikilitically surrounded by orthopyroxene crystals of En_{88} composition. In places the sill has a fine comb-texture of plagioclase-orthopyroxene in a matrix of olivine and orthopyroxenes of similar compositions. The central parts of the sill predominantly have a harrisitic texture (Sharpe and Hulbert, 1985). The exact relationship between the two textures is uncertain due to poor

exposures. The olivine crystals are bladed to dendritic with a length to width ratio of 10:1, average length 8 cm. There is no compositional zoning evident. Orthopyroxene (En_{88}), clinopyroxene and plagioclase crystallised around the network of these olivine crystals that make up 40 % of the rock volume. There are sulphides associated with this sill (Sharpe and Hulbert, 1985). Willemse (1959) make no distinction between the Wimbledon, Wildebeestkraal and Aapiesdoorndraai peridotite bodies. Furthermore, these ultramafic rocks could be equivalent to the BUS of Wilson and Chunnett (2010), the ADP in particular (Wilson, *Pers. Comm.*).

1.3. The Lower Zone

The Lower Zone in the Eastern limb is best exposed in the Olifants River Trough and according to Cameron (1978); it can be divided into the Basal Subzone, Lower Orthopyroxenite, Harzburgite Subzone and the Upper Orthopyroxenite (Fig. 1.4).

The Basal Subzone is similar in some aspects to Marginal norite described elsewhere in the Bushveld complex and its contact with the Pretoria Group is not exposed. For this reason, Cameron (1978) suggested that in the case where this unit is the 'contact rock' then it is not part of the Lower Zone but it is part of the Marginal Zone. The Basal subzone is described to be a conformable succession with gross igneous lamination observed.

The Lower Orthopyroxenite Subzone is almost entirely made of orthopyroxenite with interstitial plagioclase and clinopyroxene as important accessory minerals. Igneous layering is present, pronounced by subtle modal variations. Trace chromite and sulphides occur as interstitial minerals or as inclusions in orthopyroxene.

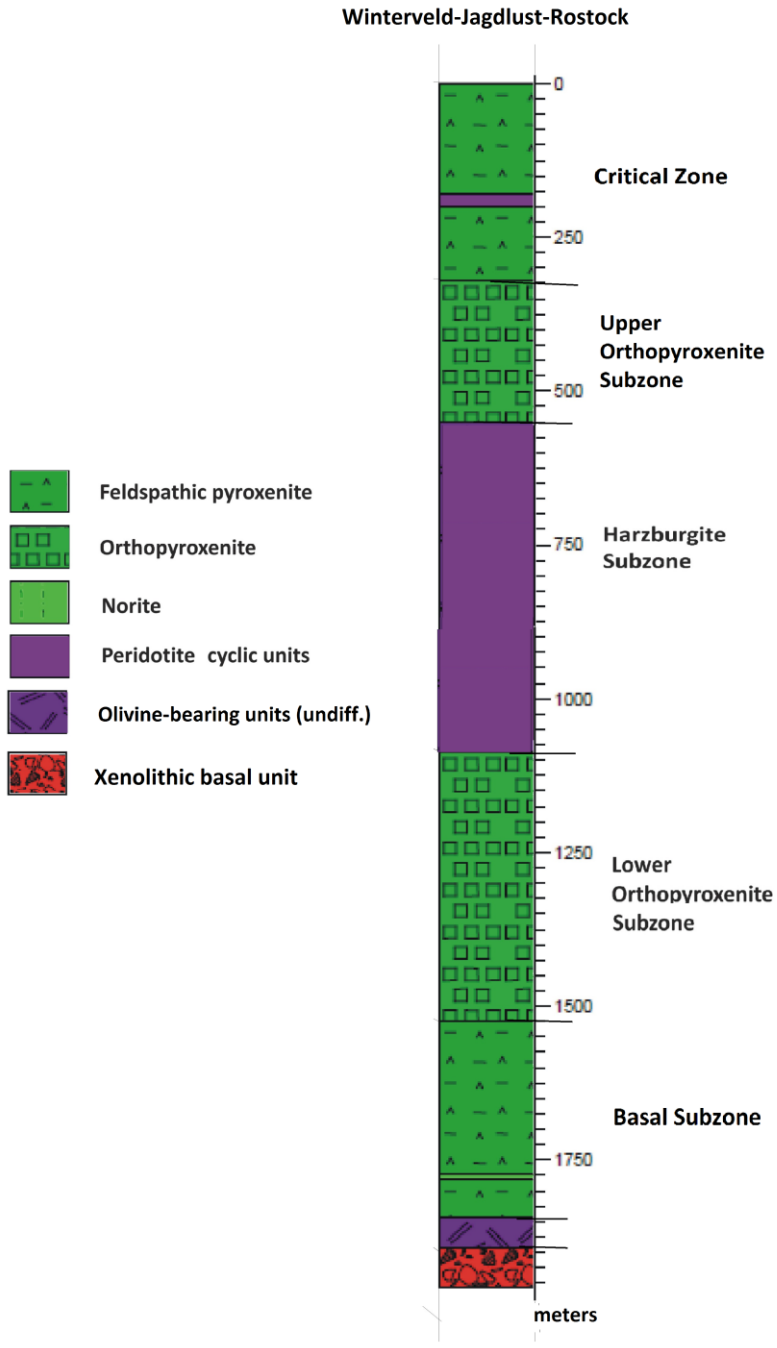

Fig. 1.4: The Lower Zone and Marginal Zone stratigraphic succession at Olifants River Trough. Section redrawn from Cameron (1978).

The appearance of cumulus olivine marks the base of the Harzburgite Subzone. This subzone is well layered and individual layers can reach up to tens of meters in thickness. The Harzburgite Subzone consists of well defined cyclic units which commonly start with

dunite (containing accessory chromite) at the base, grading upwards through harzburgites to orthopyroxenite (with or without olivine) at the top. These cyclic units are comparable to those described in the Great Dyke and Stillwater Complex, but these layers are not associated with chromitite layers (Cameron, 1978).

The Upper Orthopyroxenite is similar to the Lower orthopyroxenite with some degree of layering marked by variation of the amount of interstitial plagioclase. The Lower Zone in the eastern limb terminates in a zone where the amount of plagioclase increases to about 7 % of the rock with no evident structural break. Elsewhere in the Bushveld Complex the Lower Zone ends at the top of the Harzburgite Subzone defined by Cameron (1978) and the Upper Orthopyroxenite is taken as part of the Critical Zone because the increase in feldspar is not evident (Teigler and Eales, 1996; and Eales and Cawthorn, 1996).

1.4. Estimates of Parental Magma compositions of the Bushveld Complex

The Bushveld Complex is thought to be a result of multiple injections of at least two different magmas (Cawthorn *et al.*, 1981; Sharpe *et al.*, 1981; Cawthorn and Davies, 1983, Harmer and Sharpe, 1985). The composition of the initial magma(s) emplaced in the Bushveld Complex chamber is of importance because it has implications for the melting region(s) in the mantle and related geochemistry, as well as the source of the vast Cr and PGE deposits that occur in the intrusion (Von Gruenewaldt *et al.*, 1985; and references therein). Determining this composition is often too difficult because there are few chill margins preserved around the complex where the basal rocks abut the country rocks and the Marginal Zone norite cannot be used for this purpose because it displays evidence of layering and cumulus textures (Eales and Cawthorn, 1996).

There have been a number of attempts to determine the parental magma composition(s) of the Bushveld Complex and it is fitting to review the proposed magma compositions.

The syn-Bushveld Complex sills that intrude the floor of the intrusion and some experimental work have been used in the attempt to determine the compositions of the magma(s) responsible for the formation of the complex (Willemse, 1959; Cawthorn *et al*, 1981; Cawthorn and Davies, 1983; Sharpe and Hulbert, 1985; Barnes *et al*, 2010). The sills that Willemse (1959) described were of two groups, namely: amphibolite and norite compositions. The amphibolite sills are metamorphosed and they predate the Bushveld Complex but the latter sills are of Bushveld age and the composition is shown as column 2 in Table 1.1.

Cawthorn and Davies, (1983) described olivine-bearing, quench-textured micro-pyroxenite sills (the relationship of olivine with orthopyroxene indicates that the former crystallised first) with clinopyroxene and plagioclase as later forming minerals. Cawthorn and Davies (1983) concluded that these pyroxenite-type sills are "microcosms" of the main body of the Bushveld Complex. Sharpe and Hulbert (1985) described in detail the sills in the floor of the Bushveld Complex in the eastern limb, and the geology of the ultramafic sills that are associated with Lower Zone as summarised above (section 1.2).

Table 1.1: Major element compositions for previously proposed parental magmas to the Lower Zone of the Bushveld Complex.

	1	2	3	4	5	6	7
SiO_2	50.55	56.1	53.17	55.7	55.74	55.9	56.09
TiO_2	0.66	0.76	0.36	0.36	0.34	0.34	0.28
Al_2O_3	15.23	12.9	11.36	12.74	11.82	11.8	11.31
Fe_2O_3	1.04	1.05	1.61	1.00	1.58		1.53
FeO	10.07	8.15	9.11	7.80	8.93	10.2	7.79
MnO	0.23	0.18	0.2	0.09	0.18		0.17
MgO	8.30	10.12	14.93	12.44	11.85	12.9	13.58
CaO	11.3	6.38	7.47	6.96	6.5	6.8	6.34
Na_2O	2.24	1.48	1.57	2.02	1.63	1.7	1.43
K_2O	0.19	1.30	0.17	1.03	0.98	0.9	1.05
P_2O_5		0.18	0.07		0.08		0.07
L.O.I.	0.24	0.76		-0.39	0.31		
Total	100.05	99.36	100.02	99.75	99.94	100.54	99.64

1- Proposed parental magma by Wager and Brown (1968). 2- Chemical analysis of the parental magma proposed by Willemse (1959), analysis provided by Cawthorn and Davies, (1983). 3- B1 parental magma composition (Sharpe, 1981). 4- Proposed parental magma for the early suite of magmas to be emplaced in the Bushveld Complex (Cawthorn and Davies, 1983). 5- Average proposed B1 parental magma to the Lower Zone and Lower Critical Zone (Barnes et al, 2010). 6- B1 quenched rocks proposed to be representative of parental magma from Eales and Costin (2012). 7- B1-magma proposed by Wilson (2012) based on deep drill core samples from Clapham Trough.

The composition of the parental magma proposed by Wager and Brown (1968) (analysis 1 in Table 1.1) has been rejected based on the experimental data conducted at 3 kbars, which approximates the pressure during the emplacement and crystallization of the Bushveld Complex (Cawthorn and Davies, 1983). The crystallization sequence given by this composition does not produce the observed sequence for the Bushveld Complex. Wager and Brown (1968) pointed out that olivine crystallised first in the Bushveld

Complex followed by orthopyroxene, then plagioclase and clinopyroxene. Cawthorn and Davies (1983, their Fig. 2) showed that the composition proposed by Wager and Brown (1968), i.e. analysis 1 above, will crystallise olivine and clinopyroxene first (the order is uncertain) followed by plagioclase and orthopyroxene. This sequence is contrary to the sequence observed in the Bushveld Complex, as already indicated. The composition, therefore, cannot represent a parental magma to the Bushveld Complex.

Analysis 2 (Table 1.1) represents the Maruleng (quartz-) norite described by Willemse (1959). In the above-mentioned study, it was concluded that this type of sill represents contaminated parental magma to the Bushveld Complex and its uncontaminated equivalent is similar to the Lydenburg-type sill (amphibolite sill). However, the latter is older than the Bushveld Complex and it cannot be considered as a parental magma (Cawthorn et al, 1981), and the former lacks olivine in its crystallization sequence. As a result it is concluded that it cannot be representative of the Bushveld Complex parental magma (Cawthorn and Davies, 1983).

Sharpe (1981) suggested that the Lower Zone formed by fractional crystallization of a Mg-rich basaltic magma and the ultramafic sills resulted from crystal mushes that were 'squeezed' into the country rock as offshoots when the Lower Zone magma was emplaced. This magma is designated B1 and the average composition is shown as analyses 3 in Table 1.1. The more Mg-rich parental magmas that appear in Sharpe (1981) require more olivine to crystallise than observed in the Bushveld and the composition would have a significantly higher Mg-number as Cawthorn and Davies (1983) suggested for the lower most units of the Lower Zone (this is not impossible if there are more Mg-rich cumulates that have not yet been discovered).

The experimentally determined crystallization sequence (at 3 kbars) of analysis 4 (Cawthorn and Davies, 1983) gave the nearest approximation to the sequence of the

Bushveld Complex. That is, olivine crystallises first and shortly followed by orthopyroxene and later plagioclase and clinopyroxene also crystallise (Cawthorn and Davies, 1983). Moreover, this quartz normative magma is expected to crystallise olivine with the composition similar to those reported by Cameron (1978), of Fo_{88}. The parental magma composition presented by Cawthorn and Davies (1983), however, cannot account for the BUS of Wilson and Chunnett (2010).

The composition (analysis 5 in Table 1.1) presented by Barnes *et al*, (2010) is less Mg-rich than analysis 4 and these authors envisage a basaltic andesite for a parental magma (B1) for the Lower and Lower Critical Zones of the Bushveld Complex. This composition also shows similar crystallization sequence as that observed in the Bushveld Complex, but the composition of the olivine and orthopyroxenes are less magnesian than observed in the most primitive rocks and would not produce rock types of appropriate proportions to those observed in the Lower Zone. Furthermore, the Marginal Zone compositions are not mentioned and it is treated as a chill phase of the main body of the Bushveld Complex.

Eales and Costin (2012) presented weighted average of quenched B1-rocks estimates based on Harmer and Sharpe (1985) and Davies and Tredoux (1985) and the analysis calculated to a 'water free' composition. These data appear in column 6 of Table 1.1. The further envisage a staging chamber at depth in which crystallisation occurred prior to the emplacement in the Marginal and Lower Zone chambers. Wilson (2012) showed the occurrence of a conformable and previously unknown sequence of ultramafic rocks (the Basal Ultramafic Sequence, BUS) below the Marginal Zone rocks in the Clapham Trough area. These ultramafic rocks are in contact with the Magaliesberg Quartzite and a chill zone is preserved as described in the deep drill core CH7 by Wilson and Chunnett, 2010. The composition of B1-magma presented by Wilson (2012) is shown in column 7

of Table 1.1. The latter work arguably presents the most reliable source of estimates of B1-magma since the composition is directly derived from compositions that are measured from preserved chill phase rocks in the Bushveld Complex. It

1.5. Accumulation processes in Layered Intrusions

Amongst other issues that are generally debated in layered intrusions are the emplacement mechanisms and how the magma cools, crystallises and ultimately forms the observed layered rock sequence. The Bushveld Complex is no exception, and this aspect adds to the intricate debates about the compositions and number of pulses in each subdivision of the layered intrusion. The Marginal Zone is predominantly overlooked and afforded little attention when mechanisms of accumulation and compositions. Barnes et al., (2010), and Eales and Costin, (2012) have put proposals of how the Marginal Zone rocks fit in the Bushveld Complex stratigraphy. Their works have already been shown to have significant misgivings, especially in light of the studies of Wilson and Chunnett (2010) and Wilson (2012), as shown in the preceding subsections and this work intends to re-evaluate the previous interpretations.

Among the suggestions that have been proposed for the origin of layering in LMIs, crystal settling and in-situ crystallization are the commonly contested theories. The accepted (dominant) accumulation process for the CH6 section and the eastern Bushveld Complex must explain how both modal layering and igneous lamination occur in LMIs, the Marginal and Lower Zones in the present case. According to Naslund and McBirney (1996), crystal settling is a less favourable mechanism of layer formation, compared to *in situ* crystallization with or without gravity settling and magma current flows near the crystallization front. Moreover, crystal settling is most efficient in moving magma bodies. In a stagnant basic magma chamber, gravity settling is estimated to occur if olivine and

pyroxene grains are 3-5 cm in diameter to overcome yield strength of the magma. In the Bushveld Complex and the study area, both pyroxene and olivine are typically 2-3 mm and the long axes are sub-horizontal, defining igneous lamination, with or without trapped liquid content. Some mechanical process is responsible for separation of the crystals from the evolving magma, accumulation and layering. The removal of trapped liquid from the crystallization front and convective processes determine whether adcumulate or orthocumulate layers are formed (Wilson, 1992; McBirney and Hunter, 1995; Naslund and McBirney, 1996; and references there in). This study will re-visit this topic in greater detail later.

1.6. Methodology summary

The study area is shown in Figs. 1.1 and 1.3 and it is situated in a locality where the Marginal Zone and the base of the Lower Zone succession are well preserved. The CH6 drill core presents a complete succession, including horizons that are concealed in the field. The detailed description of CH6 is presented in Chapter 2 and the litho-stratigraphic log is shown in Appendix A. 185 samples were selected from CH6 for petrographic and geochemical analyses following the techniques stipulated in Appendix B. CH6 forms the core interest of the present study, and this work is the initial account of the latter drill core and the complete succession it presents.

In addition, samples were collected from a borehole CH1 which intersected rocks that overlap with the upper parts of the CH6 drill-core. CH1 is also described briefly in Chapter 2, and the detailed log of the preserved portions also appears in Appendix B. and the inclusion thereof in this work is mainly for correlation purposes.

A further deep drill core (not considered in this study) penetrated the rock succession underlying the CH6 and is described by Wilson and Chunnett (2010) and Wilson (2012).

This core represents the Basal Ultramafic Sequence (BUS) and contains a chill sequence in direct contact with the floor rocks of the Magaliesberg Quartzite. All of the Clapham Trough drill cores form a continuous and conformable succession of layered igneous rocks.

1.7. Aims and Objectives of the Project

The position of the Marginal Zone and the relationship with the floor rocks and the entire succession of the Bushveld Complex is still a controversial issue. The contact between the floor and the Marginal Zone is yet to be shown in outcrop. This 'lower-most' zone of the Bushveld Complex has been previously described to be a 'chill-phase' which consists of micro-norites with a large number of xenoliths and quench textures.

Wilson and Chunnett (2010) and Wilson (2012) present evidence of the occurrence of conformable ultramafic rocks between the Marginal Zone norite and the floor in the study area. Moreover, the separation between the Marginal and Lower Zones is not well defined and the relationship is not well understood. The mapping of these zones in the Clapham Trough area (study area) needs to be re-examined in light of the Bus of Wilson and Chunnett (2010) including the placement of the Marginal Zone in the context of magmatic events of the Bushveld Complex.

The Marginal Zone norite in the study area need to be further assessed in the context of parental melts and the possible compositions derived from the marginal sills. This study evaluates the section between the base of the Marginal Zone and the lowest 500 m of the overlying Lower Zone at Clapham Trough.

The aims and objectives of this study were to:

- To create a detailed stratigraphic log of the Bushveld Complex stratigraphy in this area and to collect 185-200 samples from boreholes CH6 and CH1.
- To establish field relationships of the Lower and Marginal Zones of the Bushveld Complex in the study area and their correlatives as seen from CH6 and CH1 drill cores.
- To determine the major and trace element geochemistry of the Marginal and Lower Zones, and to re-evaluate the geochemistry and petrogenesis of the Clapham Trough section and its correlatives, at least in the eastern Bushveld Complex.
- To constrain and re-evaluate proposed parental magma composition(s) that gave rise to the Lower and Marginal Zones and to model their possible evolution trend(s).
- To re-interpret the geology of the Marginal Zone and its position in the Bushveld Complex stratigraphy in context of the CH6 drill core and lastly,
- To present alternative explanation of the emplacement and accumulation of the Marginal and Lower Zone in Clapham Trough in context of the BUS.

Chapter 2

The Geology and the Stratigraphic Succession of the Clapham Trough Area

Anglo Platinum Plc drilled a series of vertical boreholes on the Clapham farm (i.e. Clapham Trough, some 25-30 km northwest of Burgersfort) to intersect the stratigraphy of the Bushveld Complex between the base of the Lower Critical Zone and the floor rocks) for research purposes. These boreholes are described as CH1, CH6 and CH7, as mentioned in Chapter 1. The collar positions for boreholes CH1 and CH6 are 24°29.324' S and 30°06.606' E; and 24°28.523' S and 30°07.305' E, respectively. The collar position of CH1 is positioned stratigraphically near the base of the Lower Critical Zone and intersects the upper units of the Lower Zone, and the CH6 was positioned to start within the bottom units of the Lower Zone through to the base of the Marginal Zone. This study considers a selected section of the lowest part of the CH1 and the entire section through CH6. Borehole CH7 intersects the bottom units of the Marginal Zone, through a previously unknown occurrence of ultramafic rocks (the Basal Ultramafic Sequence, BUS) described by Wilson and Chunnett (2010) and Wilson (2012). It is worth emphasising that CH7 drill core did not form part of this work, but it occurrence is vital in understanding the CH6 section and the early magmatic processes.

The simplified geological map compiled for the study area is shown in Fig. 2.1. In this chapter, the Lower and Marginal Zones as they occur in the Clapham Trough drill cores will be described. Furthermore, the present work draws comparisons to the field observations in the Clapham Trough to create a complete picture of how the units that are not well preserved on surface correlate with the regional geology.

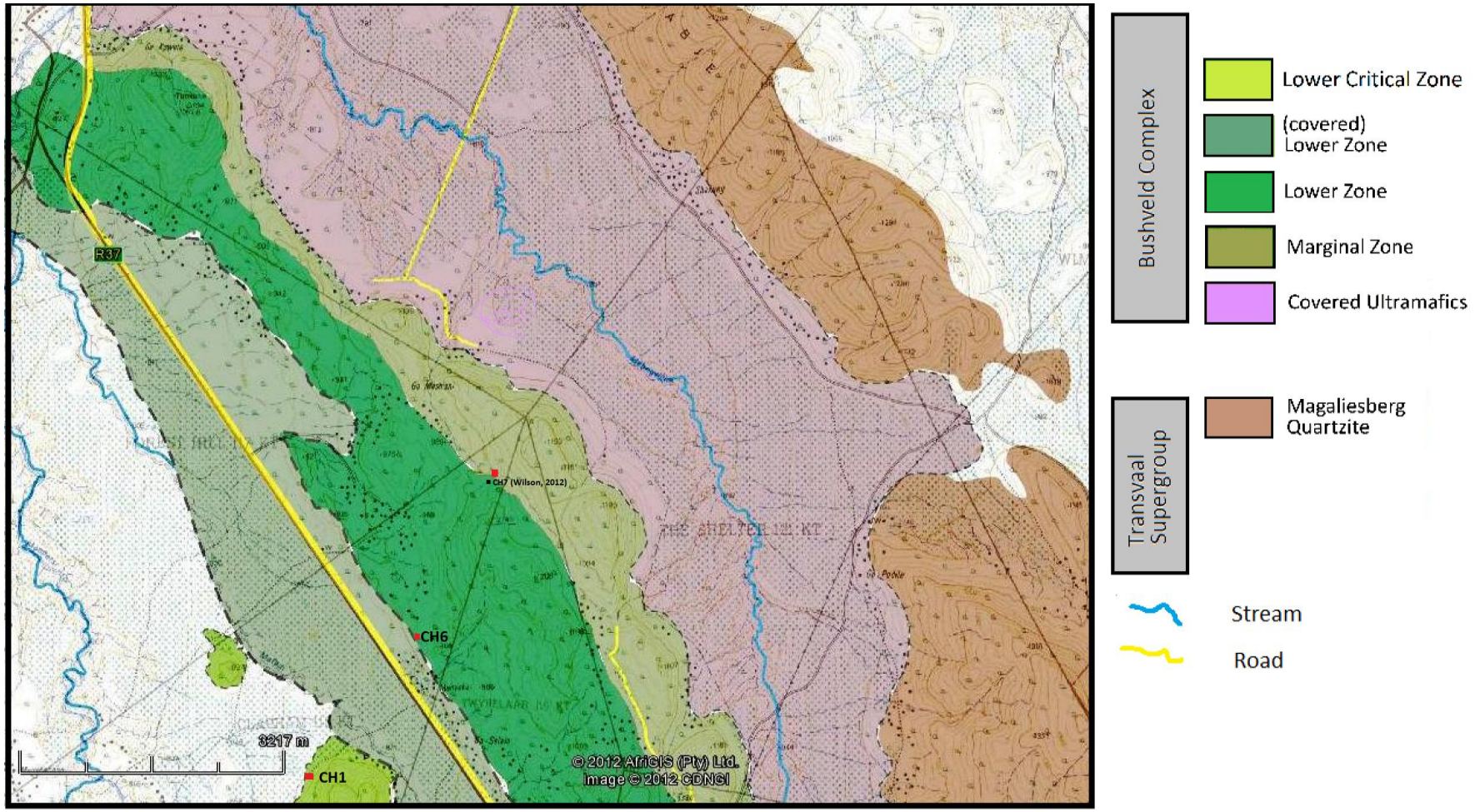

Fig. 2.1: Simplified geological map of the study area showing the lower-most succession of the Bushveld Complex. The stratigraphical relationships of the BUS, Lower and Marginal Zones are presented as seen in the Clapham Trough drill cores (red squares).

2.1. Nomenclature and subdivisions

There are numerous publications describing the lithologies and subdivisions of the layered rocks of the Bushveld Complex, including the Marginal and Lower Zones. The names used for the subdivisions of the latter zones and the rocks units that constitute them have changed (at least on an informal basis) for as long as these units have been studied. The present study adopts the subdivisions based on the informal stratigraphy as described by SACS (1980) and references therein, since it proves to be the widely used subdivision. Furthermore, in this section, the present study makes a number of basic terms that are used throughout this work.

In the Clapham Trough, the Marginal Zone consists of the lowest exposed norite units of the Bushveld Complex. The modal proportions of plagioclase in the norite range between 45-70 % of the rock. If the noritic rock contains between 35 - 45 % plagioclase, it is called a melanorite. In the present study the term mafic norite is used in preference to melanorite, since the feldspar content can, in some cases, be very low such that the rock is bordering on feldspathic pyroxenite. The term feldspathic orthopyroxenite is used to describe where the rock contains 15-30 % interstitial (post-cumulus) plagioclase. Orthopyroxenite predominantly consists of orthopyroxene with less than 10-15 % interstitial material, typically plagioclase and clinopyroxene in the present case. In some cases, the term pyroxenite is used to describe units that have both orthopyroxene and clinopyroxene, but the latter typically occurs as oikocrysts.

Other cumulate rocks occurring in the Clapham Trough area and intersected in the drill cores are olivine rich rocks, broadly referred to as peridotites. In some cases, the peridotite units are identified by their specific names such as for dunites, which are almost entirely made up of olivine, or harzburgites that contain approximately equal amounts of olivine (typically 40 to 50 %) and cumulus orthopyroxene. These peridotitic rocks were not identified in the field

(due to poor exposure) but the CH1 drill core presents fresh samples for analyses in this work. Olivine-rich rocks are not common in the CH6 drill core, but occur at specific horizons towards the top of the succession intersected.

Other than the cumulate rocks that were formed from the magmas injected into the Bushveld Complex magma chamber, there are older rocks that occur as inclusions in both the CH6 drill core and the field. Depending on their relationship with the intrusive rocks, these inclusions can be either xenoliths or autoliths. The latter refers to rocks than were possibly formed within the magma chamber and were entrained by subsequent magma injection to the present levels, whereas the former refers to rocks that predated the emplacement of the Bushveld Complex. Xenolithic rocks are typically part of the floor rocks sequence, that were carried to their present location by magma(s) emplaced in the chamber.

2.2. The Geology at Clapham Trough

This study focuses on the bottom most parts of the Lower Zone and the Marginal Zone succession, hence this work will not cover the entire Lower Zone succession in this area. All the thicknesses and depths given in subsequent sections and chapters refer to the measurements as observed in the drill cores, whose detailed logs are shown in Appendix A. The core is coherent and fresh to provide continuous sampling through the studied section of the Bushveld Complex. At the Clapham Trough, the general strike of the rocks of the Lower and Marginal Zones is approximately NW-SE with the average dip of 15° SW.

The floor rocks in the study area belong to the Magaliesberg Formation (quartzite) of the Pretoria Group. The contact rocks in this area are not exposed, but they have been studied in detail as described in the deeper drill core CH7 by Wilson and Chunnett (2010) and

subsequently by Wilson (2012). These rocks form part of approximately 1200 m of ultramafic rocks referred to as the Basal Ultramafic Sequence (BUS) by the latter authors. The BUS is completely covered by alluvium in the study area, as mentioned in earlier sections of this work. The Marginal Zone norites are the lower most exposed units of the Bushveld Complex and show conformable relations with the BUS of Wilson and Chunnett (2010). Most of the outcrops are very fresh and well preserved.

2.2.1. The Marginal Zone

Within the CH6 drill core, there are two broad groups of noritic rocks as defined by modal abundances of plagioclase and orthopyroxene. Namely, the lower Mafic Norite, which is conformable to the upper part of the BUS (Wilson and Chunnett, 2010) and grades to the overlying Shelter Norite with increasing amount of plagioclase. The Marginal Zone norite sequence (Mafic and Shelter Norites) are the lowest exposed sequence of rocks in the eastern Bushveld Complex.

The orientation of the Marginal Zone rocks in the field area varies between 347/10 W and 358/15 W, and the surface can be extremely undulating on a local scale. The Marginal Zone stratigraphic succession seen in CH6 (Fig 2.2) starts with Mafic Norite characterized by igneous lamination expressed by feldspathic lensoid features no more than 2-3 cm in the field. Similar features are observed in cyclic units identified in the Shelter Norite. The long axes of the feldspathic laminae (i.e. lensoid) are parallel to the general layering surface. The bottom most parts of the Mafic Norite are bordering feldspathic pyroxenite compositions.

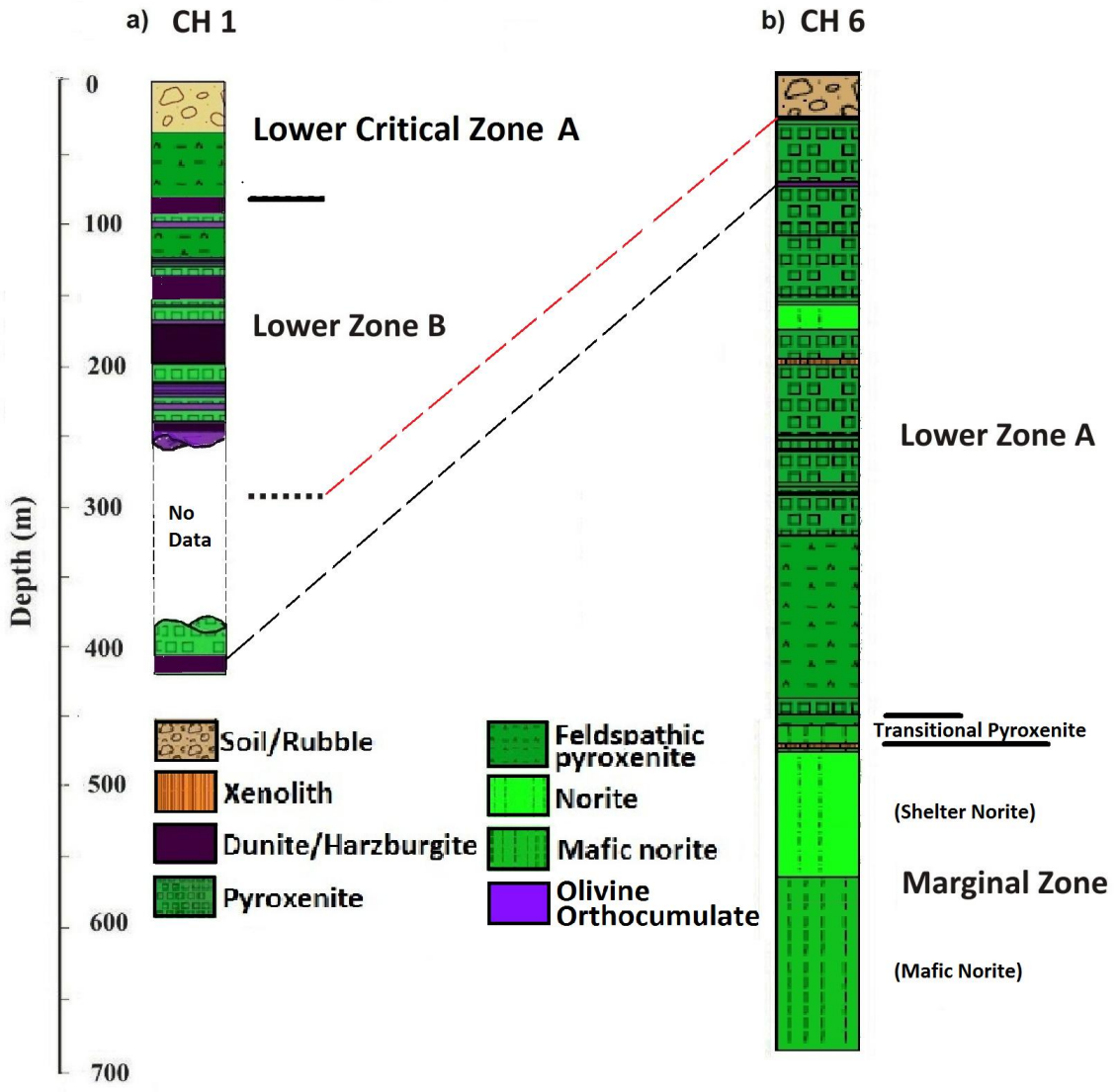

Fig. 2.2: The lithological logs of the CH1 (from Wilson, pers. com.) and CH6 drill cores. a) Shows the first and last 250 and 30 m of the stratigraphy in CH1, respectively. b) Shows the stratigraphic succession of CH6 intersecting the Lower-Marginal Zone boundary.

These igneous layering features are clearer in the field since they are developed over large distances than core samples (Fig. 2.3). The average crystal size of the Mafic Norite is 1-2 mm. The rock composition is largely made of orthopyroxene, plagioclase and post-cumulus clinopyroxene as the dominant mineral phases.

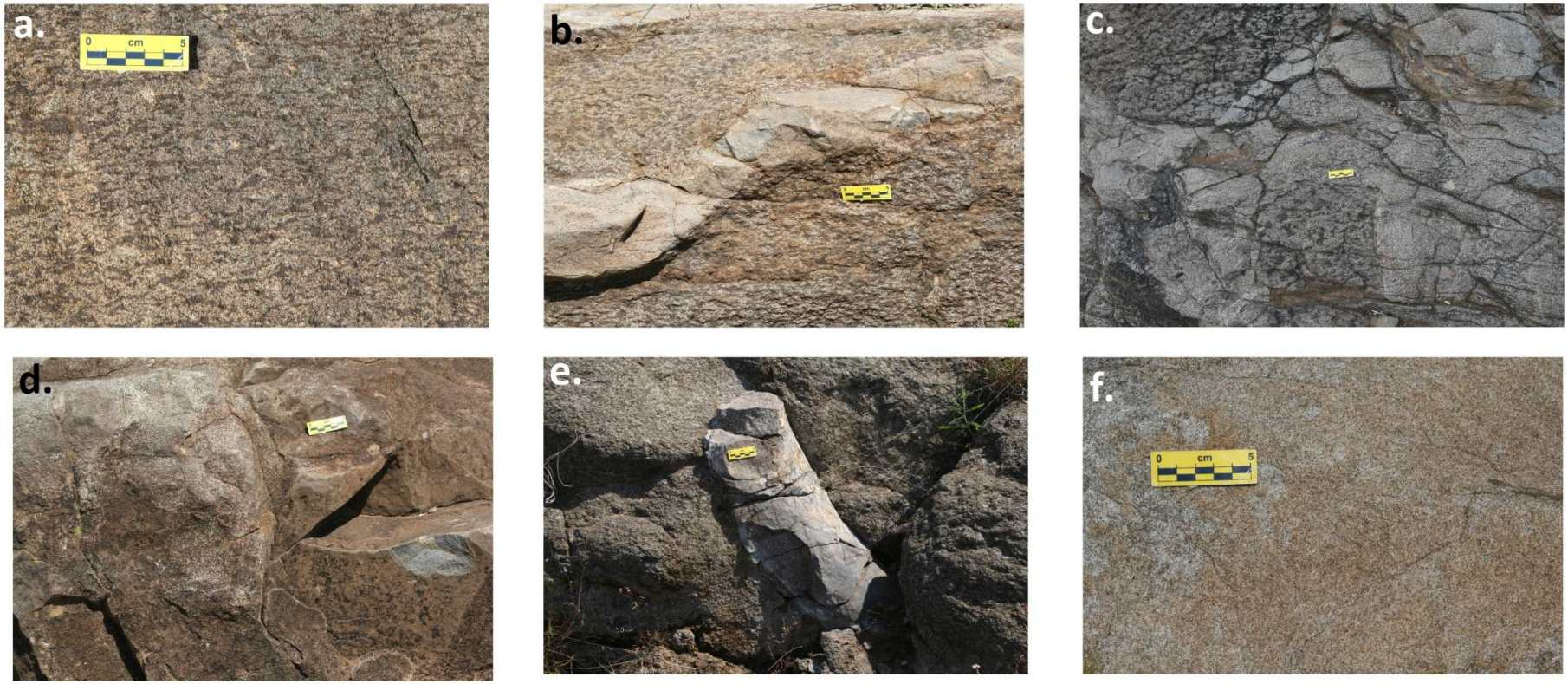

Fig 2.3: Field relations of Marginal Zone lithologies. a) Shows the Mafic Norite with sub horizontal layering expressed by feldspathic lenses. b-e) Very fine-grained norite layers conformably and transgressively associated with Shelter and Mafic Norite units. f) Shows the typical Shelter Norite. Photos courtesy of Prof. A.H. Wilson.

Orthopyroxene accounts for about 75-55 % of the modal amounts and plagioclase varies between 25-40 % and post-cumulus clinopyroxene is typically less than 10-15 volume %. In the CH6 drill core, the Mafic Norite occurs from about 570 m to the bottom of hole (692 m). It appears to have a mottled texture and details will be discussed in subsequent chapters (Chapter 4 Petrography). The amount of mafic minerals decreases gradually with increasing stratigraphic height, as the amount of cumulus plagioclase increases, particularly above 647 m depth in the CH6 drill core. The amount of plagioclase steadily increases, from about 23 % to greater than 40 volume %, with stratigraphic height. At about 566 m depth in the CH6 drill core, the amount of cumulus plagioclase increases to the compositions of a norite (*sensu stricto*, i.e. Shelter Norite in the present work). Since this change is gradational, the exact contact between the Mafic Norite and the Shelter Norite is approximated to be at 563 m. The bottom of hole is at about 692 m, and the recorded thickness of the Mafic Norite is about 129 m in the CH6 drill core.

The Shelter Norite is predominantly made up of plagioclase and orthopyroxene, with less than 10 % post-cumulus clinopyroxene. As mentioned above, the amount of plagioclase is highest in this part of the Marginal Zone, typically greater than 50 volume % of the rock. Orthopyroxene modal abundance typically varies between 22-40 volume %. Layering within the Shelter Norite sequence is expressed by the subtle variations in the amounts of plagioclase and orthopyroxene. There is poor evidence of cyclic modal variation observed in the drill core but the field mapping showed igneous lamination pronounced by the modal variations to be prevalent (Figs. 2.3a-b). Other than the amount of plagioclase, the Shelter Norite also differs from the Mafic Norite with the abundance of xenolithic and/or autolithic fragments and enclaves. These foreign rocks fragments have variable compositions and sizes. The compositions of xenoliths identified in the field were quartzite and hornfels xenoliths, particularly near the top of the Shelter Norite, both in the CH6 drill core and the field (Figs.

2.2; 2.3d). It is not as easy to identify the xenoliths/autoliths in the drill core because of the size often intersected in the drill-core, but a number of xenolith/autolithic fragments have been identified in the field.

Commonly occurring within the Shelter Norite are extremely fine-grained layers whose composition is of a quartz-rich norite. These fine-grained 'noritic' layers extend laterally for as long distances as the Shelter Norite package in which they are hosted. Moreover, there seems to be cyclicity associated with the occurrence of these fine-grained (silica-rich) noritic layers. Typically each cycle starts with the silica-rich fine 'granular-textured norite' capping norite (*sensu stricto*)-leuconorite, which in turn grades into a melanorite with relatively higher modal proportions of orthopyroxene at the base (Fig. 2.3b). At least three of these repetitive/cyclic units are identifiable in the field. The subtleties of the cyclic units in the CH6 drill core are not readily identifiable but the cyclic units could be more than the number identified in the field.

The crystal size in the Shelter and Mafic Norite packages is generally 1-2 mm, whereas the fine-grained layers have grain sizes well below 1 mm. These fine-grained layers are relatively resistant to weathering and typically form the dip surfaces in the field. The relationship between these fine-grained quartz-norite layers and the Shelter Norite is such that the former can be conformable for large distances laterally, or locally cut across and/or occur as diapirs that penetrate the overlying cyclic units (Fig. 2.3b, e). The top of the Shelter norite is estimated to be at the 471 m mark in the CH6 drill core, suggesting a thickness of about 91 m. Based on CH6 drill core, the Marginal Zone has a total thickness of about 220 m (including 129 m of Mafic Norite). The thickness in the field is variable such that the Marginal Zone, or at least the Shelter Norite succession, appears to get thicker in a southerly direction (Fig. 2.1).

2.2.2 Transitional Pyroxenite

The boundary between the Marginal Zone and the Lower Zone is marked by a zone of 'patchy' feldspathic pyroxenite (referred to from this point as the Transitional Pyroxenite, Fig. 2.4). This unit gradually changes from true (anorthositic) norite at the top of the Shelter Norite through melanorite (approximately at 471 m) to typical Lower Zone orthopyroxenite with increasing stratigraphic height. The modal abundance of plagioclase feldspar in the Transitional Pyroxenite decreases with stratigraphic height such that the most feldspathic zone is closest to the Marginal Zone norite, with the size and number of the feldspathic patches progressively decreasing towards the Lower Zone.

In the CH6 drill core and the field, there are no chill contacts observed and the lithological changes are extremely gradational. The top of the Transitional Pyroxenite is estimated at 454 m. This boundary unit in the drill core is estimated to be about 15 m but in the field it appears wider in areas, up to 30 m. The dominant mineral phases in the Transitional Pyroxenite are orthopyroxene with no apparent igneous lamination, plagioclase, which makes up the feldspathic patches (Fig 2.4) and clinopyroxene oikocrysts enclosing smaller orthopyroxene crystals. Only orthopyroxene can be positively identified as a cumulus phase in this relatively friable unit. The shallow valley between the Lower Zone and the Marginal Zone in the field marks the approximate position of the Transitional Pyroxenite (Fig. 2.1). In the field there was magnesite rubble and locally olivine bearing-rocks at this level. The CH6 drill-core does not have olivine in the Transitional Pyroxenite.

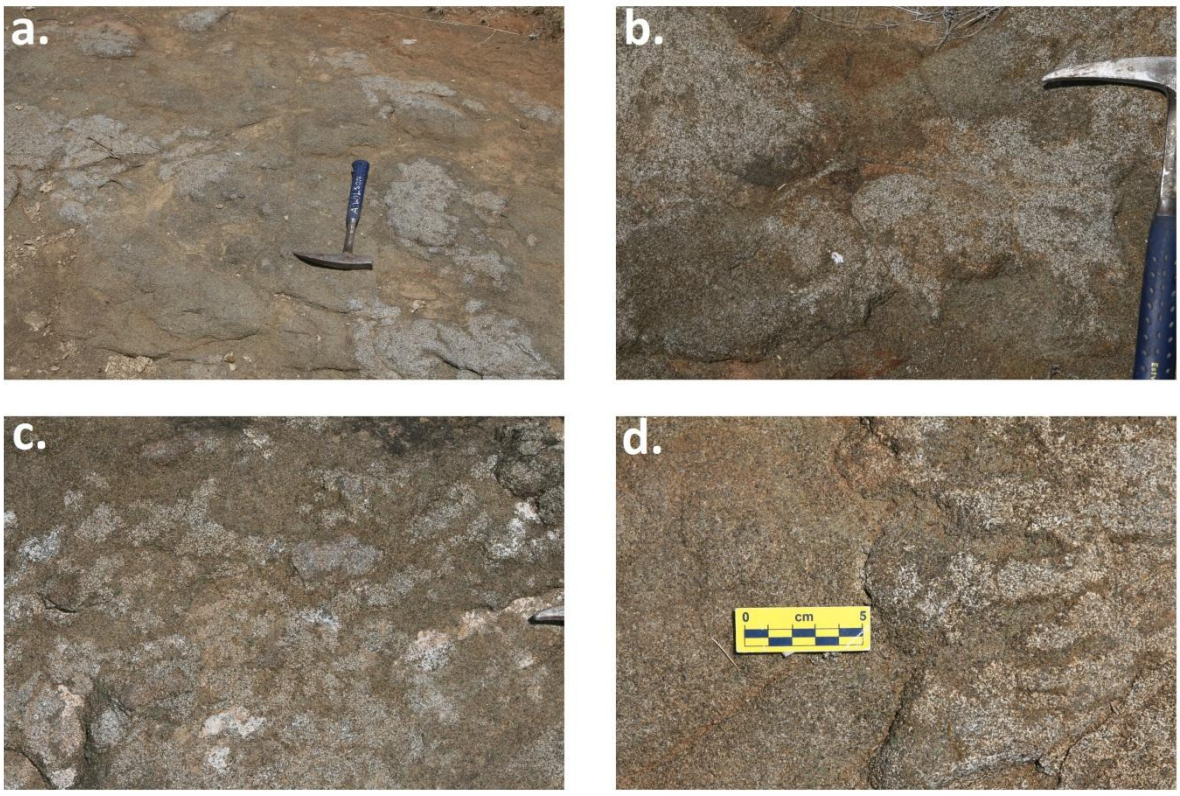

Fig. 2.4: Transitional (patchy) pyroxenite marking the Marginal-Lower Zone boundary. The accumulation (patches) of feldspar has variable sizes, generally decreasing in size closer to the Lower Zone. Photos courtesy of Prof. A.H. Wilson.

2.2.3. The Lower Zone

The Lower Zone succession as identified in the present work can be separated into two broad packages. The first, bottom succession is an orthopyroxene-rich succession, which starts from the top of the transitional (patchy) pyroxenite to the base of the olivine-rich succession, which makes the second and upper subzone of the Lower Zone succession as described in the Clapham Trough section of this study. The orthopyroxene-rich succession in the present work is referred to as the Lower Zone A (LZa) subzone. The LZa itself can be further separated into a basal 120 m thick feldspathic orthopyroxenite succession with up to 15-20 % post-cumulus plagioclase. A norite marker horizon, situated at about 290-292 m depth in the CH6

drill core, separates the lower feldspathic orthopyroxenite sequence from the upper orthopyroxenite succession.

The upper orthopyroxenite succession of the LZa contains less than 10 % post-cumulus phases, mainly plagioclase. The CH6 section shows that in the middle of the upper LZa succession there is an interlayered norite horizon, which has not been identified in the field. The separation of the LZa into two orthopyroxene subdivisions is mainly based on the amount of post-cumulus plagioclase, whose significance will be further explored in subsequent chapters. It is important to emphasise that plagioclase in the LZa predominantly occurs as an intercumulus phase, and the modal abundance thereof varies between 0-20 volume % of the rock compositions.

The variation of the amount of interstitial plagioclase is not distinct in the core, but in the field, igneous lamination is revealed by the subtle variations of the modal abundances of feldspar. Layering from centimetre to metre scale is easily identifiable in the field (Fig. 2.5). In addition to this distinct igneous layering, there are occurrences of lens-like features in the orthopyroxenite whose long axes adopt layer parallel orientations and occasionally amalgamate to form irregular layers (Fig 2.5). There is no obvious difference to the naked eye between the ‘matrix orthopyroxenite’ and the ‘lens-shaped orthopyroxenite’ except preferential weathering of the matrix relative to the lens-shaped orthopyroxenite. On a fresh surface, it seems the matrix is slightly darker (less interstitial plagioclase) than the enclosed lens-shaped objects. The subtle difference in the amount of plagioclase is the only distinction known about these features and is suspected to be the cause of the preferential weathering observed. These lens-shaped features were observed on surfaces perpendicular to the dip direction (i.e. generally parallel to strike) near the bottom of the LZa, above the transition pyroxenite.

Generally, the amount of interstitial plagioclase decreases with increasing stratigraphic height, coupled with the development good igneous lamination in the upper orthopyroxenite succession of LZa. The lamination observed is defined by the orientation of orthopyroxene crystals, whose long axes lie parallel to the layering surface (Fig. 2.5). This igneous foliation is visible in drill core and in the field exposures. In general, the long axes of the orthopyroxene grains are about 2-3 mm with an aspect ratio of up to 10:1. Orthopyroxene modal abundance generally accounts for about 80-90 volume % of the LZa succession. Minor olivine, if present, and interstitial mineral phases (mainly plagioclase and clinopyroxene) make up the rest of the assemblage. Olivine occurs as a cumulus phase in two layers, first the harzburgite layer at about 78 m, and in the variably altered dunite at about 30 m depth in the CH6 drill core. The latter unit (dunite at 30 m in CH6) is taken as the base of the harzburgite succession (LZb) of the Lower Zone (red line in Fig. 2.2).

Occasionally, plagioclase occurs as a cumulus phase hosted in the LZa within two interlayered norite horizons, one at 290-292 m and the other, between 164-181 m. Within both interlayered norite intervals, there is a well-developed millimetre-centimetre igneous layering expressed by the variations in the modal abundances of plagioclase and orthopyroxene. The well-developed igneous lamination distinguishes the LZa norite units from the plagioclase-rich Shelter (anorthositic) Norite. However, like the Shelter Norite succession, the LZa norite units are also associated with xenoliths, especially near the stratigraphically higher level (i.e. 164-181 m mark in CH6 drill core) norite unit of the LZa subzone. The bottom contact of the norite layers is gradational, whereas there is an internally sharp top contact with the fine-grained feldspathic pyroxenite. The entire package is capped by a sharp, possibly erosive contact (Fig. 2.5d). Above the fine grained pyroxenite ‘contact zone’, feldspathic pyroxenite with plagioclase stingers occurs, but the amount of interstitial

plagioclase decreases with increasing stratigraphic height to form olivine-bearing orthopyroxenite with low modal proportions of interstitial phases.

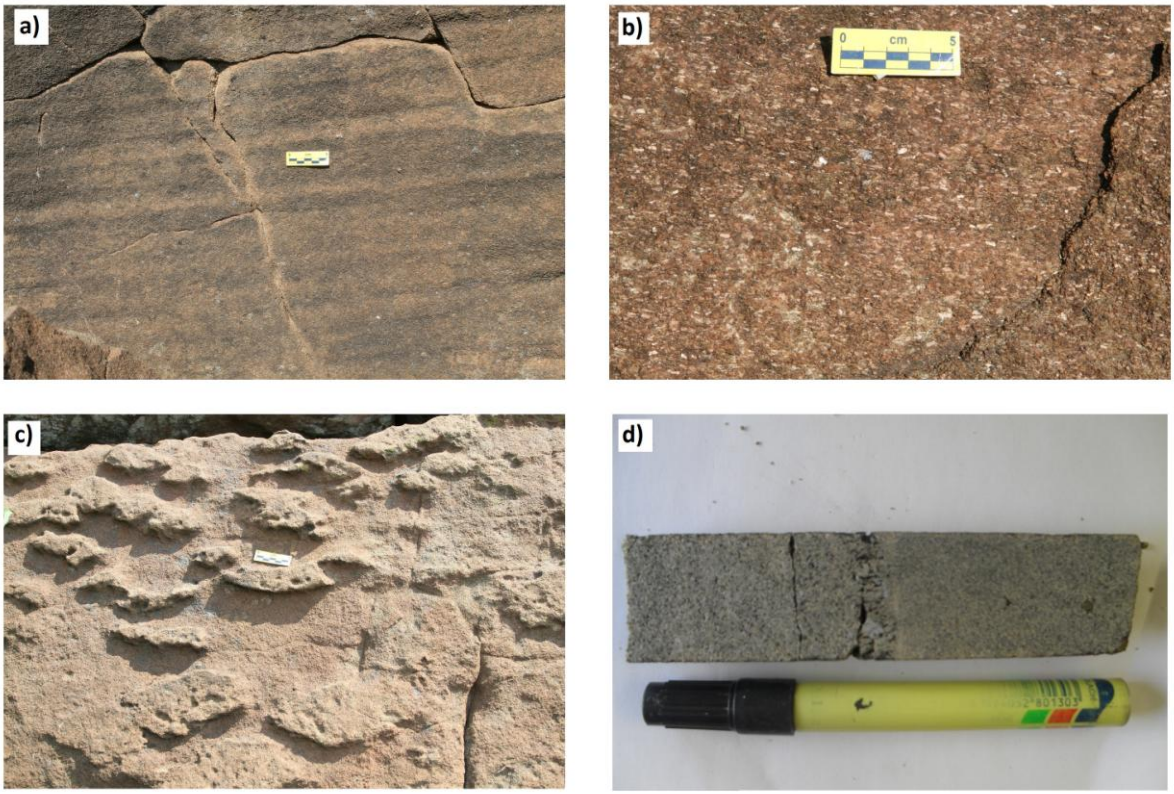

Fig. 2.5: Lower Zone orthopyroxenite showing a) subtle modal layering defined by the variation in the amount of interstitial plagioclase. There is well developed igneous foliation defined by the long axes of the orthopyroxene grains (b). Layering is also seen (vaguely) by the orientation of the lensoid features (c) whose long axes are sub-parallel to layering. d) Sharp erosive contact marking the boundary between the fine-grained and medium-grained orthopyroxenite.

As noted previously, the Lower Zone succession in the study area starts above the Transitional (patchy) Pyroxenite, whose top contact in the CH6 drill core is at 454 m depth. The base of the Lower Zone is taken to be at the level where orthopyroxene crystals exhibit well developed igneous lamination. The CH6 drill core, as mentioned earlier, is 692 m deep. In addition to the CH6 sequence, the Lower Zone succession is continued (up stratigraphy) in

borehole core CH1, which is 422 m deep. However, the CH1 collar is on Lower Critical Zone rocks, and the exact boundary with the underlying Lower Zone is not clear. In this chapter, the Harzburgite succession is taken as the top of the Lower Zone (Fig. 2.2). This suggests the Lower Zone succession at Clapham Trough is about 702 m.

The CH1 borehole was drilled such that its bottom units overlap with the top units of CH6 and therefore only the lowest part of CH1 is considered in this work. CH1 starts (from the bottom up) with about 2 m of orthopyroxenite overlain by an olivine-rich (Harzburgite) layer. Above the olivine-rich unit, there is a > 50 m thick orthopyroxenite. This Harzburgite unit is correlated with the Harzburgite unit identified in CH6 at 78 m depth as supported by the modal proportions of olivine and orthopyroxene and the association with orthopyroxenite. For the record, only the lowest part of CH1 was available for use in this work as the rest of the core had been discarded. The contact of the orthopyroxene with the olivine-rich cyclic units, where there is a sustained occurrence of olivine, is estimated (Fig. 2.2, 2.6).

In the current study, the top of LZa is taken to be the level of sustained olivine dominance as a cumulus phase. This suggests that LZa is at least 500 m thick in the Clapham area. Olivine is the dominant cumulus phase at least between 90-255 m (Figs. 2.2; 2.6) in the CH1 drill core but there is no exposure of this peridotite package in the field. There are insignificant interstitial phases in the olivine-rich units and the variation of olivine and orthopyroxene define the cyclic units observed. The cyclic units start from dunite, harzburgite, olivine-orthopyroxenite and olivine-free orthopyroxenite layers. There is no occurrence of spinel-rich (i.e. chromitite) layers (Fig. 2.2).

The peridotite-rich package in this study is referred to as the Lower Zone B (LZb) subzone. The lithological log of CH1 available suggests LZb is at least 165 m thick. Above the olivine-rich package of cyclic units, feldspathic orthopyroxenite occurs as a seemingly massive rock

sequence. Igneous layering is not observed in the core but lamination as defined by orthopyroxene crystals is present. In CH1 this orthopyroxenite is shown to be at least 54 m thick, overlain by some 30 m of rubble. Records show the CH1 borehole was collared on lower Critical Zone and nowhere in the drill core was there a boundary, either textural or structural, to mark the break between the Lower Zone and the Critical Zones. This work treats this top of the olivine-rich cyclic units (i.e. Harzburgite subzone, LZb) as the base the lower Critical Zone. Thus, the feldspathic orthopyroxenite above LZb is regarded as part of the Lower Critical Zone A (LCZ, Fig 2.6). The rocks on which CH1 is collared were mapped previously as being Lower Critical Zone lithologies by Dr. Tom Molyneux (unpublished mapping), which supports the decision to retain the top orthopyroxenite as a Lower Critical Zone succession. Since this present work focuses mainly on the LZa of the Lower Zone succession, the LZb and LCZ are only considered for correlation purposes and the discussion thereof is limited from here on.

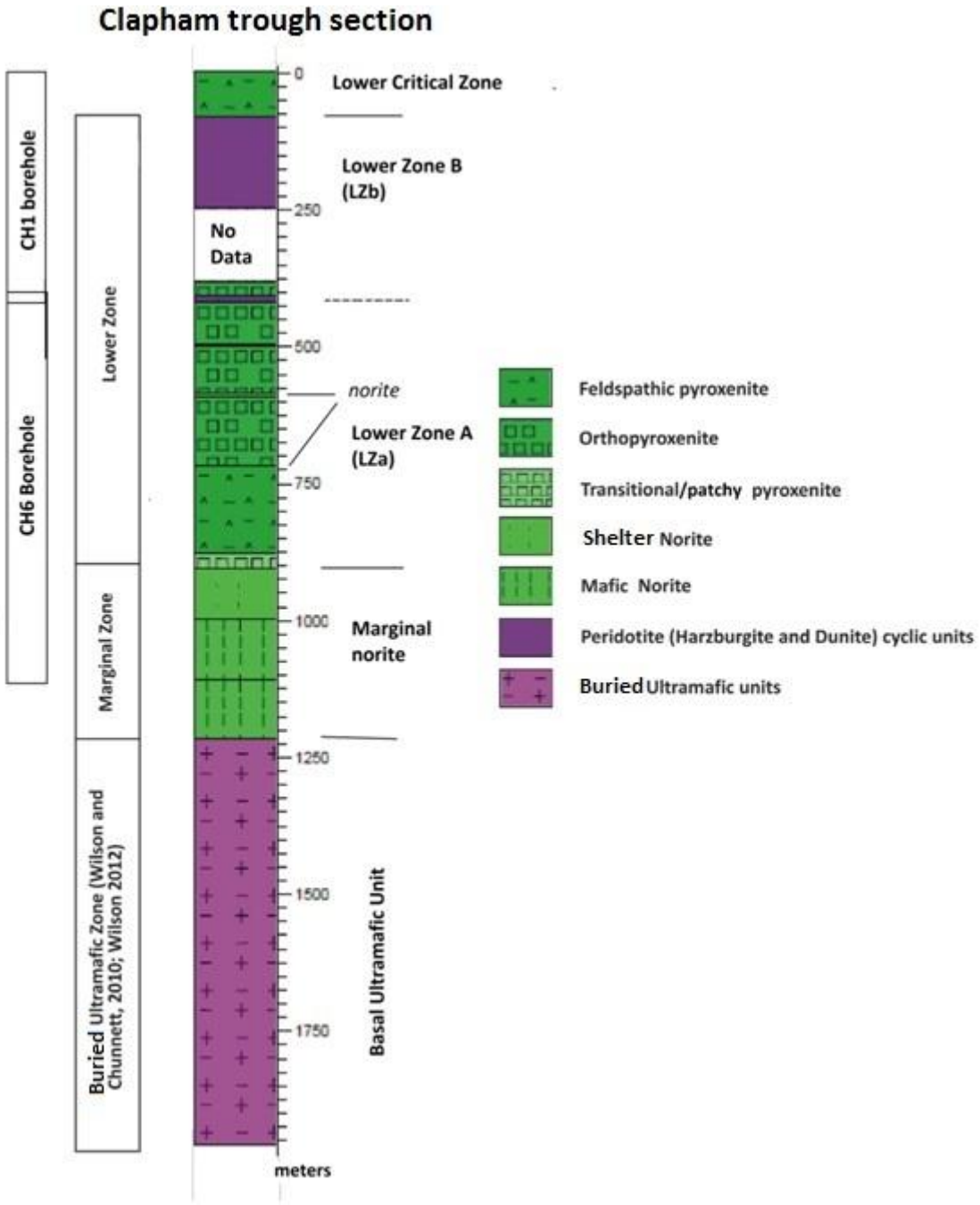

Fig. 2.6: Simplified stratigraphic succession observed in the Clapham Trough area based on intersections described in the CH1, CH6 and the CH7 drill cores. The CH7 drill core is described in Wilson and Chunnett (2010) and Wilson (2012).

2.3. Summary

The Clapham Trough drill cores were drilled for research purposes to provide a complete stratigraphic section from the bottom of the Lower Zone through the Marginal Zone to the floor of the intrusion. These boreholes are CH1, CH6 and CH7. The first two holes cover the section of the Bushveld Complex stratigraphy focused on in this project. CH7 is the subject of Wilson and Chunnett (2010), Wilson (2012) and Wilson (2014, in prep). The drill core of particular interest for the purposes of this work is CH6, which covers the Marginal-Lower Zone sequence. CH1 is a supplementary borehole, whose main purpose is for correlation of the units identified at Clapham Trough with the regional geology across the layered mafic intrusion.

The works of Wilson and Chunnett (2010), and Wilson (2012) as mentioned in the previous chapter dispel the previously accepted belief that the Marginal Zone is in contact with the Magaliesberg Quartzite under alluvial cover. Instead the latter studies showed that there is at least 1 km thick rocks designated BUS that present much more primitive compositions than previously accepted for the Bushveld Complex. Moreover, there appears to be conformable relations between the Marginal Zone rocks and the BUS of Wilson and Chunnett (2010). The key points to note in this chapter are:

- The Magaliesberg Quartzite and the Marginal Zone norite are not in contact. The latter sits conformably on a thick succession of ultramafic rocks, referred to as Basal Ultramafic Sequence (BUS).
- The Marginal Zone norite at Clapham Trough has a lower mafic norite sequence and a true norite upper portion, the best exposed part of the succession. Accordingly, the Marginal Zone norite is separated into Mafic and Shelter Norite successions with a composite thickness of at least 220 m.

- The Marginal Zone norite is relatively fine-grained and is xenolith/autolith bearing in the upper units of the stratigraphy. There is also layering (though subtle in drill core) on various scales. The layering is either expressed through modal or crystal size variations. There are at least three subtle cyclic units identified in the field within the Shelter Norite.
- The entire Marginal Zone succession in the Clapham Trough section exhibits unequivocal evidence that the rocks making up this part of the Bushveld Complex stratigraphy are cumulate rocks and they must have been subjected to some accumulation processes.
- The Shelter Norite is overlain by the Lower Zone, which shows good igneous lamination as defined by the orientation of orthopyroxene crystals. Plagioclase is largely a post-cumulus phase in the Lower Zone.
- The boundary between the Marginal and Lower Zones is marked by a feldspathic (patchy) pyroxenite unit, which is about 10-15 m thick in the CH6 drill core. This unit is called the Transition Pyroxenite.
- The patchy pyroxenite also shows vague igneous lamination defined by the patches and orthopyroxenes.
- The Lower Zone predominantly consists of orthopyroxene, with plagioclase, clinopyroxene predominantly occurring as interstitial phases. Olivine occurs mainly in specific horizons in the LZa. Based on the modal abundances, the present work separated the Lower Zone stratigraphy of the Clapham Trough section into the feldspathic orthopyroxenite (LZa) from the olivine-rich LZb subzones.
- The textures and lithological characteristics dispel earlier suggestions that the noritic rocks of the Marginal Zone were chilled melts but rather that these rocks form part of an evolving succession at the base of the Bushveld Complex.

The detailed assessment of the cumulate rocks that constitute the Marginal and Lower Zones of the CH6 drill core will provide a good understanding of the how the Marginal Zone norite fits in the stratigraphy of the Bushveld Complex, and their transition into the Lower Zone succession. Re-evaluating this section of the Bushveld Complex is critical in understanding the enigmatic early intrusive stages of the formation of the Bushveld Complex. Correlation and comparisons of similar units identified elsewhere in the intrusion will enable this study to build an understanding of local versus regional processes. The subsequent chapters will provide further details and correlations on the basis of the geochemistry.

Chapter 3

Stratigraphic Correlations in the Eastern Limb and Across the Bushveld Complex

The compositions and textures described for rocks in any particular zone of the Bushveld Complex changes from one locality to another, especially in the earliest stages of the formation of the layered mafic intrusion. The zones and rocks extend over large distances and the lateral variations are not easily identified. It is imperative that good correlation of texturally and compositionally similar rocks over these distances be conducted to allow the present study to re-assess the early magma chamber processes that were operating near and around the Clapham Trough. This section examines the drill core data from the previous chapter in light of the general stratigraphy of the eastern Bushveld Complex. Furthermore, it evaluates how the stratigraphic succession in the Clapham Trough area compares with studies conducted elsewhere in the Bushveld Complex, the Olifants River Trough (at the northern parts of the eastern limb) in particular. For the sake of completeness and relevance, comparison and correlation with Lower and Marginal Zone stratigraphy of the western Bushveld Complex will be included later in this section.

Based on the modal abundances and textures observed in the Clapham Trough drill cores and field relations observed in the study area, the Marginal Zone (and the pre-Marginal Zone rocks of the Bushveld Complex) is a separate lithological entity from the Lower Zone. The ultramafic 'pre-Marginal Zone' (i.e. the so-called B1-Ultramafic sills like the Aapiesdoringdraai Peridotite body) rocks occurring between the quartzite floor and the Marginal Zone norite elsewhere in the Bushveld Complex are tentatively designated the

correlatives of the (unexposed) Buried Ultramafic Sequence (Wilson, *pers. comm.*). The thicknesses of units at Clapham Trough are reported as measured in the CH1 and CH6 boreholes. A simplified lithological succession of the Clapham trough section has been shown already in the previous chapter (Fig. 2.6).

The thickness of the BUS is recorded in Wilson and Chunnett (2010) to be approximately 800 m and the compositions of these earliest magma(s) are discussed in Wilson (2012). These rocks are olivine and orthopyroxene cumulates ranging from dunite through harzburgite to orthopyroxenite. Conformably over the BUS occurs rocks that are defined as the Mafic Norite at least 129 m thick in CH6 drill core, but the total thickness of the Mafic Norite in the Clapham Trough area is as thick as 200 m, when including the top units described in the CH7 drill core by Wilson and Chunnett (2010).

Previous studies took the Shelter Norite succession as the stratigraphic equivalent to Hendriksplaats/Maruleng norite occurring elsewhere in the Bushveld Complex (Willemse, 1959). However, there has been enough evidence to suggest that the latter rocks pre-date the Bushveld Complex and were formed through unrelated events (Vermaak, 1970). The Mafic and Shelter Norite sequences constitute what is referred to as the Marginal Zone norite at Clapham Trough. The thickness of this Marginal Zone norite is quite variable in the study area. The CH6 drill core suggests that the Marginal Zone norite is at least 220 m thick. The Marginal Zone is separated from the Lower Zone by the 'patchy' Transitional Pyroxenite described in Chapter 2. This patchy feldspathic orthopyroxenite unit marks the base of the Lower Zone Succession.

The Lower Zone, whose thickness is some 700 m based on the Clapham Trough drill cores described in the preceding chapter, conformably overlies the Marginal Zone norite. The Lower Zone is medium grained, with well-developed igneous lamination that is everywhere

parallel to the general layering in the area. This lamination is expressed by the orientation of the long axes of the orthopyroxene crystals. As mentioned in the previous chapter the lower Zone succession is divided into the orthopyroxene-rich (Lower Zone A, LZa) and olivine-rich (Harzburgite, Lower Zone B, LZb) Subzones. The bottom orthopyroxenite sequence of the LZa is relatively feldspathic and is capped by a thin norite marker. This is succession called the Clapham Orthopyroxenite succession. Above the marker norite layer, there is relatively little modal abundance of post-cumulus phases and this succession is correlated to the Rostock Orthopyroxenite (formerly Bronzite) of SACS (1980).

The appearance of persistent olivine cyclic units is taken as the base of the Harzburgite (Lower Zone B, LZb) Subzone, which is correlated to the dunite unit near the top of CH6 drill core. This olivine-rich zone contains numerous cyclic units starting with dunite through harzburgite to olivine-bearing pyroxenite, occasionally feldspathic orthopyroxenite. Above the LZb there is approximately 80 m of feldspathic orthopyroxenite, which is taken here as part of the Lower Critical Zone as explained in the previous chapter (Fig. 2.6).

3.1. Olifants River Trough (eastern limb)

The Olifants River Trough is located on the northern-most parts of the eastern limb of the Bushveld Complex. In that area the rocks that occur below the Critical Zone are exposed on Jagdlust and Winterveld farms; and are referred to as the Lower Zone (Cameron, 1978). This term is taken to include the Lower and Transition Zones from the latter author's work. The mapping conducted in the area by Cameron (1978) has led to the compilation of approximately 1580 m of Lower Zone succession. The simplified Lower Zone stratigraphic succession, based on the work of Cameron (1978), at the Olifants River Trough is shown in

Fig. 3.1; and comparisons with the Clapham Trough stratigraphic section based on the drill cores discussed in chapter 2 of the present work appear in Fig. 3.2.

The floor of the Bushveld Complex at the Olifants River Trough is the Magaliesberg Quartzite but there is no apparent contact with the lowest exposed rocks of the layered mafic intrusion in the area. The lowest exposed rocks at the Olifants River Trough belong to the Basal Subzone which is part of the Lower Zone of Cameron (1978). The Basal Subzone consists of xenolith-bearing norite, olivine-rich and feldspathic pyroxenite units. Cameron (1978) drew similarities between his xenolithic norite with the Marginal Zone norite (previously correlated with the Hendrikplaats norite of Willemse, 1959) identified elsewhere in the Bushveld Complex. Cameron (1978) seems to be uncertain whether the norite is in contact with the quartzite floor. However, the latter author made an admission that if the xenolithic norite described at the Olifants River Trough is in contact with the Magaliesberg Quartzite, it should be considered Marginal Zone.

There are ultramafic rocks (magnesite residuum, a weathering product of olivine-rich rocks) that the latter author makes reference to in the vicinity of the floor contact. The fact that Cameron recognizes that his Xenolithic Norite might not be in contact with the Magaliesberg Quartzite suggests that there might be rocks that are not exposed between the norite and the floor, possibly the correlative units of the BUS (Wilson, *Pers. Comm.*). This xenolithic norite is correlated with the Marginal Zone norite described in the Clapham Trough, the Shelter Norite in particular with its abundance of xenoliths. The norite is overlain by at least 200 m of feldspathic pyroxenite associated with olivine-rich rocks, followed by orthopyroxenite (with little or no interstitial material) formerly referred to as the Lower Bronzitite Subzone. Since the terms bronzite and bronzitite are no longer used, the present study refers to the above subzone as the Lower Orthopyroxenite Subzone. The appearance of (cumulus) olivine above this orthopyroxene-rich zone defines the Harzburgite Subzone of Cameron (1978) (Fig.

3.1). The disappearance of olivine marks the base of an orthopyroxenite succession zone capping the Lower Zone at the Olifants River Trough, referred to by the latter author as the Upper Orthopyroxenite (Bronzitite) Subzone.

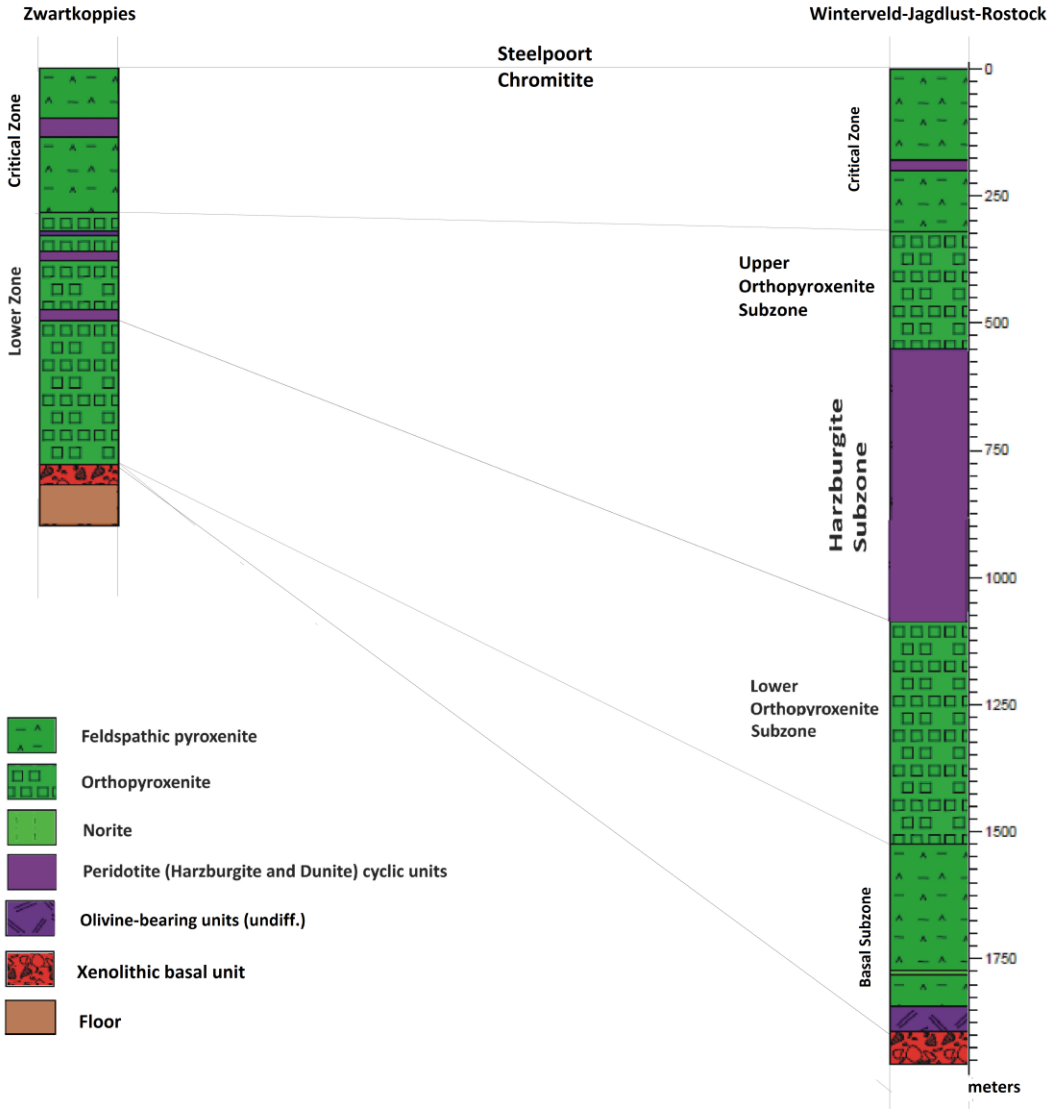

Fig. 3.1: Simplified lithological Succession at the Olifants River Trough. Stratigraphic succession adopted from Cameron (1978).

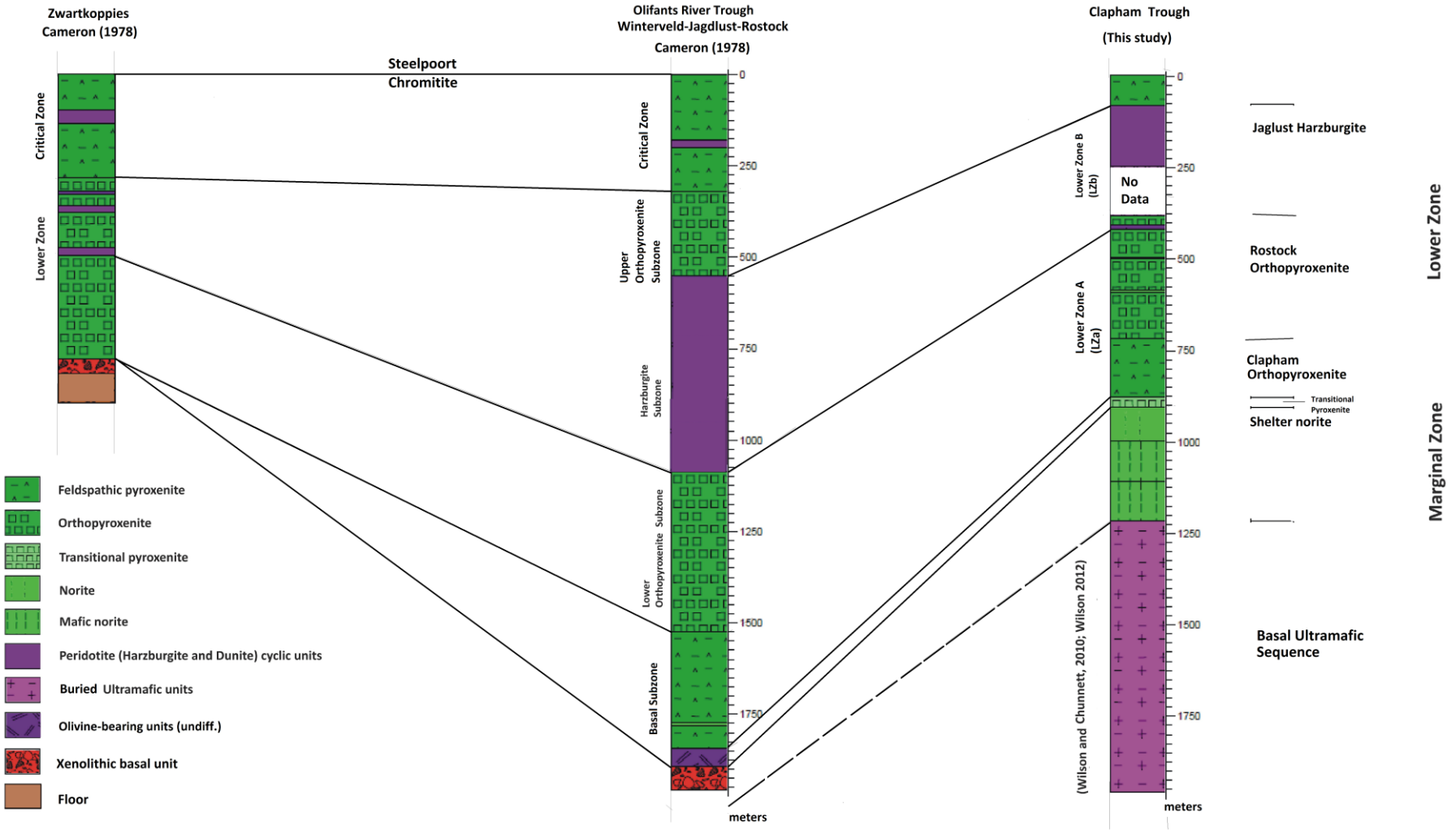

Fig. 3.2: Correlation of units across the eastern Bushveld Complex between the Clapham and the Olifants River Troughs. Note the different scales, all in meters. The thicknesses reported are as recorded in the respective areas.

There is well-developed igneous foliation in the entire Lower Zone of Cameron (1978). The part of the stratigraphy that is of great interest in the present study is the Lower Orthopyroxenite, the Basal Subzones and xenolithic norite (Marginal Zone) of Fig. 3.1. The correlation of the Marginal and Lower Zones at the Olifants River Trough with the equivalent units at Clapham Trough is shown in Fig. 3.2. The subdivision of the Marginal and Lower Zones in the Clapham Trough area, as adopted in the present study differs slightly from the work of Cameron (1978).

As mentioned above, the collar of the CH1 borehole is in the lower Critical Zone. The rock is a massive feldspathic orthopyroxenite. There is no structural and/or textural break observed anywhere within this feldspathic orthopyroxenite that would serve as a clear boundary between the Lower and Critical Zones. It is less ambiguous in the present work to take the top of the spinel free Harzburgite Subzone as the boundary between the Lower and Critical Zones (Fig. 3.2) similar to the studies in the western Bushveld Complex, as discussed later.

Since the xenolith-bearing norite in Olifants River Trough is similar to the Marginal Zone norite identified elsewhere in the Bushveld Complex, it is correlated with the Shelter Norite, which is the top of the Marginal Zone observed at Clapham. The absence of an apparent contact between the floor and the xenolith-bearing norite described by Cameron (1978), as it is at Clapham, together with the occurrence of magnesite residuum west of the area studied by Cameron (1978) suggest that there are unexposed ultramafic units that could be correlatives of the BUS described by Wilson and Chunnett (2010). Thus, the stratigraphic position of the Shelter Norite is similar to the norite unit at the bottom of the stratigraphic succession presented by Cameron (1978).

The Marginal Zone norite in both the Olifants River and Clapham Troughs is capped by a feldspathic pyroxenite with varying modal abundances of plagioclase, clinopyroxene (±

chromite and olivine at Olifants River Trough). The topmost unit in the Olifants River Trough is olivine-rich as opposed to the equivalent unit at Clapham, the "patchy" Transitional Pyroxenite, where the olivine-bearing rocks (magnesite residuum abundant in places) appear to be lenses with limited lateral extent. This difference might have been caused by lateral compositional variations of the same unit. There are also additional differences between the Marginal Zone rocks between the Clapham Trough area and that of the Olifants River Trough (i.e. Cameron, 1978) section. Among others, the Marginal Zone is measured to be thicker at the Clapham trough than in the Olifants River Trough. In addition, the Mafic Norite occurring below the xenolith-bearing Shelter Norite is not discussed in the latter area. This could mean it is not well exposed or even entirely absent. Thick olivine-rich rocks cap the Marginal Zone at the Olifants River Trough. By contrast, the Shelter Norite at Clapham Trough is marked by a feldspathic (i.e. patchy Transitional Pyroxenite) pyroxenite without olivine observed in the CH6 core. This pyroxenite unit represents a significant mineral assemblage and textural changes in the Clapham Trough section, and it is fitting that it is taken as a boundary between the Marginal Zone and Lower Zone. This unit shows well-developed igneous lamination defined by the orientation of orthopyroxene crystals. In both the Olifants River and the Clapham Troughs, the Marginal and the Lower Zones are perfectly conformable and the former (Marginal Zone) is unequivocally described as cumulate rock succession. The occurrence of a BUS correlative at the Olifants River Trough conformably underlying the Marginal Zone norite in the area might need to be re-evaluated.

3.2. Comparisons of the Marginal and Lower Zones between the western and eastern limbs

Comparisons of the sequences relating to the Marginal and the Lower Zone would not be complete without consideration of the western limb. The western and eastern limbs of the Bushveld Complex are believed to be continuous and linked at depth (Cawthorn and Webb, 2001; Webb *et al.*, 2011) and therefore similarities and differences between the two limbs could provide important information about local and regional processes that were operating in the Bushveld magma chamber. The work of Vermaak (1970), SACS (1980), and Teigler and Eales (1996) provide comprehensive information and ideal comparisons. The western limb shows remarkable similarities with the eastern limb, as well as notable differences from the eastern limb based on comparisons with the Clapham Trough succession (Fig. 3.3).

The type sequence presented here for the western Bushveld Complex is a simplified stratigraphy from the South African Committee on Stratigraphy (SACS, 1980). The mapping and the study of the Kashane borehole carried out by Vermaak (1970) showed a norite-rich Marginal Zone, referred to as a "chill zone". Of interest here is the fact that the few boreholes studied in the above mentioned work show conformable relationships with the overlying pyroxenite lithologies, of which some are olivine bearing. In contrast, a more recent study by Teigler and Eales (1996) on the Nooitgedacht (NG) boreholes at Union Section shows no indication that a noritic Marginal Zone was intersected in the area, and the floor is believed to be hornfels instead of quartzite, as is the case for the Clapham Trough. Instead of a noritic Marginal Zone, the Union section appears to have basal olivine-rich lithologies equated to the Marginal Zone (Teigler and Eales, 1996), with a thin (approximately 40 cm) gabbroic/mafic norite unit at the very base. However, it should also be noted that Teigler and Eales have reservations about the hornfels intersected at the base of the NG holes and suggest that it may also be a xenolithic fragment.

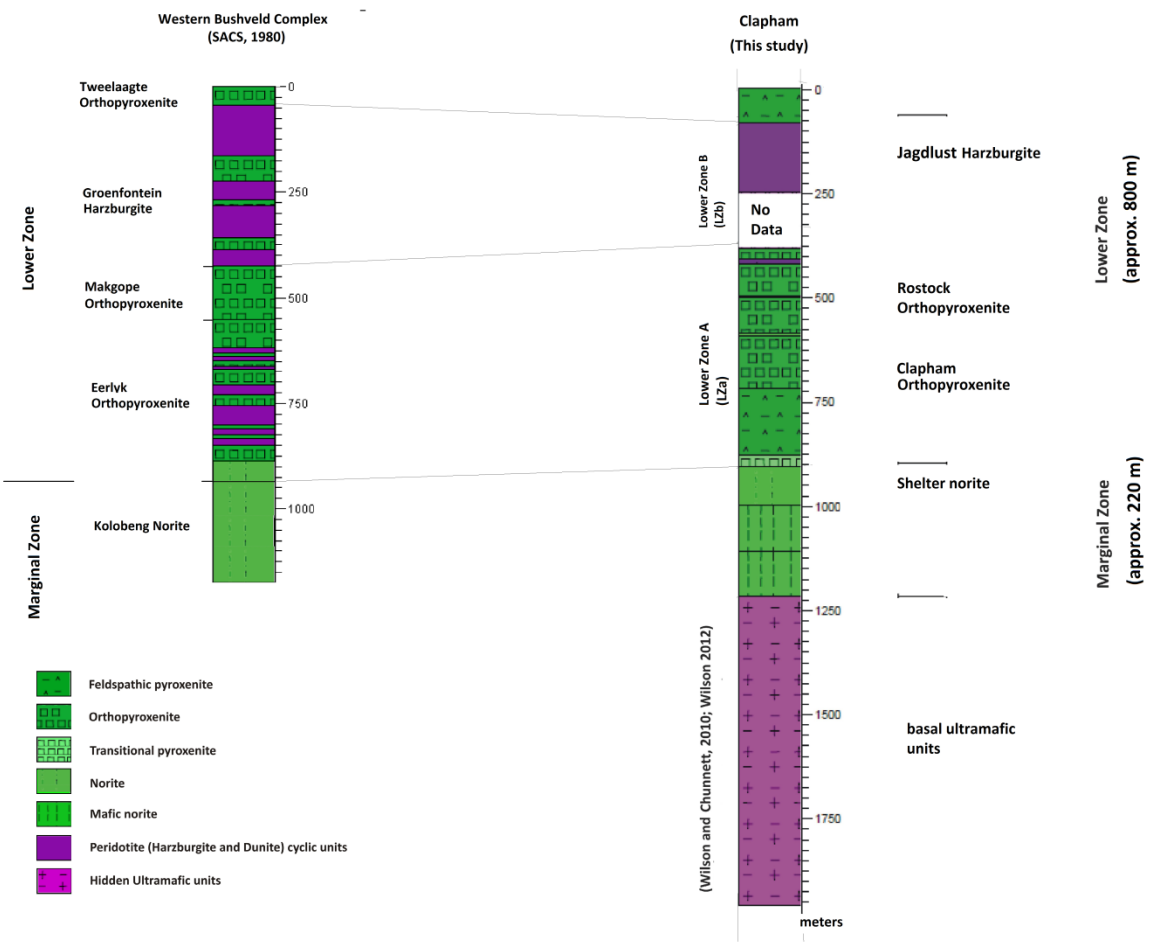

Fig. 3.3: Comparisons of the Clapham Trough litho-stratigraphic succession with the type sequence of the western Bushveld Complex, modified after SACS (1980).

The type sequence of the Lower Zone succession of the western limb shows some similarities to the accepted stratigraphic sequence of the eastern limb, based on Cameron (1978). Ultramafic rocks occur below the Marginal Zone norite in the western limb but it is not clear whether these rocks are sills or pre-Marginal Zone lithologies equivalent to the Basal Ultramafic Sequence of Wilson and Chunnett (2010). The equivalent of the Shelter Norite at Clapham in the western limb is the Kolobeng Norite, which also shows a number (eight) of cyclic units defined by variable grain sizes. The maximum thickness of the Kolobeng Norite unit, the Marginal Zone norite in the western limb, reported by SACS (1980) is about 230 m.

The studies by Vermaak (1970), Cameron (1978), and Teigler and Eales (1996) indicate that the thickness of the Marginal Zone norite is variable. The Marginal Zone norite in the western limb is overlain by feldspathic orthopyroxenite, norite and harzburgite units which are collectively referred to as the Basal Subzone. This Basal Subzone is also known as the Eerlyk Orthopyroxenite (SACS, 1980).

The Eerlyk Orthopyroxenite in the western Bushveld is overlain by almost mono-mineralic rock mass, the Makgope Orthopyroxenite. Both the Eerlyk and Makgope Orthopyroxenites are taken as distant correlatives of the LZa Subzone defined in the present study. The LZa is defined as the combination of the Basal and Lower (Bronzitite) Orthopyroxenite Subzones defined by Cameron (1978). The Lower Zone sequence of the western limb succession (below the Harzburgite Subzone) shows the occurrence of a number of olivine-rich layers. This is different from the eastern limb, which shows only one olivine rich unit capping the Marginal Zone norite at Olifants River Trough. The Clapham Trough section of the LZa (i.e. CH6) is relatively olivine poor compared with possible equivalent units in the western limb. There are no olivine-bearing cumulates in CH6 drill core near the Marginal-Lower Zones boundary and the Shelter Norite is not capped by olivine-bearing rocks, at least in CH6. However, magnesite residuum and weathered olivine-bearing rocks were observed in the field. The Orthopyroxenite Subzone (correlative of the LZa at Clapham Trough) in the western limb is conformably overlain by the Groenfontein Harzburgite, which is the equivalent of the Jagdlust Harzburgite (i.e. the Harzburgite Subzone at the Olifants River Trough, and LZb described in CH1 drill core).

3.3. Summary of the Lithological variations

In Summary, the lower most units of the Clapham Trough area present similarities and some significant differences with other areas in the Bushveld Complex, both in the eastern and western limbs. The key similarities are:

- The Marginal Zone norite forms the lowest exposed rocks of the Bushveld Complex, with no apparent floor contact.
- Some units in the norite are relatively fine-grained compared to the overlying Lower Zone, but coarse-grained rocks also occur within the Shelter Norite.
- The equivalent rocks to the Shelter Norite in the western Bushveld Complex are the Kolobeng Norite, which also shows a number of cyclic units defined by variations in grain size. At least three of these cyclic units were identified at Clapham (chapter 2).
- Lateral variations in the thickness of the Marginal norite are apparent, such that it is not developed everywhere, e.g. Zwartkoppies and Nooitgedacht in the eastern and western Bushveld Complex, respectively.
- There are possible correlatives of the BUS separating the Marginal Zone norite and the floor of the intrusion in the eastern and western limbs.
- More primitive rocks (both ultramafic and mafic) of the Lower Zone conformably overlie the correlatives of the Shelter Norite described in the Clapham trough area, marked by changes in texture and mineral assemblages but with no structural breaks.
- The LZa in the present study is the equivalent of the Basal and Lower Orthopyroxenite Subzones defined by Cameron (1978). Strong igneous lamination is everywhere parallel to gross layering in the Bushveld Complex.

Even though remarkable similarities are present in the Marginal and Lower Zones, there are also important differences. The differences can either be related to the geology of the areas compared to the Clapham and Shelter farms or lack of detailed mapping and drill core data. These differences are:

- The Shelter Norite is definitely not in contact with the quartzite floor, but it lies over a thick ultramafic sequence, which is nowhere exposed on surface.
- The Shelter Norite is less feldspathic at depth and it is characterised by significant amounts of mafic minerals, orthopyroxene in particular.
- Olivine-free Transitional (patchy) Pyroxenite marks the Marginal-Lower Zone boundary at Clapham Trough. On the contrary, olivine cumulates or olivine-bearing rocks cap (or occur in close proximity to) the boundary in other areas, like the Olifants River Trough.

The occurrence of ultramafic units below the Marginal Zone has been previously associated with the intrusion of ultramafic sills whose relationship with the rest of the Bushveld Complex and with each other is not clear, as discussed in chapter 1. Wilson and Chunnett (2010), Wilson (2012) and the present study support the view that the unexposed ultramafic units that occur between the Shelter norite and the Magaliesberg Quartzite in Clapham Trough represent the earliest units of the Bushveld Complex and they have conformable relations with the overlying Marginal Zone rocks. Cameron (1978) suggested the possibility of ultramafic units occurring between the Marginal norite and the floor at Olifants River Trough. These rocks were postulated to be thin sills intruding the Marginal Zone and the floor. Even though Vermaak (1970) suggested the occurrence of ultramafic rocks, it is even more difficult to deduce whether they occur as sills or as earlier cumulates of the Bushveld Complex. Further considerations of these important questions are interesting but they are not part of the present study.

The Shelter Norite and the bottom most parts of the Lower Zone (LZa) are the key issues of focus in the present study. As much as the thickness of the Marginal Zone norite is reported to be variable from place to place, the factors that control these reported variations remain unclear. The suggested compositional and textural variations revealed in the present study thus far are yet to be explained fully. Moreover, the magma compositions of the Marginal Zone and the overlying Lower Zone are still issues to be discussed, as mentioned previously (Chapter 1). Various models have been proposed for the formation of the Marginal norite. Many of these models treat the Marginal Zone as the quenched equivalent of the earliest magma intrusion and go as far as suggesting that the norite is representative of liquid compositions of the magma that crystallised to form the Lower Zone (e.g. Barnes *et al*., 2010). The cumulus nature of the Marginal Zone and the modal variations suggest fractional crystallization played a key role in the formation of the Marginal Zone and is consistent with the conformable ultramafic rocks described by Wilson and Chunnett (2010) and Wilson (2012). The relationship of the Marginal Zone norite and the Lower Zone needs to be re-evaluated.

By contrast, the Lower Zone is relatively more studied than the Marginal Zone, and is therefore understood better than the latter. Earlier studies of the Lower Zone (and in fact the Marginal Zone), however, base their interpretations of the petrogenesis, geochemical evolution and to some extent the isotopic trends on the so-called B-1 parental magma, whose composition is largely arguable. The importance of re-evaluating the Lower Zone evolution is immediately apparent since the parental magma(s) on which its interpretation is based on is primarily questionable.

Chapter 4

Petrology and Textures in the Marginal Zone Norite and Part of the Lower Zone at Clapham Trough

The mineral assemblages of the Marginal Zone norite and the Lower Zone A (as discussed in the preceding chapters) are the same, but the modal proportions, crystal sizes and the textures in these zones differ considerably. The modal abundances and textural variations to this point have been based on descriptions of field samples and the Clapham Trough drill core samples described in the preceding chapters. In the present chapter petrographic features of the CH6 drill core, which straddles the Marginal-Lower Zone boundary, will be described. The objective here is to outline the key petrographic features of both the Marginal and Lower Zones. Thus, the description of petrographic features of the rocks from the Clapham Trough and comparisons with the rest of the Bushveld Complex (and other layered mafic intrusions, LMIs) is necessary to understand the processes that operated during the formation of the Marginal-Lower Zone succession in the Clapham Trough area.

The petrography of the Lower and Marginal Zones has been published in many previous works, e.g. Willemse (1959), Cameron (1978), and briefly in Hulbert and Sharpe (1985). The present work outlines the petrographic features as observed in the Clapham Trough drill cores and then draws comparisons with the earlier studies. The samples that were analyses in greater detail with transmitted optical microscopy were also taken for the electron microprobe analyses. The run conditions and preparation is described in the methodology section in Appendix B.

4.1. Nomenclature

The dominant silicate minerals in the rocks considered in this study are orthopyroxene, plagioclase, clinopyroxene and olivine (typically restricted only in specific layers) in decreasing order of abundance. The main difference between the Marginal and Lower Zones in terms of petrography is the modal abundances of the cumulus phases, such that the Marginal Zone is plagioclase-rich whereas the Lower Zone is orthopyroxene-rich. The modal abundance estimates of these minerals in the rocks, however, are not accurate even for the almost mono-mineralic layers, because the polished thin sections only represent a small 2D section of the cumulate rocks, and the preparation processes of the thin sections may remove some of the minerals. More accurate and internally consistent modal abundance estimates are based on CIPW norms calculated from the chemical analyses (Appendix C).

For the purposes of the present work, rocks that contain only interstitial plagioclase are termed orthopyroxenite ranging to feldspathic orthopyroxenite, with the amount of feldspar ranging between 0-20 volume percent (consistent with the definitions in Chapter 2). This translates to about 0-5 wt. % Al_2O_3 content in the chemical analyses of the whole rocks. The other common rock types are mafic norite and norite (*sensu stricto*), which contain 20-40 %, and 40-65 volume % plagioclase (translating to 5 - 11 and 11 - 18 wt. % Al_2O_3 in the whole rock analysis), respectively. Leuconorites and anorthosite are not common in the CH6 drill core and were not identified in the field, but they contain between 65-85 % and 85-100 volume % plagioclase feldspar, respectively. In all of these rock types the remainder of the rock composition is made up of cumulus orthopyroxene, with or without the inclusion of post-cumulus mineral phases.

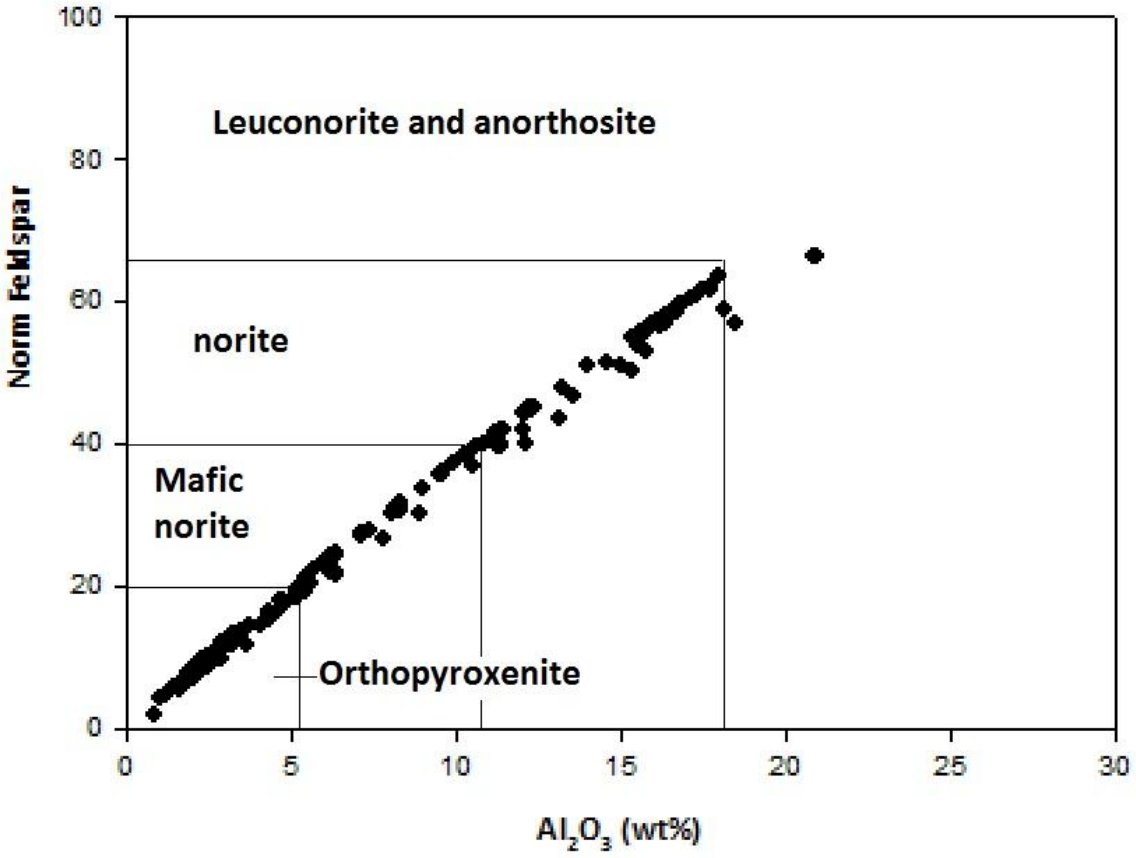

Fig. 4.1: Nomenclature for plagioclase-orthopyroxene dominant rocks in the CH6 borehole based on whole rocks Al_2O_3 and normative feldspar (i.e. plagioclase in this case).

Fig. 4.1 shows a continuum between orthopyroxenite and norite based on the normative plagioclase content of the CH6 drill core, and as related to the whole rock Al_2O_3 content it allows distinction between the different rock types. The distinction between the Marginal and Lower Zones is also mainly based on the mode of occurrence of plagioclase as mentioned previously. Typically, the Lower Zone plagioclase is largely post-cumulus and it is only cumulus in the interlayered norite horizons described in Chapter 2. Describing the petrographic features of the CH6 succession, and the changes in textures thereof does not only have lithological implications, but it suggests that there were also changes in the magma chamber processes. These changes can be either chemical (relating to parental magma compositions) or physical changes, or even both.

4.2. Orthopyroxenite

The Lower Zone A (LZa, correlative of the Orthopyroxenite Subzone of Cameron, (1978)) Subzone described in the CH6 drill core predominantly consists of orthopyroxenite, with norite and olivine-rich horizons. Orthopyroxene accounts for about 80-90 volume % of the 450 m thick LZa recorded in the CH6 borehole. The top 254 m contains less than 10 volume % interstitial plagioclase and is classified as the Rostock Orthopyroxenite succession. Clinopyroxene occurs as an interstitial phase, which poikilitically encloses orthopyroxene crystals. This post-cumulus monoclinic pyroxene typically accounts for less than 5 volume % of the mode in the Rostock Orthopyroxenite. In addition, there are re-equilibration textural relationships, similar to decomposition rims, between the clinopyroxene and orthopyroxene observed at crystal boundaries (Fig 4.2 b, c).

Generally, the entire orthopyroxenite subzone consists of subhedral orthopyroxene crystals averaging 2-3 mm in size. Elongate orthopyroxene crystals show the presence of igneous lamination, defined by the long axes, parallel to the gross layering of the intrusion. Moreover, the orthopyroxene crystals show numerous thin exsolution lamellae. The orthopyroxene crystals near interlayered norite horizons exhibit thicker lamellae, similar to those expected in the inverted pigeonite (Fig. 4.2 c). Annealing and triple junction boundaries in some places are observed, especially near contact zones, where the crystal size changes from less than 1 mm to the typical 1-3 mm size. Igneous lamination is not preserved in such case by the orthopyroxene crystal orientation (Fig 4.2 a).

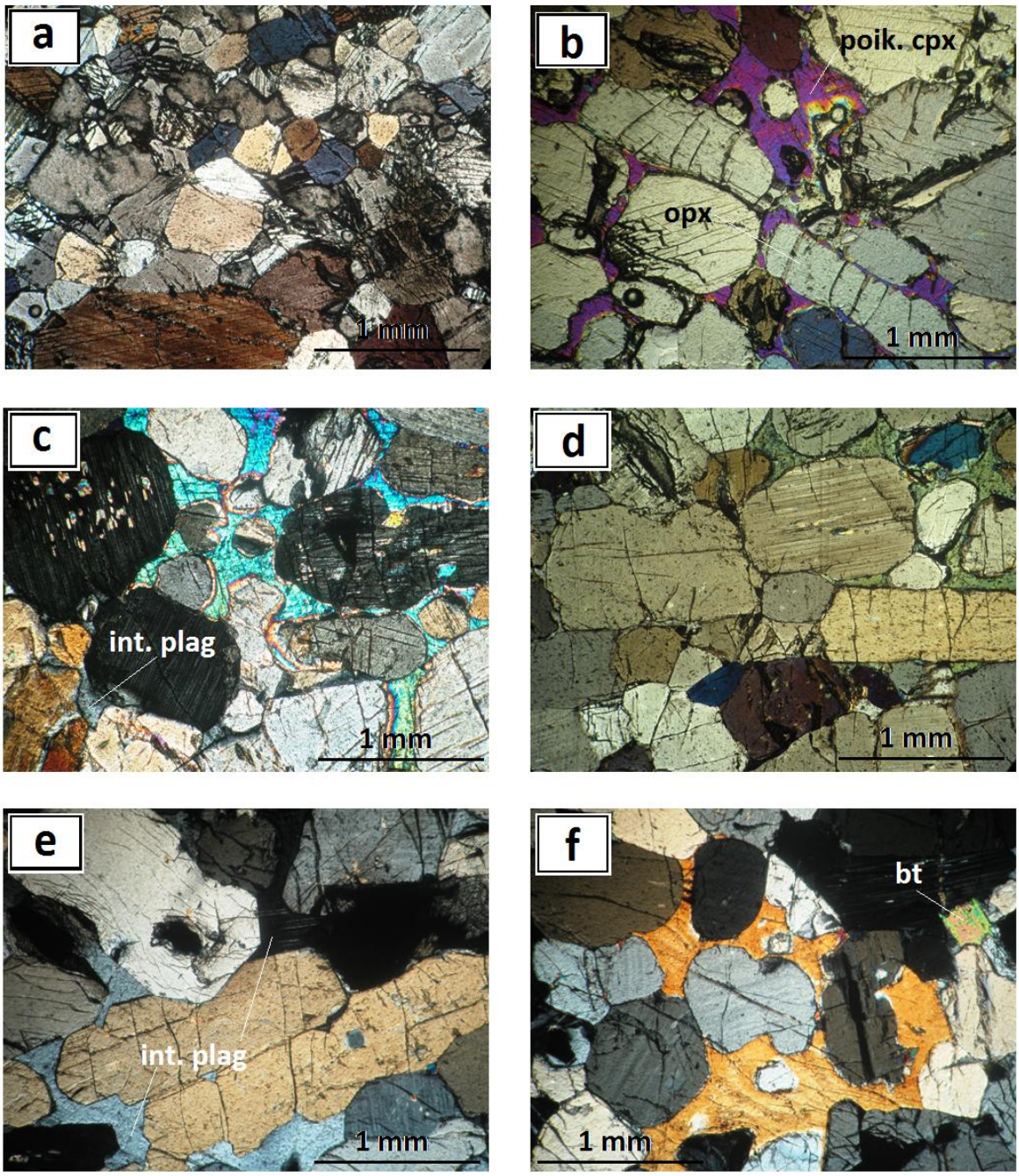

Fig 4.2: Photomicrographs of selected samples from the LZa orthopyroxenite showing the common textures seen in the CH6 drill core. Grain size (a. CH6/7, depth 55.05 m) and modal layering are the common types of layering. Igneous lamination is commonly expressed by the orientation of orthopyroxene grains (b, CH6/22, 103.71 m; d, CH6/56, 218.54 m; and e, CH6/62, 235.70 m). Pictures b) and e) show the 'true' layer orientation and in d) the trace of the layering surface is rotated to a sub-horizontal position. Re-equilibration between opx and interstitial cpx is seen in c. (CH6/36, 153.52 m).

Below 268 m depth in the CH6 drill core, the amount of post-cumulus plagioclase increases, varying between 10-20 %. This part of the LZa succession is defined as the Clapham Orthopyroxenite succession (Fig. 3.2). The textures described for the Rostock Orthopyroxenite succession above are prevalent throughout the Lower Zone A Subzone. That is, the relatively feldspathic Clapham Orthopyroxenite is not texturally different from the Rostock Orthopyroxenite. The crystal sizes, igneous lamination and in places the annealed (120° triple-junction) boundaries are also observed in the (relatively feldspathic) Clapham Orthopyroxenite succession.

Biotite occurs as an accessory mineral throughout the LZa; and the amount of clinopyroxene generally remains constant throughout the entire subzone. Throughout the LZa, clinopyroxene displays poikilitic relationships (and in some instances re-equilibration textures) with orthopyroxene at grain boundaries, as mentioned above. The Lower Zone A orthopyroxenite succession hosts two norite horizons, at 157-181 and 298-302 m depth (see Chapter 2), in which layering is predominantly expressed by variations of the modal abundances of orthopyroxene and plagioclase on a centimetre scale.

4.3. Transitional Pyroxenite

The boundary between the Marginal Zone and Lower Zones at Clapham is a patchy feldspathic pyroxenite (referred to as the Transitional Pyroxenite in preceding chapters). The petrographic data shows that this unit occurs in the CH6 drill core between 454-471 m (suggesting that it is about 15 m thick), but the thickness in the field is quite variable as mentioned in Chapter 2. The petrographic features of this unit are of great importance since it is the boundary zone between the Shelter norite and the Lower Zone.

The dominant mineral assemblage in this transitional boundary zone is orthopyroxene (varying between 40-84 volume %) and plagioclase, which occurs as both a cumulus mineral (within the feldspathic patches, up to 50 volume %) and as a post-cumulus phase. Poikilitic clinopyroxene (typically about 5-10 vol. %) and accessory biotite are the other important minerals. In the field, the clinopyroxene oikocrysts are 5-10 mm in general but can be as large as 20 mm.

Fig. 4.3: Photomicrograph of typical patchy Transitional pyroxenite (sample CH6/119, 454.69 m) showing the shattered, clinopyroxene lamellae with anhedral-subhedral orthopyroxene and plagioclase. Sub-horizontal igneous lamination observed.

In thin section, the poikilitic clinopyroxene appears to be re-equilibrated with the orthopyroxene crystals, which contain thick shattered clinopyroxene exsolution lamellae. Subhedral orthopyroxene crystals define the igneous lamination within the patchy pyroxenite, similar to the LZa pyroxenite units. The feldspathic patches appear to be nuclei for further crystallization and in places act as matrix of the mafic minerals. Closer to the Shelter norite,

the feldspathic patches display many similarities to the norite in thin section but there is poor igneous lamination observed in the plagioclase and the orthopyroxene crystals are generally subhedral-anhedral in shape. The common texture throughout the Transitional Pyroxenite suggests mixing and re-equilibration of seemingly unrelated (non-cotectic) mineral phases. Closer to the Marginal Zone, plagioclase is dominant but closer to the LZa succession, orthopyroxene is dominant with plagioclase inclusions in places.

4.4. Norite

There are three norite sequences of interest in the CH6 drill core, first is the Marginal Zone norite which consists of a bottom Mafic Norite and the upper Shelter Norite. These norite sequences account for at least 229 m thick Marginal Zone rocks at the Clapham Trough. The plagioclase content varies between 20 to 40 % in the Mafic Norite and 40 to 62 volume % in the Shelter Norite. Fig. 4.1 shows the spread in the modal abundance of plagioclase for the Mafic and Shelter Norite sequences. Other than the Marginal Zone norite, the CH6 drill core shows that there are two norite marker horizons in the LZa Subzone, as mentioned above. Even though the modal abundances and grain sizes of the Lower and Marginal Zone norite sequences are comparable, they show different petrographic features in some respect.

4.4.1. Marginal Zone Norite

Igneous lamination in the Marginal Zone is defined by modal variations over preferred orientation of orthopyroxene crystals and subtle variations of interstitial plagioclase as in LZa. Moreover, in the Marginal Zone orthopyroxene crystals are typically subhedral-anhedral and with poikilitic texture enclosing plagioclase crystals. Exsolution lamellae of

clinopyroxene (in the case of inverted pigeonite) are abundant in the orthopyroxene. The modal abundances of plagioclase and orthopyroxene vary even on a centimetre scale to form the subtle layering in the Shelter Norite described in preceding chapters. Unlike the overlying Lower Zone, optically continuous (i.e. poikilitic) clinopyroxene grains do not only enclose the relatively large orthopyroxene crystals, but both pyroxenes engulf smaller plagioclase and other (smaller) pyroxene crystals, which are typically sub-millimetre in scale (Fig. 4.3c). The extremely fine crystals seen in Fig. 4.3 are part of the resistant fine noritic layers mentioned in preceding chapters, which are persistently continuous over considerable distances within the Marginal Zone norite.

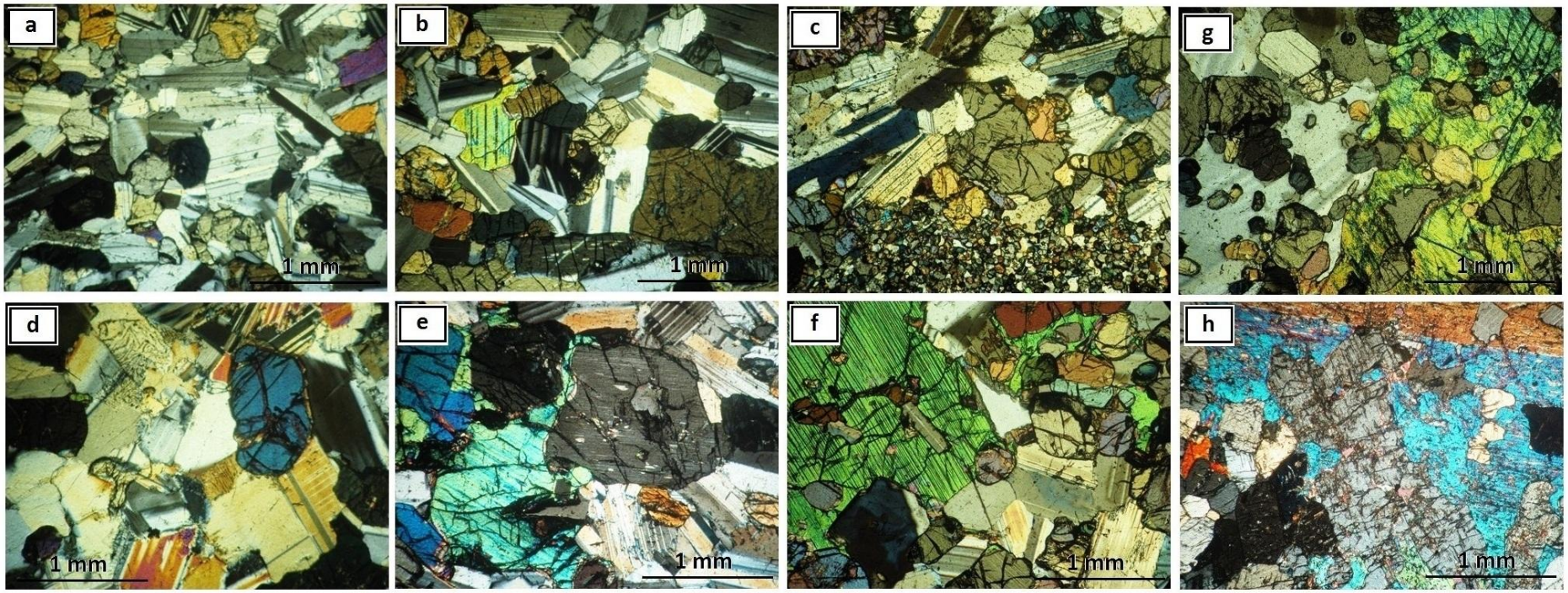

Fig 4.4: Photomicrographs of Marginal Zone norite textures. Diagrams a-d (a. CH6/122, depth 462.59 m (Transitional Pyroxenite feldspathic patch); b. CH6/126, 477.34 m; c. CH6/131, 492. 53 m; d. CH6/150, 555.34 m) show Shelter Norite textures. Diagrams e-h (e. CH6/155, depth 573.51 m; f. CH6/161, 595.01 m; g. CH6/176, 649.10 m; h. CH6/180, 672.39 m) show mafic norite units. Throughout the Marginal Zone norite, there are occurrences of extremely fine-grained norite layers (c) and inclusions (f-g, poikilitically enclosed).

The top unit of the Marginal Zone norite, the Shelter Norite in preceding chapters, is a norite (sensu stricto) containing 40-65 plagioclase and 22-30 volume % orthopyroxene. Clinopyroxene accounts for about 10-15 volume % of the Shelter Norite. Plagioclase occurs as tabular, subhedral-euhedral crystals, whereas both pyroxenes typically occur as anhedral mineral clusters, which show re-equilibrated (similar to decomposition rims) grain boundaries. The crystal sizes observed in the Shelter Norite (orthopyroxene crystals at least) is variable, from well below 1 mm to a maximum of 2 mm. In addition to the tabular habit of plagioclase, there are occurrences of worm-like intergrowths (symplectite) of feldspar and quartz (Fig. 4.4d). The CIPW norm suggests that quartz in the Shelter Norite accounts for about 1-2 volume %. This symplectite appears to be 'consuming' the subhedral plagioclase grains. There are also pyroxene grain boundary 'replacement' re-equilibration textures (Fig. 4.3 e-h) similar to those identified in the poikilitic clinopyroxene grains in the Lower Zone A Subzone (see Fig. 4.2).

The amount of plagioclase decreases with depth in the Marginal Zone such that below 560 m the Shelter norite is replaced by the less feldspathic variety of the Marginal zone norite, the Mafic Norite as it is referred to in the previous chapters. The key difference between the upper (Shelter) Norite and the bottom Mafic Norite in CH6 drill core is the modal abundances of plagioclase and clinopyroxene. The amount of plagioclase and orthopyroxene in the mafic norite vary between 20-40 and 42-66 volume %, respectively. In the same interval the amount of clinopyroxene decreases from greater than 10 % in the Shelter Norite to about 5-7 volume % in the Mafic Norite. Clinopyroxene occurs as (relatively) large optically continuous grains that typically enclose tabular, subhedral plagioclase grains and anhedral orthopyroxene crystals. Moreover, there are numerous decomposition rims (re-equilibration textures at grain boundaries) observed between the pyroxenes of the Mafic Norite. These rims seem to be more penetrative than in the Lower Zone and Shelter norite. In addition, larger plagioclase and pyroxene crystals engulf smaller anhedral crystals of quartz (and possibly feldspar). The small mineral inclusion crystals

are similar in form to those making up the fine-grained layers and inclusion identified in the upper units of the Shelter norite (Fig 4.3h). Exsolution between the two pyroxenes is also prevalent showing extensive lamellae of one pyroxene in the other (Fig. 4.3h).

4.4.2. Lower Zone A Norite

The modal abundances of plagioclase and orthopyroxene in the LZa Subzone norite units are comparable to those seen in the Shelter Norite succession of the Marginal Zone. Two interlayered norite horizons are present in the LZa, at 160-180 and 297-304 m. In both units, the plagioclase varies from 20-65 volume % and the orthopyroxene typically accounts for 40-65 volume %. The amount of the cumulus plagioclase increases towards the centre of the interlayered norite units. Clinopyroxene occurs as an interstitial phase and shows re-equilibration rims where it is in contact with the orthopyroxene crystals. Clinopyroxene accounts for 10-15 volume % of the rock composition in the upper (occurring between 160-180 m in CH6, within the Rostock Orthopyroxenite) interlayered norite, and about 5 volume % in the lower norite unit separating the Clapham and Rostock Orthopyroxenite sequences.

The modal variation in these norite units defines the thin, centimetre scale igneous lamination observed in the CH6 drill core. Plagioclase is subhedral, with the long axes aligned sub-parallel to the general layering observed in the CH6 drill core. Generally, both norite units are relatively fine-grained, with orthopyroxene crystals about 1-2 mm in size. Unlike the Marginal Zone norite, the LZa norite units are not quartz bearing and do not show the occurrence of symplectite. The equigranular plagioclase and pyroxene crystals exhibit annealing textures as supported by the 120° triple-junction boundaries observed.

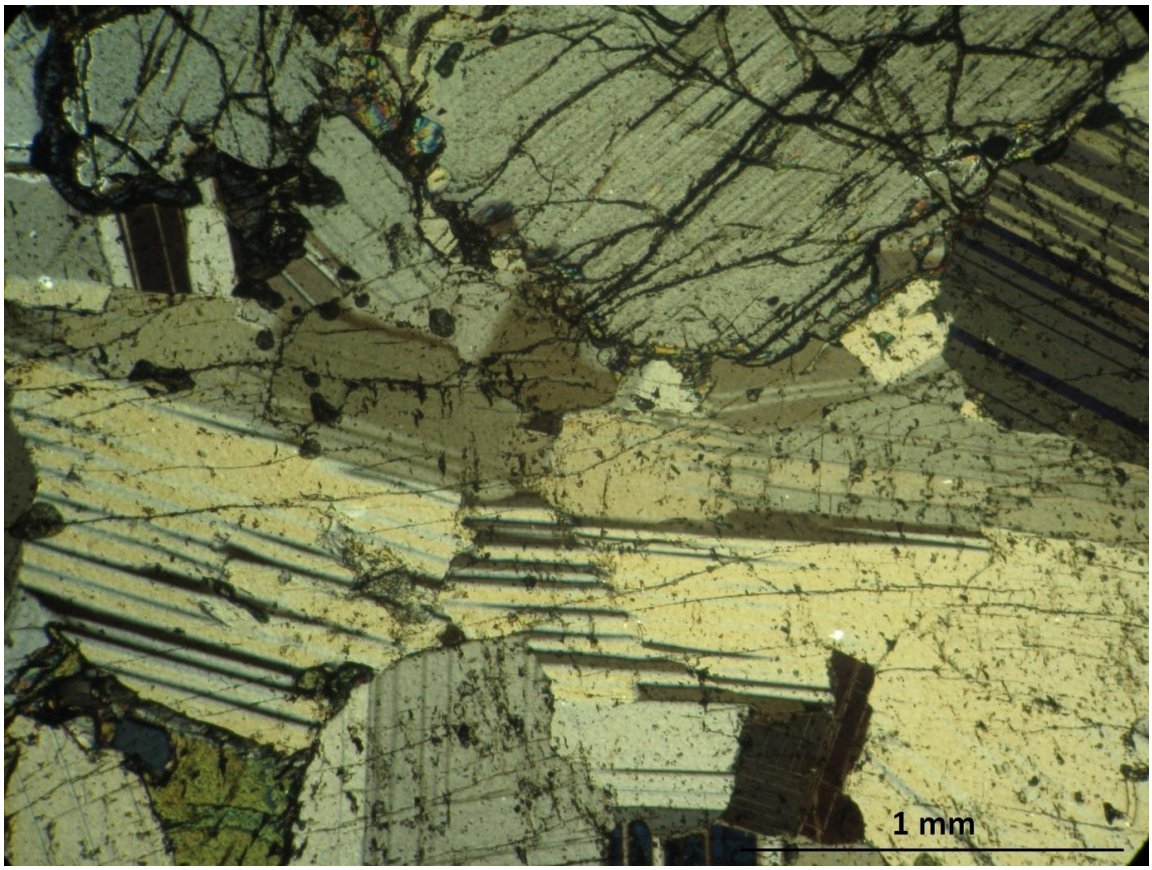

Fig. 4.5: Photomicrograph showing typical LZa norite features. Orthopyroxene and plagioclase show igneous lamination defined by both modal variations and the long axes of the plagioclase, sample CH6/45 (depth 179.52m).

4.5. Summary

The processes by which layering and mineral accumulation occur are arguably some of the contentious topics regarding the formation of layered mafic intrusions (LMIs) as mentioned in chapter 1. In the Lower Zone A (LZa), 2-3 mm orthopyroxene with preferred sub-horizontal are the predominant cumulus phase, except in the interlayered units where plagioclase is the predominant. This orthopyroxene-rich subzone has variable amount of interstitial (post-cumulus) silicate minerals, but the primary post-cumulus phase is plagioclase. The amount of the interstitial phases in the LZa is estimated to vary from 10-30 % suggesting there was insufficient removal of trapped

liquid, thus making the studied section (at least) orthocumulate succession. By contrast, only quartz and clinopyroxene are post-cumulus phases in the entire Marginal Zone succession, and they typically account for less than 7-10 volume % of the rocks, combined. This suggests that the Marginal Zone rocks are meso-adcumulates. However, since there is evidence above for post-magmatic textural re-equilibration, like the annealing and development of symplectite (in the Shelter Norite), the use of terms like orthocumulate and adcumulate must be treated with caution.

This aspect will be re-visited and will be advanced by the geochemistry in later chapters, but here it will suffice to emphasises that the textures discussed and the petrography indicate that there was mechanical alignment of cumulus minerals to form igneous lamination, modal and grain-size layering, especially in the Marginal Zone. This chapter further supports the aims and objectives of re-evaluating the CH6 section with and the Marginal Zone rocks to propose alternative processes since the field relations and the descriptions of the rocks and petrography cast unequivocal doubt on the interpretation that these rocks represent a chill phase to the Bushveld Complex.

Chapter 5

Whole Rock and Mineral Geochemistry

185 Samples from the drill core CH6 were analysed for major and trace elements by X-ray fluorescence (XRF) and Inductively Coupled Plasma Mass Spectrometry (ICP-MS), as described in the Methodology section in Appendix B. All the geochemical data and the sample lists, depths and lithologies are presented in Appendix C. Mineral separates were also analysed using the above equipment and electron microprobe analyses were carried out with a CAMECA SX 100 at the University of Johannesburg.

5.1. Whole-rock Geochemistry

The whole-rock major element (as oxides) compositional variations are associated with the modal abundances of the mineral assemblages that constitute the rock. By contrast, some trace elements are influenced by small amounts of rare phases that formed from trapped melt and their compatibility with respect to the major cumulus mineral phases that constitute the bulk rock. The measured whole rock major and trace elements are tabulated in Appendix C. The samples were analysed for the following major element oxides SiO_2, $Al_2O_{3,}$ TiO_2, FeO, MnO, MgO, CaO, Na_2O, K_2O, and P_2O_5. The list of trace elements of interest includes Cr, Ni, Co, Cu, Rb, Sr, Ba, REE, and Zr.

5.1.1. Major Elements

A common way of presenting whole-rocks major element variations is by way of Harker-type diagrams using MgO as the proxy for differentiation (Fig. 5.1). The whole-rock data shows that there is a positive correlation between MgO and SiO_2 (except in olivine-rich lithologies, which form a different trend to the one seen in norites and pyroxenites), FeO, and to some extent MnO. For these oxides, the Shelter Norite contains lower concentrations than both the Mafic Norite and the orthopyroxenite-dominant Lower Zone succession. In fact, all the major elements that are controlled by orthopyroxene are low in the Shelter Norite compared to the major elements that are controlled by plagioclase. Fig. 5.2 shows the major elements concentration variations for the CH6 section. MgO, FeO, SiO_2 and MnO decrease with stratigraphic height in the Marginal Zone succession.

SiO_2 and MgO in the Shelter norite averaged at 52.84 ± 0.45 and 11.98 ± 2.16 wt. %, respectively. On the other hand, the Mafic Norite yielded 54.42 ± 0.55 and 19.23 ± 2.58 wt. % for SiO_2 and MgO, respectively. Similarly, the LZa orthopyroxenite yielded slightly higher SiO_2 and higher MgO abundances of 54.76 ± 2.10 and 29.76 ± 2.68 wt. %, respectively. The LZa norite yielded 52.29 ± 1.65 and 20.10 ± 6.28 wt. % for SiO_2 and MgO, respectively (Table 5.1). There are negative correlations between MgO and Al_2O_3, CaO and Na_2O in both the Marginal and Lower Zones. Unlike in the Marginal Zone succession, TiO_2 and MgO show negative correlation in the Lower Zone succession, excluding the norite-dominant units. There is no defined relationship between K_2O and MgO in either the Marginal or Lower Zone rocks. The notable difference in the K_2O concentration is that the Marginal Zone rocks generally contain higher abundances of K_2O than Lower Zone cumulates.

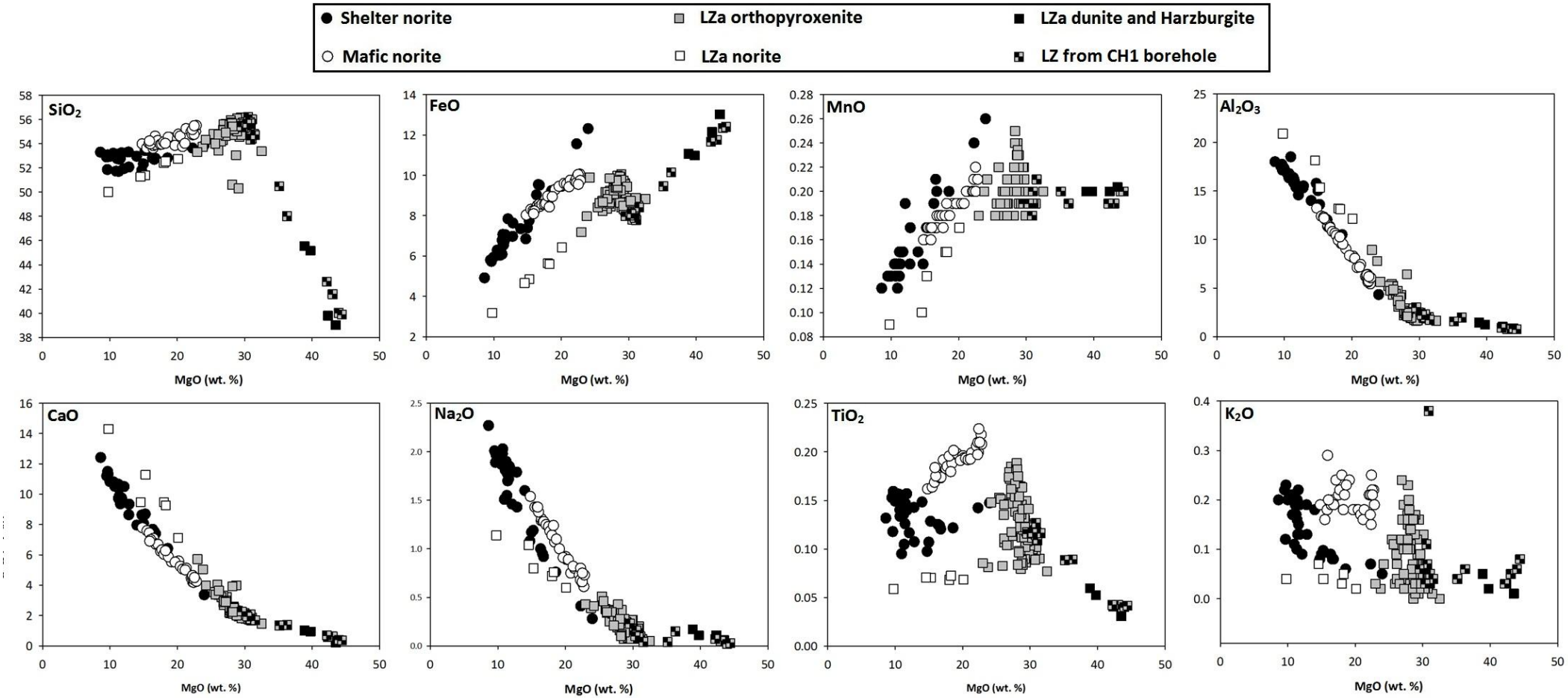

Fig 5.1: Harker-type diagrams of the major elements of the CH6 borehole whole-rock samples plotted against MgO.

Whole-rock Mg# (defined as the molecular ratio 100×(MgO/(MgO+FeO)) in the LZa vary between 86-83. In contrast, in the Marginal Zone the whole-rock Mg# vary between 81-74 with increasing stratigraphic height in the CH6 drill core (Fig. 5.2). Unlike the whole-rock Mg#, the whole rock An# in the Marginal Zone (An# defined as molecular 100×(CaO/(CaO+2*Na_2O]) increases from 74 at the bottom of the Mafic Norite to 81 near the Lower-Marginal Zone boundary. Near constant, though highly variable whole rock An# (82-88) is characteristic of the Lower Zone A. For all elements and Mg#, there is a significant change in the concentrations recorded along the Lower Zone-Marginal Zone boundary (i.e. as noted in the previous chapters, and referred to as the Transitional Pyroxenite) coinciding with changes described in the mineral assemblages across this narrow zone (Fig 5.2).

The Marginal Zone contains MgO concentrations that are less than 20 wt. % and about 9-15 wt. % for Al_2O_3. By contrast, the Lower Zone contains approximately 29 wt. % MgO and ≤ 3 wt. % Al_2O_3. The LZa interlayered norite units are slightly lower in MgO and FeO, and higher in Al_2O_3 and Na_2O than the orthopyroxenite units, following the different mineral assemblages in the respective units. The average MgO concentration in the former (norite units) is approximately 20 wt. % and the average Al_2O_3 concentration is about 11 wt. % (Table 5.1). However, the LZa norite horizons are more magnesium-rich and less sodic than the Marginal Zone norite succession. Similarly, the other major elements show that the Marginal Zone is relatively evolved compared to the Lower Zone A sequence (Fig.5.2). Across the Transitional Pyroxenite, there is evidence of a major geochemical change. The Mg# rapidly increases across the 8-15 m Transitional Pyroxenite from about 74 in the Shelter Norite to reach a maximum of 86 (Fig. 5.2; Table 5.1).

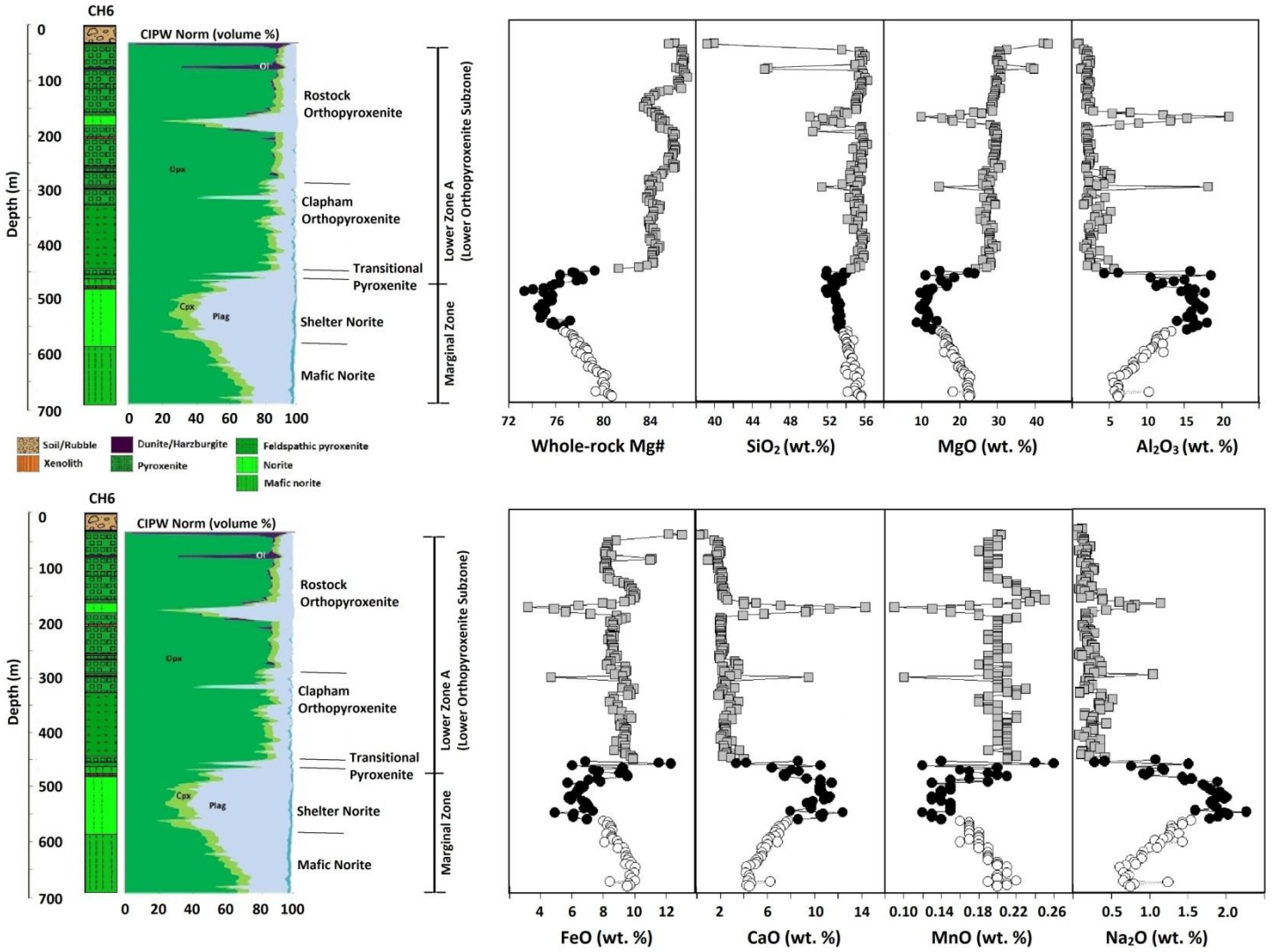

Fig. 5.2: Major element variations with height in the CH6 section. The Marginal Zone shows relatively evolved compositions compared to the Lower Zone A.

Table 5.1: Averages and standard deviations of major element compositions of the common lithologies occurring in the Lower and Marginal Zones of the CH6 borehole.

Lithology	n	Statistics	SiO_2	Al_2O_3	CaO	FeO	MgO	TiO_2	Na_2O	K_2O	Cr_2O_3	NiO	Mg#	An#
LZa orthopyroxenite	52	Mean	54.76	2.53	2.21	8.69	29.76	0.11	0.18	0.05	0.45	0.09	85.91	86.96
		STD Dev.	2.10	1.83	1.15	0.82	2.68	0.02	0.10	0.04	0.07	0.03		
LZa feldspathic orthopyroxenite	36	Mean	55.22	2.84	2.71	9.28	27.60	0.14	0.26	0.09	0.39	0.09	84.38	86.10
		STD Dev.	0.45	0.93	0.44	0.38	0.99	0.02	0.11	0.06	0.04	0.01		
LZa norite	8	Mean	52.29	11.54	7.93	6.39	20.10	0.08	0.61	0.04	0.24	0.07	84.87	87.69
		STD Dev.	1.65	5.69	3.94	2.05	6.28	0.03	0.31	0.03	0.17	0.05		
Transitional Pyroxenite	6	Mean	53.03	10.16	6.19	9.32	19.13	0.13	0.74	0.07	0.24	0.07	78.39	83.26
		STD Dev.	1.10	5.86	2.88	2.50	5.40	0.02	0.48	0.02	0.12	0.02		
Shelter norite	29	Mean	52.84	15.59	9.91	6.89	11.98	0.14	1.69	0.16	0.10	0.03	75.53	76.59
		STD Dev.	0.45	1.72	1.29	1.08	2.16	0.02	0.35	0.05	0.04	0.01		
Mafic norite	33	Mean	54.42	8.99	5.57	9.10	19.23	0.19	1.03	0.20	0.22	0.05	78.90	75.93
		STD Dev.	0.55	2.41	1.10	0.64	2.58	0.02	0.28	0.03	0.04	0.01		

5.1.2. Trace Elements

Trace element variations also show significant geochemical differences between the Marginal Zone and Lower Zone successions in the CH6 section (Fig. 5.3). Orthopyroxene and plagioclase are the most abundant mineral phases in the Marginal and Lower Zones of the CH6 drill core (See chapters 2-4). The Marginal Zone is slightly enriched in large ion lithophile elements and high field strength elements (i.e. LILE and HFSE, incompatible elements) relative to the Lower Zone A succession. In addition, trace elements that are compatible with respect to plagioclase are abundant in the rocks that are feldspar rich (i.e. lower MgO content in Figs. 5.2 and 5.4). Even though the whole-rock Mg# suggest that the Mafic Norite is relatively primitive than the Shelter Norite, the trace elements (Figs. 5.3 and 5.4) show that the former is relatively enriched in incompatible trace elements (LILE and HFSE) with the exception to Sr because of its compatibility in plagioclase.

By contrast, the Lower Zone succession is relatively enriched in compatible trace elements (with respect to orthopyroxene in particular). The LILE and HFSE (Ba, K, Zr and Ti in particular) in the Lower Zone show widely varied concentrations such that a cyclic compositional variation is observed. These variations in the trace elements are observed in the Clapham Orthopyroxenite succession. By comparison, the Rostock Orthopyroxenite succession shows little compositional variation, with nearly constant concentrations for tens of metres, with the exception to the interlayered norite unit (Figs. 5.3, 5.4). The CH1 samples that are included in Fig. 5.4 are stratigraphically continuous with the CH6 units above the Harzburgite unit at 76-78 m, and they (CH1 samples) are part of the transition from the LZa to LZb of the Lower Zone succession at Clapham Trough.

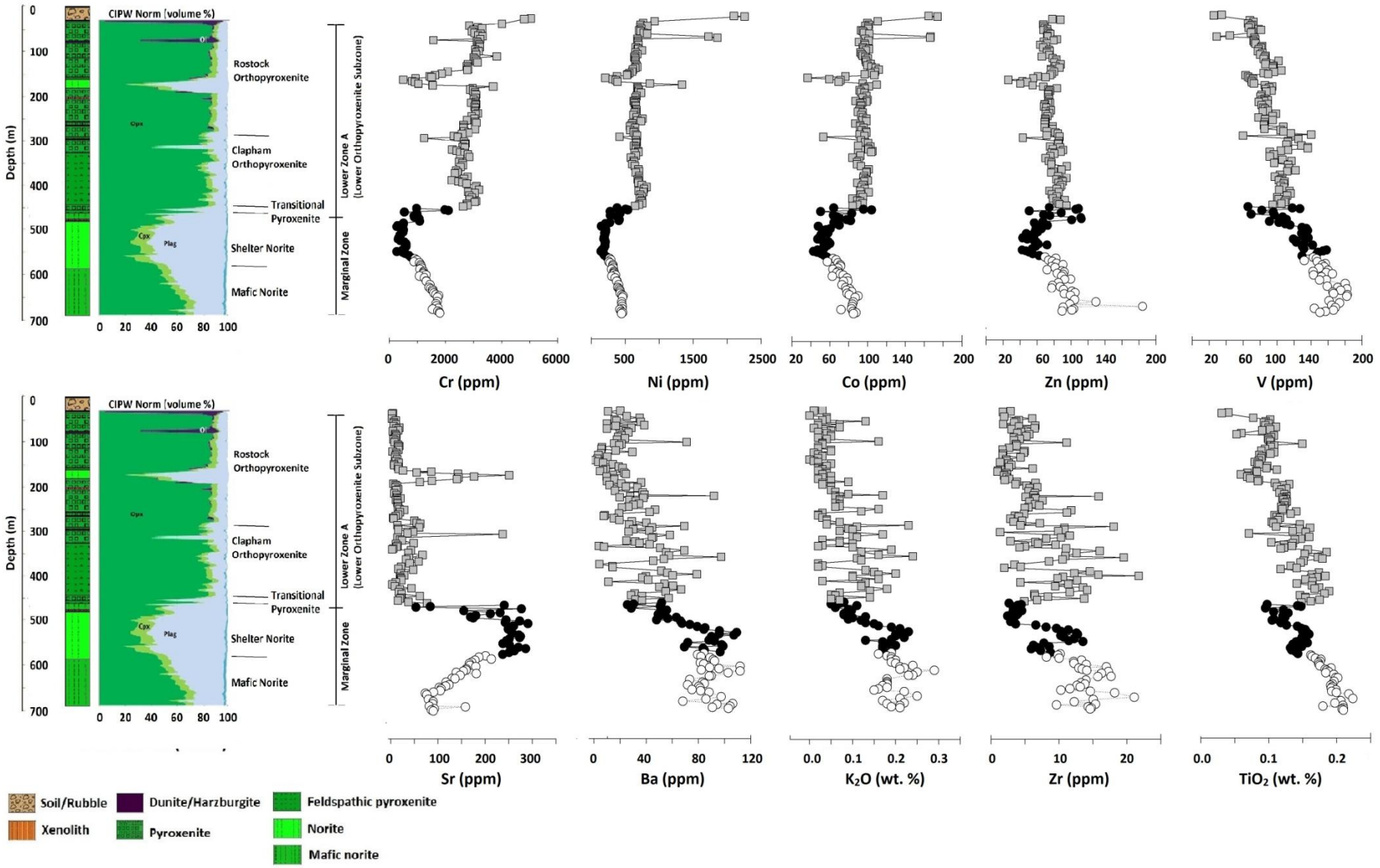

Fig. 5.3: Trace element (including K_2O and TiO_2) variations with depth in the CH6 drill core.

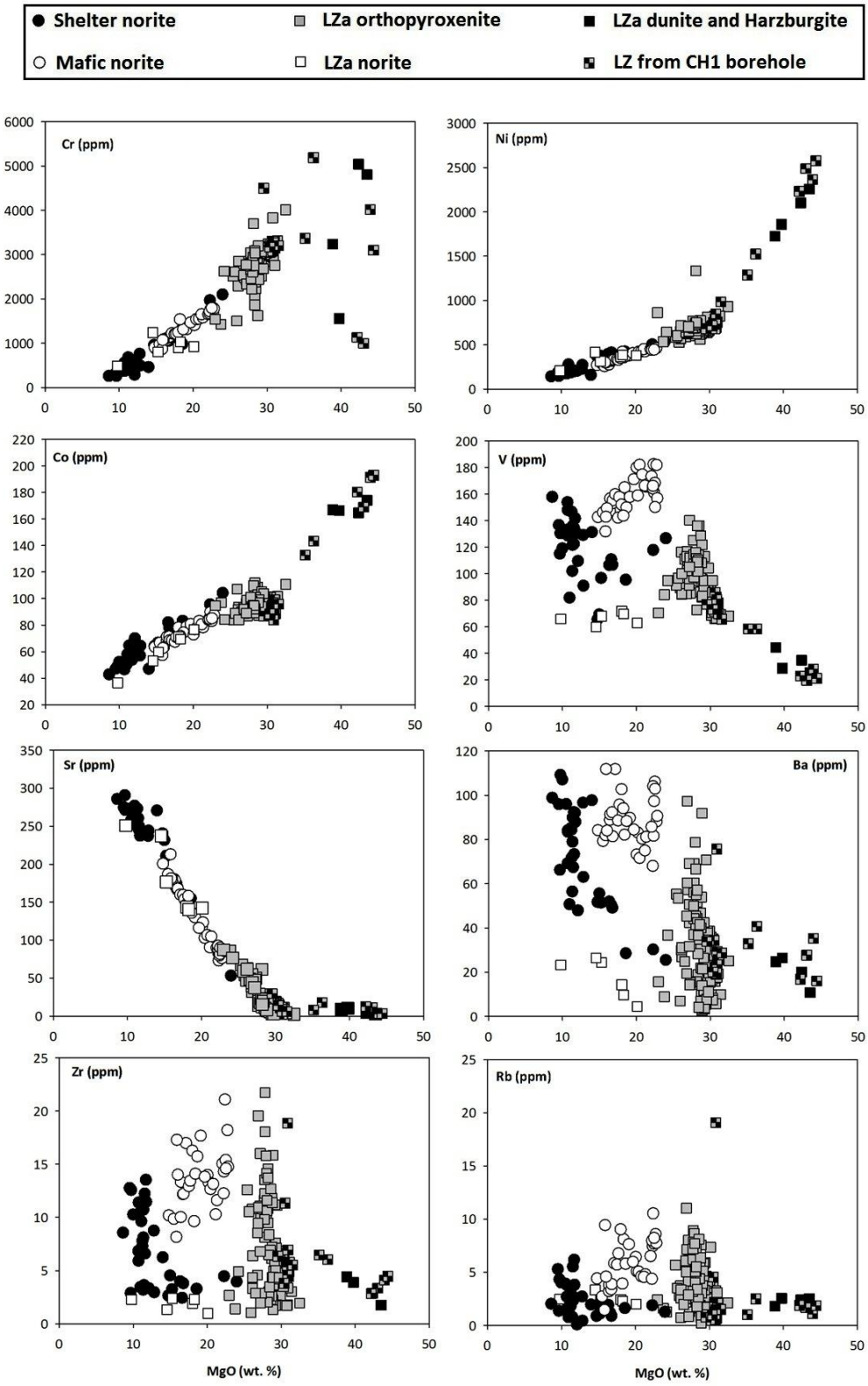

Fig. 5.4: Whole-rock variation diagrams of trace elements plotted against wt.% MgO for CH6 and a comparative selection of samples from the base of the CH1 borehole as a continuum from the top of CH6.

There are positive correlations between MgO and Cr, Ni, and Co in CH6; and negative correlations with Sr, V (with MgO content, and specifically increasing olivine content for V, since it has low partition coefficient with respect to olivine). Less defined relationships between MgO and Ba, Zr and Rb (Fig. 5.4).

Compatible trace elements (with respect to orthopyroxene, Cr, Ni and Co) concentrations in the Marginal Zone are lower than the Lower Zone abundances. The average Cr content in the LZa was recorded to be 2761±660 ppm (n= 118) whereas the Shelter and mafic norite contain 668± 421 (n= 34) and 1391±281 ppm (n= 33), respectively. Ni and Co show similar trends in the CH6 to Cr, and in turn they are positively correlated with MgO and to some extent the occurrence of olivine (Figs. 5.3 and 5.4). Concentrations of incompatible trace elements (Zr, K_2O, TiO_2, and Rb) in the Marginal Zone are comparable in some instances to those of the Lower Zone. Even though the Marginal Zone contains slightly higher averages than the LZa, there is less defined distinction in the concentration of incompatible trace elements in the some instances in Marginal Zone compared to the Lower Zone (Fig. 5.3).

Sr (and to a lesser extent, Ba) is the only incompatible trace element (with respect to orthopyroxene) that is significantly enriched in the Marginal Zone succession than in the LZa succession. Sr is compatible in plagioclase, which is the dominant mineral phase in the Marginal Zone, especially the Shelter Norite. The Shelter Norite yielded the highest Sr values, averaging 253 ± 53 ppm, and the Mafic Norite average is 131 ± 40 ppm. Chapter 4 of this study showed that the Lower Zone rocks contain very small amount of cumulus plagioclase (CIPW norm vs. Al_2O_3, Fig. 4.1) which is virtually confined in the interlayered norite units. Accordingly the Sr average (18 ± 14 ppm excluding the interlayered norite units) in the LZa is very low compared to the Marginal Zone succession.

In contrast, Zr has comparable average concentrations in the whole CH6 succession, which are 6 ± 4 ppm in the LZa; and 7 ± 4 and 14 ± 3 ppm in the Shelter and Mafic Norite sequences, respectively. Similar relative concentration levels are seen for other incompatible elements (V, K_2O, TiO_2 and Rb). Generally, Fig. 5.3 shows that there is a significant decrease in incompatible trace element (with respect to the mineral assemblages described in Chapter 4) concentrations in passing from the Marginal Zone to the Lower Zone.

5.1.3. Rare Earth Elements

The Rare Earth Elements (REE) is a unique group of incompatible trace elements that have not been investigated in detail at Clapham Trough. The REE have the atomic numbers from 57 to 71 (i.e. Lanthanum to Lutetium). The progressive decrease in the ionic size of the REE systematically controls the partitioning of the REE. Each of the cumulus phases in CH6 (orthopyroxene and plagioclase) has a different control on the distribution on these trace elements. REE patterns are also influenced by the source region of the magma, where the concentrations of individual elements depend on the partitioning in the melting mineral phases and the residuum in the source area. REE are largely incompatible with respect to the CH6 mineral assemblages, except for Eu, which is compatible with plagioclase in its divalent state. The occurrence of cumulus plagioclase imparts positive Eu anomalies, whose magnitude is expressed by Eu/Eu*, defined by Taylor and McLennan (1985) to be $Eu/Eu^* = Eu_N/\sqrt{[(Sm_N).(Gd_N)}$. The REE data presented in this section are normalised relative to a primitive mantle source of McDonough and Sun (1995). The source of the magmas that were emplaced in the Lower Zone and its supposed chill phase (i.e. the Marginal Zone) is largely believed to be the mantle, regardless of other processes that might have altered the primary magma composition (Eales and Costin, 2012; Barnes et al., 2010 and Wilson, 2012). The REE

data are shown with the rest of the whole-rock data in Appendix C and Fig. 5.5 shows the resulting REE patterns from the CH6 data, separated by the dominant lithologies in the section.

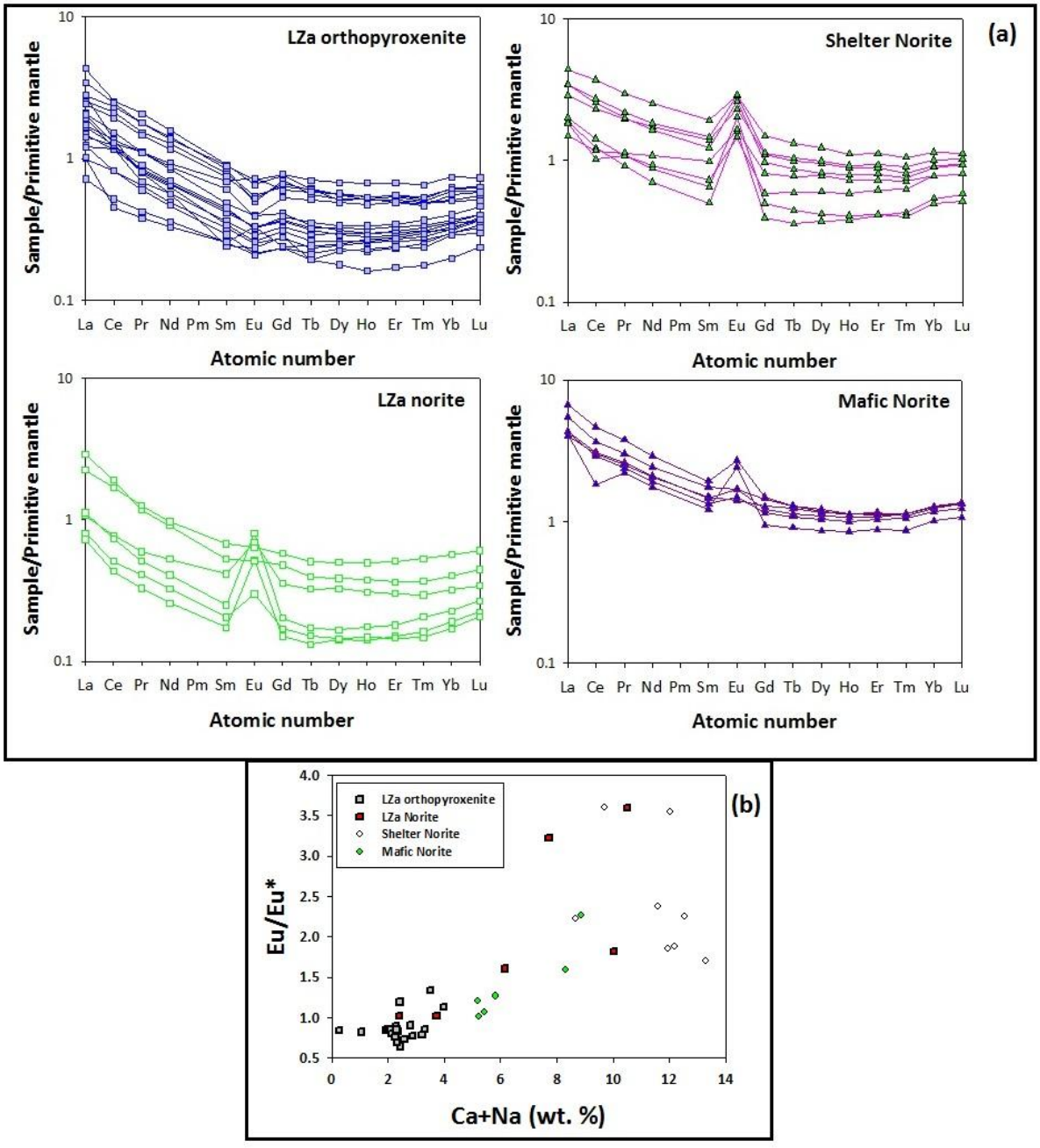

Fig. 5.5: (a) Whole rock REE trends for the Lower and Marginal Zones in the CH6 section. (b) Eu/Eu variation with the amount of plagioclase with (Ca+Na) for proxy of normative plagioclase.*

The patterns observed for both the Marginal and Lower Zones in the Clapham Trough section are Light Rare Earth Element (LREE) enriched relative to the primitive mantle of McDonough and Sun (1995) (Fig. 5.5). Eu is compatible with respect to plagioclase and rocks that contain cumulus plagioclase (dominant phase), Eu will have a positive Eu/Eu* anomaly such as occurs in the Marginal Zone norite. The Mafic and Shelter Norite have average Eu/Eu* of 1.4 and 2.4, respectively, whereas the LZa norite average Eu/Eu* is 2.1. By contrast, the LZa orthopyroxenite units show a subtle negative (to zero) Eu anomaly with the average Eu/Eu* of 0.9. Fig. 5.5b shows that there is a positive correlation between the amount of plagioclase (Ca+Na for proxy of normative plagioclase) and the magnitude of the Eu anomaly (i.e. Eu/Eu*) in the CH6 section. The Shelter Norite contains the highest amount of plagioclase and the Eu anomaly is highest in this part of the Marginal Zone. In contrast, the LZa orthopyroxenite units show the lowest Eu anomaly (0.64-1.19), and have the lowest amount of plagioclase in the whole rock.

In addition to anomalies (peaks and troughs), REE patterns are also interesting because they are affected by the crystal-melt association during the formation of the rock. The REE patterns observed in the CH6 section are of petrological interest and they bear implications of the magmatic processes that formed the cumulate rocks under consideration. There are two basic REE patterns, the light or heavy REE enriched patterns. Either pattern is influenced by the composition of the parental magma and the partition coefficients of the REE in the mineral phases that form the rock. The light rare earth element (i.e. LREE) enrichment patterns suggest that there is plagioclase control on the REE composition since they are relatively more compatible with respect to the feldspar than in mafic minerals. By contrast, heavy REE (i.e. HREE) patterns are controlled by the mafic minerals (in which they are relatively more compatible) in the rock. In the CH6 section, orthopyroxene is the most significant mafic mineral, thus the observed whole-rock REE patterns will be predominantly affected by the latter mineral phase.

The degree of enrichment of the REE can be quantified with the ratio $(La/Yb)_N$, where values > 1 suggest LREE enrichment and < 1 suggest that there HREE. The LZa orthopyroxenite and LZa norite units have $(La/Yb)_N$ ratios of 4.78 and 4.44, respectively, compared to the Shelter and Mafic Norite units of the Marginal Zone, which have 3.33 and 4.00 $(La/Yb)_N$ ratios, respectively. Fig. 5.6 shows the degrees of LREE and HREE enrichment in the CH6 expressed as $(La/Yb)_N$ vs. Ce_N. There is a positive correlation between the $(La/Yb)_N$ and Ce_N in both the Lower Zone and Marginal Zone rocks. The Lower Zone A succession shows a relative heavy rare earth elements (LREE) enrichment compared to the Marginal Zone succession (Figs. 5.5, 5.6).

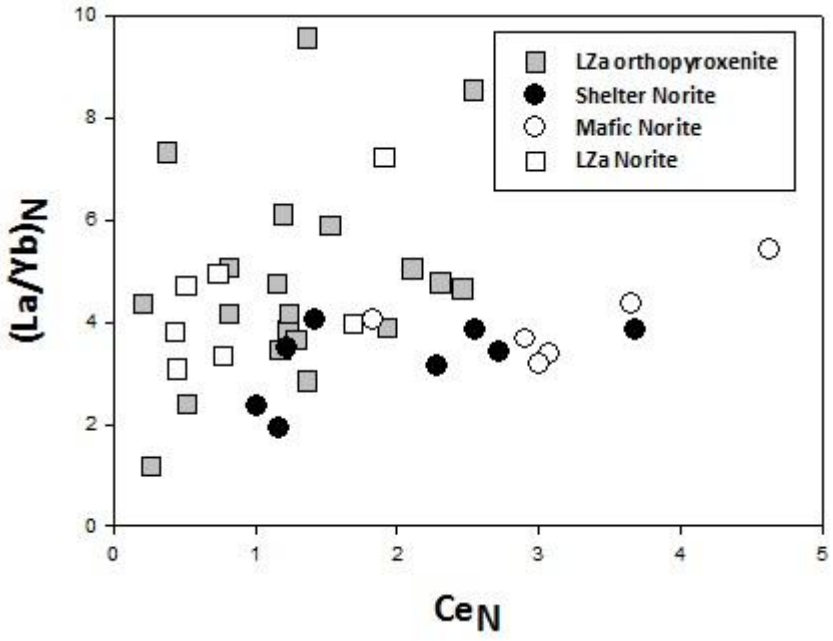

Fig. 5.6: (La/Yb)N vs. CeN as a measure of the degree of enrichment of LREE compared to HREE in the CH6 succession.

5.2. Mineral Geochemistry

49 samples were selected for mineral composition analyses throughout the CH6 drill core. Two different techniques for the mineral analyses were used in the present study. One set of analyses was done on polished thin section samples using a CAMECA SX 100 electron probe micro

analyser (EMPA, technique is described in Appendix B); and the other sets of analyses were done using XRF (for major elements) and ICP-MS (trace elements) on mineral separates. Additional trace element analyses were done using LA-ICP-MS by Prof. AH. Wilson. The combined data are presented in Appendix C and in the figures below.

5.2.1. Orthopyroxene compositions

The orthopyroxene magnesium number (defined as the molecular ratio Mg# =100*(MgO/(MgO+FeO), also expressed as En) is used to express the compositional variations with stratigraphic height through the CH6 drill core (Fig. 5.6). The Lower Zone shows the most primitive compositions (En_{86-82}) in the studied section, with the most primitive compositions predominant in the upper units (i.e. Rostock Orthopyroxenite) of the Lower Zone A section of CH6. In the Marginal Zone, the orthopyroxene compositions show a steady and continuous decrease from En_{78-70} with increasing stratigraphic height (Fig. 5.7). In the Mafic Norite orthopyroxene compositions range from the En_{78-73} whereas the most evolved orthopyroxenes compositions occur in the Shelter Norite, ranging between En_{73-70}.

Similarly, the Al_2O_3 and Cr_2O_3 concentrations in the orthopyroxene crystals are generally lower in the Marginal Zone than in the Lower Zone succession. There is a continuous decrease in the Cr_2O_3 concentrations, from 0.25-0.21 wt. %, in the Mafic Norite to 0.16-0.08 wt. % in the Shelter Norite. The Cr_2O_3 concentrations in the Lower Zone are typically greater than 0.25 wt. % (averaging 0.41 ± 0.08 wt. %, n=24). The Clapham Orthopyroxenite succession shows gently decreasing Cr_2O_3 concentration at the bottom, followed by an increase with stratigraphic height. In the same interval, Al_2O_3 shows a gentle upward increase similar to MgO and Mg#. (Fig. 5.7).

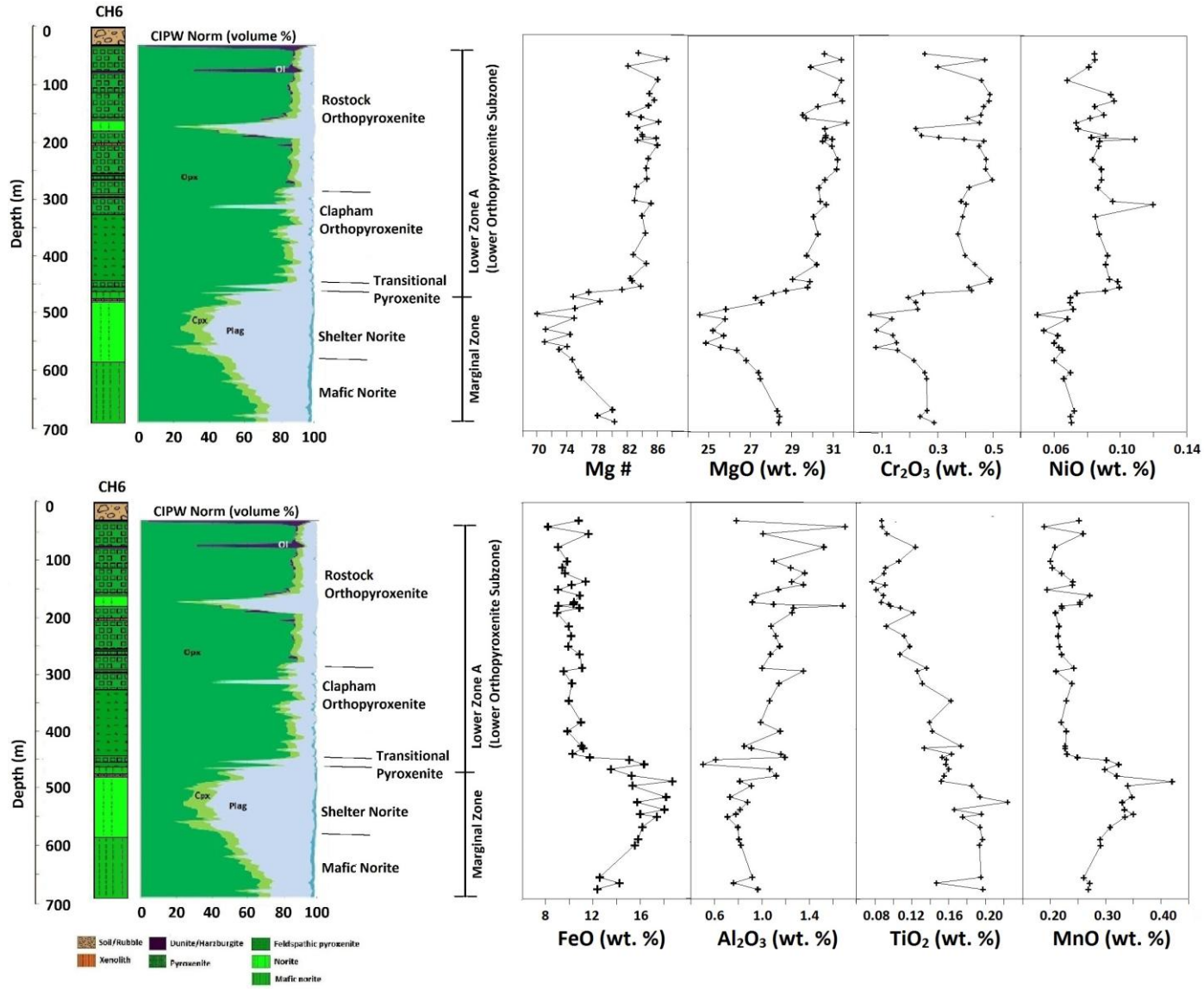

Fig. 5.7: Orthopyroxene major element compositions for the CH6 section.

The average Al_2O_3 content for the Lower Zone A orthopyroxene is measured to be 1.16 ± 0.22 wt. %. The Marginal Zone orthopyroxene yielded 0.89 ± 0.19 for the Shelter Norite and 0.85 ± 0.08 wt. % Al_2O_3 for the Mafic Norite succession.

The orthopyroxene compositions in the Shelter Norite succession show cyclic compositional variations compared to the relatively continuous and smooth progressive changes in the concentration of the major elements observed in the Mafic Norite succession. There are cyclical variations that are also observed in the interlayered norite unit in the Rostock Orthopyroxenite. The orthopyroxene compositions show a significant geochemical change between the Marginal Zone and the Lower Zone (i.e. LZa) succession of CH6, through the Transitional Pyroxenite.

Trace element compositions for orthopyroxene were acquired through analysis of mineral separates using ICP-MS and LA-ICP-MS (analyses carried out by Prof. A Wilson) of polished sections as indicated in Appendix C. The data are presented in Figs. 5.8 showing stratigraphic variation and in 5.9 against the composition of the orthopyroxene as Mg#. The Lower Zone orthopyroxene crystals generally have higher concentrations of compatible trace elements (Cr and Ni) compared to the Marginal Zone orthopyroxene. In contrast, the Marginal Zone orthopyroxene crystals contain higher incompatible trace elements than the Lower Zone A orthopyroxene.

Across the Transitional Pyroxenite, all the trace elements show gradual geochemical change, particularly Cr, Ni, Co, V and Sc. The Lower Zone orthopyroxene show near constant concentrations for these elements (excluding the LZa norite samples) compared to the steady and continuous compositional evolution observed between the Mafic and the Shelter Norite succession Marginal Zone. The HFSE in the CH6 orthopyroxene are generally low. In the Lower Zone A succession Ti, Zr, and Hf show generally decreasing concentrations with increasing

stratigraphic height. In the Marginal Zone orthopyroxene, the Shelter Norite shows generally depleted incompatible trace elements concentrations than the Mafic Norite.

There are positive correlations between orthopyroxene Mg# and compatible trace elements (Cr and Ni in particular) and negative correlation with Co, V and Sc. There is no defined relationship between orthopyroxene with LILE (large ion lithophile elements) and HFSE (High field strength elements), with the exception to Y, REE and Ti which show subtle but negative correlation (Figs. 5.8 and 5.9). These elements (including rare earth elements) are largely incompatible with respect to orthopyroxene and this is seen by the low concentrations in the mineral phase. The Shelter Norite succession shows the most evolved orthopyroxene compositions, and they are associated with slightly higher concentration of incompatible trace elements. In the latter section of the Marginal Zone, orthopyroxene shows evidence of cyclic compositional variations such that there is a systematic compositional reversal unlike the smooth progressive compositions seen in the Mafic Norite. This phenomenon has been also identified in the orthopyroxene major elements, and in the whole rock geochemistry presented above (Figs. 5.2-5.3).

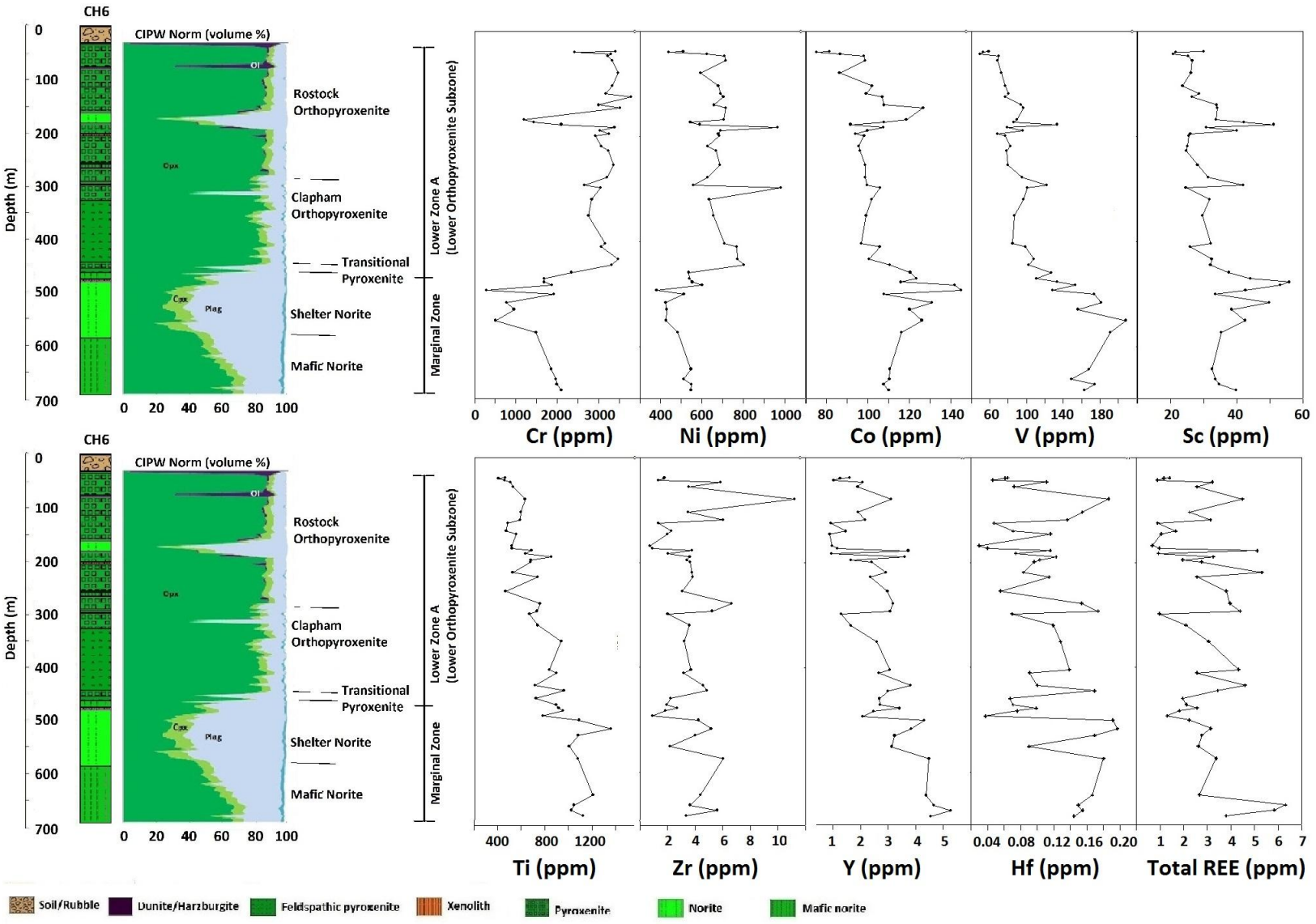

Fig. 5.8: Orthopyroxene trace elements variations for the CH6 section.

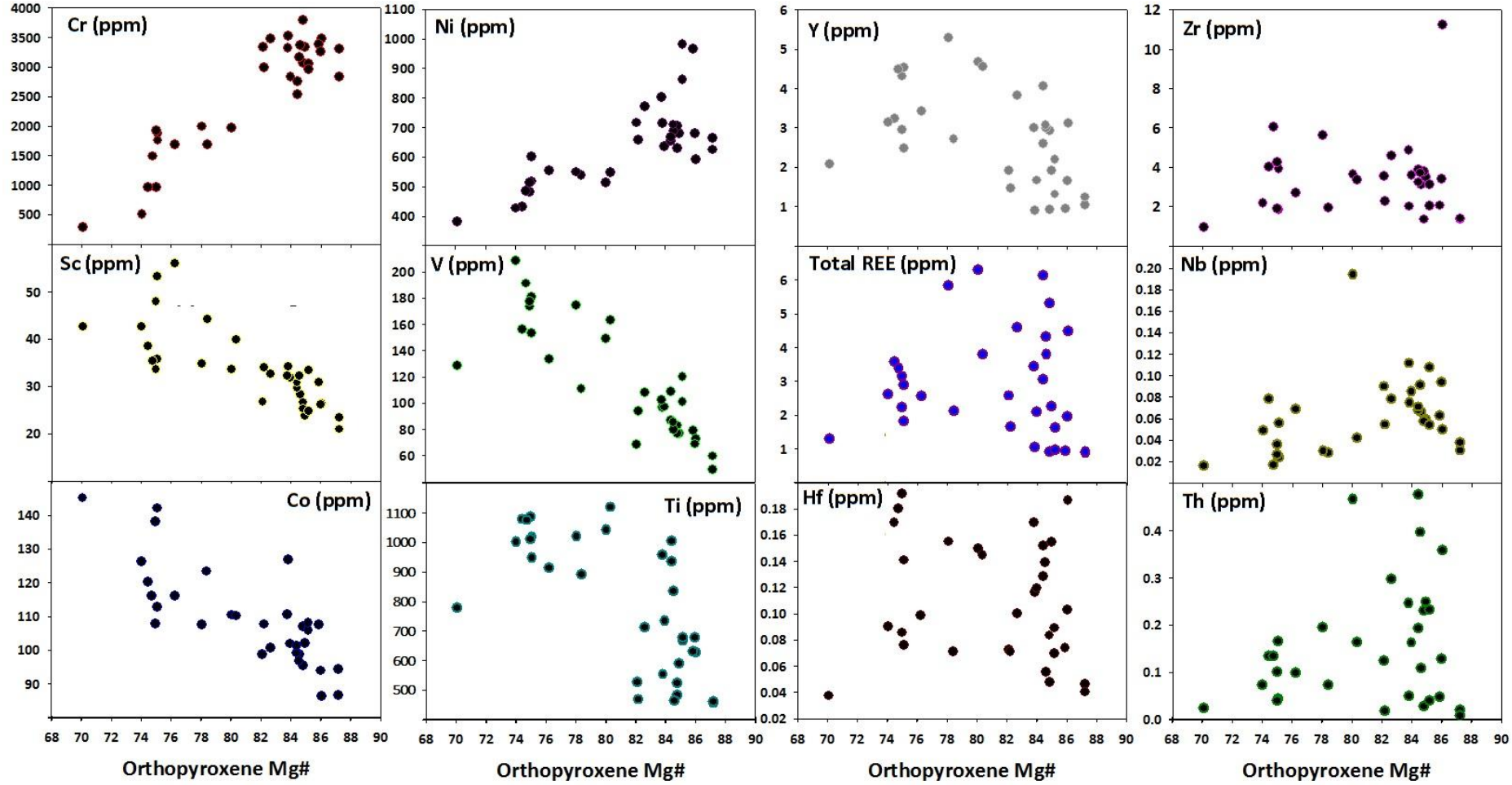

Fig. 5.9: Orthopyroxene trace elements concentrations plotted against the orthopyroxene Mg#.

5.2.2. Plagioclase compositions

In the CH6 section, plagioclase is the second most abundant mineral after orthopyroxene. Compositional data in the studied stratigraphic section are shown in Fig. 5.10. With the exception of samples from the interlayered norite units, all the reported plagioclase compositional data in the LZa section represent interstitial plagioclase. The composition of plagioclase is expressed by the anorthite (An#) content defined by the molecular ratio $100\times CaO/(CaO+2*Na_2O)$. The An# values in the Marginal Zone show steady and continuous variation between the Mafic and Shelter Norite. However, the An# values progressively becomes more calcic (i.e. more primitive compositions) with stratigraphic height in the Marginal Zone succession, unlike the orthopyroxene compositions, which progressively become evolved in the same interval. There is a compositional reversal that adopts a normal compositional trend, in line with progressively sodic compositions (decreasing temperature regime) between 574-542 m (Fig. 5.7). The Mafic Norite contains the most evolved plagioclase compositions (An_{68-66}), and becomes more calcic in the Shelter Norite (An_{76-63}) towards the Marginal-Lower Zone boundary (i.e. the patchy pyroxenite).

The LZa plagioclase compositions vary tremendously from those in the Marginal Zone (Fig. 5.10). From about 280 to 192 m depth in the CH6 drill core there is a gradually decreasing composition from An_{82-81} (measured from cumulus plagioclase near the base of the Rostock Orthopyroxenite succession) to An_{60} stratigraphically below the interlayered norite in the middle of the Rostock Orthopyroxenite. There is a major compositional reversal within the interlayered norite at 165-192 m to An_{84-81} at the centre of this norite unit. The second composition decrease occurs above the interlayered norite (Fig 5.10).

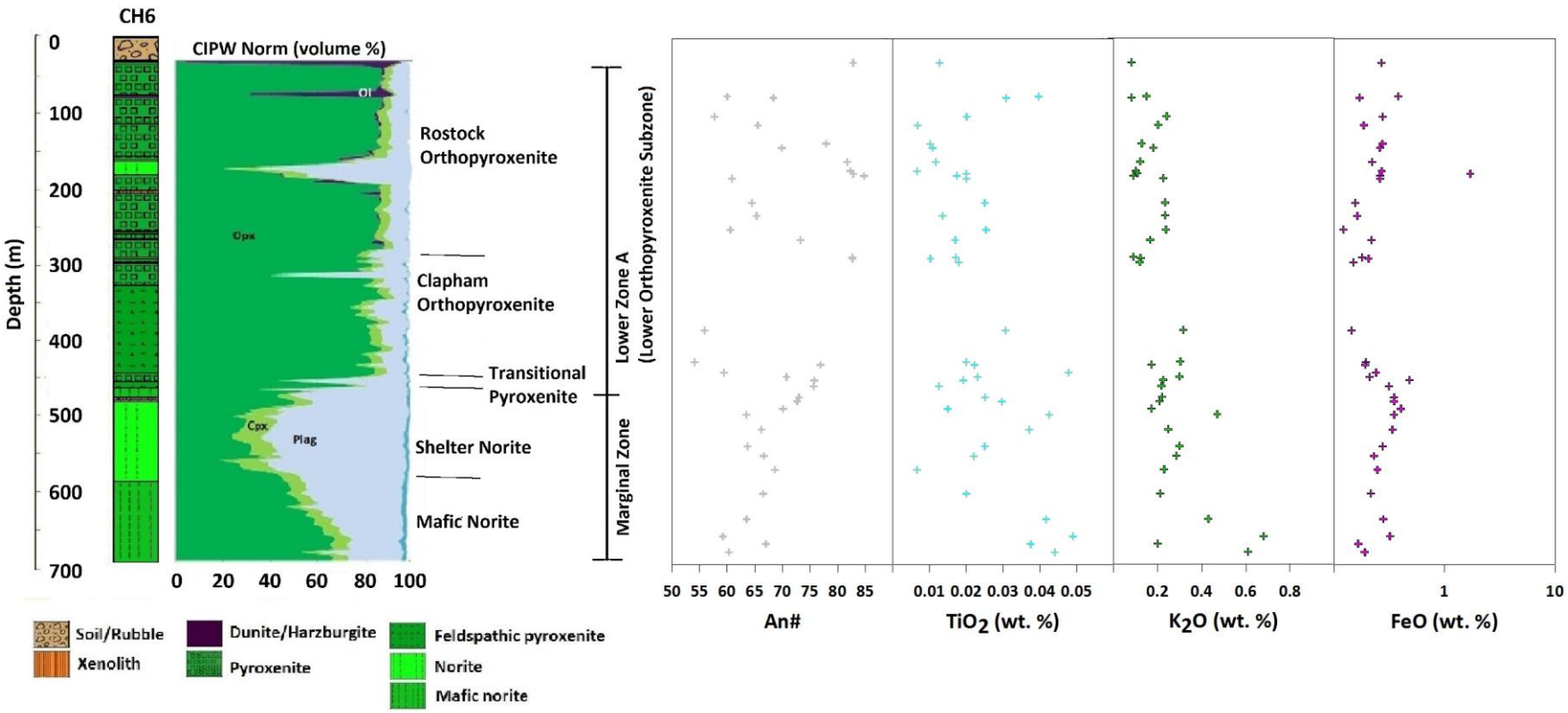

Fig. 5.10: Plagioclase major elements variations in the CH6 section of the Bushveld Complex.

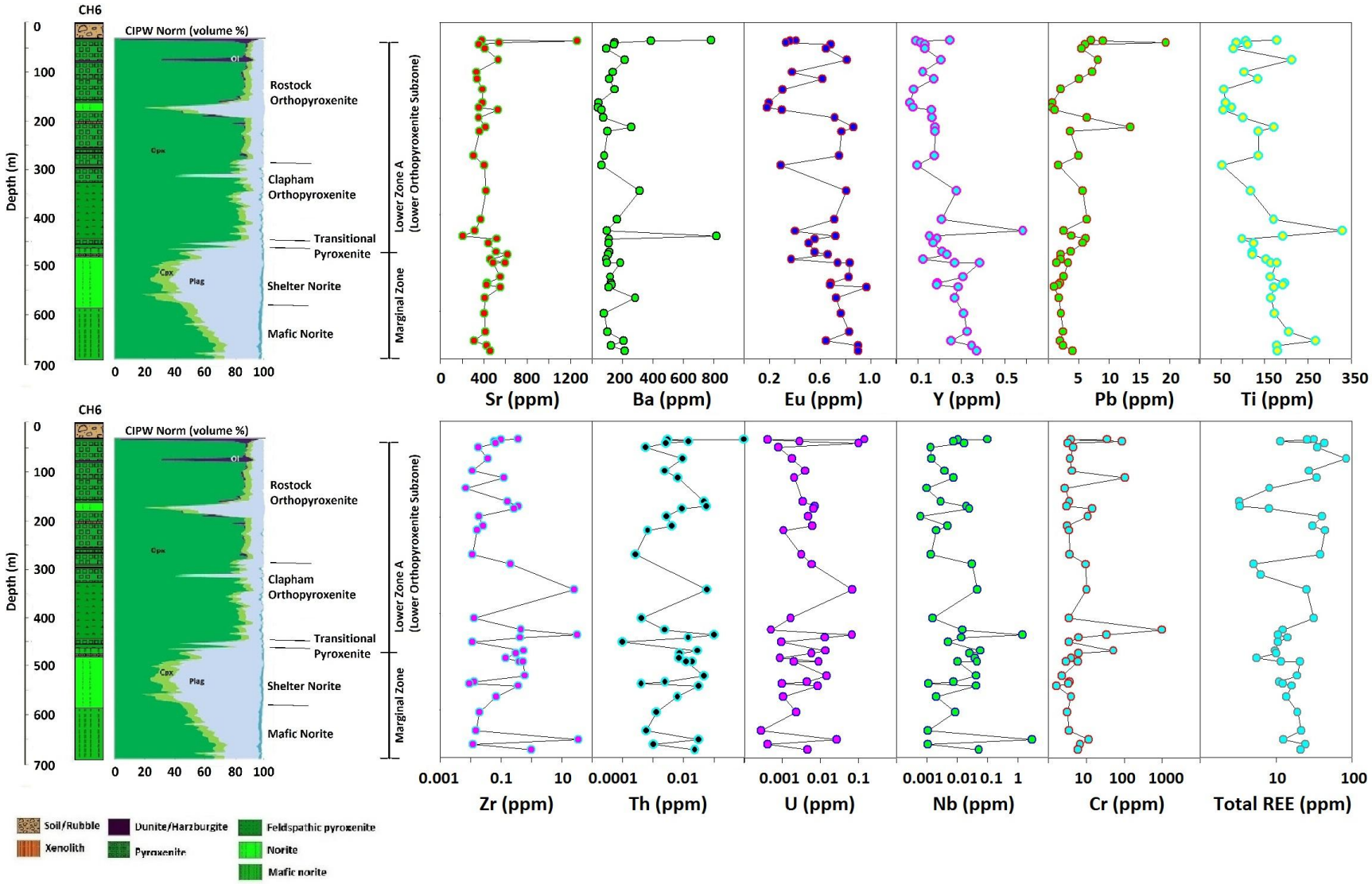

Fig. 5.11: Plagioclase trace elements variations for the CH6 section.

The K_2O and TiO_2 concentration variations also show subtle evidence of compositional change of plagioclase in the intervals mentioned above. The cumulus plagioclase samples have the lowest TiO_2 and K_2O concentrations, which systematically increase in the interstitial plagioclase above each of the norite units in the LZa. This is however different from the trend observed in the Marginal Zone, such that the most primitive plagioclase crystals are associated with the highest TiO_2 and K_2O (Fig. 5.10).

Strontium is compatible with respect to plagioclase and in the CH6 section, the highest Sr concentrations were measured in the Shelter Norite compared to the Mafic Norite. There is a steady and continuous Sr increase with stratigraphic height in the Marginal Zone of CH6. Unlike the evolved orthopyroxene Mg# and depleted compatible trace elements in the Shelter Norite, the co-existing plagioclase becomes more primitive (i.e. more calcic) with height. Sr and Eu show subtle cyclic compositional variations in the Shelter Norite. Th, U, REE, Ti and Y also suggest steady and continuous compositional variation between the Mafic and Shelter Norite successions of the Marginal Zone.

In the LZa, there is almost no difference in the amount of Sr in cumulus and interstitial plagioclase samples. In addition, the Marginal Zone plagioclase is slightly enriched in Sr than the Lower Zone A samples (Fig. 5.11). Generally, the trace element variations diagrams show that Eu (and Total REE), Ba, Y, Pb and Ti have the lowest concentrations within the interlayered norite unit of the Rostock Orthopyroxenite succession. Above the latter unit, the concentrations of these elements progressively increase as the An# decreases (Figs. 5.10, 5.11).

.

5.3. Summary and Discussion

The whole rocks and mineral compositional data presented in this section show that the CH6 core intersected two geochemically distinct packages of the Bushveld Complex. The lower part is the Marginal Zone which has been separated into the Shelter and Mafic Norite sequences as presented in previous chapters. The geochemical and mineral compositional data presented are in accord with the stratigraphic subdivisions.

There is continuous uninterrupted composition change in compositions between the Mafic and Shelter Norite interpreted as resulting from fractionation. The whole-rock and orthopyroxene compositions suggest that the Shelter Norite is the most compositionally evolved section of the Marginal Zone succession (Figs 5.2-5.4, Table 5.1). However, the measured compositions of plagioclase are contradictory to this observation. The Marginal Zone plagioclase compositions become more primitive (more calcic) as the co-existing orthopyroxene progressively presents evolved compositions with increasing height. The mineral compositions measured in the Shelter Norite were En_{73-70} and $An_{76-63,}$ compared to the Mafic Norite whose mineral compositions are En_{78-73} and An_{68-66}.

Cameron (1978) in his Fig. 3 (and possibly equivalent to the section discussed in this work) showed three samples within the xenolithic norite that show increasing An# with stratigraphic height and the orthopyroxene behaviour showing the opposite, i.e. decreasing in the same interval. The latter author did not explain this behaviour in the Marginal Zone and generally focused on the plagioclase compositions that were measured higher in the Olifants River Trough succession. Teigler and Eales (1996) presented analyses of only one sample in the Marginal Zone and Barnes *et al*., (2010) does not place any stratigraphic relationship between the samples that are taken to represent the Marginal Zone rocks (i.e. B1-type). This disparity in the compositional variation of co-existing minerals in this work

is taken in this work as resulting from accumulation processes during the formation of these cumulate rocks.

There is a significant geochemical change at the Lower Zone-Marginal Zone boundary. This abrupt change occurs over a narrow package referred to as the Transitional Pyroxenite in the present study. This compositional reversal in the section intersected by the CH6 at Clapham Trough is consistent with the significant changes in the cumulus phases described in the CH6 section in Chapters 2-4. The gradual compositional reversal is interpreted as having resulted from mixing of a two geochemically distinct liquid compositions during the emplacement of Lower Zone magma.

The Transitional Pyroxenite is a narrow zone of compositional reversal emphasising that the Marginal Zone and the Lower Zones are geochemically distinctly different packages. Stratigraphically above the Transition Pyroxenite, the rocks of the LZa progressively show near constant and relatively primitive compositions, except in the interlayered norite units. This constancy is contrary to the steady and continuous compositional variation described in the Marginal Zone. Cameron (1978) showed that at least the orthopyroxene compositions in the LZa correlative (Lower Orthopyroxenite Subzone) are near constant at Olifants River Trough. However, the subtle variations of the geochemical data support the separation of the LZa succession into the Clapham and Rostock Orthopyroxenite successions (Chapters 2-4). The near constant compositions in the LZa suggest the Lower Orthopyroxenite Subzone did not undergo fractionation and the Bushveld Complex must have experience a long period of virtually little or no changes in the chemical and physical process that were prevalent during the formation of at least the Lower Zone. The data indicate that the Marginal Zone and the Lower Zone A rocks were produced from markedly different magmas and accumulation processes in the Bushveld Complex with a possible time lapse between the two zones.

Chapter 6

The Parental Magma Compositions of the Marginal and Lower Zones at Clapham Trough

The currently accepted argument that the Marginal Zone represents the chill phase (Barnes *et al.*, 2010; Eales and Costin, 2012; and references therein) to the earliest intrusion of mafic/ultramafic magma(s) within the Bushveld Complex chamber, thus they are related to the magma parental to (at least) the Lower Zone is flawed on many fronts (see Chapter 1). It is generally accepted that the entire Bushveld Complex intrusion is a result of multiple injections of large volumes of magma(s) with at least three distinct compositions (Sharpe, 1981). The earliest of these compositions, the so-called B1-magma, is the composition believed to be parental to the Marginal and Lower Zones of the Bushveld Complex (Chapter 1 and references therein). Previously proposed compositions are presented in Table 6.1.

The B1-magma composition of Wilson (2012), which is derived from the chill units in contact with the Magaliesberg Quartzite floor intersected in CH7 drill core, is the most reliable B1-magma composition of all the previous estimates. This chill zone is not exposed anywhere in the Bushveld Complex and is only intersected in drill core (CH7) described by Wilson and Chunnett (2010). According to Wilson (2012), the B1-magma must have formed from a more primitive magma composition that would have been in equilibrium with the most primitive orthopyroxene compositions that occur in the chill zone and in the Basal Ultramafic Sequence (BUS). Moreover, there is evidence for more primitive (komatiitic) magma composition associated with olivine cumulates in the BUS described by Wilson and Chunnett (2010) and Wilson (2012).

Modelling to put in context Marginal Zone and Lower Zone as seen in the CH6 section is immediately imperative in light of the new data presented Wilson (2012). Furthermore, the B1-magma compositions previously proposed by other workers are not adequate to explain the BUS, and by implication, the conformable cumulus rocks of the Marginal Zone sequence at Clapham Trough and correlatives identified in Chapter 3.

Table 6.1: Previously proposed parental magmas of the Lower Zone rocks

	1	2	3	4	5	6	7	8
SiO_2	56.07	55.70	55.24	55.74	55.90	56.09	56.90	53.30
TiO_2	0.34	0.36	0.38	0.34	0.34	0.28		
Al_2O_3	11.47	12.74	12.13	11.82	11.80	11.31	9.60	9.80
Fe_2O_3	1.58	1.00	1.57			1.53		
FeO	8.48	7.80	7.79	10.50	10.20	7.79	7.90	9.10
MnO	0.18	0.09	0.15	0.18		0.17		
MgO	12.96	12.44	12.97	11.85	12.90	13.58	16.4	19.00
CaO	6.68	6.96	6.84	6.50	6.80	6.35	5.10	5.80
Na_2O	1.68	2.02	1.75	1.63	1.70	1.43		
K_2O	0.80	1.03	0.88	0.98	0.90	1.05		
P_2O_5	0.07		0.01	0.08		0.07		
Cr_2O_3	0.20		0.16		0.15	0.22		
NiO					0.05			
TOTAL	100.51	100.14	99.87	99.62	100.74	99.87	96.10	97.00
Mg#	0.73	0.74	0.75	0.67	0.69	0.76	0.79	0.79

Column 1- B1-magma proposed by Hulbert and Sharpe (1985), 2- Experimental parental magma proposed by Cawthorn and Davies (1983) , 3- Davies (1982) , 4- Barnes et al., (2010) , 5- Eales and Costin (2012), 6- B1-magma of Wilson (2012), 7- Primitive magma fractionated to the B1-magma of Wilson (2012), 8- Komatiitic magma of Wilson (2012).

6.1. Modelled crystallisation of previous magmas

All of the proposed B1-magma compositions (Columns 1-6, Table 6.1) and the primitive compositions (columns 7 and 8, Table 6.1) were run for model fractional crystallization using Petrolog 3.1.1 (algorithms and software described in Danyushevsky and Plechov, 2011). The various output data were evaluated in comparison with the observed mineral phases in the Lower and Marginal Zones of the Bushveld Complex, particularly CH6 section described in the present study. Modelling of the crystallization from the above starting compositions (Table 6.1) was conducted at 20.0, 7.0, 3.0 and finally at 2.0 kbars pressure levels (kept constant during each crystallization run), simulating the possible depths of the Bushveld Complex magma chambers (and sub-chambers) and QFM buffer (model after Borisov and Shapkin, 1990). 2-3 kbars is the accepted pressure range for magma chamber in which the currently exposed Bushveld Complex rocks were formed (Cawthorn and Davies, 1983; Cawthorn, 1996; Eales and Costin, 2012). 7-20 kbars are pressures proposed for staging chamber(s) in which early crystallization could have occurred prior to the emplacement of the Marginal and Lower Zones magmas at the currently exposed level (Eales and Costin, 2012).

The preferred orthopyroxene composition model of the Petrolog 3.1.1 software in the present work is after Bolikhovskaya *et al.* (1995) on the basis that the model by the latter author is specifically developed for the crystallization of low-Ca pyroxene, a dominant phase in the CH6 section. The plagioclase and clinopyroxene models are after Danyushevsky (2001) but the Langmuir *et al.* (1992) model offers comparable results. The used model (Danyushevsky, 2001) is favoured because it takes into account both pressure and water content in the magma. Olivine composition model is after Danyushevsky (2001). All of the above models take into account the effects of pressure and are able to produce Bushveld Complex appropriate compositions right from the starting magmas depending on the pressures used. The calculation steps were carried out at 0.01 % crystallization intervals and the liquid was

allowed to crystallise uninterrupted until 20% liquid was remaining (i.e. up to 0.8 degree of crystallization, *F*). The orthopyroxene composition ranges produced from the magma compositions proposed by the earlier authors listed in Table 6.1 are shown in Figure 6.1, and the complete model data are attached in Appendix D.

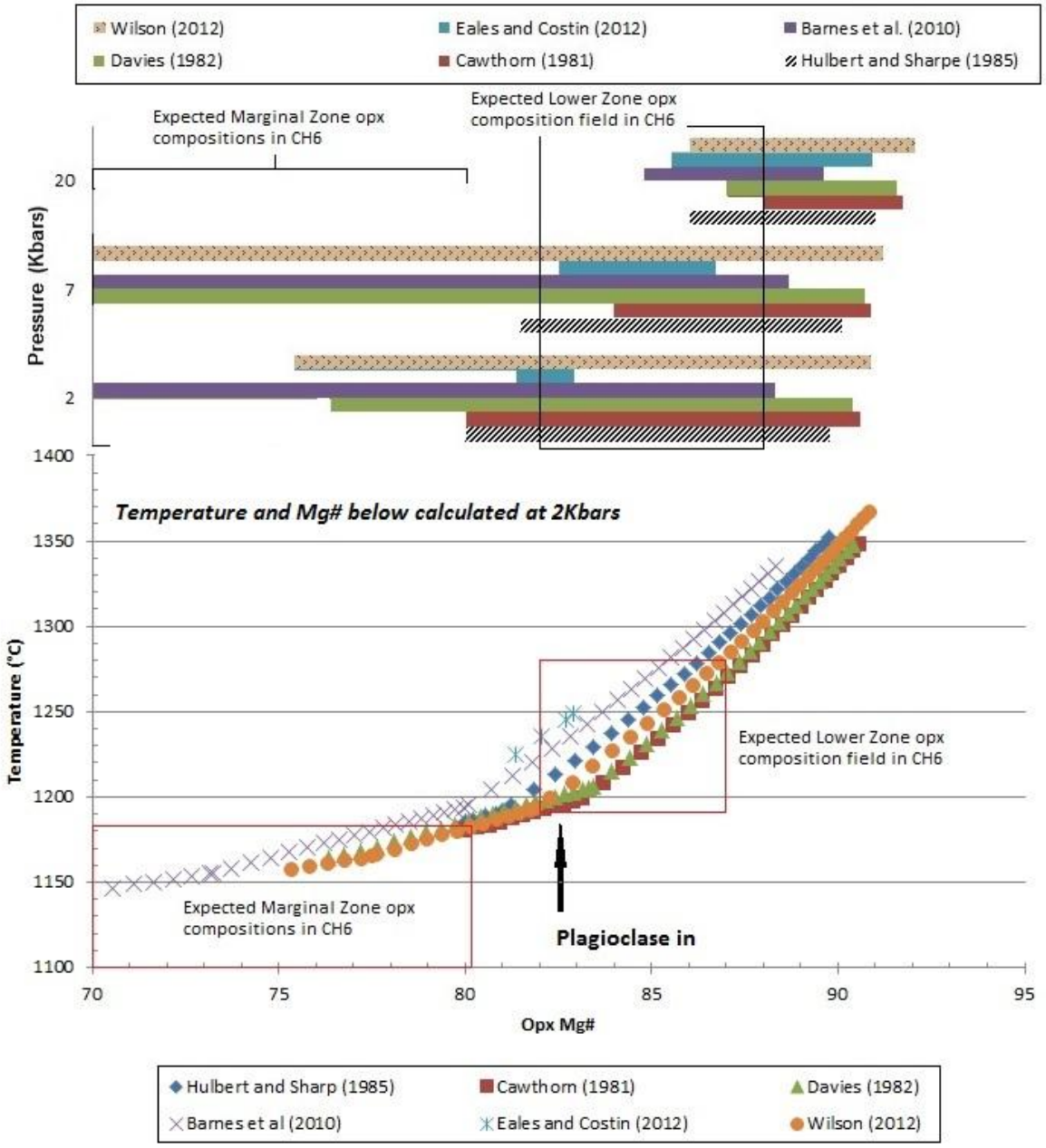

Figure 6.1: Orthopyroxene crystallization predicted at pressures between 20-2 kbars from previous B1-magma compositions.

The orthopyroxene compositions presented in chapter 5 for the Lower Zone A of CH6 are expected to fall in the demarcated rectangles (red square for temperature and the black rectangle for pressures in Fig 6.1). The predicted temperature range for the crystallization of the appropriate compositions in CH6 is 1280-1190° C at 2 kbars. The accepted starting B1-magma composition in the present study is that of Wilson (2012) because the orthopyroxene compositions and the crystallization order observed in CH6 can be readily produced by initially crystallizing compositions equivalent to the BUS. In addition, unlike the other B1-magmas, the composition of Wilson (2012) is derived from a tangible chill phase of the most primitive known rocks in the Bushveld Complex itself rather from marginal sills, the exact origin of which remains unclear.

The present study already presented in chapter 1 the short falls and inadequacies that render the earlier B1-magma compositions unlikely parental magmas to the Lower (i.e. Lower Orthopyroxenite Subzone) and Marginal Zones of the Bushveld Complex, at least at the Clapham Trough section. The B1-magma composition presented by Eales and Costin (2012) is disregarded because it is mainly derived from theoretical modelling that does not take into account the BUS of Wilson and Chunnett (2010). However, their work correctly emphasises that the magmas emplaced at the level of the currently exposed Bushveld Complex chamber were most likely crystal mushes (Marsh 1988; Mondal and Mathez, 2007; Latypov, 2009; Eales and Costin, 2012; Roelofse and Ashwal, 2012). Furthermore, Fig. 6.1 shows that some of the orthopyroxene compositions observed in the BUS and the base of the Lower Zone are producible from the B1-magma of Wilson (2012) at 20-7 kbars. This means that between about 60-20 km depth range a staging chamber could have existed in which up to 30 % crystallization of the B1-magma is possible (Appendix D). The modelling supports the emplacement of primitive orthopyroxene carried in suspension for both the BUS and Lower Zones of the Bushveld Complex, thereby validating the important role crystal mushes could have played in the origin of the Bushveld Complex. Contrary to the BUS and the Lower

Zone, the Marginal Zone orthopyroxene compositions could not have formed in pressures greater than 4 kbars because at higher pressures the accepted crystallization order for the Bushveld Complex (at least at Clapham Trough, i.e. (± olivine) orthopyroxene, plagioclase and poikilitic clinopyroxene) in the Petrolog model falls away and clinopyroxene crystallizes before plagioclase.

The accepted crystallization order of the silicate mineral phases for the Bushveld Complex is olivine, which is replaced early on by orthopyroxene, then plagioclase and clinopyroxene that crystallised at relatively lower temperatures (Cameron, 1978; Sharpe, 1981; Cawthorn and Davies, 1983; Hulbert and Sharpe, 1985; Eales and Cawthorn, 1996). In the Lower and Marginal Zones of the CH6 section olivine is a minor phase, occurring only at specific intervals making orthopyroxene the dominant liquidus mineral phase. This observation is applicable across the eastern limb of the Bushveld Complex, with only minor lateral variations in modal abundances and subtle geochemical composition (Cameron, 1978; Eales and Cawthorn, 1996). This observation allows focus on the crystallization of orthopyroxene as essentially the primary phase to crystallise from the B1-magma. This is supported by the work of Wilson (2012) that showed two different magma compositions represented in chill zone rocks of the Bushveld Complex. The latter author presented B1-magma that is in equilibrium with orthopyroxene only (his Fig. 24) and the other komatiitic composition associated with the olivine units.

6.2. Compositional variations of Marginal and Lower Zones

The whole-rock and mineral compositions, particularly MgO and Mg# in the Marginal Zone show steady and continuous compositional variations with increasing stratigraphic height (see Chapter 5) such that they become progressively evolved with increasing height (Fig 6.2). The Mg# variations in the Marginal Zone are interpreted as having formed from continuous and

uninterrupted differentiation in the magma prior to emplacement of new magma. The relatively lower Mg#, S.I. (solidification index defined by Thornton and Tuttle, 1960) and MgO content support the interpretation that the Marginal Zone succession formed from a relatively evolved magma composition compared to the overlying LZa sequence (Fig. 6.2). The steady and continuous differentiation during the formation of the Marginal Zone was interrupted by the emplacement of the Lower Zone which resulted in mixing of primitive magma with the evolved magma that must have been crystallizing orthopyroxene compositions (i.e. inverted pigeonite) equivalent to the top of the Shelter Norite. This interpretation is supported by the occurrence of the Transitional 'patchy' Pyroxenite, which marks a gradual but significant compositional change from the Marginal Zone rocks to the more primitive LZa compositions over a narrow interval. The LZa compositions remain constant above the Transitional Pyroxenite with increasing stratigraphic height, with the exception of the interlayered norite units (see Figs. 5.1-5.3, 5.7, 6.2).

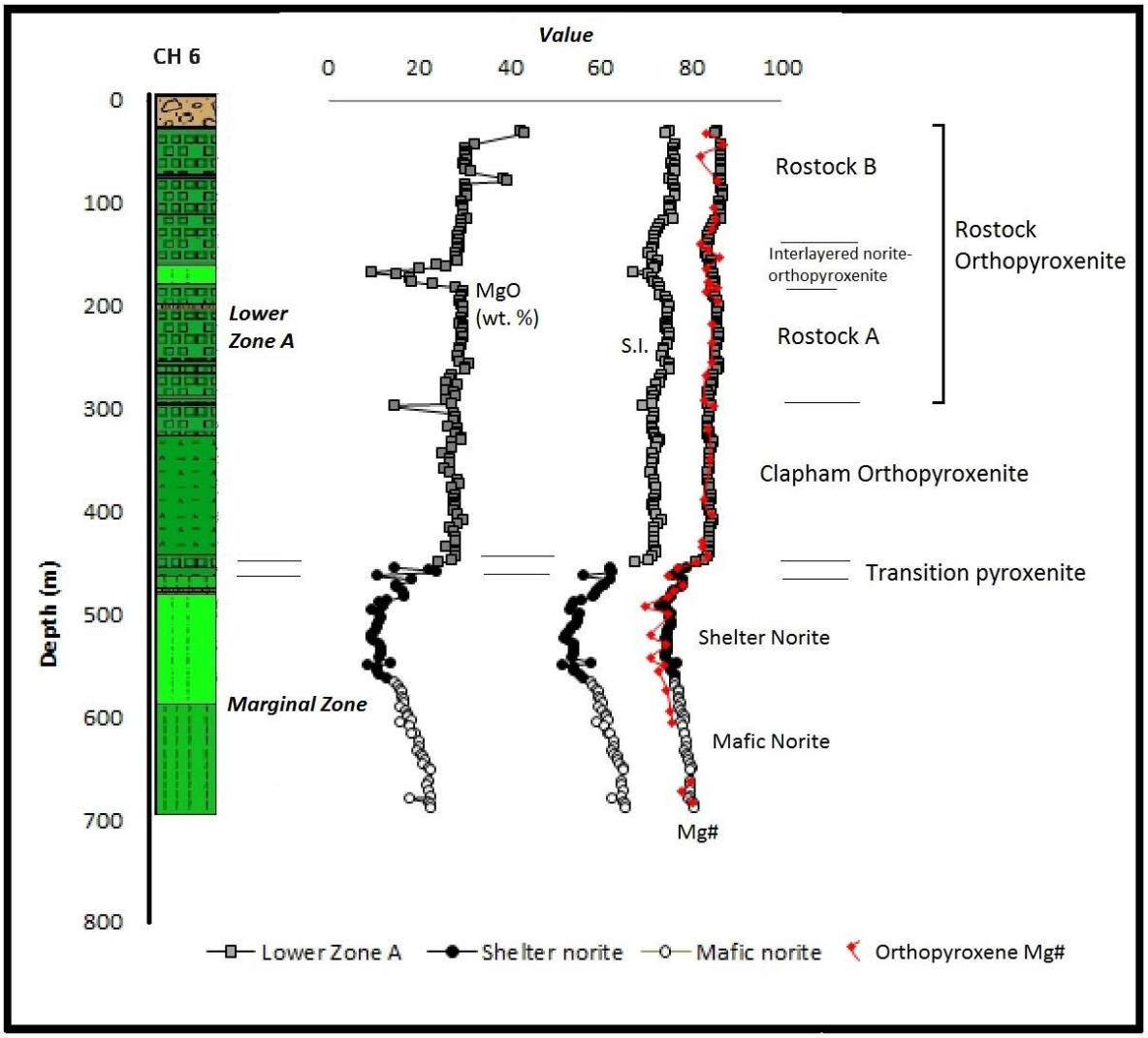

Fig. 6.2: Compositional variation of the LZa and Marginal Zone of the CH6 section. Marginal Zone shows progressive differentiation with height compared to relatively constant (i.e. effectively poorly differentiated) composition of the Lower Orthopyroxene Subzone (LZa) package of CH6. The S.I is the Solidification index, with no units and MgO is the whole-rock composition is wt. %. Mg# number refers to both whole-rocks and orthopyroxene data (in red).

The Marginal Zone formed by crystallization and accumulation of progressively differentiating magma in equilibrium with orthopyroxene and (cumulus) plagioclase within the chamber as presently exposed. Clinopyroxene is a post cumulus phase throughout (excluding the inverted pigeonite identified in chapter 4). Contrary to the Marginal Zone,

plagioclase and clinopyroxene in the LZa both occur both occur as post-cumulus phases. The LZa and the Marginal Zone rocks described in CH6 cannot be readily produced by an unmodified B1-magma of Wilson (2012) since it would crystallize more primitive compositions than observed. A significant amount of differentiation of the B1-magma must have taken place to form the Marginal and the Lower Zones at Clapham Trough. This chapter evaluates the possible compositions of the magmas, on the basis of the modelling, that are most likely to be parental to the CH6 section.

6.3. Modelling Parental Magmas for the Clapham Trough

The crystallization order of the mineral phases that make-up the rocks in the study area is orthopyroxene - plagioclase - clinopyroxene. Wilson (2012) showed that the B1-magma is largely associated only with orthopyroxene cumulates (Fig. 24 in the latter work), and its postulated composition was formed from extraction of approximately 13 % En_{92-90} orthopyroxene. We have already shown above that this magma composition is not in equilibrium with the mineral compositions presented in chapter 5 and it cannot be the parental magma responsible for the CH6 section described in this work. The present study therefore considers the magma composition that occupied the presently exposed Marginal Zone to be a derivative of the B1-magma, formed from the continued extraction of primitive orthopyroxene.

The parental magma to the LZa must have been more primitive than the magma which gave rise to the Marginal Zone rocks. However, the orthopyroxene compositions in the LZa are themselves more evolved compared to the orthopyroxene compositions in equilibrium with the B1-magma of Wilson (2012). Plausible Marginal Zone and LZa parental magma compositions must therefore satisfy this primary relationship. That is, that the magma responsible for the Marginal Zone must be very close or at the orthopyroxene-plagioclase

cotectic and produce the compositions comparable to the CH6 section. In addition, the magma composition appropriate for the LZa section of CH6 must be in equilibrium almost exclusively with orthopyroxene. In this work, the Marginal Zone is modelled to have crystallised in a (temporarily) closed magma chamber, without injection of new (primitive) magma because the whole-rocks and orthopyroxene Mg# show continuous evolution without any abrupt compositional reversals. Furthermore, this study assumes little or no magma escaped through the roof and the BUS was either completely solid or little trapped liquid escaped upwards. Therefore, a state of (relative) quiescence in the Bushveld Complex chamber during the formation of the Marginal Zone is envisaged.

The most primitive orthopyroxenes in the Marginal Zone of the CH6 section (at the top of the BUS, below the Mafic Norite) have the composition of En_{81-79} at the base of the Mafic Norite. Wilson and Chunnett, (2010) showed that the Marginal Zone is conformable to the BUS and there is no structural and textural change at the contact. The residual liquid (from evolving B1-magma of Wilson) in equilibrium with En_{81-79} orthopyroxene is postulated to approximate the parental magma to the Marginal Zone cumulates observed at least in Clapham Trough. This premise is acceptable considering the preponderance of B1-magma units in the BUS (Wilson and Chunnett, 2010; Wilson, 2012).

6.3.1 Run Conditions and applying the model

During the modelling, the B1-magma was allowed to crystallise in a stepwise manner at constant pressure with crystallization runs at 7.5, 4.5, 3.0 and then finally at 2.0 kbars. The present study accepts the minimum pressure inside the Bushveld Complex chamber as 2.0 kbars (after Eales and Costin, 2012). The model data below refer to this pressure as applicable. The buffer used in the model is the QFM buffer with 0.01 % of mineral phase extracted in each crystallization step. The modelling was carried out under both dry and

water saturation. The results are comparable but dry magma data is applicable since the amount of water required for water saturation is very high and water-bearing phases (biotite-phlogopite) in the CH6 section are post-cumulus and of minor proportions. The LZa modelling was carried out under similar conditions, however, the amount of crystallization allowed was restricted since the compositions reflected in the previous chapter (and Fig. 6.2) are near constant. The composition postulated to be parental to the LZa is taken as a mixture of the B1-magma and the residual liquid that must have ponded at the top of the Marginal Zone before the abrupt emplacement of large volumes of new (primitive, B1) magma. This assumption is justified because of the gradual compositional change at the base of the LZa (within the narrow Transitional Pyroxenite), rather than an abrupt change without any intermediate compositions between the LZa and Shelter Norite units (chapter 5, Fig. 6.2).

The orthopyroxene and plagioclase compositions appropriate for the Marginal Zone are expected to be within the ranges $En_{80\text{-}71}$ and $An_{78\text{-}63}$, respectively. The expected orthopyroxene compositions in the LZa as measured in CH6 are $En_{87\text{-}82}$. Table 6.2 shows the modelling parameters and compositions used in different stages of the Marginal and LZa sections of the CH6 sequence. The complete results of the modelling are attached in Appendix D and the relevant data are shown in the Figs. 6.3-6.4.

Table 6.2: Summary table of the Petrolog model output for the Marginal Zone at Clapham Trough as described in CH6 core.

	Starting magma composition*	**Residual liquid after crystallization**							**Magma at base of Marginal Zone[#]**	**Magma at top of Marginal Zone[##]**
	B1-Magma	**5%**	**10%**	**15%**	**20%**	**25%**	**30%**	**35%**	**Postulated Magma (31%)**	**Residual Magma (54%)**
SiO_2	56.09	56.22	56.24	56.28	56.34	56.45	56.67	57.06	**56.7**	**59.45**
TiO_2	0.28	0.30	0.31	0.33	0.35	0.37	0.40	0.43	0.41	0.47
Al_2O_3	11.31	11.75	12.20	12.71	13.26	13.88	14.19	13.77	**14.13**	**12.49**
Fe_2O_3	1.53	1.21	1.18	1.15	1.12	1.10	1.12	1.21	1.13	1.64
FeO	7.79	8.24	8.40	8.54	8.63	8.65	8.67	8.92	**8.73**	**9.87**
MnO	0.17	0.18	0.19	0.20	0.21	0.23	0.24	0.26	0.25	0.34
MgO	13.58	12.50	11.35	10.10	8.75	7.29	6.12	5.62	**6.05**	**3.59**
CaO	6.35	6.68	7.02	7.40	7.81	8.27	8.58	8.56	8.58	6.94
Na_2O	1.43	1.51	1.59	1.69	1.79	1.91	2.00	2.00	2.01	2.18
K_2O	1.05	1.11	1.17	1.24	1.32	1.40	1.50	1.50	1.52	2.29
P_2O_5	0.07	0.07	0.08	0.08	0.09	0.09	0.10	0.11	0.10	0.15
Cr_2O_3	0.22	0.23	0.25	0.26	0.28	0.39	0.32	0.32	0.32	0.47
Temp (°C)	1356.6	1345.7	1322.6	1295.5	1263.3	1224.2	1190.9	1180.7	1189.5	1139.32
Density ($g.cm^{-3}$)	2.619	2.619	2.618	2.617	2.616	2.614	2.612	2.611	2.612	2.60
Lg(fO_2)	-6.63	-6.81	-7.03	-7.29	-7.62	-8.03	-8.41	-8.52	-8.42	-9.02
Mg#_melt	90.82	91.91	91.17	90.28	89.19	87.81	85.99	83.46	81.3	71.38
Fo_ol	-1	-1	-1	-1	-1	-1	-1	-1	-1	-1
Mg#_Opx	90.82	89.97	88.95	87.68	86.05	83.88	81.5	79.83	81.30	69.94
An#_Pla	-1	-1	-1	-1	-1	-1	73.79	72.15	73.56	66.26
Melt %	99.99	94.999	89.996	84.992	79.995	74.998	69.997	64.998	71.71	45.99
Opx %	0.01	5.0009	10.004	15.008	20.005	25.002	30.003	35.003	28.28	35.38

**Composition re-calculated by Petrolog to normalise starting composition. # Residual Magma at the base of the Mafic Norite postulated to be parental to Marginal Zone rocks. ## Residual magma remaining at the top of Marginal Zone.*

6.3.2a. Marginal Zone magma

The modelling showed that the B1-magma at 20-2 kbars is in equilibrium with En_{92-90} orthopyroxene at 1366° C (2 kbars pressure). Orthopyroxene is the sole liquidus mineral phase until plagioclase joins the cotectic at 1190° C with the compositions of An_{74-73} after approximately 28-31 % crystallization (Table 6.2). The co-existing orthopyroxene compositions at the stage where plagioclase joins the cotectic as predicted by Petrolog are En_{82-81}. This cotectic assemblage is comparable with the compositions measured at the base of Mafic Norite in the CH6 drill core (En_{81-80} and An_{78-77}) except the measured plagioclase compositions are more primitive compared to the calculated compositions. The magma at this point contains about 6.0 wt. % MgO and 56.5 wt. % SiO_2. These oxide concentrations are consistent with the compositions of a basaltic andersite. Clinopyroxene (pigeonite) is largely a post-cumulus phase and it crystallizes at a point where the magma reaches the peritectic point at 1165° C. This order of crystallization and the compositions are acceptable and comparable to those observed in the Marginal Zone succession of the CH6 section.

After 52-54 % crystallization, the residual liquid composition is estimated to have 3.6 wt. % MgO and is enriched in SiO_2 (59.45 wt. %) with the mineral compositions being En_{71} and An_{67}. The model output for the 40-54 % crystallization range shows pigeonite co-existing with orthopyroxene. Inverted Pigeonite is observed in the CH6 core as a cumulus phase with thick broken clinopyroxene lamellae in orthopyroxene host (Chapter 4). The top of the Marginal Zone shows mineralogy that coincides with the mineralogy predicted by the model after approximately 50-54 % crystallization of the B1-magma of Wilson (2012). This suggests that the Marginal Zone compositions observed in CH6 can be produced at 2 kbars after 30-55% crystallization, corresponding to temperatures between 1190-1139° C. The complete model output data are shown in Appendix D and the magma

composition proposed here for the Marginal Zone is shown in Table 6.2 and column 8 in Table 6.3.

The modelled parental composition for the Marginal Zone magma is significantly depleted in MgO compared to B1-magmas previously postulated to be responsible for the Lower and Marginal Zone rocks through quenching or other mechanisms (see Chapter 1). In earlier studies, the Marginal Zone was believed to be a chill phase of the Lower Zone magma whose composition is tholeiitic basalt to basaltic andesite. Earlier chapters of the present work have already shown this to be invalid since the Marginal Zone is cumulus in nature showing ample evidence of fractionation, and in itself does not represent a chilled liquid (Fig. 6.3). The postulated magma composition modelled from the fractionation of the B1-magma (Wilson, 2012) produces mineral phases comparable to the mineral phases observed in CH6 as shown in Fig. 6.3.

The fractionation of primitive orthopyroxene from the B1-magma to form part of the BUS (Wilson and Chunnett, 2010) drives the magma to progressively more evolved compositions resulting in the liquid postulated to be responsible for Marginal Zone (Red-border and green-filled hexagon in Fig. 6.3). The present study shows that, unlike the work of Eales and Costin (2012), the Marginal Zone was produced by a basaltic andesite liquid formed by the fractionation of primitive orthopyroxene observed in the BUS of Wilson and Chunnett (2010). The BUS orthopyroxene compositions could have started crystallizing at pressures of about 20 kbars (about 60 km depth). This is important to emphasise because it supports the previous works that suggested the Bushveld Complex could have been emplaced as crystal charged mushes. The prolonged evolution of the B1-magma eventually would produce the mineral compositions consistent with the Marginal Zone.

This study suggests that the cumulate rocks in the Marginal Zone formed by steady and uninterrupted differentiation of the postulated magma (Table 6.2) and accumulation of plagioclase and orthopyroxene mixed with variable amount of trapped liquid. The accumulation process, a physical phenomenon, is responsible for the trends observed in CH6 and of importance here is the enigmatic and reversed plagioclase compositional changes compared to the orthopyroxene (discussed in section 6.3.1b).

The mixing of the orthopyroxene, plagioclase and liquid components to form the CH6 Marginal Zone succession is represented by the green triangle in Fig. 6.3. Very little contribution to the whole-rock composition from the liquid (as trapped liquid) is predicted by the triangle. This is in line with the observation that the post-cumulus clinopyroxene in the Marginal Zone is typically less than 15-10 volume % of the whole-rock composition. Since there is no evidence of complete fractionation of the liquid inside the Marginal Zone chamber (supported by the absence of complete granophyric compositions, associated with the zone), there must have been residual liquid ponding at the top of the Marginal Zone cumulates inside the chamber prior to the emplacement of the LZa magma (B1-magma). The proposed residual (composition after 54 % crystallization in Table 6.2) magma must have either been expelled from the chamber or mixed with the primitive B1-magma to produce a different liquid composition that could have continued to produce mineral compositions different from the Marginal Zone succession.

In this work, the mixing of fresh B1-magma and the residual magma from the Marginal Zone is postulated to responsible for the LZa cumulates. There is no evidence of extrusive rocks of mafic Bushveld Complex-type compositions and the possibility of this residual magma being expelled from the magma chamber cannot be supported by field evidence. Nevertheless, the expulsion of magma from the chamber has been previously proposed (Cawthorn and Walraven, 1998) and occasional expulsion of magma is a possibility,

which might have occurred to a lesser extent during the emplacement of the Marginal and lower Zones.

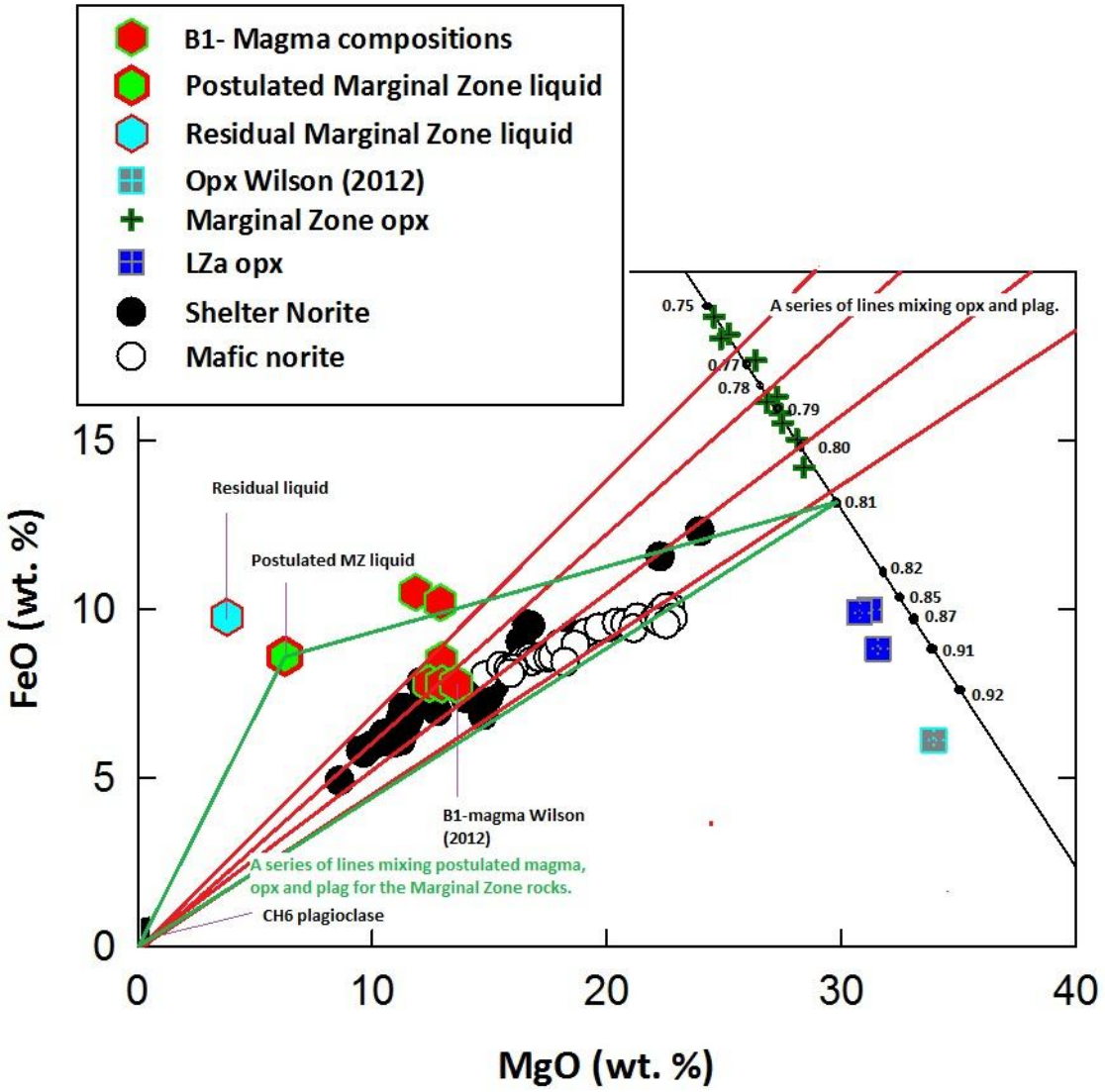

Fig. 6.3: MgO vs. FeO for the Marginal Zone rocks, showing the orthopyroxene, whole-rocks and postulated magma compositions based on modelling using the B1-magma of Wilson (2012). Red lines represent mixing-lines between orthopyroxene compositions and plagioclase. Solid black line represents extrapolated orthopyroxene compositions based on the measured Marginal Zone orthopyroxene compositions (green crosses), inclusive of both Mafic Norite and Shelter Norite.

6.3.2b. Reverse Plagioclase compositions

The compositions of co-existing (cotectic) mineral phases in normal (uninterrupted) fractionation are expected to become simultaneously evolved. This principle is what underpins predicted crystallization compositions of Petrolog (and other similar programs) and composition calculations. As mentioned above, the observed Mg# and An# compositions in CH6 are comparable to the values calculated by Petrolog from the progressive differentiation of B1-magma at 2 kbars. However, the measured An# compositions from the CH6 section are reversed from the expected 'normal' fractionation trend (Fig. 6.4). That is, the observed plagioclase compositions in CH6 become more primitive (more calcic) with stratigraphic height instead of becoming (more sodic) evolved as predicted by the Petrolog modelled compositions (see chapter 5).

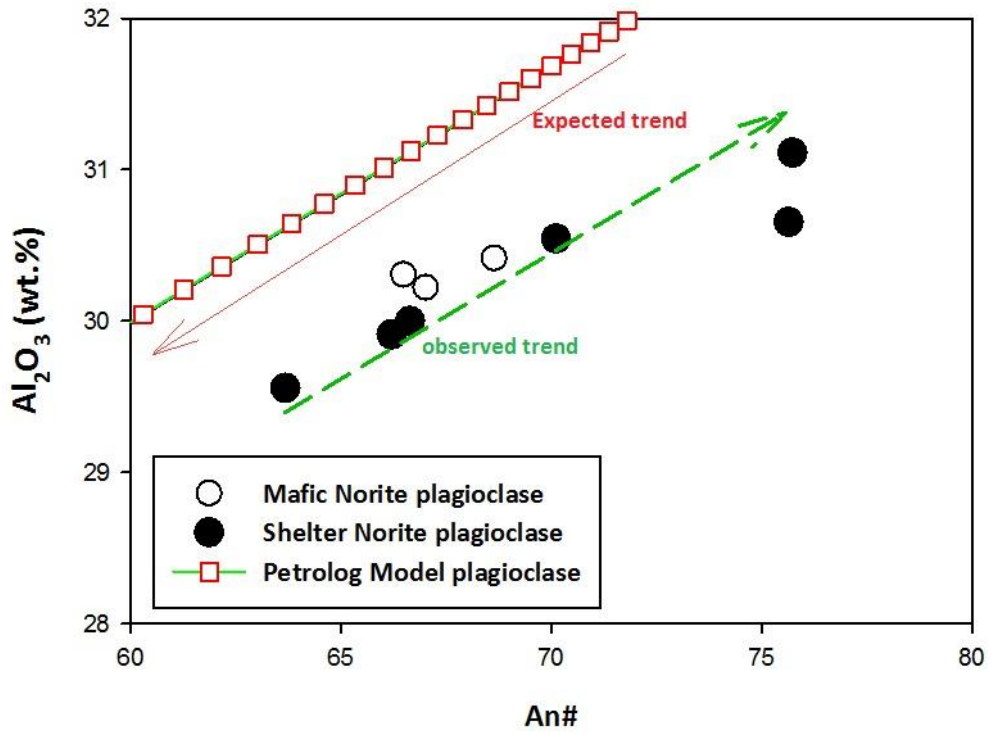

Fig. 6.4: Al_2O_3 vs. An# plot showing the contrasting modelled and the measured plagioclase compositional trends.

In the same interval, co-existing orthopyroxene (and whole rock) compositions become progressively evolved (more Fe-rich) starting with relatively primitive compositions at the bottom of the Mafic Norite to more evolved orthopyroxene at the top of the Shelter Norite. On the other hand, the plagioclase compositions increase from the Mafic Norite sequence through to the Shelter Norite. The Mg# and An# of co-existing orthopyroxene and plagioclase in the Shelter Norite evolve in opposing directions. The orthopyroxene Mg# evolution is in agreement with normal fractionation trends whereas the plagioclase composition goes against normal differentiation (Fig .6.2).

The disequilibrium between co-existing mineral phases cannot be a chemically driven process in the magma. The same liquid composition cannot simultaneously stabilise mineral compositions that have opposing thermodynamic evolution. This orthopyroxene and plagioclase relationship is interpreted as physical separation and different responses to the accumulation processes that must have occurred in the chamber controlled by the density of the evolving magma. This enigmatic relationship between the co-existing orthopyroxenite and plagioclase highlights the cumulus nature of the Marginal Zone rocks versus the prevalent historic interpretation that these rocks represent a 'chill phase' formed by quenching of Lower Zone magma.

6.3.3. Lower Zone magma

The Lower Zone rocks in the CH6 section (LZa in Fig. 6.2) are more primitive than the Marginal Zone rocks with higher whole rock and orthopyroxene Mg#, suggesting that it formed from a relatively more primitive magma. However, the orthopyroxene compositions measured in CH6 cannot be produced from the B1-magma composition without the prior extraction of more primitive orthopyroxene. Since this study has already shown that the LZa in CH6 is a correlative of the Lower Orthopyroxenite Subzone

described at Olifants River Trough, similarly the compositions presented by Cameron (1978) cannot have been directly produced directly from B1-magma, not even at 2-3 kbars. The boundary zone between the Marginal Zone and Lower Zone at Olifants River Trough is marked by an olivine-bearing unit at the base of the so-called 'Basal Subzone' of Cameron (1978). The equivalent of the boundary zone at Clapham Trough in this work is referred to as the Transition Pyroxenite described in earlier sections this study (Chapters 2-4). The Transition Pyroxenite is not olivine bearing in the CH6 drill core but magnesite rubble and weathered olivine rocks were observed in the field. The Transitional Pyroxenite is a '*mix-textured and patchy'* feldspathic pyroxenite (Chapter 2-5). This unit is interpreted in this work to represent mixing between two different magmas (possibly crystal mushes) of different compositions.

The orthopyroxene compositions reported for the Lower Orthopyroxenite Subzone are in the range En_{89-82} (Cameron, 1978). These data are comparable to the measured compositions in the present study (En_{87-82}). By contrast, the B1-magma would have been in equilibrium with En_{92-90} orthopyroxene. The liquid parental to the Lower Orthopyroxenite Subzone (LZa) at the Clapham trough must have been an evolved liquid descendent of the B1-magma. The present study suggests mixing of primitive B1-magma with the siliceous residual liquid postulated to have been at the top of the Marginal Zone to produce a slightly evolved magma composition. The liquid composition postulated to be parental for the LZa in the CH6 section is shown in Table 6.3. This study suggests that the emplacement of the Lower Zone magma interrupted on-going differentiation in the Marginal Zone, and mixing between the primitive B1-magma and residual liquid produced an intermediate magma composition (Table 6.3). Magma mixing in layered chambers is commonly used to explain the general whole-rocks and mineral compositions, including the formation of economic horizons, especially in the Bushveld Complex (like Irvine, 1977; Eales and Cawthorn, 1996; Naldrett *et al*., 2009).

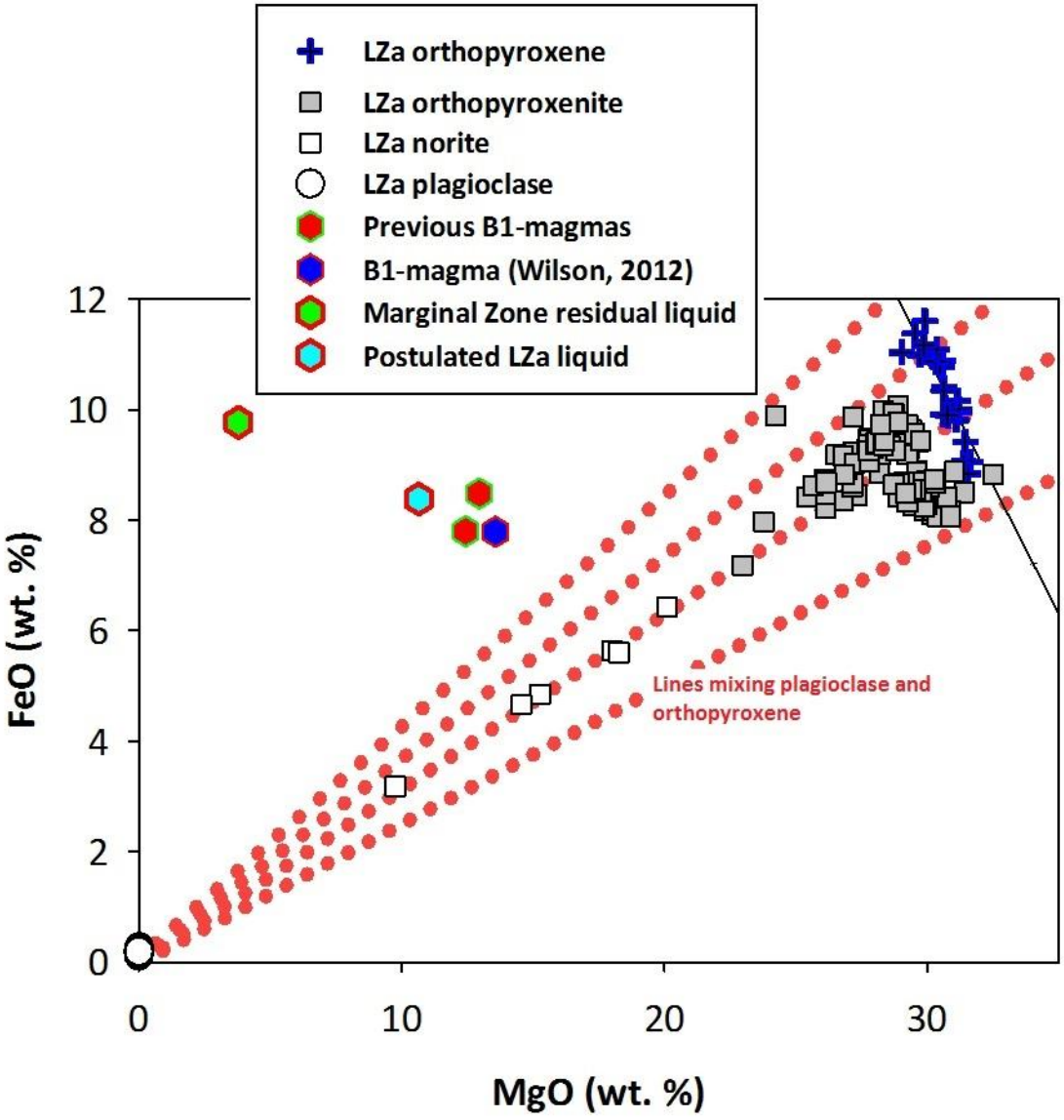

Fig 6.5: MgO vs. FeO for the Lower Orthopyroxenite Subzone (LZa), showing the orthopyroxene, whole-rocks and postulated magma compositions based on modelling with mixing between the B1-magma of Wilson (2012) and the evolved residual liquid predicted for the Marginal Zone. Solid black line represents the extrapolation of orthopyroxene compositions.

Table 6.3: Summary table of the Petrolog model output for the Lower Orthopyroxenite Subzone (LZa) as described in CH6.

	Possible starting magma compositions*					Postulated LZa magma	Residual liquid after LZa crystallization			
	10%	20%	30%	40%	50%	**30:70**	6%	10%	15%	20%
SiO_2	56.43	56.76	57.1	57.43	57.86	**57.1**	56.92	56.99	57.11	57.26
TiO_2	0.30	0.32	0.34	0.36	0.38	**0.34**	0.34	0.36	0.38	0.40
Al_2O_3	11.43	11.55	11.66	11.78	11.92	**11.66**	12.08	12.46	12.97	13.54
Fe_2O_3	1.54	1.55	1.56	1.57	1.32	**1.56**	1.23	1.21	1.18	1.17
FeO	8.00	8.21	8.41	8.62	9.08	**8.41**	8.64	8.72	8.77	8.75
MnO	0.19	0.20	0.22	0.24	0.256	**0.22**	0.21	0.22	0.24	0.25
MgO	12.58	11.58	10.58	9.58	8.596	**10.58**	10.25	9.29	8.00	6.62
CaO	6.41	6.47	6.53	6.59	6.66	**6.53**	6.86	7.13	7.51	7.91
Na_2O	1.51	1.58	1.65	1.73	1.81	**1.65**	1.68	1.76	1.86	1.98
K_2O	1.17	1.30	1.42	1.55	1.67	**1.42**	1.38	1.45	1.53	1.63
P_2O_5	0.08	0.09	0.09	0.10	0.11	**0.09**	0.09	0.10	0.10	0.11
Cr_2O_3	0.24	0.27	0.29	0.32	0.34	**0.29**	0.29	0.30	0.32	0.34
Temp (°C)	1351.6	1336.0	1319.3	1301.04	1281.10	**1319.3**	1307.7	1285.60	1253.33	1214.47
Density ($g.cm^{-3}$)	2.62	2.61	2.61	2.61	2.60	**2.61**	2.61	2.61	2.61	2.60
$Lg(fO_2)$	-6.75	-6.90	-7.06	-7.24	-7.44	**-7.06**	-7.17	-7.39	-7.72	-8.14
Mg#_melt	90.03	89.03	87.93	86.64	85.13	**87.93**	87.67	86.5561	84.78	82.43
Fo_ol	-1	-1	-1	-1	-1	**-1**	-1	-1	-1	-1
Mg#_Opx	90.03	89.03	87.93	86.64	85.13	**87.93**	88.38	87.88	87.17	86.
An#_Pla	-1	-1	-1	-1	-1	**-1**	-1	-1	-1	-1
Melt %	99.99	99.99	99.99	99.99	99.99	**99.99**	93.996	89.99	84.99	79.99
Opx %	0.01	0.01	0.01	0.01	0.01	**0.01**	6.00	10.04	15.00	20.0

*Compositions are determined by mixing the residual liquid from Marginal Zone and B1-magma.

The liquid composition proposed to be in equilibrium with the LZa orthopyroxene can be produced by mixing approximately 80-70 % of B1-magma and 20-30 % residual liquid (Table 6.3, Fig. 6.5). The resulting liquid is in equilibrium with orthopyroxene composition of En_{89-87}. This orthopyroxene composition is appropriate for the Lower Orthopyroxenite Subzone at Clapham Trough and other areas in the eastern Bushveld Complex described by Cameron (1978), and Hulbert and Sharpe (1985). The most primitive orthopyroxene compositions in the Clapham Trough were measured to be En_{87-86} (Chapter 5).

The postulated magma (30:70 mixture of Marginal Zone residual liquid and b1-magma) would need to undergo about 7-8 % fractionation to be in equilibrium with orthopyroxene compositions of En_{87-86}. Kruger (2005) and Clarke *et al.*, (2009a) proposed that the feeders of the Lower Zone are the near the Thabazimbi-Murchison Lineament (TM) and the Burgersfort Bulge. These authors documented compositional variations and changes in the thickness of rock units away from the proposed feeder zones. The present study postulates that the magma modelled to be parental to the Lower Zone A (i.e. Lower Orthopyroxenite Subzone correlatives, Tables 6.3 and 6.4) was emplaced near the TM, forming the relatively primitive rocks described at the Olifants River Trough by Cameron (1978). Cooling and fractionation occurred during lateral expansion of the magma chamber such that the magma parental to the Clapham Trough section had undergone through additional fractional crystallization while spreading inside the chamber. Hence, relatively evolved compositions are observed in the Clapham Trough compared to the Olifants River Trough. Thus, according the work of Clarke (2009a), the LZa at Clapham Trough in this case is interpreted as distal facies of the Lower Orthopyroxenite Subzone (i.e. proximal facies) of Cameron (1978).

The postulated liquid composition for the LZa section of the eastern Bushveld Complex contained lower MgO than the B1-magma composition. This proposed parental liquid contained about 10.59 wt. % MgO and 57.1 wt. % SiO_2, as shown in Table 6.4 along with previous magma estimates and in Fig. 6.5 with whole-rocks and orthopyroxene. The compositions of cumulate rocks formed in the LZa appear to be solely controlled by the accumulation of orthopyroxene with the appropriate compositions with little trapped liquid (interstitial plagioclase in thin section) involved.

Table 6.4: Proposed Parental magmas for the Lower Orthopyroxenite Subzone.

Wt %	1	2	3	4	5	6	7	8
SiO_2	56.07	55.70	55.24	55.74	55.90	56.09	**57.1**	**56.55**
TiO_2	0.34	0.36	0.38	0.34	0.34	0.28	**0.34**	0.39
Al_2O_3	11.47	12.74	12.13	11.82	11.80	11.31	**11.66**	**14.33**
Fe_2O_3	1.58	1.00	1.57			1.53	**1.56**	1.09
FeO	8.48	7.80	7.79	10.50	10.20	7.79	**8.41**	**8.61**
MnO	0.18	0.09	0.15	0.18		0.17	**0.22**	0.24
MgO	12.96	12.44	12.97	11.85	12.90	13.58	**10.59**	**6.28**
CaO	6.68	6.96	6.84	6.50	6.80	6.35	**6.53**	8.59
Na_2O	1.68	2.02	1.75	1.63	1.70	1.43	**1.65**	2.00
K_2O	0.80	1.03	0.88	0.98	0.90	1.05	**1.42**	1.47
P_2O_5	0.07		0.01	0.08		0.07	**0.09**	0.11
Cr_2O_3	0.20		0.16		0.15	0.22	**0.29**	0.31
NiO					0.05			
TOTAL	100.51	100.14	99.87	99.62	100.74		99.49	99.78
$Mg\#_{melt}$	0.73	0.74	0.75	0.67	0.69	0.79	0.69	0.54

Column 1- B1-magma proposed by Hulbert and Sharpe (1985), 2- Experimental parental magma proposed by Cawthorn (1981) , 3- Davies (1982) , 4- Barnes et al., (2010) , 5- Eales and Costin (2012), 6- B1-magma of Wilson (2012) , 7- This study Lower Zone parental magma, 8- This study, liquid proposed for the Marginal Zone. The compositions presented in this study for the Lower and Marginal Zone (columns 7 and 8) are more evolved than previous compositions.

The most evolved (En_{84-82}) orthopyroxene compositions in the CH6 section are strictly associated with the interlayered norite units described in earlier chapters, with the lowest Mg# measured near the centre of these plagioclase-rich zones (Fig. 6.2). The present study proposes a brief period of relatively prolonged fractionation and super cooling of the postulated parental liquid composition inside the magma chamber to produce the orthopyroxene compositions in the interlayered norite units. This interpretation is in line with the explanation of the norite layers of the Lower Zone by Cawthorn and Walraven (1998). The volume of magma that would have been required to produce the observed cumulates in the Lower Zone would have been enormous. The interlayered norite layers are interpreted as the volume of magma that was at the top of the magma chamber prior to emplacement of new magma as the magma chamber increased in size.

6.4. Summary and Discussion

The modelled compositions presented above are qualitative estimates, and illustrate alternative magma compositions to those previously proposed for at least the Marginal Zone and the Lower Orthopyroxenite Subzone sequences based on the section studied at the Clapham Trough (CH6). Furthermore, they allow re-evaluation of the mechanism by which the Lower Orthopyroxenite Subzone and Marginal Zone (at least in the eastern Bushveld Complex) formed, taking into account the unexposed (most primitive) Basal Ultramafic Unit and the most primitive orthopyroxene compositions from the work of Wilson (2012).

There are a number of assumptions used in the modelling above. First, the starting B1 parental magma composition from Wilson (2012) is the only magma subjected to differentiation and the subsequent mixing to produce the derivative magmas proposed to be responsible for the CH6 section. This assumption is made on the widespread preponderance

of B1-type magmas, and that the komatiite-type magma composition presented by Wilson (2012) was of limited involvement in this section. Second, the olivine-rich units in the Basal Ultramafic Sequence were most likely produced by injection of crystal mushes derived from the higher-Mg composition (i.e. the komatiitic magma). Third, the differentiating B1-magma was not modified by any other geochemical processes like mixing or contamination in any significant manner to affect the bulk compositions of the Marginal Zone. However, this in itself is a simplification considering the numerous xenolithic fragments that were identified in the field (Chapters 2-3). Lastly, the relatively 'cool' and evolved liquid remaining from the fractionation in the Marginal Zone chamber mainly ponded at the top of the cumulate pile and mixed with new B1-magma (at an estimated 30:70 mixing ratio) to produce the appropriate orthopyroxene compositions for the Lower Orthopyroxenite Subzone (i.e. LZa correlative at Clapham Trough).

Tables 6.2, 6.3 and 6.4 show the relevant compositions and their comparisons with previous estimates of parental magmas for the Marginal and Lower Zone sections of the CH6 section. The compositions observed in CH6 could not have been directly produced by the B1-magma since it is MgO-rich and is in equilibrium with En_{92-90} orthopyroxene, as mentioned above. The magma postulated to be parental to the LZa (column 7 of Table 6.4) produce comparable orthopyroxene compositions to the measured orthopyroxene compositions in this work and earlier studies (see chapter 5, and Cameron, 1978). The magma responsible for the LZa section (i.e. the Lower Orthopyroxenite Subzone) must have initially contained about 10.58 % MgO, and must have been in equilibrium with orthopyroxene compositions (En_{89-87}) described in the Olifants River Trough. About 7-8 % fractionation must have occurred during lateral expansion of the magma chamber, such that the modelled magma composition reached the Clapham Trough containing about 9 wt. % MgO and 57.3 wt. % SiO_2, and in equilibrium with orthopyroxene compositions of En_{87-86}.

The Marginal Zone described in the present work conformably overlies the BUS without abrupt compositional variations, showing that they are related through differentiation (Wilson and Chunnett, 2010). The Mg# and whole-rocks MgO progressively become evolved with increasing stratigraphic height in CH6. The chemical variations are coupled with variable modal abundances of cumulus phases. Mainly increasing plagioclase and decreasing orthopyroxene abundances. The continuous Mg# decrease and modal variations suggest uninterrupted differentiation of the magma occupying the Bushveld Complex chamber at the time the Marginal Zone was forming. The Marginal Zone magma crystallised and accumulated in a period of relative quiescence. During this time, the Bushveld Complex chambers were relatively dormant and a temporarily closed system is envisaged. The postulated parental liquid composition for the Marginal Zone section of the Bushveld Complex contains approximately 6.05 % MgO and 56.7 wt. % SiO_2. This composition is of basaltic andesite affinities and it is more appropriate to account for the formation of the relatively evolved and differentiated Marginal Zone minerals and rock compositions presented in Chapter 5. The formation of the Marginal Zone from an evolved liquid (derived from B1-magma) is a significant departure from the historic interpretation that these rocks represent a chill phase. The Marginal Zone rocks are cumulate as supported by field evidence, CH6 drill-core data, and geochemistry. Furthermore, the parental magma model presents an alternative explanation of the compositional variations and formation of the Marginal Zone rocks.

However, the modelling predicts (as expected) mutually evolving Mg# and An# for co-existing orthopyroxene and plagioclase. The data presented in Chapter 5 show that the plagioclase compositions are reversed in the Shelter Norite, contrary to normal fractionation as prescribed by thermodynamics and evolving magma compositions. Instead, the plagioclase crystals are not the appropriate cotectic compositions for the co-existing orthopyroxene

crystals and whole-rocks evolution trends. The accumulation of orthopyroxene and mixed with 'foreign' plagioclase is a physical phenomenon that engineered the observed reverse An# values. That is, the accumulation processes that formed the Marginal Zone resulted in a compositional 'mismatch' between plagioclase and orthopyroxene compositions that did not crystallise together (mixing of mineral phases). That is, the cotectic mineral phases were physically separated during accumulation to form the observed trends in CH6. The interpretation and the model predict that the plagioclase at the bottom of the Shelter Norite must be cotectic equivalent of the orthopyroxene at the top of the Shelter Norite and vice versa. The subsequent chapter will discuss the reverse compositional variation and general accumulation processes further based on the CH6 data and drawing similarities and differences throughout the eastern Bushveld Complex.

Chapter 7

Geochemical Modelling: Constraints on Primary Processes.

This study showed that the whole-rock compositional variations are related to the modal abundances and compositions of the cumulus mineral phases making up the rock sequence. That is, the concentration of any element is dependent on the amounts and compositions of mineral phases constituting the rock together with variable amounts of trapped melt which in turn crystallised to form late-stage phases. In turn, the compositions and (indirectly) the modal abundances of the mineral phases present in a rock are related to the composition of the parental magma; and the accumulation processes that occurred within the magma chamber influence the whole-rock compositions. This section uses trace elements to address the relationship of the CH6 section with the proposed parental magma compositions and the accumulation (magma chamber) processes that were dominant inside the Bushveld Complex chamber during the formation of the Lower Zone A and the Marginal Zone.

Plagioclase and orthopyroxene are the dominant phases in the Marginal and Lower Zone rocks described in the CH6 section (chapters 2-4). The concentrations of the elements that are compatible with respect to plagioclase and orthopyroxene are related to their compositions (i.e. plagioclase or orthopyroxene) and modal abundance at any point in the studied Clapham Trough section (CH6). On the other hand, the concentration of the elements that are incompatible in either plagioclase or orthopyroxene would have been controlled by the amount (and composition) of trapped liquid, which is represented by the post-cumulus phases present. If the amount of trapped liquid is very small, low concentrations of incompatible elements will be measured in the whole rock compositions. The corollary is that low concentrations of incompatible trace elements in the bulk rock composition suggest the rock

was formed with low amounts of trapped liquid. The variation of the incompatible trace elements in the rock is indicative of the variations of the amount and/or composition of the trapped liquid content. The amount of trapped liquid in any rock is determined by the predominant accumulation processes in the chamber (McBirney and Hunter, 1995). Thus, constraints on the amount of trapped liquid prior to post-cumulus processes that could have altered the rock are essential to predicting the primary accumulation processes.

The compositions of the cumulus and post-cumulus phases vary with the composition of the differentiating magma. As differentiation of the magma proceeds, trace elements either get enriched or depleted in the remaining (residual magma in a closed system) magma as a function of their compatibility with respect to the cumulus phases (i.e. partition coefficients, D). Eales *et al*. (1986) assumed that even if the compositions of the elements will change in response to differentiation processes, the ratio of trace elements shows progressive change in the mineral phase, hence the whole rock. Furthermore, sharp/abrupt changes in the ratios are indicative of changes in the magma composition and/or emplacement of new/primitive magma. Seabrook (2005) showed that the latter assumption was an over simplification and that the accumulation processes affect the modal abundances of the cumulus phases (thus also the whole rock geochemistry) more significantly than the magma composition. In turn, this affects the variations of the concentrations of trace elements that are measured in the whole rock. The result is that changes in trace element ratios in the whole rock compositions do not necessarily reflect changes in the magma compositions but more so the accumulation processes that are prevalent in the magma chamber.

7.1. Orthopyroxene fractionation

As already shown, the proposed parental magma compositions are capable of producing the observed CH6 mineral assemblages and the compositions observed in the CH6 section between 4-2 kbars pressure (Chapter 6). It is commonly accepted that the currently exposed rocks of the Bushveld Complex accumulated between 3-2 kbars (Chapter 1 and references therein). In addition, the orthopyroxene compositions can be reasonably produced, under the correct temperature and pressure, from as deep as 60 km (i.e. 20 kbars). This supports the theories that the Bushveld Complex may have been emplaced as crystal-charged mushes carried by the magma from depth (Eales and Cawthorn, 1996; Mondal and Mathez, 2007; and Eales and Costin, 2012; Roelofse and Ashwal, 2012). Therefore, the assumption of equilibrium between the magmas and orthopyroxene crystals is not misguided since there must have been a great deal of time of crystal-liquid association between formation and accumulation. The assessment of the trace element compositions of the magmas involved in the CH6 section, this study focuses on these ratios: Cr/MgO, Cr/Ni, Cr/Co, Cr/V, Cr/Ti, Cr/Y, Cr/Tot REE, Co/V, Ti/Y and Th/U.

7.1.1. Cr/MgO ratio

Cawthorn (1999) and Cawthorn (2007) showed that there is a positive relationship between Cr and MgO content in the whole-rocks and orthopyroxene compositions. MgO and Cr are highly compatible with respect to orthopyroxene, and MgO is a major component of enstatite (orthopyroxene Mg-end member). There is an overall positive correlation between the orthopyroxene Cr and MgO concentrations and therefore also the whole rock MgO compositions in the CH6 section (chapter 5). The orthopyroxene Cr/MgO ratio is especially useful because both Cr and Mg are depleted together as the magma progressively crystallises

orthopyroxene. Cawthorn (1999) used this principle to distinguish Critical (CZ) and Main (MHZ) Zone magmas in the Bushveld Complex chamber. The present work applies this investigative technique to evaluate the changes in the Cr and MgO concentrations of the cumulus phases and the whole rock to estimate the variations in the composition of the liquids (i.e. parental magmas) that must have been in equilibrium with the Marginal and Lower Zones of the Clapham Trough section (CH6 section). The liquid Cr and MgO can be calculated using partition coefficients, assuming equilibrium between the mineral phases and the magma. The equation below which defines the bulk partition coefficient of a trace element in a rock that consists of a number of different coexisting phases is used to calculate the Cr liquid composition.

$$\text{Bulk } \mathbf{D_{El}} = \sum x_i D_{El} \qquad (7.1)$$

Where x_i is the weight fraction of mineral phase *i* and D_{El} is the partition coefficient of the element (Cr in this case) in mineral phase *i*. Plagioclase is a cumulus in the LZa specifically in the horizons, the interlayered (marker) norite unit described in (Chapters 2-4). Cr is incompatible with respect to plagioclase and its partition coefficient in olivine is negligible compared to orthopyroxene. Moreover, olivine is restricted to specific horizons for most part of the Lower Orthopyroxenite Subzone (i.e. LZa). The CH6 section does not have (cumulus) chromite and clinopyroxene is a post cumulus phase throughout the CH6 section (chapter 4), thus the Cr content in the clinopyroxene is largely related to the trapped liquid and to some extent (possibly) post-cumulus re-equilibration. However, the modal abundance of clinopyroxene is insignificant compared to orthopyroxene (even though the partition coefficient of Cr in clinopyroxene is higher compared to orthopyroxene, being approximately 10 according to Wilson, 1992) in the Clapham Trough section (CH6). Thus, the clinopyroxene contribution is less in the estimates of the liquid Cr content in this part of the Bushveld Complex stratigraphy. Taking into account these various considerations, the above

equation can be simplified to estimate the liquid Cr content from the orthopyroxene compositions. Equation 7.1 can be then replaced by the simple equation of the partition coefficient of Cr in orthopyroxene.

$$D = Cr_{Opx} / Cr_{Liq} \quad (7.2)$$

Therefore, the liquid Cr content is related to the orthopyroxene in the following manner

$$Cr_{Liq} = Cr_{Opx} / D \quad (7.2.1)$$

This equation is in the form of "method 1" used by Godel *et at*. (2011) in calculating estimated equilibrium concentrations of elements in liquid from which the analysed minerals crystallised. These authors pointed out flaws in using this equation in calculating concentrations of elements in the parental magma. However, discrepancies are only evident in incompatible elements and for the orthopyroxene-rich CH6 section, assuming that MgO and Cr concentrations are largely controlled by orthopyroxene is tenable, at least for the LZa section.

In the Marginal Zone, the magma must have been in equilibrium with orthopyroxene and plagioclase, with pigeonite joining the crystallization when the magma reaches a peritectic point. As shown in the modelling in chapter 6, the mineral phases in the Marginal Zone must have crystallised in an essentially closed system. Chemical equilibrium must have existed between the mineral phases during fractional crystallization. Furthermore, the physical separation of cotectic plagioclase and orthopyroxene, and trapped liquid must have retained the initial compositions of orthopyroxene and prevented post-cumulus re-equilibration proceeding to completion. Thus, the measured orthopyroxene compositions can be used to estimate representative parental magma compositions. Cawthorn (2007) used partition

coefficient of 3 for Cr in orthopyroxene similar to the work of Barnes (1986b) for Lower Zone rocks, unlike the 6.5 used in Seabrook (2005) for Critical and Main Zone rocks. This study prefers the former value which consistent with the work of Cawthorn (2007) and Barnes (1986b).

Table 7.1 shows a summary of average compositions of Cr and MgO for the parental magmas that must have been in equilibrium with the CH6 section. The data show that if the average Marginal Zone orthopyroxene contains 1300 ppm Cr (n=19), then the average magma composition that must have be in equilibrium with orthopyroxene of that composition is 440 ppm Cr. Similarly, if the average Cr composition in the Lower Zone (LZa) orthopyroxene is 2900 ppm Cr (n= 30), the liquid that would have been responsible for the observed sequence must have contained about 960 ppm Cr. This shows that the average Lower Zone A parental magma composition must have been at least twice as rich in Cr than the average Marginal Zone parental magma composition. This Marginal Zone parental magma Cr concentration is lower than the Cr concentration (770 ppm) predicted by the Rayleigh fractionation (equation 7.3, assuming D = 3) based on the Wilson (2012) B1-magma starting composition (C_0, i.e. 1576 ppm Cr) and 0.73-0.69 *F* (i.e. 28-31 % crystallization) in line with the modelling of the Marginal Zone parental magma in Chapter 6. This discrepancy in the two calculations for Cr in the parental magma is explained as some of the Cr budget is in the chromite-bearing units described in the BUS of Wilson and Chunnett (2010).

$$C_L/C_0 = F^{(D-1)} \qquad (7.3)$$

Table 7.1: Calculated average Cr and MgO contents for the Marginal and Lower Zone A of the CH6 section.

		Orthopyroxene Composition		D_{opx}	Liquid Composition	
		Marginal Zone	**Lower Zone**		**Marginal Zone**	**Lower Zone**
CH6 data	Cr (ppm)	1317	2877	3	439	959
	MgO (wt. %)	26.58	30.44	3.6	7.38	8.45
	Cr/MgO	49	95		27	52

Similar to the calculation of liquid Cr, the calculations show that the magma parental to the LZa rocks contained between 8.1-8.8 wt. % MgO (average 8.45 wt. %) assuming an enrichment factor of 3.6 similar to that estimated by Seabrook (2005). The modelled liquid composition in equilibrium with the entire LZa succession at Clapham Trough section lies between 7.40-8.99 wt. % MgO, derived from a parental magma modelled to have (maximum) 10.59 wt. % MgO (Chapter 6). The modelled parental liquid composition is consistent with the calculated liquid composition. The orthopyroxene Cr/MgO, orthopyroxene Cr and MgO compositional variations with depth in the CH6 section are shown in Fig. 7.2.

The Marginal Zone cumulates and orthopyroxenes show positive correlation trends between the Cr/MgO and MgO supporting the interpretation that the Marginal Zone succession was formed through systematic and continuous (uninterrupted) fractionation as shown by the orthopyroxene MgO and Cr compositions. There is no evidence in the Cr/MgO to suggest that there might have been a change in magma composition in the entire Marginal Zone succession. The Shelter Norite Cr/MgO is generally less than 60, whereas the Mafic Norite values generally range 60-80. In contrast, the LZa sequence does not show a strong correlation between Cr/MgO and MgO; instead, there is a clustered composition pattern (Fig. 7.1), which supports the interpretation that the LZa orthopyroxene crystals are relatively non-fractionated, at least with respect to major element content. However, there is a clear

distinction in the compositions of the orthopyroxene between the orthopyroxenite and the norite units, such that the latter hosts relatively evolved compositions, with subtle negative correlation between Cr/MgO and MgO in the latter cluster (Figs. 7.1-7.2). The Cr/MgO in the LZa is typically greater than 80, except in the interlayered norite horizons, where the values range 40-60. Relatively evolved orthopyroxene compositions associated with the norite units is consistent with the modelling of the LZa sequence in Chapter 6. That the norite layers reflect periods of temporal cessation of the magma emplacement, thereby allowing a period of relatively projected fractionation of super-cooled magma in the chamber. The subtle change in Mg# and Cr/MgO at the level 292 m in CH6 supports the textural and geochemical boundary between the Clapham and Rostock Orthopyroxenite sequences. This subtle change in composition is interpreted as emplacement of a relatively larger volume of new magma.

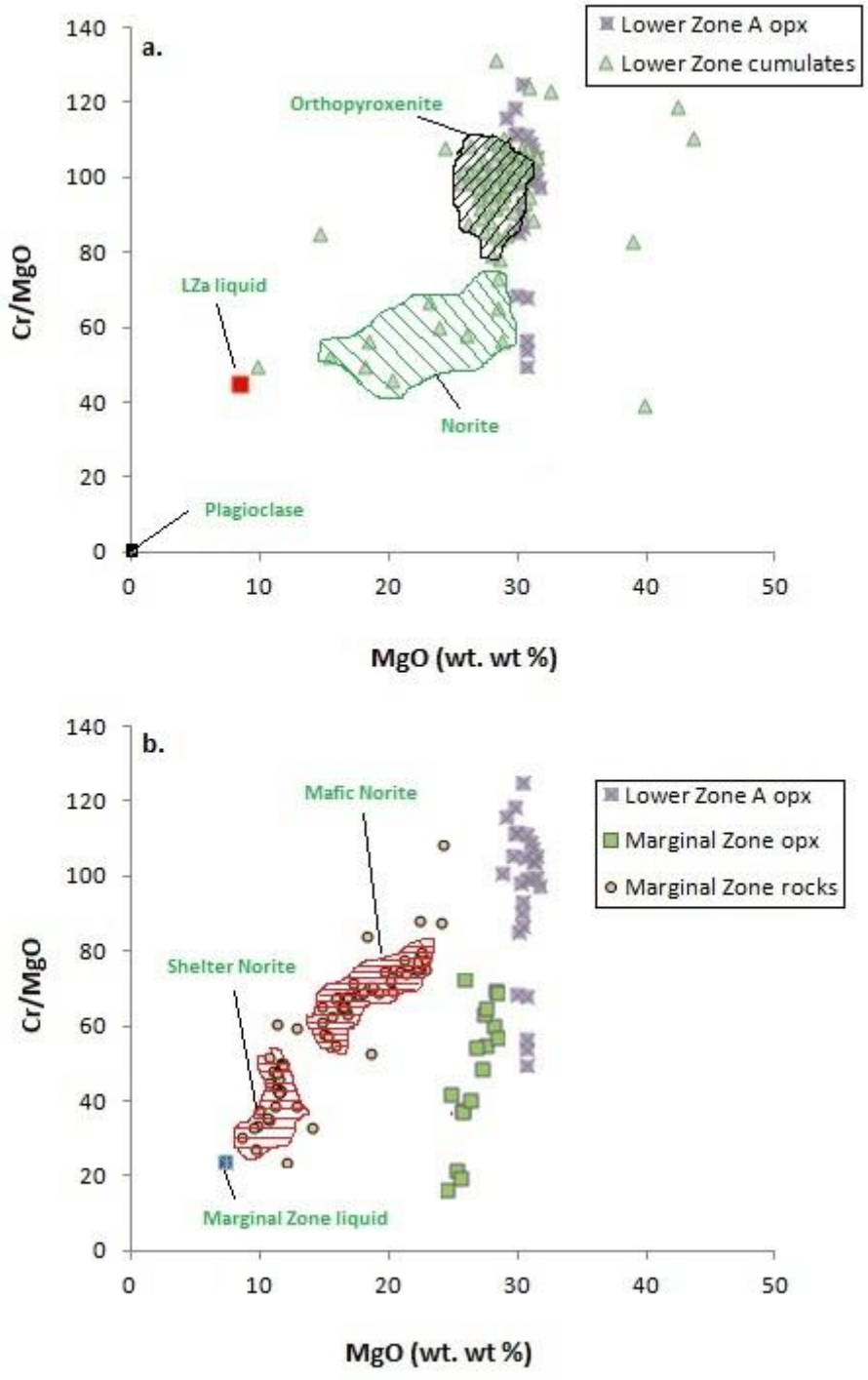

Fig. 7.1: Cr/MgO vs. MgO for the measured whole-rock and orthopyroxene compositions for the CH6 section. a. LZa cumulates, orthopyroxene compositions and calculated liquid composition (red square). b. Marginal Zone cumulates, orthopyroxene compositions and the calculated liquid composition (blue square) for the Marginal Zone.

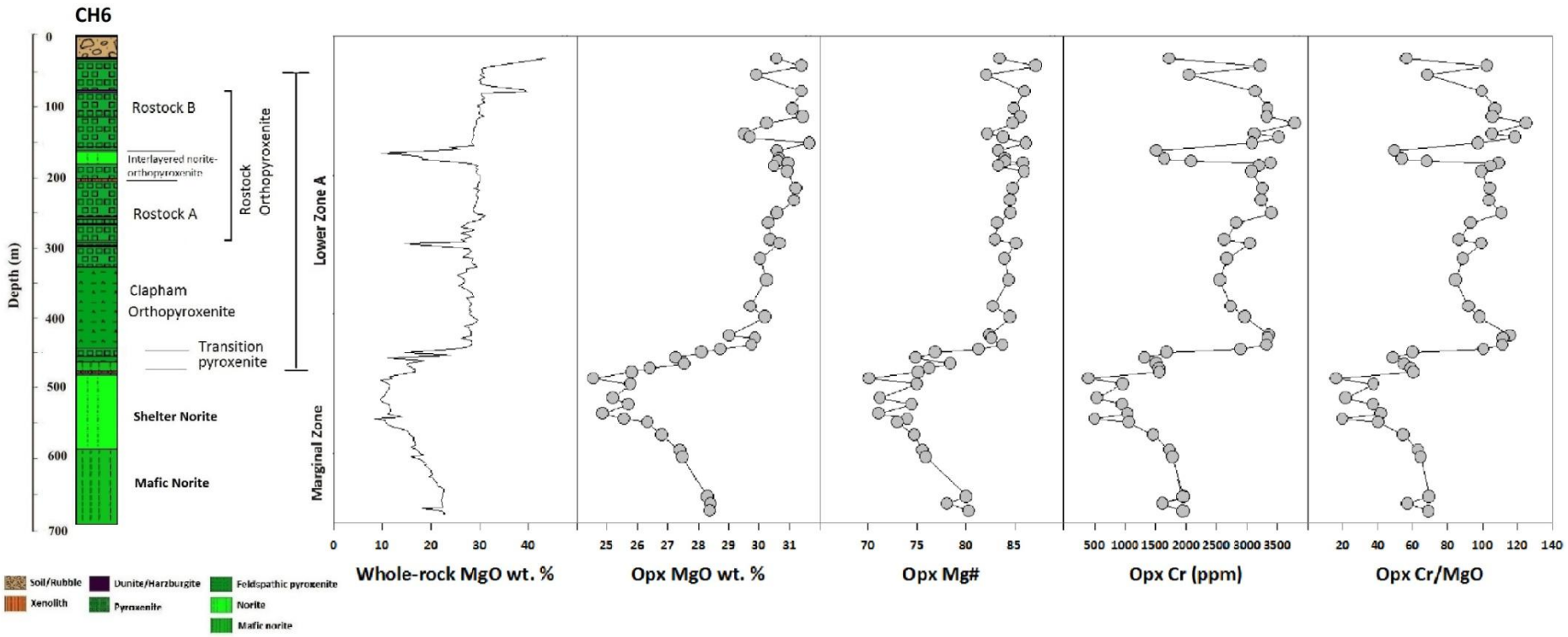

Fig. 7.2: Compositional variation of CH6 orthopyroxene. Marginal Zone compositions show systematic compositional variation compared to the near constant LZa orthopyroxene.

7.1.2. Other Trace Element ratios in Orthopyroxene

This section evaluates the CH6 through the detailed analysis of other trace element ratios shown in Fig 7.3. The majority of the orthopyroxene trace ratios are of the form Cr/X, where X represents the elements in the ratios displayed in Fig. 7.3. The reason for the use of these ratios is because of the high compatibility of Cr in orthopyroxene; and the positive correlation Cr has with Mg# (Chapter 5, Figs. 7.1-7.2). Thus, Cr is an appropriate proxy for changes in the composition (i.e. fractionation, which is not observed in the major elements concentrations) of orthopyroxene (similar to Cawthorn, 2007; and Tanner *et al.* 2014). Variations in the Cr/X have, therefore, bear implications of changes in the magma and fractionation patterns.

The trace element ratios shown in Fig. 7.3 corroborate data already presented above (i.e. Cr/MgO), such that there is evidence of continuous fractionation between the Mafic and Shelter Norite orthopyroxene compositions. The most evolved orthopyroxene compositions occur in the Shelter Norite as supported by the lower Cr/X ratios, with progressively decreasing Cr concentration in the progressively evolving orthopyroxene. In addition, the ratios in the Shelter Norite succession show evidence of cyclic compositional variation, also supporting the orthopyroxene Mg# which suggests the variable accumulation of cumulus minerals to form the cyclic compositional layering observed in the Marginal Zone (Fig. 7.3). Field observations also show strong evidence of modal layering in the Shelter Norite as noted in chapter 2 (but far more difficult to identify in fresh core samples). These data emphasise that the Marginal Zone consists of cumulus assemblages that must have accumulated inside the chamber to form the layered rocks observed both in the field and through the CH6 section. The coherently continuous geochemical trends shown in Figs 7.1-7.3 support the modelling interpretation that the entire Marginal Zone formed from a single batch of continuously evolving magma prior to the emplacement of the Lower Zone A magma. The

transition from the Marginal Zone rocks to the Lower Zone A (LZa) is marked by a gradual geochemical change over a narrow zone termed here the Transitional Pyroxenite. This gradual compositional reversal over a narrow interval is consistent with emplacement and mixing of two geochemically dissimilar magma compositions to produce the observed range of cumulus mineral compositions. This discontinuity is interpreted as having been formed by the mixing of (70-80 wt. %) primitive B1-magma and 20-30 wt. % of residual magma from the Marginal Zone.

The ratios Cr/Co, Cr/V, Cr/Ti and Cr/(Tot REE) show clear evidence of fractionation leading to the changes of Cr content within the Clapham Orthopyroxenite succession with lowest concentration occurring at the interlayered unit separating the Clapham and Rostock Orthopyroxenite packages (Fig. 7.3). There are subtle trace element ratio reversals above the norite separating the Clapham and Rostock Orthopyroxenite packages marking the boundary between the two packages. The Rostock Orthopyroxenite shows relatively constant composition with the exception to the units that are associated with the interlayered norite in the middle of the Rostock Orthopyroxenite succession (Fig. 7.3).

Both Th and U are highly incompatible high field strength elements (HFSE). In the evolving magma, they are controlled almost entirely by the trapped liquid content and as differentiation progressed, these elements were also enriched in the remaining magma. These elements are also relatively enriched by contamination from crustal rocks. Abrupt changes in the Th and U concentrations may reflect contamination and assimilation processes. The Th/U ratio in the orthopyroxene of the CH6 section is relatively constant, with the exception of the Marginal Zone, where higher Th/U values are observed.

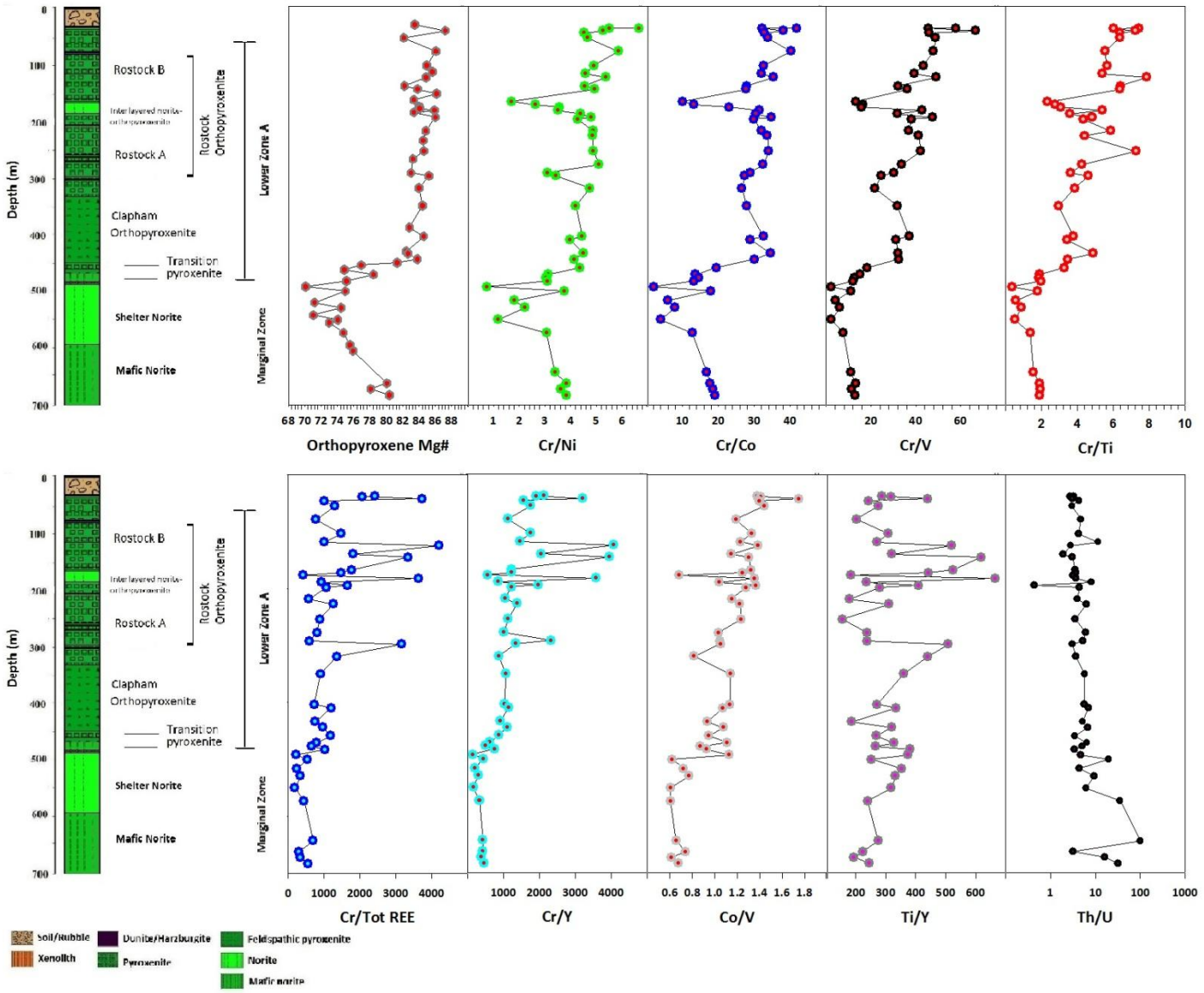

Fig. 7.3: Trace element ratios in CH6 orthopyroxene. The Marginal Zone ratios show continuous, systematic variations compared to the LZa.

The entire LZa succession shows relatively constant Th/U ratios suggesting that there was very little assimilation of the crustal rocks by the magma, keeping the overall magma composition near constant with respect to these elements. The exception is only observed in the rocks making up the interlayered norite unit at the middle of the Rostock Orthopyroxenite succession. By Contrast, the Marginal Zone Th/U varies dramatically, particularly near the Mafic-Shelter Norite transition. Chapters 2-3 and field mapping showed that there are innumerable xenoliths (crustal rocks) in this part of the Clapham Trough section, particularly above 570 m depth in CH6. This variation in Th/U is interpreted to be indicative of the assimilation of crustal rocks by the Marginal Zone magma compared to the LZa, which is poorly affected by assimilation and contamination.

7.2. Trace Element ratios in Plagioclase

After orthopyroxene, plagioclase makes up a significant proportion of the whole rock compositions of the CH6 section. With the exception to the bulk of the LZa Orthopyroxenite succession, plagioclase occurs as a cumulus phase and its occurrence is enigmatic, especially in the Marginal Zone. In chapters 5, supported by the modelling in chapter 6, this study showed that there is a geochemical dissociation in the coexisting compositions of plagioclase and orthopyroxene crystals, such that the plagioclase does not coexist with its appropriate cotectic orthopyroxene in the Shelter Norite. In fact, the composition of plagioclase suggests a reversed fractionation trend when compared to the orthopyroxene compositions and the whole rocks Mg# within the same section of the Marginal Zone. In the LZa, the Rostock Orthopyroxenite succession fractionation of plagioclase was observed (Chapter 5), but not reflected by the orthopyroxene compositions. Of course, the plagioclase in the LZa mainly occurs as the interstitial phase and represents trapped liquid content. The fractionated An#

(chapter 5) and trace elements in plagioclase are interpreted as evidence of post-cumulus fractionation of trapped liquid content with minimal migration of trapped liquid. Sr is relatively compatible with plagioclase and it can be used as proxy for understanding the variation of the composition in conjunction with large ion lithophile and high field strength elements (i.e. LILE and HFSE). Fig. 7.4 shows the trace element ratios in plagioclase of the CH6 section.

The trace element ratios displayed in Fig. 7.4 corroborate the reversed plagioclase composition trend observed in Chapter 5, and that the Marginal Zone reflects continuous fractionation between the Mafic and Shelter Norite sequences (Sr/Ba, Sr/Eu, Sr/total REE, Sr/Ti, Eu/Zr). There is evidence of cyclic compositional variations in the Shelter Norite section of the Marginal Zone as showed by the Sr/Ga and to some extent Pb/Y. These data corroborate the major elements data in chapter 5. In the LZa, the trace element ratios generally support evolved and fractionating plagioclase compositions, except for the cumulus plagioclase samples in the interlayered norite horizons. The cumulus plagioclase has the highest compositions (Sr/element ratios), with low concentrations in LILE and HFSE elements. There are subtle differences in the Clapham and Rostock Orthopyroxenite plagioclase compositions as pronounced by the Sr/Ba, Sr/Ti, Sr/Cr ratios. These data corroborate the subtle compositional variations and fractionation observed in plagioclase major elements in Chapter 5.

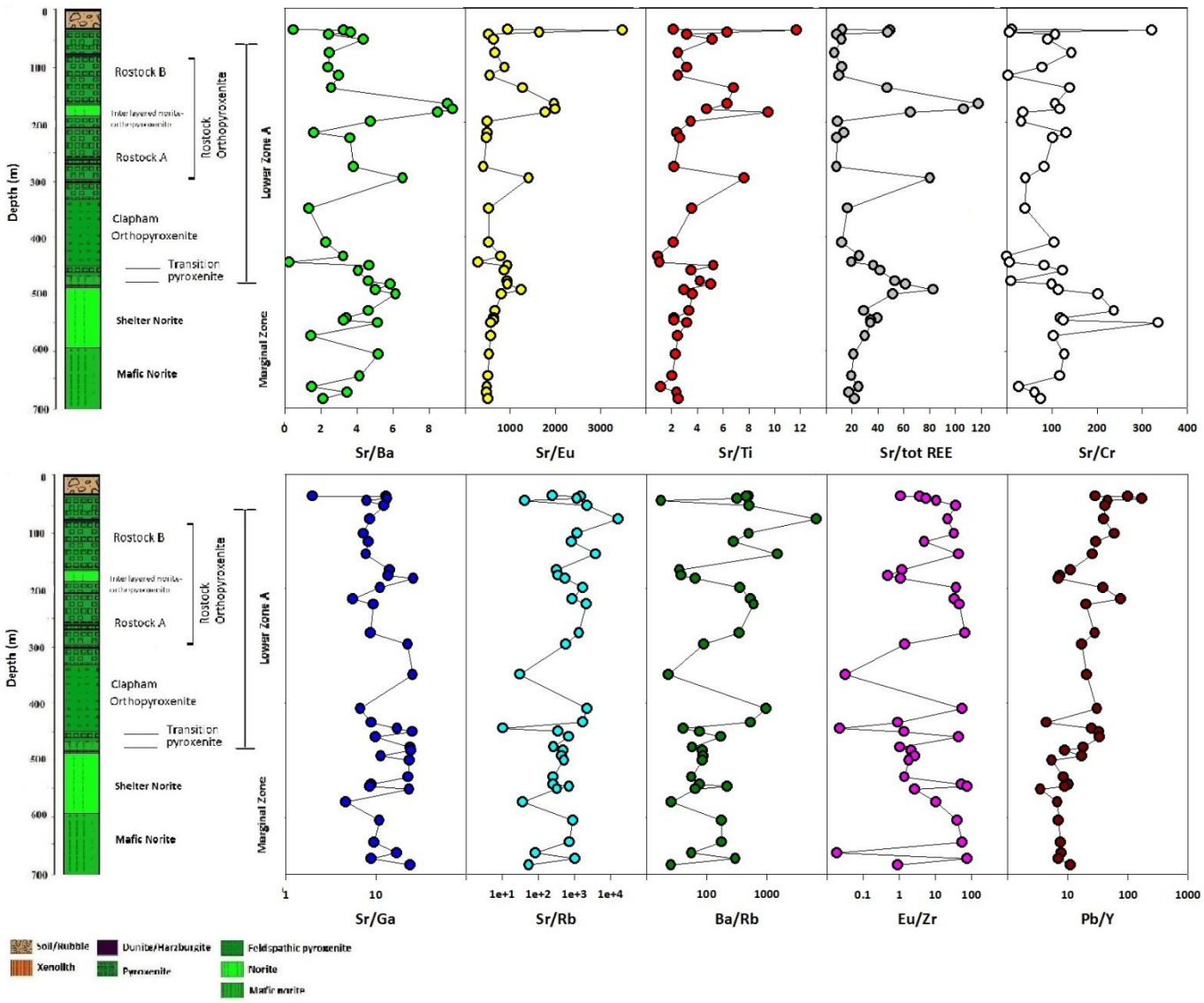

Fig. 7.4: Trace element ratios in CH6 plagioclase. Data support continuous, systematic variation in Marginal Zone compared to LZa.

7.3. Incompatible Trace Elements and Trapped Liquid content

Up to this point, only the composition of cumulus phases and their variations in the CH6 drill core has been considered. The influence of trapped liquid on the whole-rock compositions and mineral phases has been noted previously but not fully evaluated. The initial amount and concentration of trapped liquid is not easily determined due to changes related to post-cumulus processes. Modal abundances (i.e. CIPW Norm estimations) of clinopyroxene and interstitial plagioclase cannot be directly taken to represent the original amount of trapped liquid (i.e. porosity between the cumulus mineral frame work) when the Clapham Trough succession accumulated because post-cumulus processes are not fully known. Moreover, the post-cumulus processes could have altered the volume and the composition of the trapped liquid content during the formation of the rocks in the CH6 section. CIPW Norm calculations are qualitative and do not discriminate between cumulus and post-cumulus (trapped liquid) phases. The amount of trapped liquid in the Marginal Zone would be even more difficult to estimate from CIPW norms because some of the clinopyroxene (pigeonite) crystallised from the magma as a cumulus phase, and there was also post-cumulus clinopyroxene (poikilitic textures) that formed around the cumulus mineral framework (Chapter 4).

In this section, this study evaluates the variations in the incompatible trace elements and their ratios in the whole rocks and their relationship to the amount and composition of the trapped liquid. The concentration of the incompatible trace elements in the parental magma must be known in order to estimate the amount of trapped liquid in the whole rock. The Marginal Zone in Chapter 6 was modelled to have formed from a liquid composition that resulted from about 28-31 % fractional crystallization of the B1-magma composition proposed by Wilson (2012). In that case we can use the postulated trace element compositions in this starting B1-magma of Wilson (2012), and the estimated degree of fractionation (i.e. 1-*F*, where *F* is the fraction of liquid remaining after fractionation) to predict the trace element compositions in the Marginal Zone chamber. Elements

of particular interest in this section are LILE and HFSE (which are typically incompatible with respect to both orthopyroxene or plagioclase) namely, Rb, Cs, Th, U, Y, Pb, Zr and Nb. Up to the base of the Marginal Zone, B1-magma is assumed to have predominantly equilibrated with only orthopyroxene. Therefore, the bulk partition coefficients of these incompatible trace elements are assumed to be similar to that of orthopyroxene. Using equation 7.3, we can estimate the approximate trace element composition of the parental magma of the Marginal Zone sequence. Table 7.2 shows the relevant data, and Fig. 7.5 shows the calculated ratios in whole-rocks and mineral phases in the CH6 section.

Generally, elements that have comparable incompatibility with respect to the CH6 mineral assemblage display near constant ratios for the whole-rocks and clinopyroxene. In particular, the U/Rb, Th/U and Y/Pb ratios do not change throughout the Marginal Zone and most of the LZa succession. The near constant ratios are interpreted as a response to prevailing and stable accumulation processes in the Marginal Zone and parts of the LZa, with comparable volumes of trapped liquid content (i.e. the amount of trapped liquid remaining is generally constant with very little variation). The U/Rb, Th/U and Y/Pb ratios qualitatively show that the volume of trapped liquid in the Marginal Zone remained constant during accumulation. To estimate the amount of trapped liquid this study uses equation 7.4 and the measured average concentration of Zr, Nd and U in the Lower and Marginal Zones of the CH6 section (Table 7.2). The fundamental assumption in carrying out these trapped liquid estimates is that these trace elements are completely incompatible and their concentration reflects the (average) trapped liquid content, and that melt or fluid is lost from the local system at a later stage.

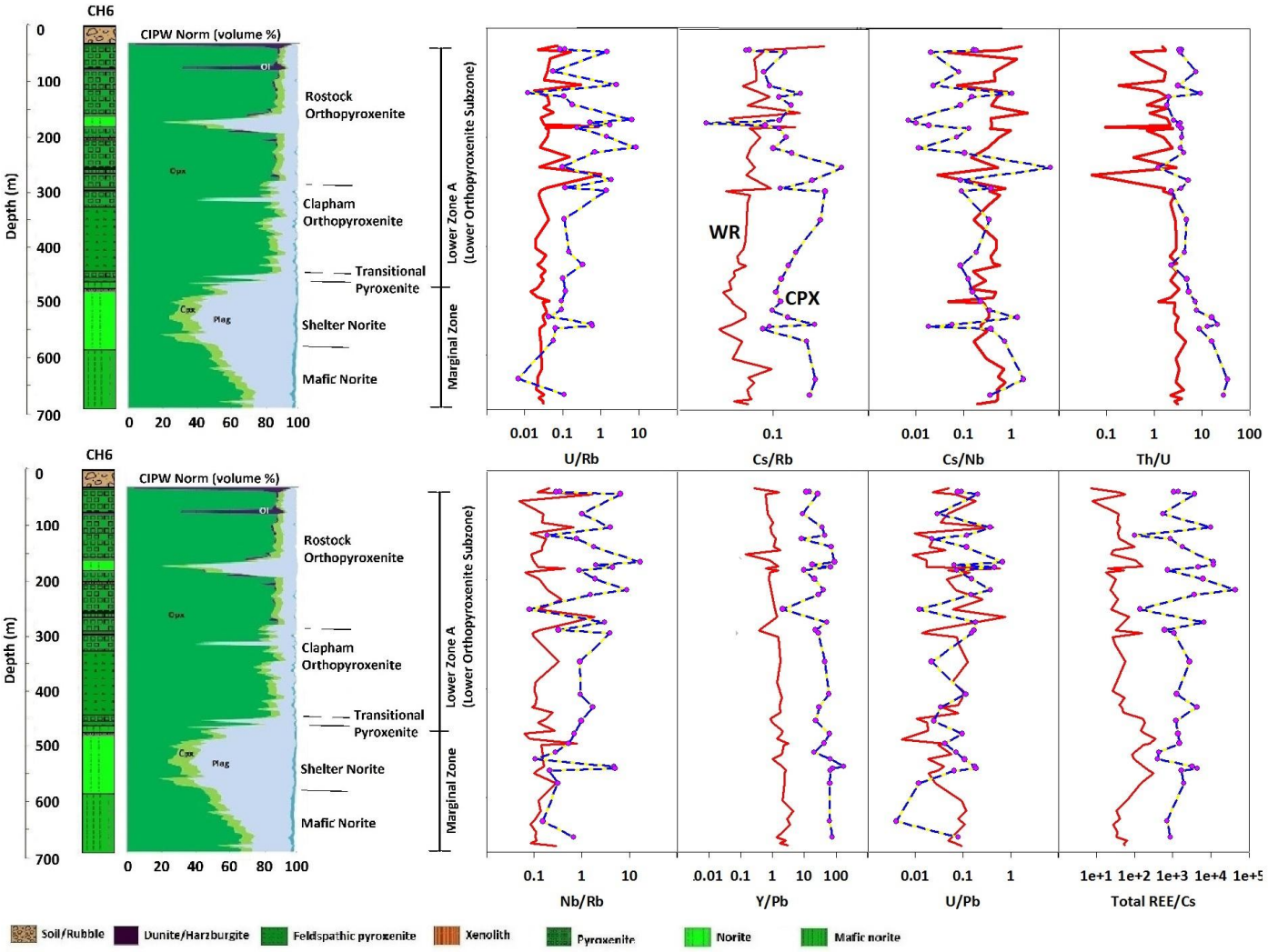

Fig. 7.5: whole-rocks and clinopyroxene (post-cumulus phase) incompatible trace element ratios in the CH6 section. U/Rb, Th/U and Y/Pb show that the trapped liquid content variation is minimal through the CH6 section, especially in the Marginal Zone.

Table 7.2: Estimation of trapped liquid proportion from parental magma estimates and whole-rock composition

	Parental Magma*			Average Whole-rock composition			Trapped liquid proportion (%)		
	Zr (ppm)	Nb (ppm)	U (ppm)	Zr (ppm)	Nb (ppm)	U (ppm)	Zr	Nb	U
Lower Zone A	84.90	4.75	1.11	7.77	0.50	0.15	9.15	10.52	13.49
Marginal Zone	66.00	3.80	0.87	9.80	0.51	0.10	14.85	13.42	11.49

* Parental magma estimates calculated from Rayleigh fractionation (and mixing for LZa) of B1-magma of Wilson (2012).

Using the modified relationship from Maier and Barnes (1999) the amount of trapped liquid can be calculated as follows:

$$\text{Trapped Liquid \%} = 100 \times (\mathbf{El}_{WR}/\mathbf{El}_{B1\text{-}magma}) \quad (7.4)$$

El refers to the incompatible trace elements. According to the data in Table 7.2 the Marginal Zone had 11-15 % average trapped liquid and the Lower Zone A about 10 % on average. This suggests that both zones are adcumulate-mesocumulate sequences and there must have been enough time for the removal of trapped liquid to be as low proportions as 10 %. This interpretation is in line with the definitions of Irvine (1982). The comparable trapped liquid proportion is consistent with the comparable incompatible trace element concentrations and ratios for the Marginal Zone and Lower Zone A (Fig. 7.5). It is important to emphasise that the calculations in Table 7.2 are only semi-quantitative but their credence can be supported by the CIPW Norm of post-cumulus phases. This agreement between the estimated amount of trapped liquid and the CIPW Norm (Fig. 7.5) support the interpretation that there was only minimal or no post-cumulus trapped liquid migration that occurred during the accumulation period in either the Marginal Zone or the Lower Zone A succession.

7.4 Summary

The variation of the measured Cr and Cr/MgO and other trace elements in the orthopyroxene of the CH6 section show that the Marginal Zone rocks formed from differentiation of one liquid composition with no (major) interruption of the magma chamber. The data support that the Marginal Zone formed from single magma batch, without input of new magma. That is, the sequence resulted from uninterrupted continuous fractionation in a 'temporarily' closed magma chamber. In addition, there must have been constant operation of accumulation processes, allowing for small variation in the amount of trapped liquid. The Marginal Zone is interpreted as an adcumulate-mesocumulate sequence of progressively differentiated rocks. The amount of incompatible trace elements in the Marginal Zone is very low and comparable to the LZa in general suggesting that there was significant separation and removal of trapped liquid from the cumulus phases at an early stage of the accumulation process. Furthermore, there is evidence of cyclic compositional variation in the Shelter Norite.

Contrary to the Marginal Zone, the LZa shows at two geochemically different packages (Fig. 7.2). These trends are consistent with the subdivision of the LZa section at Clapham Trough to the Clapham and the Rostock Orthopyroxenite sequences based on the SACS (1980) formal stratigraphy of the Bushveld Complex. The former (Clapham Orthopyroxenite) shows Cr differentiation with height, towards the interlayered norite horizon between 290-292 m in the CH6 section. Above this norite horizon, the Clapham Orthopyroxenite becomes progressively more primitive towards the overlying Rostock Orthopyroxenite. The Rostock Orthopyroxenite consists of a thicker interlayered norite marker horizon almost in the middle of the succession in the CH6 section. The most distinctive visual difference between the Rostock and Clapham orthopyroxenite sequences is the amount of interstitial plagioclase (see chapters 2-4). This reflects the variations in the amount of trapped liquid in the LZa. The Clapham Orthopyroxenite reflects constant amounts of trapped liquid compared to the cyclic

and systematic variation in the Rostock Orthopyroxenite package (Fig. 7.5). Generally, the LZa shows fractionated trace elements and the Rostock Orthopyroxenite sequence has relatively primitive compositions compared to the Clapham Orthopyroxenite sequence (Fig. 7.2).

Chapter 8

Magma Emplacement and Accumulation Processes

The mode of emplacement of the parental magmas and the accumulation processes have a considerable effect on the compositional variations in layered intrusions, regardless of the size and the shape. The Bushveld Complex magma chamber is no exception. The Skaergaard intrusion, in Greenland, is believed to be a result of as a single injection of tholeiitic magma with indications of lateral and vertical compositional variations (McBirney, 1996, 1989). The compositional variations are explained in terms of the accumulation processes. In layered intrusions where multiple injections of magma may have occurred, more complex compositional variations occur.

The Marginal and Lower Zones of the Bushveld Complex are associated with at least two separate (and compositionally distinct magmas) major injections of magma. Sharpe (1981) proposed the timing of magma influxes in the Bushveld Complex based on the Marginal Zone rocks in the eastern limb. Cawthorn and Walraven (1998) modelled the mode and number of magma pulse to explain the observed lithological and compositional variations in the Bushveld Complex. The Feeder positions to the Bushveld Complex are debatable but it is only in a study by Kruger (2005) that the locations of the feeder zones were proposed. Clarke *et al.* (2009a, b) presented comprehensive geometrical and related compositional variations.

The present chapter re-evaluates the emplacement of the Lower and Marginal Zones at the Clapham Trough within the broader scope of the eastern Bushveld Complex, including the cumulus processes controlling the chemical trends observed in CH6 in light of the recent works of Wilson and Chunnett (2010) and Wilson (2012). The lateral continuity of units and

the remarkable similarities of zones in the western and eastern limbs of the Bushveld Complex suggest that some processes (which were functional in the early stages of the magma chamber) were similar over large distances, with only (local) differences. This allows the present study to extend the interpretations made for Clapham Trough and make comparisons across the entire Bushveld Complex.

8.1. Emplacement of Lower and Marginal Zone Magmas

Sharpe (1981) and other workers therein agree that the Lower Zone magmas are a separate influx of magma from the Marginal Zone, whose compositions have been subject to great debate. The previous chapters of the present study also showed that the two zones formed from two distinct magma compositions, and at least two different magma emplacement events. For the section starting from the base of the Lower Zone to the Upper-Lower Critical Zone transition, Cawthorn and Walraven (1998) modelled six (1 km thick columns) major magma impulses to explain the 1.5 km thick ultramafic succession. The latter authors further suggested that there was rapid cooling to produce the most evolved orthopyroxene compositions (En_{82}) at about 1200° C. Cawthorn and Walraven (1998) did not model the emplacement and cooling/accumulation rate for the Marginal Zone. In addition, the emplacement of 1 km (or more) thick magma column that differentiates to form the near-constant 400-500 m Lower Orthopyroxenite Subzone in a single injection is improbable.

Eales and Costin (2012) described the Marginal Zone as the emplacement and rapid cooling (approximately 2 kbars pressure) of a relatively siliceous component of a basaltic magma, which was formed by differentiation in a staging chamber that was located at depths equivalent to 4.5-10 kbars pressure. Moreover, these workers suggest that the relatively primitive component of the latter magma is parental to the Lower Zone. However, the latter

authors did not present any plausible composition of the "siliceous cap" tapped by conduits of the Marginal Zone. In addition, their model does not account for the occurrence of the BUS (Basal Ultramafic Sequence of Wilson and Chunnett, 2010) intersected at Clapham Trough. Generally previous workers have treated the composition of the Marginal Zone as uniform, and the 'chill zone' in the work of Eales and Costin (2012) is no exception. The present study has unequivocally shown that the composition of the Marginal Zone rocks adjacent (formerly referred to as B1-type) to the Lower Zone is variable, showing evidence of systematic compositional variation and fractionation (Chapters 5-7). The Marginal Zone rocks are not representative of a chill zone.

8.1.1. Compositional reversal in the Marginal Zone

The data presented in the previous chapters show steady and continuous fractionation of orthopyroxene and concurrent evolution of whole-rock composition (i.e. Mg#), without any compositional reversals observed in the Marginal Zone. In the same interval, the co-existing plagioclase trend adopts a generally continuous but opposing trend from that of the orthopyroxene and whole-rocks Mg#. That is, the plagioclase compositions follow a reversed trend to 'normal' differentiation from the bottom of CH6 section, from most evolved compositions (lowest An#) in the Mafic Norite being more primitive with increasing height, with the Shelter Norite presenting the most primitive An# (Chapters 5-7). The orthopyroxene compositions, however, progressively become evolved in the same height interval (En_{81} and An_{63} at the base of Mafic Norite compared to En_{71} and An_{78} at the top of the Shelter norite). The latter trend (orthopyroxene) is the 'normal trend' of differentiation consistent with decreasing temperature and corresponding compositions (Chapter 5, Fig 8.2). Plagioclase and orthopyroxene show continuous differentiation trends with mutually opposing compositional

trends, especially above 560 m depth, approximately at the (gradational) contact between the Shelter Norite and Mafic Norite sequences. As previously mentioned, the latter norite sequence (i.e. Mafic Norite) is bordering feldspathic orthopyroxenite, as defined by the modal abundances (chapter 4), but plagioclase is a cumulus phase throughout the Marginal Zone (Chapter 4, Fig 8.1). Al_2O_3 and Sr are significant components in plagioclase; whereas TiO_2, K_2O, Rb and Zr are concentrated in interstitial phases (i.e. represent trapped liquid). A positive relationship between the abundance of plagioclase and Al and Sr is observed, whereas a negative or no apparent relationship with Ti, K, Rb and Zr is observed (Fig. 8.1). These data support that all the Marginal Zone plagioclase is a cumulus phase. Therefore, plagioclase and orthopyroxene must have formed as cotectic minerals, supporting the modelling of the parental liquid composition in chapter 6.

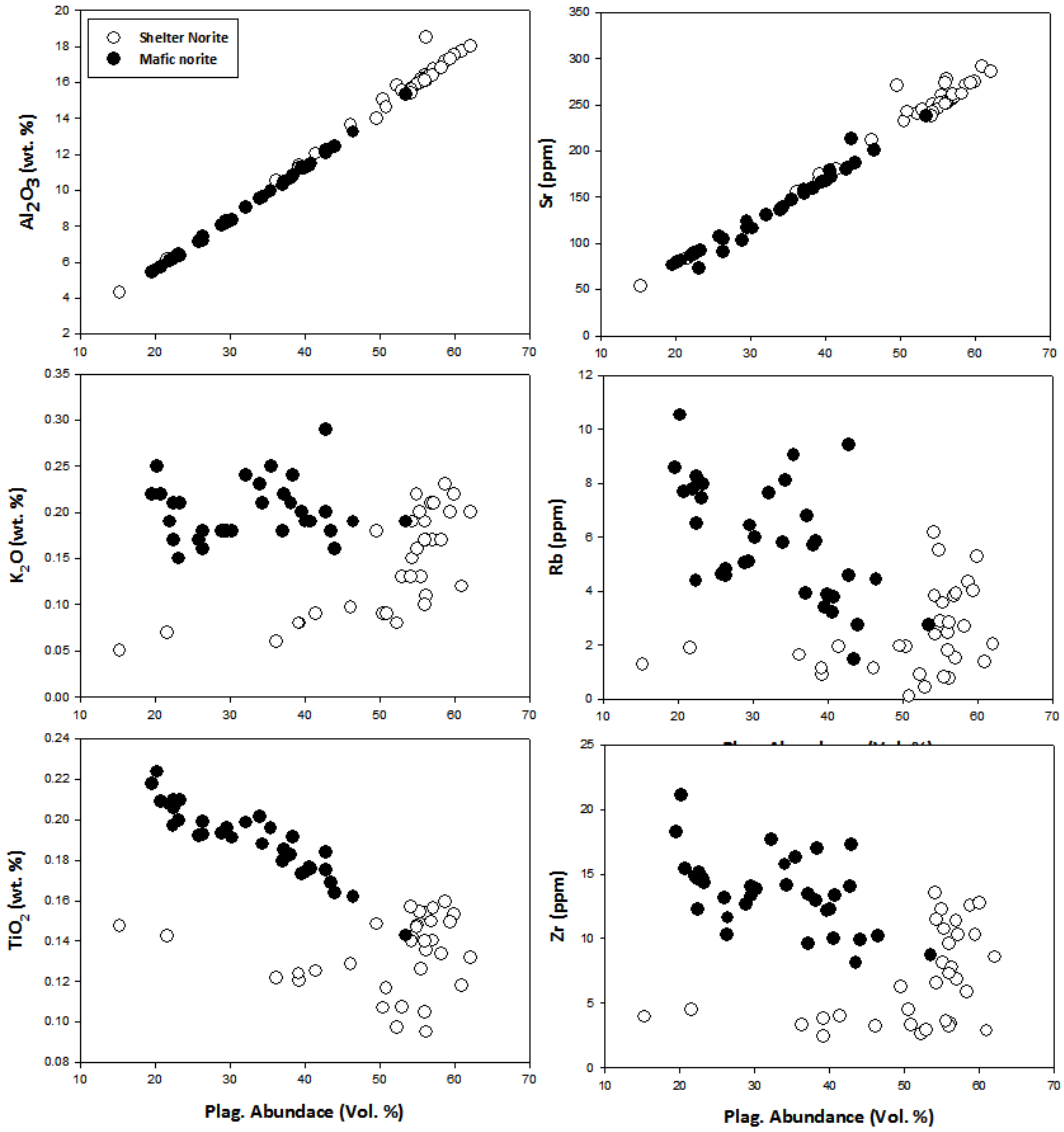

Fig. 8.1: Plagioclase modal abundance (CIPW) versus whole-rocks major and trace elements. Plagioclase shows positive correlation with Al_2O_3 and Sr and negative correlation with trapped liquid components.

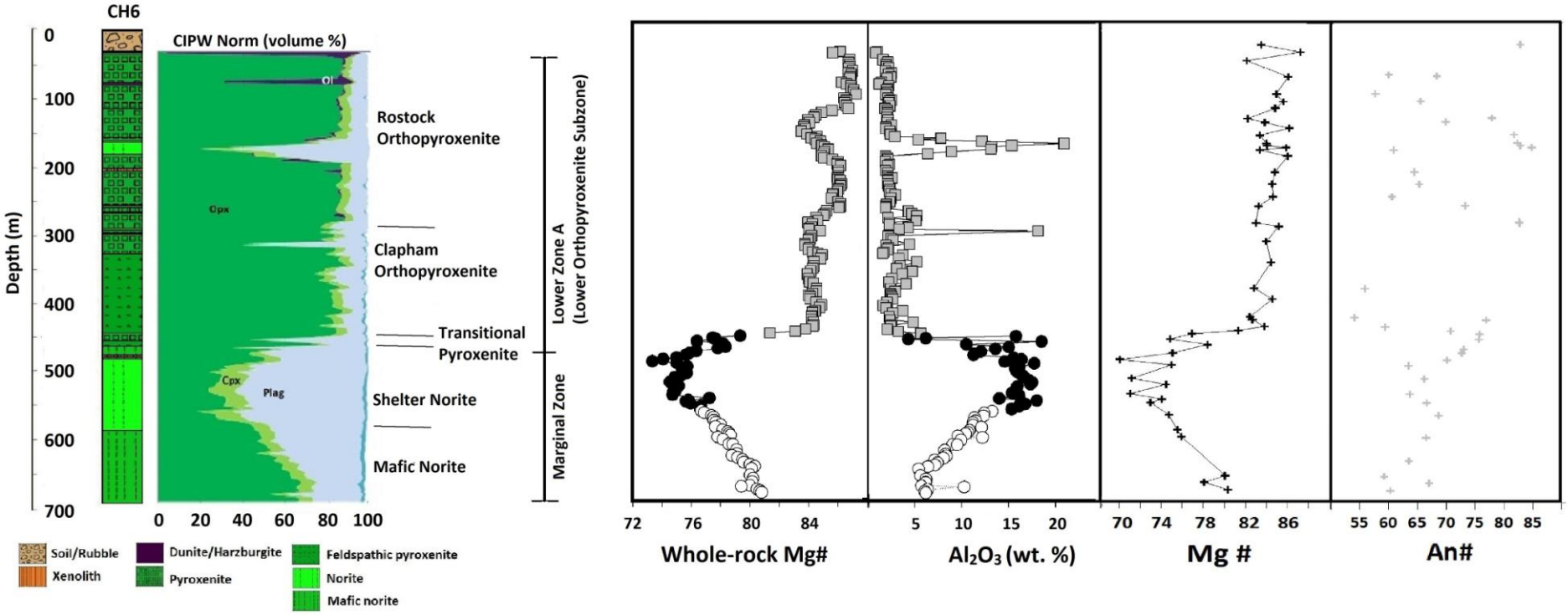

Fig. 8.2: The variation of orthopyroxene Mg# and plagioclase An# with depth in CH6. The Shelter Norite shows reverse plagioclase evolution to co-existing orthopyroxene crystals. Al_2O_3 as proxy for plagioclase composition and its modal abundance.

The observed reversed fractionation trend in plagioclase is against normal differentiation and thermodynamics because co-existing mineral phases, forming from the same liquid, must show complimentary evolution paths in the same direction of temperature/composition change as predicted by the Petrolog model (Fig. 8.3). That is the compositions must become more evolved with increasing height. Increasingly primitive plagioclase composition (thus increasing whole-rocks An#) necessitates increased temperature conditions in the chamber, whereas the opposite is true for more evolved Mg# compositions. The appropriate temperature (thus composition) conditions at the time of crystallization cannot drive the evolution of one mineral in an opposite trend to that of a simultaneously (cotectic) formed mineral (Figure 8.3). i.e. plagioclase, in the present case, cannot show reversed compositional evolution path to that of the orthopyroxene formed from the same liquid if normal differentiation is in operation.

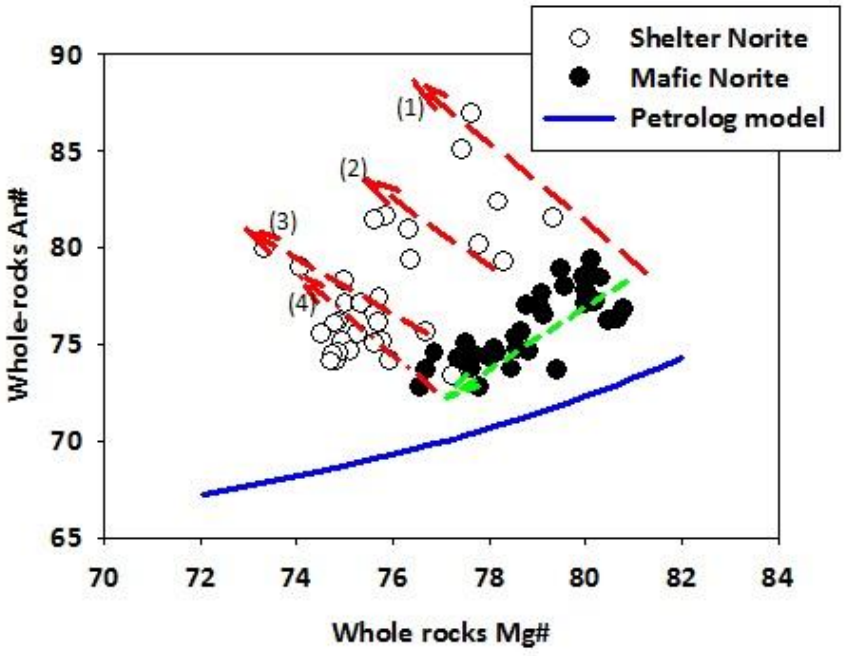

Fig. 8.3: Whole rocks An# and vs., Mg# for the Marginal Zone. Shelter Norite largely shows negative correlations between An# and Mg#. Arrows show the accumulation and fractionation directions, and the numbering next to the Shelter Norite samples shows cyclic units with increasing depth. Green arrow shows Mafic Norite evolution trend.

The orthopyroxene and whole-rocks geochemistry in the Marginal Zone show 'normal fractionation' as consistent with a cooling temperature regime. It is worth noting that the reversed Shelter Norite (and plagioclase) compositions positively correlate with the modal abundances of plagioclase, and the increasing compositions are coupled with decreasing whole-rocks and orthopyroxene Mg# (i.e. negative correlations with Mg#). The process by which plagioclase and orthopyroxene of contrasting evolution trends co-exist in the same package of rocks is not an ordinary accumulation process (whether by crystal settling and/or *in-situ* crystallization). The orthopyroxene-clinopyroxene-plagioclase (Opx-Cpx-Plag) ternary system is useful in showing the evolution of the marginal Zone liquid (Fig. 8.4). As expected the composition of the proposed parental magma (red hexagon) plots near the cotectic boundary between the orthopyroxene and plagioclase fields.

There is a disparity between the modelled magma composition and the modal abundances observed in the core (CH6) and chemical modelling. The expected distribution from the magma is a linear trend around the plagioclase-orthopyroxene cotectic boundary, traversing towards the eutectic point. However, the chemical data suggest the CH6 cumulates must have formed from an opx-normative liquid. There is a 'misfit' between the Marginal Zone compositions and the model liquid in the form of the compositional reversal and the modal proportions that are predicted. This is interpreted to be influenced by the accumulation processes after the crystallization.

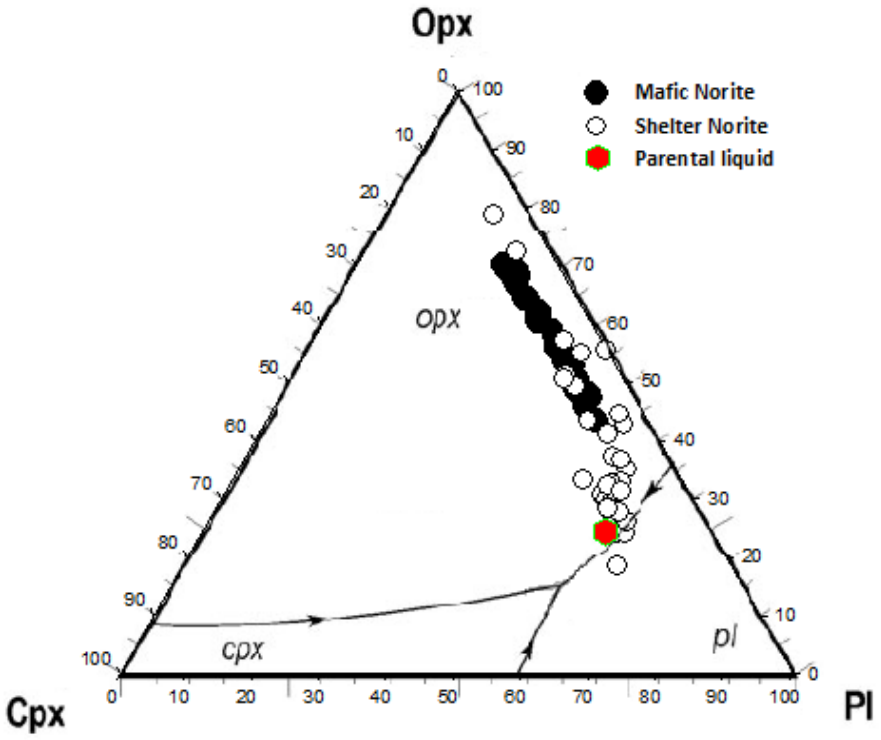

Fig. 8.4: Opx-Cpx-Plag ternary diagram for the Marginal Zone. The proposed liquid composition to the Clapham section of the Marginal Zone lies close to the cotectic boundary between opx and plag. The whole-rocks compositions in the Marginal Zone contrast the modelled crystallization from the liquid.

8.1.2. Floatation of Cotectic Plagioclase

The crystallization front in the Marginal Zone magma chamber is envisaged as a crystal-mush zone in which plagioclase and orthopyroxene crystallised simultaneously (as a cotectic assemblage), with convection currents operating mainly in the crystal-free liquid zone of the chamber (Fig. 8.5). Orthopyroxene must have been the dominant cumulus phase below the crystallization front (assuming upward propagation of the crystallization front). This zone is equated to the base of the Mafic Norite. According to Scoates (2000) the densities of plagioclase and orthopyroxene vary between 2.63-2.74 and 3.23-3.29 $g.cm^{-3}$, respectively. In addition, the density of the andesitic liquid proposed to be parental (SiO_2 and MgO of 56.7 and 6.05 wt. %, respectively, see section 6.3) to the Marginal Zone is predicted to be 2.61

$g.cm^{-3}$. The density of basalt to basaltic andesite magma in literature is about 2.6-2.8 $g.cm^{-3}$ (Scoates, 2000; Murase and McBirney, 1973). The density of the plagioclase is comparable to slightly lower than the magma proposed to be parental the Marginal Zone, whereas the orthopyroxene has a greater density than the predicted parental magma. Because the density of plagioclase is comparable with the density of the basaltic andesite liquid (parental magma to the Marginal Zone) it is expected to remain in suspension more readily than orthopyroxene. That is, there is no density separation expected between the magma and plagioclase.

The present study postulates that upon crystallization, convection currents carry plagioclase in suspension and leaving a stagnant crystal-mush zone that is orthopyroxene-rich and some volume of 'immobile' trapped liquid. The trapped liquid is envisaged to crystallise (cumulus) plagioclase at a lower temperature than the cotectic plagioclase carried in suspension by the convection in the magma above the stagnant crystal-mush zone. The plagioclase carried in suspension makes up the bulk of the Shelter Norite. Floatation of plagioclase is a common mechanism to explain the occurrence of mainly plagioclase rich layers. Common examples to support the above statements are the occurrence of large anorthosite massifs and the anorthosites that form the Lunar highlands crust (Namur *et al.*, 2011; Walker and Hays, 1977). Mafic minerals that form simultaneously with plagioclase from these magma bodies (lava lakes as in the case of Lunar crust) sink to the bottom of the same mafic liquid reservoir (Walker and Hays, 1977; Scoates, 2000; Namur *et al.*, 2011).

Whether the mafic mineral, orthopyroxene, in the case of the Marginal Zone, accumulated through in-situ crystallization with or without contribution of crystal settling, it is conceivable that plagioclase independently floated to achieve gravitational stability, and concentrated in units forming at a (relatively) higher stratigraphic level (horizon) than their cotectic orthopyroxene crystals. Relatively later formed plagioclase crystallised at lower temperatures

from stagnant magma column that was in association with the orthopyroxene zone (Fig. 8.5). The separation of the plagioclase from orthopyroxene must have occurred soon after crystallization. Complete solidification of the Marginal Zone however, happened at a later stage allowing the evolved plagioclase to mingle with relatively evolved orthopyroxene and vice versa. This study proposes that the Marginal Zone formed largely through in-situ crystallization, with floatation of plagioclase to create mechanical separation between the cotectic mineral assemblages.

The proposed accumulation mechanism can account for both the observed compositional variations of orthopyroxene and plagioclase, such that the trends would get more evolved (Mg#) and primitive (An#) with height, respectively. Moreover, it is conceivable the most primitive An# compositions associated with evolved Mg# in the cyclic units in the Shelter Norite, as defined by the trends identified in Fig. 8.3, are therefore accounted for.

In addition, the proposed accumulation process also presents a plausible manner in which the conformable siliceous (micro-norite) layers that were described in Chapters 2-4 of the current study were formed. That is, upon separation of the plagioclase crystals from the cotectic orthopyroxene, there is a volume of magma that must be relatively depleted in MgO, CaO and Al_2O_3 but SiO_2 enriched than the associated norite layers. The micro norite layers support a mechanical separation of orthopyroxene and plagioclase leaving a siliceous sandwich/boundary layer (Fig. 8.5). These layers in the field help delineate the cyclic units in the Marginal Zone, especially within the Shelter Norite sequence. These layers represent the last liquid to solidify within each cyclic unit, hence the more siliceous nature and the fine crystals. The localised diapiric structures identified in the field (see Chapter 2) also support that the layers must have solidified after the overlying cyclic unit had started forming.

Because the magma is crystallizing both plagioclase and orthopyroxene with interstitial clinopyroxene, the fusion temperature will be the same for the cumulus phases at any point.

However, as mentioned earlier, the opposing compositional trends suggest that the temperature varied dramatically to form the observed CH6 Marginal Zone compositions. It is improbable that temperature could vary dramatically within millimetres even in an intrusion the size of the Bushveld Complex. The above account assumes an upward migrating crystallization front. In theory, crystallization could also form from the roof down, as in the Upper Border Series in the Skaergaard intrusion, forming congelation cumulates. Whether the crystallization was from the bottom of the chamber or at the (paleo-) roof of the Marginal Zone (prior to the emplacement of the Lower Zone A magma) the mechanical separation of plagioclase and orthopyroxene could have equally been produced by the density contrasts mentioned above. i.e. it is equally plausible that the Marginal Zone formed as congelation cumulates but the denser orthopyroxene crystals sank to the bottom of the crystallization pile.

In the latter case plagioclase also behaves the same way as the 'roof' reversal of the S-shaped marginal reversal of Latypov (2003a, b), where cotectic orthopyroxene is separated from the plagioclase. The mechanical separation of cotectic plagioclase and orthopyroxene in this case also depends on the density (with or without the Soret fractionation described by Latypov, 2003a) contrasts between the resident magma and the orthopyroxene crystals. The challenges against this interpretation of the congelation cumulates mechanism are first, the roof rocks of the Bushveld Complex (Rooiberg felsite) would not support the weight of the would-be congelation cumulates. Moreover, the heat from the underlying magma chamber would have caused the roof rocks to be partially molten by the time the Marginal Zone formed. Second, according to Naslund and McBirney (1996, and references therein) it is improbable that the orthopyroxene crystal-sizes observed in the Marginal Zone accumulated through gravity settling. Before the crystals could begin to sink through the magma chamber, Stoke's law (i.e. controls by density contrast and radius of orthopyroxene) requires large enough crystals to be formed such that the yield strength of the magma is exceeded by the weight of the crystals

(Naslund and McBirney, 1996). Lastly, the congelation cumulates would require that there must be an internal border zone similar to the Sandwich Horizon described in the Skaergaard Complex, in which most if the xenolithic fragments would be found. This is not the case with the Marginal Zone described in the CH6 drill-core and observed in the Clapham Trough. It seems, therefore, unlikely that the Marginal Zone compositional trends are a result of significant influence of gravitation settling regardless of the role of convection in the Marginal Zone magma chamber.

Latypov (2003a) explained Marginal compositional reversals using the Soret fractionation. The involvement of the latter process in explaining the observed compositions of the plagioclase in the Marginal Zone is not clear in the present study. However, it is unlikely that the composition evolution is related with the Soret effect. If that were the case, the compositions of the plagioclase and orthopyroxene must get more evolved and primitive with increasing height, respectively. This is the opposite of the observed trend in the present study.

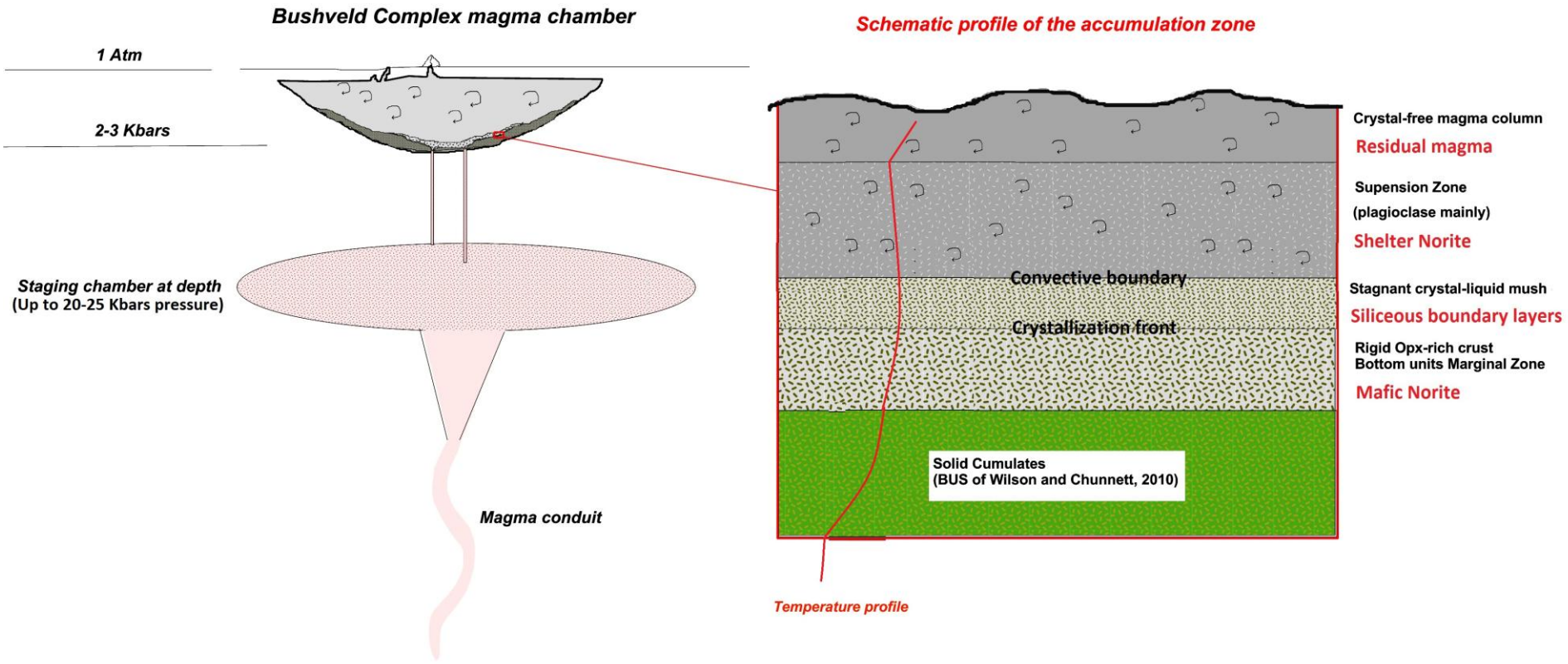

Fig. 8.5: Schematic model for the Marginal and Lower Zones of the Bushveld Complex as observed at Clapham Trough.

8.1.3. Emplacement of the Lower Zone

The boundary zone between the Marginal and Lower Zone of the Bushveld at Clapham Trough in the present study is a relatively friable zone referred to as the Transitional Pyroxenite (Chapter 2). In chapters 5 and 6 the present study showed that the composition of the Transitional Pyroxenite shows an increasing trend from the evolved Marginal Zone towards more primitive Lower Zone. The increasing composition (MgO and Mg#) suggests that there was a gradual influx of new primitive Lower Zone magma.

The composition of this new magma is presented in Chapter 6 as the B1-magma proposed by Wilson (2012) which progressively mixes with the residual liquid trapped at the top of the Marginal Zone chamber. The gradual compositional change described in the CH6 section supports the mixing between the B1-magma and the evolved (silica-rich) residual magma as predicted by the modelling in Chapter 6. The proposed composition of the parental magma of the Lower Orthopyroxenite Subzone (LZa) is produced by a 20- 30 % mixture of residual and 70-80 % primitive B1-magma, respectively. In the Opx-Cpx-Plag ternary system, the LZa magma composition is marked by the red hexagon in Fig. 8.6.

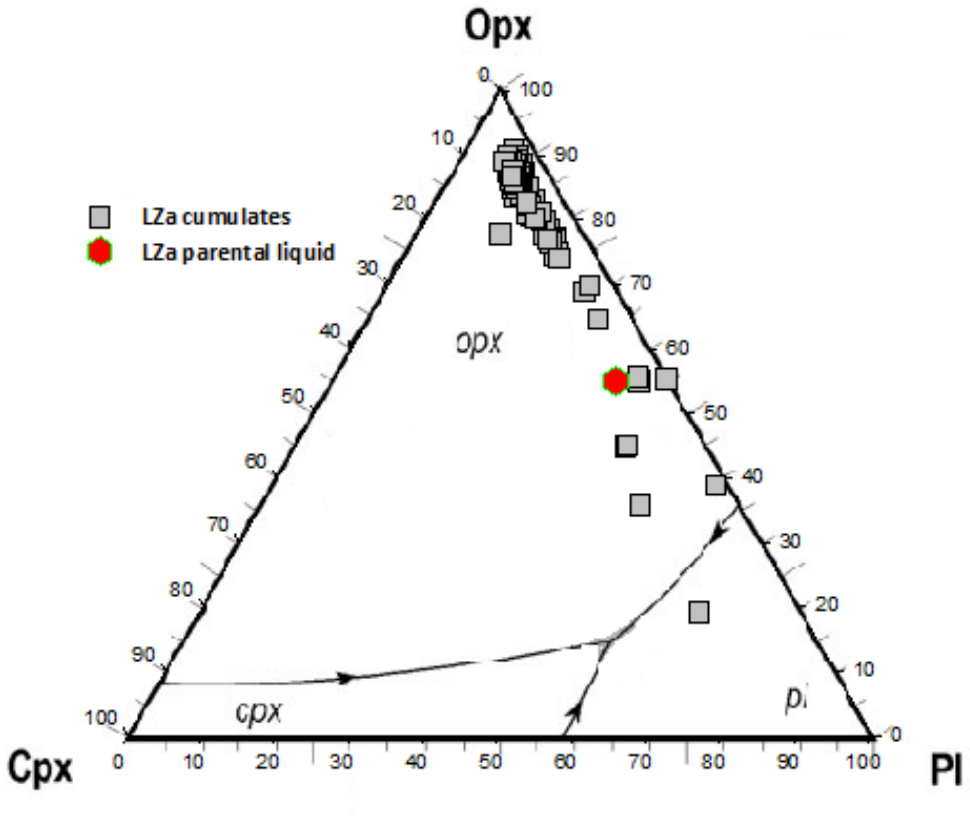

Fig. 8.6: Opx-Cpx-Plag ternary system for the Lower Zone showing the LZa cumulates and the proposed magma composition responsible for the cumulates. The magma lies on a liquid-line of descent going through the Opx apex and the cumulates.

The Lower Zone geochemistry is generally constant, varying only at specific intervals. The variations are confined largely to norite marker horizons within the Lower Zone succession, namely the interlayered norite units described in earlier chapters. This near-constant composition is evident in Fig. 8.6, indicated by the close grouping of the CH6 samples near the Opx apex. The LZa is interpreted to have formed from a parental magma that was kept relatively constant by simultaneous crystallization and continued emplacement of new, crystal charged, magma. The residual liquid composition was not allowed by the system to evolve significantly before it is replenished and restored to (or close) to the proposed parental magma. Hence, the near constant chemistry and the modelling of the Lower Zone

composition require that there must have been constant replenishment of the magma chamber or at least the crystallization zone (crystal-mush magma zone). The latter requires effective convection systems to be in operation in the Bushveld Complex chamber at least at the time the LZa accumulated. Equilibrium between the crystals and the melt must have been maintained effectively through the convection.

The Lower Orthopyroxenite Subzone (LZa) in the CH6 section is at least 450 m thick, and the Clapham Trough section suggests that the Lower Zone is at least 850 m thick (chapters 2 and 3). The Harzburgite Subzone (LZb overlying LZa) is olivine-rich, and it is believed to be a separated magma impulse (and composition) from that responsible for the LZa. According to Cawthorn and Walraven (1998) the (estimated) thickness of the Lower Zone is about 800-1300 m thick, and they roughly projected (as seen in Fig. 8 therein) about 3-4 km magma column is necessary to produce the observed thickness of the cumulates. Cawthorn and Walraven (1998) inferred 4-5 separate stages of recharge and extrusion to account for the Lower and Lower Critical Zones. Practically, it is unlikely that the magma column was 3-4 km at any given stage of the accumulation of the Lower Zone cumulates. The weight of the 3-4 km magma column combined with the weight of the overlying roof rocks (Transvaal Supergroup) would produce pressures that possibly exceed 2-3 kbars pressure putative for the Bushveld Complex magma chamber, at least during the Lower Zone accumulation (Cawthorn and Davies, 1983; Eales and Costin, 2012). Estimating the thickness of the magma column during the accumulation of the Lower Orthopyroxenite Subzone is complex. However, it seems reasonable to suggest that the crystallization and accumulation of the Lower Zone must have occurred contemporaneously with steady magma injection to keep the near constant composition observed in CH6. Modelling of the crystallization in the previous chapter showed that the Lower Zone orthopyroxene formed within the present Bushveld

Complex chamber, under at least 2.0 kbars pressure through mixing of B1-magma and residual magma.

This study postulates that the orthopyroxene crystals were formed and emplaced in a convective crystal-charged zone reaching equilibrium (at temperatures of about 1282° C) with the magma prior to accumulation. The zone of equilibration is the stagnant crystal-much zone with the temperature between 1140-1190° C. The crystallization front marks the boundary where the remaining trapped liquid in the interstitial zone of the cumulus network solidified below 1140° C (average temperature of crystallization of interstitial clinopyroxene and plagioclase). The convective and crystal-free magma body is envisaged to be separated from the zone of accumulation/crystallization by the convective boundary, below which a stagnant crystal-liquid mush is dominant (Fig. 8.7). The stagnant magma-crystal zone is proposed to be the accumulation zone, through in situ crystallization with or without the contribution of crystal settling. The total thickness of the crystallization column is not known, however, the magma recharge is envisaged to replenish the convective suspension (i.e. crystal-mush) and the crystal free magma columns prior to accumulation.

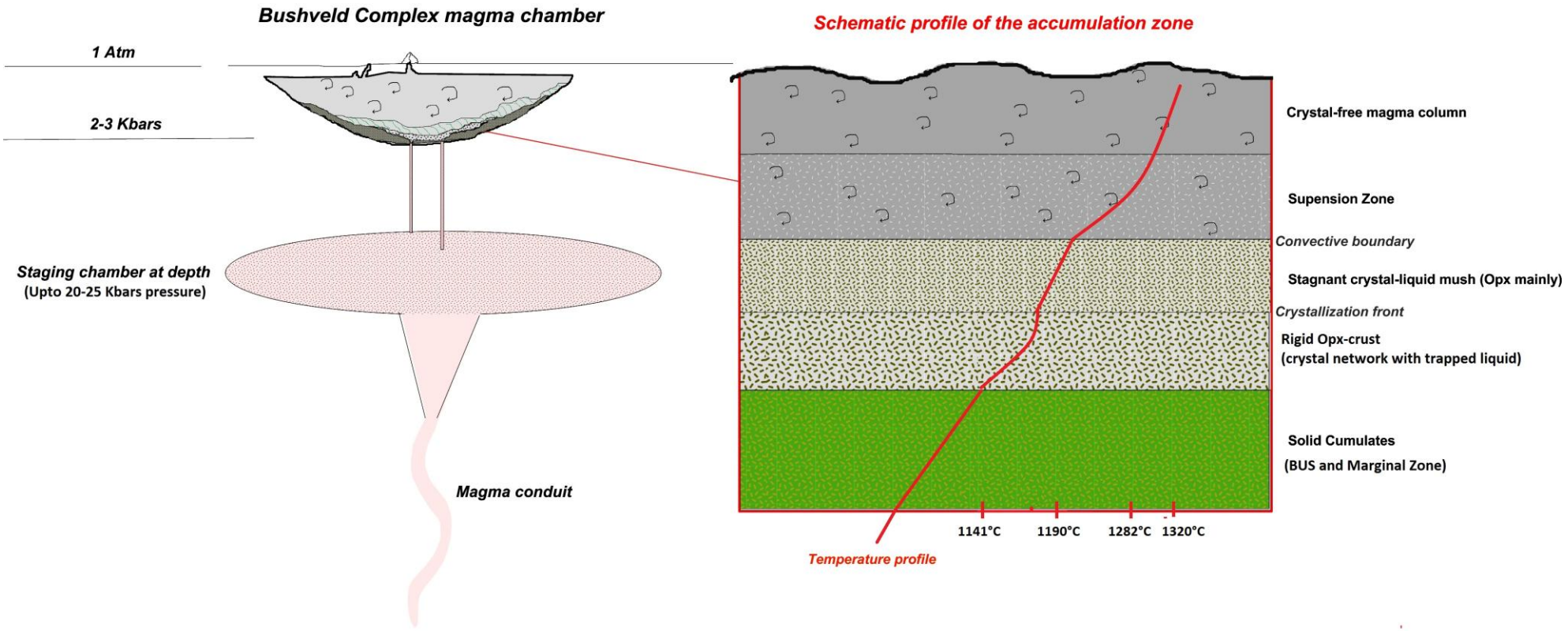

Fig. 8.7: The schematic diagram of the accumulation of the Lower Zone A as described at Clapham Trough. The temperatures are as predicted in Petrolog model in Chapter 6. Lower temperature trend in BUS is taken to be subsolidus cooling.

8.2 Summary and Discussion

The process most likely formed the observed Marginal Zone trends was modified *in-situ* crystallization, coupled with the floatation and suspension of relatively lower-density plagioclase. The mechanical separation of cotectic cumulus phases results in the compositional reversals described in chapters 5, and accounts for the modal variations described in chapters 2-4. This separation resulted in a compositional 'mismatch' and disequilibrium of the cumulus phases in the Marginal Zone, such that the Mg# generally becomes increasingly evolved with increasing stratigraphic height. The opposite is true for the An# compositions of plagioclase and the whole rock. Moreover, the accumulation process accounts for the enigmatic siliceous layers observed in the field and described in an earlier section.

The plagioclase-charged suspension was achieved through convection currents that separated the solid cumulate rocks from the residual magma ponding at the top of the Marginal Zone chamber. This crystal-free residual magma near the top of the Marginal Zone magma chamber must have been in contact with the paleo-roof prior to the emplacement of the Lower Zone magma. The latter interface (i.e. residual magma-roof interface) also being the location of the emplacement of new, more primitive, magma(s).

The new magma impulse(s) formed the Transitional Pyroxenite and the Lower Orthopyroxenite Subzone (LZa) through mixing with the residual magma (as discussed in chapter 6). The magma emplaced must have been carrying some orthopyroxene crystals in suspension. The present study proposes that there must have been adequate time for the magma and the crystals to achieve chemical equilibrium, at least to the point of accumulation. The crystals in the convective zones must have been in equilibrium with the magma.

Effective convection and the pressure applied on the magma chamber by the mass of the overlying country rocks and the magma column is proposed to have reduced the amount of trapped liquid in

the cumulus crystal network. Diffusion, convection and periodic emplacement of new magma are responsible for the replenishment of the magma chamber and the convective suspension-charged zone where major crystallisation and re-equilibration occurred. The constant replenishment at the crystallization zone/front with near constant orthopyroxene compositions provides near constant compositions observed in the trend in the Lower Orthopyroxenite Subzone.

This study favours a modified *in-situ* crystallization mechanism, in which the crystallization occurs in a crystal-liquid (suspension-charged) magma zone, maintaining equilibrium close enough to the accumulation zone where there is negligible convection. The decreasing temperature of the crystallization front and the size of the orthopyroxene crystals suggest that the crystals could not have overcome the yield strength of the magma (Naslund and McBirney, 1996), thus there must have been minor input (if any) of gravity settling in the accumulation process. The suspension-charged and accumulation zones are envisaged to be no more than a few tens of centimetres thick as the solidification front progressed.

Chapter 9

Summary and Conclusions

The present study undertook to investigate the relationship of the Marginal Zone and the Lower Zone in the Clapham Trough area, eastern Bushveld Complex. The study was approached in context of the works of Wilson and Chunnett (2010), and insights from Wilson (2012) regarding the earlier events in the Bushveld Complex. Based on the observations, a model to account for the Marginal Zone rocks and the immediately overlying rocks of the Lower Zone was developed.

9.1 Summary of key points

The important findings in this work, based on the study of the CH6 drill core section and mapping at Clapham Trough, are as follows.

- Nowhere in the study area, or in the entire eastern limb of the Bushveld Complex is the Marginal Zone in contact with the floor rocks.
- The Marginal Zone conformably overlies the Basal Ultramafic Sequence (BUS) described by Wilson and Chunnett (2010), and Wilson (2012).
- The Marginal Zone is relatively fine grained compared to the Lower Zone. However, the former displays cumulus textures together with evidence of cyclic units in the field.
- The CH6 drill core shows two broad lithological subdivisions in the Marginal Zone, the Mafic and Shelter Norite Sequences. The latter is leuconorite to norite (*sensu stricto*) and the former is a melanorite, bordering on feldspathic pyroxenite.

- The whole-rock and mineral geochemistry shows that the Marginal Zone is a fractionated sequence of cumulus rocks. The Mg# changes progressively through the sequence and steadily becomes evolved with stratigraphic height. Contrastingly, the amount and composition of plagioclase show reversed trends to orthopyroxene, such that the An# progressively become primitive upwards in the same interval.

- The cumulate rocks of the Marginal Zone consist of non-cotectic plagioclase and orthopyroxene due to mechanical separation and accumulation processes. However, the modelling shows that the Marginal Zone sequence must have formed from one composition of magma during a period in which the magma chamber was temporarily closed.

- The trapped liquid content in the Marginal Zone is very low and the rocks are classified as adcumulates-mesocumulates. The sequence is interpreted as having formed from in-situ crystallization with floatation of plagioclase, thereby separating cotectic assemblages, mixing minerals resulting in non-cotectic minerals coexisting in the same rock.

- Whole-rock incompatible trace elements compositions in the Marginal Zone support the interpretation that this section of the Clapham Trough contains very low trapped liquid content.

- The Marginal Zone formed from a liquid of andesitic basalt composition with a starting composition of 6 wt. % MgO and 56.7 w. % SiO_2 derived from about 30 % differentiation of B1-magma of Wilson (2012). The composition sequence of the Marginal Zone is producible with up to 54 % crystallization.

- The residual magma from the 54 % crystallization ponded at the top of the magma chamber (as it existed at that stage) with the composition of 3.5 wt % MgO and 59.45 wt. % SiO_2.

- Mixing of a large volume of B1-magma and the residual magma from the Marginal Zone formed the parental magma of the Lower Zone A described in the CH6 section. The mixing ratio is 20-30 wt % of residual magma to 70-80 wt. % B1-magma.
- The Transitional Pyroxenite in Clapham Trough hosts evidence of mixing and gradual compositional variation from the Marginal Zone to the Lower Zone. The textures described in this unit and the geochemistry support the interpretation that the narrow zone is a result of magma mixing.
- The Lower Zone A sequence is a correlative of the Lower Orthopyroxenite unit of Cameron (1978).
- The parental magma of the Lower Zone A is modelled to have about 10.58 wt. % MgO and 56.76 wt. % SiO_2.
- This composition is capable of producing orthopyroxene composition of En_{88-86}, which is consistent with the Clapham and Olifants River Troughs.
- The CH6 sequence has two marker interlayered norite horizons. The orthopyroxene is En_{83-82} and is interpreted as rapid cooling and fractionation of relatively evolved composition.
- Apart from the interlayered norite horizons, the Lower Zone succession has relatively constant whole-rocks and orthopyroxene compositions (in terms of Mg#).
- The Lower Zone A formed through contemporaneous crystallization and emplacement of new B1-magma and the norite is interpreted as the zone that was in contact with the roof prior to the emplacement of large volume of new magma that formed the Lower Zone.
- The whole-rocks and mineral geochemistry show that the Lower Zone A can be separated into the lower Clapham Orthopyroxenite sequence and the upper Rostock Orthopyroxenite

sequence. The boundary between the two is marked by the stratigraphically lower norite horizon.

9.2. Conclusions

The Marginal Zone succession present at the Clapham Trough represents a fractionated sequence of cumulate rocks that formed from the earliest intrusion of the B1-magma, after 30 % crystallization had occurred. The fractionation formed a pyroxene-rich Mafic Norite and a plagioclase-rich Shelter Norite. During the crystallization and accumulation of the Marginal Zone rocks, the Bushveld Complex magma chamber was temporarily closed and no new injection of magma occurred. The accumulation was a relatively slow process, such that most of the trapped liquid was removed prior to complete solidification. The accumulation occurred through modified *in-situ* crystallization that was coupled with floatation of plagioclase through convection currents. The mineral disequilibrium between plagioclase and orthopyroxene in the same rock is interpreted as a direct cause of the mutually reversed evolution trends between the minerals phases through separation (floatation) of cotectic cumulus minerals by convective currents. This study presents strong evidence that the Marginal Zone rocks do not represent a chill phase of the Lower Zone magma, but represent the evolved part of the an earlier emplacement of B1-magma.

After 54 % crystallisation another major impulse of B1-magma was emplaced into the fractionating chamber, and it interrupted the residual magma from completing the fractionation trajectory. The mixing of this residual magma and primitive B1-magma is parental to at least the Lower Zone A, which is the correlative of the Lower Orthopyroxenite Subzone at Olifants River Trough. At this stage the Bushveld Complex magma chamber may have been an open system, with contemporaneous magma emplacement and differentiation taking place. The result of these simultaneous process resulted in maintaining an almost constant composition of the cumulate rocks and mineral phase (orthopyroxene). The exception is only in the interlayered norite marker horizons

that are envisaged to have been near the roof of the chamber at the time of formation, and formed from a relatively rapidly cooled (and slightly evolved) liquid derived from the parental magma.

References

Ashwal, LD; Webb, SJ and Knoper, MW. 2005. *Magmatic stratigraphy in the Bushveld Northern Lobe: continuous geophysical and mineralogical data from the 2950 m Bellevue drillcore*. South African Journal of Geology, **108**, pp. 199-232.

Barnes, S-J; Maier, WD and Curl, EA. 2010. *Compositions of the Marginal Rocks and Sills of the Rustenburg Layered Suite, Bushveld Complex, South Africa: Implications for the formation of the Platinum-Group Element Deposits*. Economic Geology, **105**, pp. 11491-1511.

Bolikhovskaya SV, Vasil'eva MO, Koptev-Dvornikov EV. 1995. *Modelling of low-Ca pyroxene crystallization in basic systems (New versions of geothermometers)*. Geokhimia, **12**, pp. 1710-1727.

Cameron, EN. 1978. *The Lower Zone of the eastern Bushveld Complex in the Olifants River Trough*. Journal of Petrology, **19**, pp. 437-462.

Cawthorn, RG; Davies, G; Clubley-Armstrong, A; and McCarthy, TS. 1981. *Sills associated with the Bushveld Complex, South Africa: an estimate of parental magma composition*. Lithos, **14**, pp. 1-15.

Cawthorn, RG and Davies, G. 1983.*Experimental Data at 3 Kbars pressure on parental magma to the Bushveld Complex*. Contributions to Mineral Petrology, **83**, pp. 128-135.

Cawthorn, RG and Walraven, F. 1998. *Emplacement and Crystallization Time for the Bushveld Complex*. Journal of Petrology, **39**, pp. 1669-1687.

Cawthorn, RG. 1999. *Platinum-group element mineralization in the Bushveld Complex- a critical reassessment of geochemical models*. South African Journal of Geology, **102**, pp. 268-281.

Cawthorn, RG and Webb, SJ. 2001. *Connectivity between the western and eastern limbs of the Bushveld Complex*. Tectonophysics, **330**, pp. 195-209.

Cawthorn, RG. 2007. *Cr and Sr: Keys to parental magmas and processes in the Bushveld Complex, South Africa*. Lithos, **95**, pp. 381-398.

Cheney, ES and Twist, D. 1991. *The conformable emplacement of the Bushveld mafic rocks along a regional unconformity in the Transvaal succession of South Africa*, Precambrian Research, **52**, pp. 115-132.

Clarke, B; Uken, R and Reinhardt, T. 2009. *Structural and compositional constraints on the emplacement of the Bushveld Complex, South Africa*. Lithos, **111**, pp. 21-36.

Clarke, B; Uken, R and Reinhardt, T. 2009. *The Geometry and emplacement mechanics of a Bushveld Complex peridotite body, South Africa*. South African Journal of Geology, **112**, pp. 141-162.

Danyushevsky, LV. 2001. *The effects of small amounts of H_2O on crystallization of mid-ocean ridge and back-arc basin magmas*. Journal of Volcanology and Geothermal Research, **110**, pp. 265-280.

Danyushevsky, LV and Plechov, P. 2011. *Petrology3: Integrated software for modeling crystallization processes*. Geochem., Geophys., Geosyst., **12**, Q07021, doi:10.1029/2011GC003516.

Eales, HV; Marsh, JS; Mitchell, AA; De Klerk, WD; Kruger, JH and Field, M. 1986. *Some geochemical constraints upon models of the crystallization of the Upper Critical Zone – Main Zone interval, northwestern Bushveld Complex*. Mineralogical Magazine, **50**, pp. 567-582.

Eales, HV and Cawthorn, RG, 1996. *The Bushveld Complex.* In: RG. Cawthorn (Ed.). 1996. Layered Intrusions, Elsevier Science, Amsterdam, Netherlands, pp. 181-230.

Eales, HV and Costin, G. 2012. *Crustally Contaminated Komatiite: Primary Source of the Chromitites and Marginal, Lower, and Critical Zone Magmas in a Staging Chamber Beneath the Bushveld Complex*. Economic Geology, **107**, pp. 645-665.

Godel, B; Barnes, S-J and Maier, WD. 2011. *Parental Magma composition inferred from trace elements in cumulus and intercumulus silicate minerals: An example from the Lower and Lower Critical Zones of the Bushveld Complex, South Africa*. Lithos, **125**, pp. 537-552.

Harmer, RE and Sharpe, MR. 1985. *Field Relations and Strontium Isotope Systematics of the Marginal Rocks of the Eastern Bushveld Complex*. Economic Geology, **80**, pp. 813-837.

Irvine, TN. 1977.*Origin of chromitite layers in the Muskox intrusion and other stratiform intrusions: a new interpretation*. Geology, **5**, pp. 273-277.

Irvine, TN. 1982. *Terminology for Layered Intrusions*. Journal of Petrology, **23**, pp. 127-162.

Kinnaird, JA; Hutchinson, D; Schurmann, C; Nex, PAM and de Lange, R. 2005. *Petrology and mineralization of the southern Platreef: Northern limb of the Bushveld Complex, South Africa*, Mineralium Deposita, **40**, pp. 576-597.

Kruger, JF. 2005. *Filling the Bushveld Complex magma chamber: lateral expansion, roof and floor interaction, magmatic unconformities, and the formation of giant chromitite, PGE and Ti-V-magmatic deposits*. Mineralium Deposita, **40**, pp. 451-472.

Latypov, RM. 2003a.*The Origin of Marginal Compositional Reversals in Basic-Ultrabasic Sills and Layered Intrusions by Soret fractionation*. Journal of Petrology, **44**, 1579-1618.

Latypov, RM. 2003b.*The Origin Basic-Ultrabasic Sills with S-, D- and I-shaped Compositional Profiles by in Situ Crystallization of a Single Input of Phenocryst-poor Parental Magma*. Journal of Petrology, **44**, 1619-1656.

Latypov, R. 2009. *Testing the Validity of the Petrological Hypothesis 'No Phenocrysts, No Post-emplacement Differentiation'*. Journal of Petrology, **50**, pp. 1047-1069.

Maier, WD and Barnes, S-J. 1999. *Platinum-Group Elements in Silicate Rocks of the Lower, Critical and Main Zones at Union section, Western Bushveld Complex*. Journal of Petrology, **40**, pp. 1647-1671.

Marsh, JS. 1988. *Crystal capture, sorting and retention in convecting magma*. Geological Society of America, Bulletin, **100**, pp. 1720-1737.

McBirney, AR. 1989. *The Skaergaard Layered Series: I. Structure and average compositions*. Journal of petrology, **30**, pp 363-397.

McBirney, AR and Hunter, RH. 1995. *The Cumulate Paradigm Reconsidered*. Journal of Geology, **103**, pp. 114-122.

McBirney, AR. 1996. *The Skaergaard Intrusion*. In: Cawthorn, RG (Ed.). 1996. Layered intrusions. Elsevier Science, Amsterdam, Netherlands, pp. 147-180.

Mondal, SK and Mathez, EA. 2007. *Origin of the UG2 chromitite layer, Bushveld Complex*. Journal of Petrology, **48**, pp. 495-510.

Murase, T and McBirney, AR. 1973.*Properties of some common igneous rocks and their melts at high temperatures*. Geological Society of America, Bulletin, **80**, pp. 3563-3592.

Naldrett, AJ; Wilson, A; Kinnaird, J and Chunnett, G. 2009. *PGE tenor and metal ratios within and below the Merensky reef, Bushveld Complex: Implications for its genesis*. Journal of Petrology, **50**, pp. 625-659.

Namur, O; Charlier, B; Pirard, C; Hermann, J; Liegeois, J-P and Auwera, JV. 2011. *Anorthosite formation by plagioclase flotation in ferrobasalt and implications for the lunar crust*. Geochimica et Cosmochimica Acta, **75**, pp. 4998-5018.

Naslund, HR and McBirney, AR. 1996. *Mechanisms of Formation of Igneous Layering*. In: RG. Cawthorn (Ed.). 1996. Layered Intrusions, Elsevier Science, Amsterdam, Netherlands, pp. 181-230.

Roelofse, F and Ashwal, LD. 2012. *The Lower Main Zone in the Northern Limb of the Bushveld Complex- a >1.3 km Think Sequence of Intruded and Variably Contaminated Crystal Mushes*. Journal of Petrology, **53**, pp. 1449-1476.

Scoates, JS. 2000. *The Plagioclase-Magma Density Paradox re-examined and the Crystallization of Proterozoic Anorthosites*. Journal of Petrology, **41**, pp. 627-649.

Seabrook, CL. 2005. *The Upper Critical Zone and Lower Main Zones of the eastern Bushveld Complex*. Unpublished PhD Thesis, University of the Witwatersrand, Johannesburg, 211 p.

Sharpe, MR, 1981. *The Chronology of magma influxes to the eastern compartment of the Bushveld Complex as exemplified by its marginal border groups*. Journal of the Geological Society of London, **138**, pp 307-326.

Sharpe, MR and Hulbert, LJ. 1985. *Ultramafic sills beneath the eastern Bushveld Complex: Mobilized suspensions of early Lower Zone cumulates in a parental liquid boninitic affinities*. Economic Geology, **80**, pp. 849-871.

SACS, 1980. *Lithostratigraphy of the Republic of South Africa, South West Africa/Namibia, and the Republics of Bophuthatswana, Transkei and Venda.* In: Kent, LE (Ed). 1980. Stratigraphy of South Africa, Part 1. Pretoria: Handbook of the Geological Survey of South Africa, **8**, 223-242 p.

Tanner, D; Mavrogenes, JA; Arculus, RJ and Jenner, FE. 2014. *Trace Element Stratigraphy of the Bellevue Core, Northern Bushveld: Multiple Injections Obscured by Diffusive Processes*. Journal of Petrology, **55**, pp. 859-882.

Teigler, B and Eales, HV. 1996. *The Lower and Critical Zones of the western limb of the Bushveld Complex as intersected by the Nooitgedacht Boreholes*. Geological Survey of South Africa, **111**, 206 p.

Wager, LR and Brown, GM. 1968. Layered Igneous Rocks. Oliver and Boyd, Edinburgh and London, 588 p.

Walker, D and Hays, JF. 1977. *Plagioclase flotation and lunar crust formation*. Geology, 5, pp. 425-428.

Webb, SJ; Ashwal, LD and Cawthorn, RG. 2011. *Continuity between eastern and western Bushveld Complex, South Africa, confirmed by xenoliths from kimberlite*. Contributions to Mineral Petrology, **162**, pp. 101-107.

Wilson, AH. 1992. *The Geology of the Great dyke, Zimbabwe: Crystallization, Layering, and Cumulate Formation in the P1 Pyroxenite of Cyclic unit 1 of the Darwendale Subchamber*. Journal of Petrology, **33**, pp. 611-663.

Wilson, AH and Chunnett, G. 2010. *New Insight into the Stratigraphy, Emplacement and Evolution of the Basal Ultramafic Succession in the Eastern Bushveld Complex, South Africa*. In: P. Jugo, J. Mungall, and H. Brown (Eds). 11th International Platinum Symposium, June, 2010, Sudbury, Extended abstracts, http://11thIPS.laurentian.ca.

Wilson, AH. 2012. *A Chill Sequence to the Bushveld Complex: Insight into the First Stage of Emplacement and Implications for the Parental Magmas*. Journal of Petrology, **53**, pp. 1123-1168.

Willemse, J. 1959. *The 'floor' of the Bushveld Igneous Complex and its relationships, with special reference to the eastern Transvaal*. Transactions and Proceedings of the Geological Society**,** **62**, pp. 22-83.

Appendix A: Lithological Logs of the Clapham Drill Cores

A.1 CH6 Drill Core

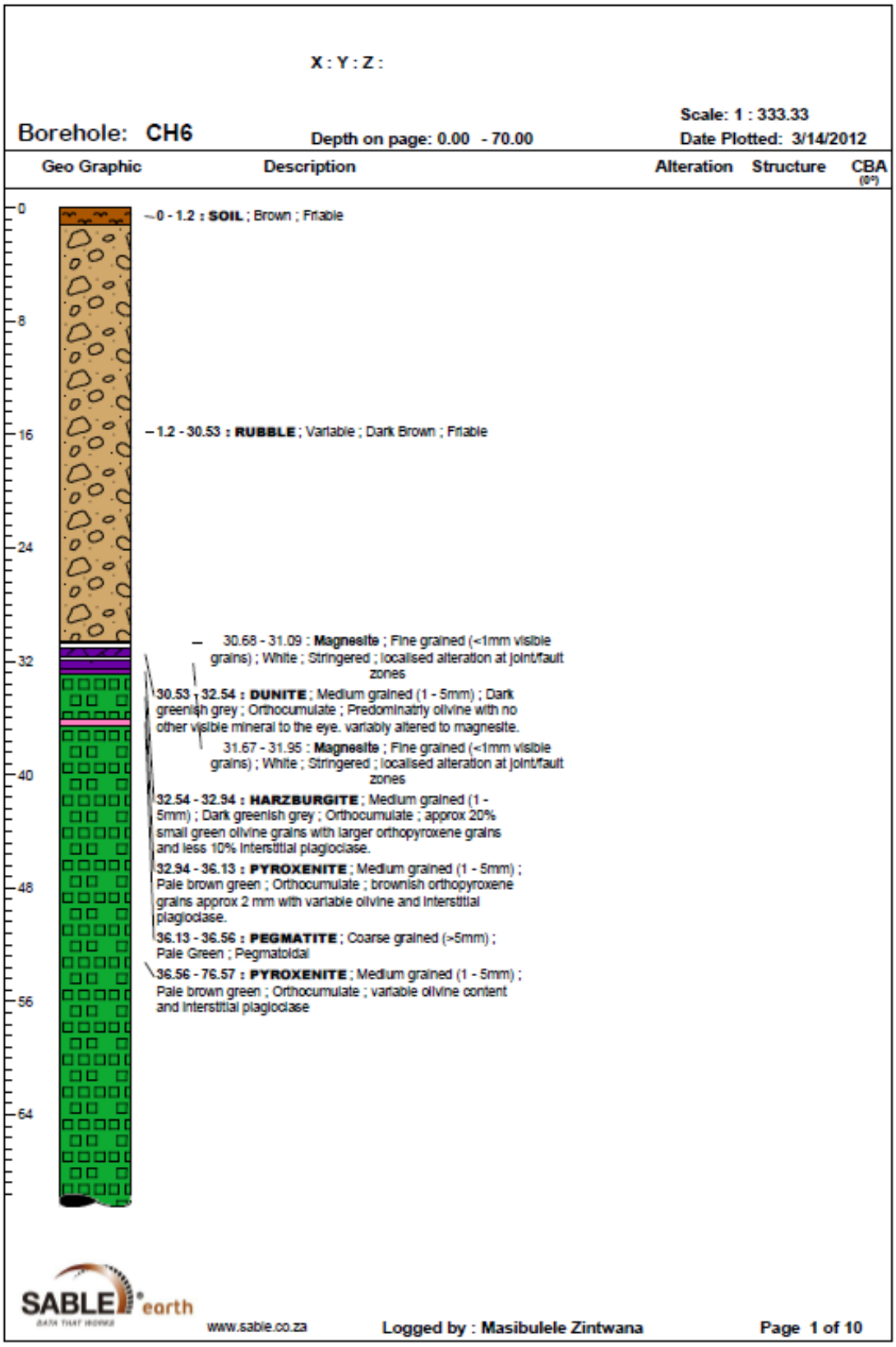

X : Y : Z :

Borehole: **CH6** Depth on page: 70.00 - 140.00 Scale: 1 : 333.33 Date Plotted: 3/14/2012

Geo Graphic	Description	Alteration	Structure	CBA (0°)
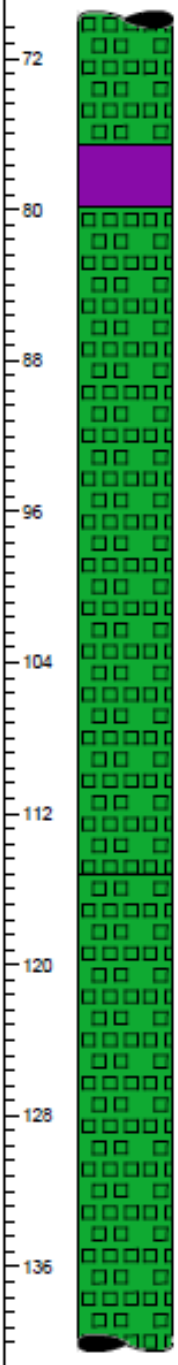	– 36.56 - 76.57 : **PYROXENITE** ; Medium grained (1 - 5mm) ; Pale brown green ; Orthocumulate ; variable olivine content and interstitial plagioclase			
	– 76.57 - 79.86 : **HARZBURGITE** ; Medium grained (1 - 5mm) ; Dark greenish grey ; Orthocumulate			76-80
	– 79.86 - 161.5 : **PYROXENITE** ; Medium grained (1 - 5mm) ; Pale brown green ; Orthocumulate ; variable olivine and interstitial plagioclase. ; the long axis of the orthopyroxene grains at a small angle (approx 10 deg) to the core axis. The bottom contact appears eroded.			76-80
	\ 115.2 - 115.2 : **PYROXENITE** ; Medium grained (1 - 5mm) ; Pale brown green ; Orthocumulate ; Interstitial plagioclase amount increases below 155.2 m			

72 80 88 96 104 112 120 128 136

SABLE earth

www.sable.co.za Logged by : Masibulele Zintwana Page 2 of 10

X : Y : Z :

Borehole: CH6 | Depth on page: 140.00 210.00 | Scale: 1 : 333.33 | Date Plotted: 3/14/2012

Geo Graphic	Description	Alteration	Structure	CBA (0°)
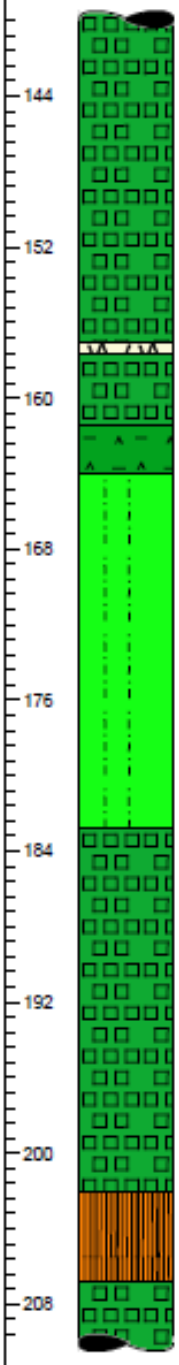	– 79.86 - 161.5 : **PYROXENITE** ; Medium grained (1 - 5mm) ; Pale brown green ; Orthocumulate ; variable olivine and interstitial plagioclase. ; the long axis of the orthopyroxene grains at a small angle (approx 10 deg) to the core axis. The bottom contact appears eroded.			76-80
	– 157.04 - 157.64 : CALC-SILICATE ; Medium grained (1 - 5mm) ; Whitish green grey ; Stringered ; bands of white and dark green silicates. Calcite and epidote with sporadic chromites along the top margins of the xenolith			
	– 161.5 - 163.96 : **FELDSPATHIC PYROXENITE** ; Fine to medium ; Pale Brown ; Laminated ; contains variable plagioclase content such that it's noritic in place.			
	– 163.96 - 182.75 : **NORITE** ; Fine to coarse ; Pale brown green ; Laminated			75-79
	– 182.75 - 257.06 : **PYROXENITE** ; Medium grained (1 - 5mm) ; Pale brown green ; Orthocumulate ; brownish orthopyroxenes with variable olivine and interstitial plagioclase. grain side varies locally to fine. ; locally contains cumulus plagioclase forming stringers of anorthosite and norite and minor olivine in lower parts of the unit, near hornfels xenolith			
	202.1 - 206.8 : HORNFELS ; Very fine ; Black ; N/A			

144 152 160 168 176 184 192 200 208

SABLE earth DATA THAT WORKS

www.sable.co.za | Logged by : Masibulele Zintwana | Page 3 of 10

X : Y : Z :

Borehole: CH6 | Depth on page: 210.00 280.00 | Scale: 1 : 333.33 | Date Plotted: 3/14/2012

Geo Graphic	Description	Alteration	Structure	CBA (g/t)

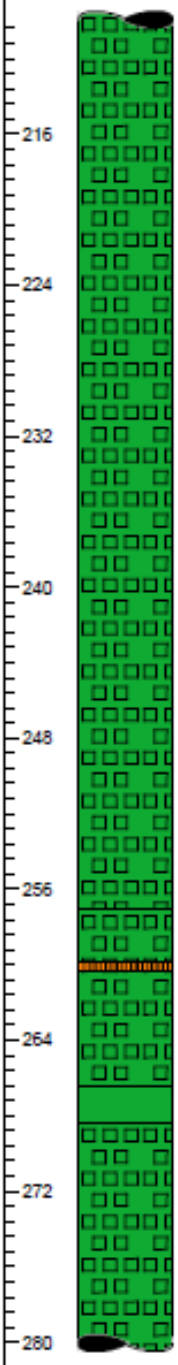

– **182.75 - 257.06 : PYROXENITE** ; Medium grained (1 - 5mm) ; Pale brown green ; Orthocumulate ; brownish orthopyroxenes with variable olivine and interstitial plagioclase. grain side varies locally to fine. ; locally contains cumulus plagioclase forming stringers of anorthosite and norite and minor olivine in lower parts of the unit, near hornfels xenolith

– 259.91 - 260.33 : **HORNFELS** ; Very fine ; Black ; N/A

– **257.06 - 266.45 : PYROXENITE** ; Medium grained (1 - 5mm) ; Dark greenish grey ; Orthocumulate ; Dark olivine grains with relatively coarse orthopyroxenes and interstitial plagioclase ; olivine content is slightly variable downwards, below the 42 cm xenolith. olivine pyroxenite

266.45 - 268.35 : PEGMATOIDAL PYROXENITE ; Fine to coarse ; Dark greenish grey ; Orthocumulate ; coarse pyroxene with smaller olivine cumulus grains and interstitial plagioclase — 77

– **268.35 - 290.46 : PYROXENITE** ; Medium grained (1 - 5mm) ; Pale brown green ; Orthocumulate ; brownish green orthopyroxene and olivine grains in variable amounts and interstitial plagioclase ; locally variable plagioclase resulting in localised stringers

SABLE earth
DATA THAT WORKS

www.sable.co.za | Logged by : Masibulele Zintwana | Page 4 of 10

X : Y : Z :

Borehole: **CH6** Depth on page: 280.00 350.00 Scale: 1 : 333.33 Date Plotted: 3/14/2012

Geo Graphic	Description	Alteration	Structure	CBA (0°)
280				
	– 268.35 - 290.46 : **PYROXENITE** ; Medium grained (1 - 5mm) ; Pale brown green ; Orthocumulate ; brownish green orthopyroxene and olivine grains in variable amounts and interstitial plagioclase ; locally variable plagioclase resulting in localised stringers			
288				
	– 290.46 - 292.36 : **NORITE** ; Medium grained (1 - 5mm) ; Pale whitish brown ; Orthocumulate ; cumulus plagioclase with brownish orthopyroxene grains ; contains stringers of plagioclase, varying from norite to pyroxenite through anorthosite in mm-cm scale layering.			77
296				
	292.36 - 297.76 : **PYROXENITE** ; Medium grained (1 - 5mm) ; Pale brown green ; Orthocumulate			
	297.76 - 298 : **NORITE** ; Medium grained (1 - 5mm) ; Pale whitish brown ; Orthocumulate ; cumulus plagioclase with brownish orthopyroxene grains			
304				
312				
	– 298 - 328.38 : **PYROXENITE** ; Medium grained (1 - 5mm) ; Pale brown green ; Orthocumulate ; orthopyroxene and plagioclase mainly with variable amounts of clinopyroxenes locally. ; grain size and plagioclase content vary.			76-80
320				
328				
336				
	– 328.38 - 443.2 : **FELDSPATHIC PYROXENITE** ; Medium grained (1 - 5mm) ; Pale whitish brown ; Orthocumulate ; Brownish-green orthopyroxene needles with cumulus plagioclase ; interlayered norite, anorthosite-pyroxenite			76-80
344				

X : Y : Z :

Borehole: **CH6**

Depth on page: 350.00 420.00

Scale: 1 : 333.33

Date Plotted: 3/14/2012

Geo Graphic	Description	Alteration	Structure	CBA (0°)

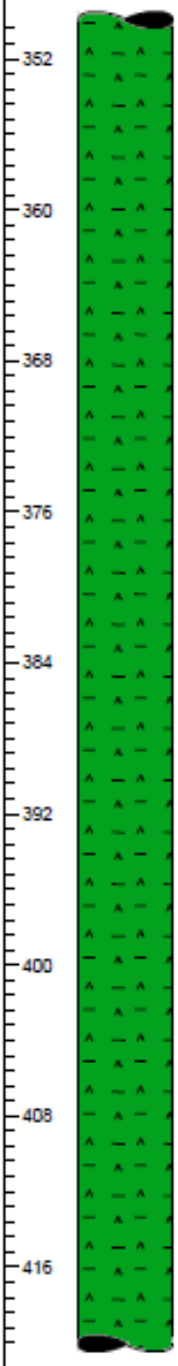

– 328.38 - 443.2 : **FELDSPATHIC PYROXENITE** ; Medium grained (1 - 5mm) ; Pale whitish brown ; Orthocumulate ; Brownish-green orthopyroxene needles with cumulus plagioclase ; Interlayered norite, anorthosite-pyroxenite

SABLE earth

www.sable.co.za

Logged by : Masibulele Zintwana

Page 6 of 10

X : Y : Z :

Borehole: **CH6** Depth on page: 420.00 490.00 Scale: 1 : 333.33 Date Plotted: 3/14/2012

Geo Graphic	Description	Alteration	Structure	CBA (0°)

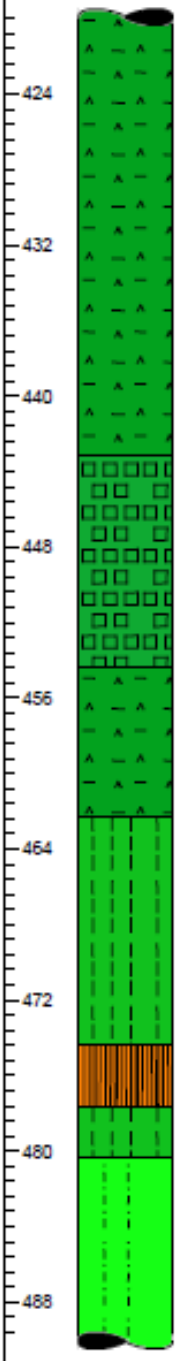

– 328.38 - 443.2 : **FELDSPATHIC PYROXENITE** ; Medium grained (1 - 5mm) ; Pale whitish brown ; Orthocumulate ; Brownish-green orthopyroxene needles with cumulus plagioclase ; interlayered norite, anorthosite-pyroxenite

– 443.2 - 454.35 : **PYROXENITE** ; Medium grained (1 - 5mm) ; Pale brown green ; Orthocumulate ; Contains brownish opx with interstitial plag and cpx oikocrysts ; contains patchy feldpathic units about 2cm resulting in 'two colours' in one pyroxenite

– 454.35 - 462.33 : **FELDSPATHIC PYROXENITE** ; Medium grained (1 - 5mm) ; Pale brown green ; Friable ; Contains opx with pockets of plagioclase and minor cpx

– 462.33 - 480.33 : **MELANORITE** ; Medium grained (1 - 5mm) ; Pale green grey ; Orthocumulate ; Cumulus, tabular plagioclase with abundant orthopyroxene ; the amount of plagioclase is slightly lower than typical norite but higher than feldspathic pyroxenite.

\ 474.35 - 477.63 : **HORNFELS** ; Very fine ; Black ; Massive ; cannot identify with naked eye.

– 480.33 - 563.51 : **NORITE** ; Fine to medium ; Pale green grey ; Granular ; Cumulus plagioclase with opc and some cpx ; fine grain norite relative to critical zone.

X : Y : Z :

Borehole: CH6

Depth on page: 490.00 560.00

Scale: 1 : 333.33

Date Plotted: 3/14/2012

Geo Graphic	Description	Alteration	Structure	CBA (0°)
496	496.19 - 497.1 : **NORITE** ; Fine grained (<1mm visible grains) ; Pale green grey ; Granular			77
	497.2 - 497.45 : **CALC-SILICATE** ; Fine grained (<1mm visible grains) ; Whitish green grey ; Stringered			
504				
512				
520				
	480.33 - 563.51 : **NORITE** ; Fine to medium ; Pale green grey ; Granular ; Cumulus plagioclase with opc and some cpx ; fine grain norite relative to critical zone.			77
528	527.77 - 527.81 : **NORITE** ; Very fine ; Whitish green grey ; Fine Grained			
536				
544				
552				
560				

X : Y : Z :

Borehole: CH6 | Depth on page: 560.00 630.00 | Scale: 1 : 333.33 | Date Plotted: 3/14/2012

Geo Graphic	Description	Alteration	Structure	CBA (0°)
560 568 576 584 592 600 608 616 624	– 480.33 - 563.51 : **NORITE** ; Fine to medium ; Pale green grey ; Granular ; Cumulus plagioclase with opc and some cpx ; fine grain norite relative to critical zone.			
	– 563.51 - 647.01 : **MELANORITE** ; Medium grained (1 - 5mm) ; Pale green grey ; Granular ; feldspar decreases with depth (varies from noritic to feldpathic pyroxenite).			77-80

X : Y : Z :

Borehole: **CH6**

Depth on page: 630.09 691.50

Scale: 1 : 333.33

Date Plotted: 3/14/2012

Geo Graphic	Description	Alteration	Structure	CBA (0°)

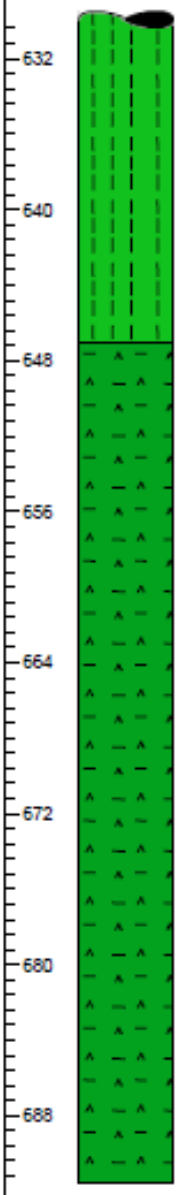

563.51 - 647.01 : **MELANORITE** ; Medium grained (1 - 5mm) ; Pale green grey ; Granular ; feldspar decreases with depth (varies from noritic to feldpathic pyroxenite).

647.01 - 691.5 : **FELDSPATHIC PYROXENITE** ; Fine to medium ; Dark greenish grey ; Granular ; contains more feldspar and cpx (<10%) than the feldpathic pyroxenite in the LZ

SABLE earth
DATA THAT WORKS

www.sable.co.za

Logged by : Masibulele Zintwana

Page 10 of 10

A.2: CH1 Drill Core as logged by Prof. A.H. Wilson

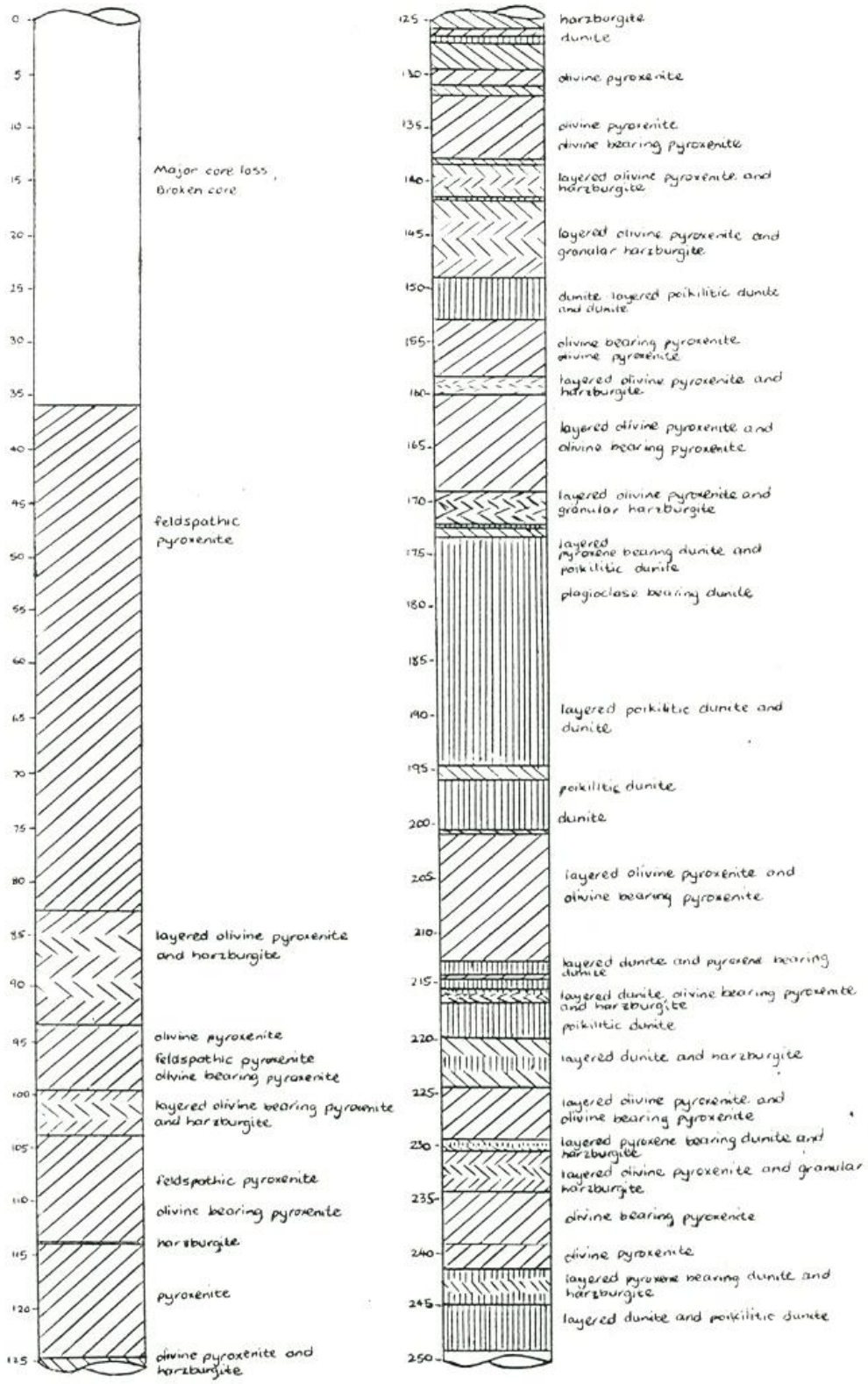

FIGURE 2 STRATIGRAPHIC SECTION THROUGH THE FIRST 250 m OF BOREHOLE CORE CH1

A.3: CH1 with added 30 m at bottom

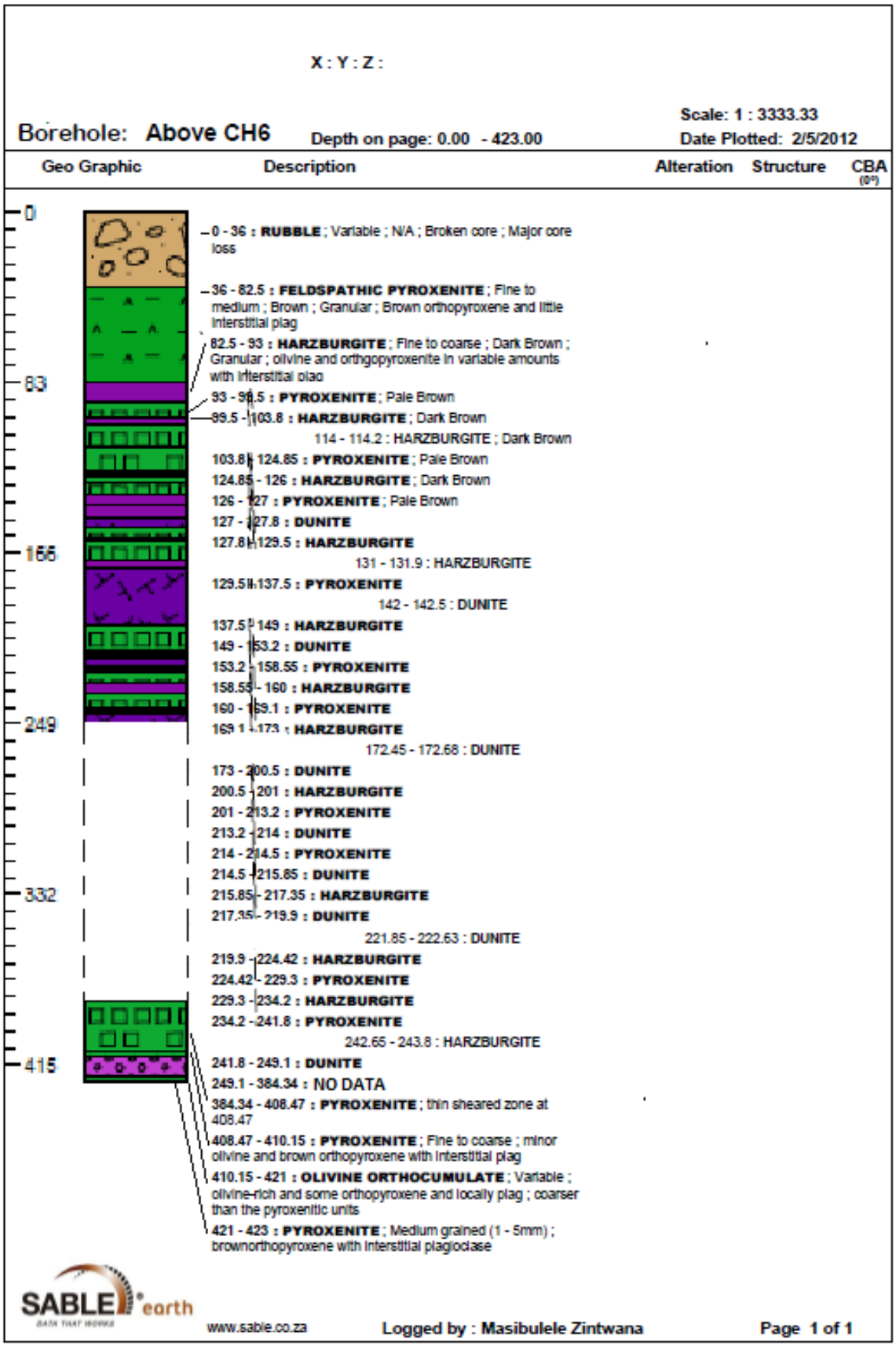

X : Y : Z :

Borehole: Above CH6 Depth on page: 0.00 - 423.00 Scale: 1 : 3333.33 Date Plotted: 2/5/2012

Geo Graphic	Description	Alteration	Structure	CBA (0°)

0 – 0 - 36 : **RUBBLE** ; Variable ; N/A ; Broken core ; Major core loss

36 - 82.5 : **FELDSPATHIC PYROXENITE** ; Fine to medium ; Brown ; Granular ; Brown orthopyroxene and little interstitial plag

82.5 - 93 : **HARZBURGITE** ; Fine to coarse ; Dark Brown ; Granular ; olivine and orthgopyroxenite in variable amounts with interstitial plag

83 – 93 - 99.5 : **PYROXENITE** ; Pale Brown

99.5 - 103.8 : **HARZBURGITE** ; Dark Brown

114 - 114.2 : HARZBURGITE ; Dark Brown

103.8 - 124.85 : **PYROXENITE** ; Pale Brown

124.85 - 126 : **HARZBURGITE** ; Dark Brown

126 - 127 : **PYROXENITE** ; Pale Brown

127 - 127.8 : **DUNITE**

127.8 - 129.5 : **HARZBURGITE**

131 - 131.9 : HARZBURGITE

166 – 129.5 - 137.5 : **PYROXENITE**

142 - 142.5 : DUNITE

137.5 - 149 : **HARZBURGITE**

149 - 153.2 : **DUNITE**

153.2 - 158.55 : **PYROXENITE**

158.55 - 160 : **HARZBURGITE**

160 - 169.1 : **PYROXENITE**

249 – 169.1 - 173 : **HARZBURGITE**

172.45 - 172.68 : DUNITE

173 - 200.5 : **DUNITE**

200.5 - 201 : **HARZBURGITE**

201 - 213.2 : **PYROXENITE**

213.2 - 214 : **DUNITE**

214 - 214.5 : **PYROXENITE**

214.5 - 215.85 : **DUNITE**

332 – 215.85 - 217.35 : **HARZBURGITE**

217.35 - 219.9 : **DUNITE**

221.85 - 222.63 : DUNITE

219.9 - 224.42 : **HARZBURGITE**

224.42 - 229.3 : **PYROXENITE**

229.3 - 234.2 : **HARZBURGITE**

234.2 - 241.8 : **PYROXENITE**

242.65 - 243.8 : HARZBURGITE

415 – 241.8 - 249.1 : **DUNITE**

249.1 - 384.34 : NO DATA

384.34 - 408.47 : **PYROXENITE** ; thin sheared zone at 408.47

408.47 - 410.15 : **PYROXENITE** ; Fine to coarse ; minor olivine and brown orthopyroxene with interstitial plag

410.15 - 421 : **OLIVINE ORTHOCUMULATE** ; Variable ; olivine-rich and some orthopyroxene and locally plag ; coarser than the pyroxenitic units

421 - 423 : **PYROXENITE** ; Medium grained (1 - 5mm) ; brownorthopyroxene with interstitial plagioclase

SABLE earth www.sable.co.za Logged by : Masibulele Zintwana Page 1 of 1

Appendix B: Methodology

B.1 Sample selection

A total of 185 samples were selected from the CH6 drill core for geochemical analyses. A detailed lithological logging of CH6 was done at the Wits University Earth Lab, Johannesburg, RSA. The samples were taken at least three metres apart, taking into account the dominant cumulate rocks. 20-30 cm long half-core (BQ diameter) samples were selected for all the different geochemical analyses performed in the present study. An additional 20 samples were selected from the bottom 30 m of the CH1 drill core. All the samples selected for the purposes of this study are coherent and fresh, and representative of the lithologies samples at all intervals. Thirty samples were selected at regular intervals for polished thin sections preparations from the CH6 drill core. These thin sections were extensively examined with transmitted light optical microscopy and electron microprobe analyses (EMPA). Additional twenty samples were selected (between the samples that were selected for thin section preparations) for mineral separate analyses.

B.2 Analytical techniques

The core samples were cut to half core and cleaned to remove any traces of cutting fluids and dust contamination. The other halves are preserved in the remaining CH6 drill core. Representative 3-5 cm blocks of the samples that were selected for the polished thin sections were cut and submitted for preparation at the Wits Geosciences rock laboratory. The rest of the samples were crushed in a Mo-steel jaw crusher to fragments less than 1 cm. In between sample exchange the jaw-crusher was stripped and scrubbed with a wire brush, then thoroughly vacuumed to remove the rock dust and wiped with acetone. The sample pan was vacuumed, washed with water and thoroughly cleaned with acetone. 30-60 seconds was allowed between samples for the crusher and sample pan to be

dry. At least 80 g of each sample fine milled and powdered in a carbon case-hardened pure iron rotary mill to produce homogenised powdered samples for the preparation of X-ray Fluorescence (XRF) and Inductively Coupled Plasma Mass Spectrometry (ICP-MS) analyses.

B.2.1 X-ray Fluorescence (XRF)

Whole rock major and trace element analyses were carried out with a Panalytical WD 2404 X-ray Fluorescence (XRF) spectrometer with a Rh tube running at 50 kV and 50 mA. Instrument calibration for major element analyses appears below and the running instrument parameters for trace element analyses were as per guidance of the software ProTrace. The homogenised, powdered rock samples were prepared in two different forms; first pressed pellets in 5 mm diameter aluminium dishes for trace element analyses. Second, fused glass beads (with lithium metaborate or tetraborate flux) were prepared for major element analyses.

Table B.1: Instrumental calibration parameters for major element analyses.

Element	Crystal	Collimator	Detector
Ti	LiF 200	150 µm	Flow
Ca	LiF 200	150 µm	Flow
K	PE 002-C	550 µm	Flow
Si	PE 002-C	550 µm	Flow
Al	PE 002-C	550 µm	Flow
Mg	PX1	550 µm	Flow
Na	PX1	550 µm	Flow
P	Ge 111-C	550 µm	Flow
Ni	LiF 220	150 µm	Duplex
Fe	LiF 220	150 µm	Flow
Mn	LiF 220	150 µm	Duplex
cr	LiF 220	150 µm	Duplex

The glass beads were fused using Johnson Matthey Spectroflux 105 at about 1100° C for about 40 minutes. The flux that was used is a commercially available flux with the composition of 47 % $Li_2B_4O_7$, 36.7 % Li_2CO_3 and 16 % La_2O_3. The major element concentrations were determined by running comparisons with known standard materials, namely: W2, GSP1, BCR2, NIM N, NIM P, NIM S, NIM 2 D, BHVO2, AGV2, G2, DTS1, PCC1, NIM G. In every five analyses instrumental drift test and compensation was also tracked by running measurements on an internal standard. The standards used for the trace element concentration determination were GSP2, NIM D, AGV2, BHVO2, and NIM S. These standards and the ProTrace drift standards ensured that the analytical data produced were accurate and precise.

B.2.2 Inductively Coupled Plasma Mass Spectrometry (ICP-MS)

55 of the whole rock samples of the 185 samples selected from the CH6 drill core were analysed for additional trace elements and rare earth elements (REE) using ICP-MS technique with a Perkin Elmer Elan Instrument. The instrument has low detection limits, and good accuracy and precision. The sample digestion used HF-HNO_3 solution in CEM Mars microware set at 235° C and 450 PSI for 40 minutes. After the drying, the samples were taken up into solution with 2 ml HNO_3 in capped beakers simmering at 60° C overnight (± 24 hours).

The samples were diluted 1000 times and mixed with internal Re, Rh, Bi to cover the required mass range. Primary external calibration standards were made up to cover the concentration range 5-100 ppb. Each ICP-MS analysis included the US Geological Survey Analysed Basalt BCR-1, Hawaiian Basalt BHVO-1, Icelandic Basalt BIR-1 control standards. All elements the standard deviation was less than 10 % from the reported standard values.

The LA-ICP-MS analyses were done and provided for use in this work by Prof. AH Wilson from the samples that were analysed with Electron Microprobe for major elements (below). The data

were provided as single point data and are treated in this work in similar fashion as the solution ICP-MS data.

B.2.3 Electron Microprobe

The major element compositions of the mineral phases were analysed with a CAMECA SX100 electron microscope at Spectrau laboratory at the University of Johannesburg. Standard operating conditions included a filament current of 30 nA at 20 kV and a beam diameter of 5 μm. The instrument calibrations were done internally by Dr C. Reinke using Almandine and Diopside standards. The calibration data appear below.

Point	Na	Mg	Al	Si	K	Ca	Ti	Cr	Mn	Fe	Ni	O	Total
1 / 1 .	0.01	1.40	11.16	17.41		2.93	0.04		0.18	27.75		39.88	100.76
2 / 1 .	0.00	1.43	11.22	17.43		2.94	0.05		0.21	27.75		39.99	101.02
3 / 1 .	0.01	1.42	11.17	17.50		2.71	0.03		0.20	27.85		39.95	100.85
4 / 1 .	0.05	10.99	0.02	25.93		18.29	0.03		0.07	0.65		44.33	100.36
5 / 1 .	0.05	11.02	0.02	25.76		18.32	0.03		0.06	0.64		44.18	100.09
6 / 1 .	0.03	10.96	0.02	25.92		18.49	0.04		0.05	0.64		44.38	100.54

sil_ni1a_chk_20120906a, mass %:

Point	Na	Mg	Al	Si	K	Ca	Ti	Cr	Mn	Fe	Ni	O	Total
1 / 1 .	0.00	1.40	11.19	17.54		3.05	0.05		0.18	27.54		40.06	101.02
2 / 1 .	0.01	1.44	11.14	17.55		2.94	0.04		0.16	27.95		40.11	101.34
3 / 1 .	0.01	1.45	11.21	17.61		2.65	0.04		0.17	28.01		40.15	101.31
4 / 1 .	0.04	10.95	0.02	25.89		18.17	0.03		0.08	0.70		44.23	100.10
5 / 1 .	0.04	10.98	0.02	25.80		18.28	0.04		0.08	0.65		44.19	100.08
6 / 1 .	0.03	11.08	0.03	25.88		18.26	0.03		0.07	0.67		44.34	100.39

Relative difference, %:

Na	Mg	Al	Si	K	Ca	Ti	Cr	Mn	Fe	Ni
	0.94	-0.03	0.69		0.70				0.18	
	0.12		-0.05		-0.71					

Appendix C: Geochemistry

Table C.1: Whole-rock major element geochemistry (XRF data) of the CH6 Drill Core in wt. %.

Sample No.	Depth (m)	Lithology	SiO_2	TiO_2	Al_2O_3	Fe_2O_3	FeO	MnO	MgO	CaO	Na_2O	K_2O	P_2O_5	Cr_2O_3	NiO	TOTAL	L.O.I.
CH6/1	30.59	Dunite	39.79	0.04	1.02	1.50	12.15	0.20	42.35	0.57	0.11	0.03	0.02	1.10	0.28	99.17	6.8
CH6/2	31.93	Dunite	39.03	0.03	0.85	1.61	13.02	0.20	43.50	0.21	0.06	0.01	0.02	1.13	0.31	99.99	9.22
CH6/3	42.60	Orthopyroxenite	53.38	0.08	1.63	1.09	8.82	0.20	32.51	1.46	0.05	0.00	0.01	0.63	0.12	99.97	-0.06
CH6/4	46.23	Orthopyroxenite	55.24	0.10	2.13	1.03	8.31	0.19	30.41	1.85	0.11	0.04	0.01	0.42	0.10	99.95	-0.07
CH6/5	50.26	Orthopyroxenite	55.65	0.10	1.96	1.03	8.31	0.19	30.65	1.75	0.14	0.04	0.01	0.48	0.09	100.40	-0.26
CH6/6	52.75	Orthopyroxenite	55.32	0.09	1.98	1.03	8.30	0.20	30.70	1.74	0.13	0.03	0.01	0.51	0.11	100.14	-0.23
CH6/7	55.18	Orthopyroxenite	55.87	0.10	2.23	1.01	8.22	0.19	30.14	1.79	0.14	0.13	0.01	0.46	0.09	100.38	-0.18
CH6/8	59.10	Orthopyroxenite	55.59	0.09	1.88	1.02	8.23	0.19	30.85	1.72	0.13	0.02	0.01	0.45	0.09	100.27	-0.41
CH6/9	62.53	Orthopyroxenite	55.63	0.11	2.49	1.01	8.17	0.18	29.89	2.00	0.22	0.07	0.01	0.45	0.09	100.31	-0.19
CH6/10	64.19	Orthopyroxenite	55.28	0.10	2.21	1.00	8.10	0.19	30.18	1.88	0.15	0.02	0.01	0.49	0.09	99.69	-0.24
CH6/11	68.23	Orthopyroxenite	55.30	0.10	2.45	1.01	8.16	0.19	30.21	1.90	0.18	0.07	0.01	0.46	0.10	100.14	-0.19
CH6/12	70.15	Orthopyroxenite	54.81	0.09	2.04	1.05	8.50	0.19	31.40	1.68	0.07	0.01	0.01	0.50	0.10	100.45	-0.14
CH6/13	76.27	Harzburgite	45.54	0.06	1.44	1.37	11.07	0.20	38.88	1.01	0.17	0.05	0.01	0.54	0.21	100.55	-0.42
CH6/14	78.71	Harzburgite	45.17	0.05	1.24	1.36	10.98	0.20	39.76	0.94	0.11	0.02	0.02	0.25	0.23	100.31	-0.41
CH6/15	81.49	Orthopyroxenite	55.54	0.11	2.25	1.01	8.17	0.19	30.38	1.81	0.16	0.04	0.01	0.48	0.09	100.23	-0.2
CH6/16	85.53	Orthopyroxenite	55.66	0.10	2.15	1.01	8.20	0.20	30.48	1.81	0.12	0.05	0.01	0.47	0.08	100.34	-0.22
CH6/17	88.25	Orthopyroxenite	55.71	0.10	2.01	1.01	8.16	0.19	30.88	1.74	0.16	0.05	0.01	0.49	0.09	100.60	-0.22
CH6/18	91.55	Orthopyroxenite	55.17	0.10	2.10	1.00	8.06	0.19	30.39	1.83	0.10	0.02	0.01	0.48	0.09	99.54	-0.21
CH6/19	94.42	Orthopyroxenite	55.87	0.10	1.93	1.00	8.07	0.19	30.90	1.81	0.20	0.04	0.01	0.49	0.09	100.69	-0.01
CH6/20	99.88	Orthopyroxenite	56.17	0.15	2.17	1.02	8.26	0.19	29.45	2.01	0.17	0.16	0.02	0.46	0.08	100.31	-0.17
CH6/21	102.89	Orthopyroxenite	55.58	0.10	2.48	1.02	8.28	0.19	29.96	2.15	0.27	0.03	0.02	0.48	0.09	100.65	-0.21
CH6/22	103.86	Orthopyroxenite	55.52	0.11	2.32	1.02	8.29	0.19	29.96	2.12	0.23	0.03	0.01	0.48	0.09	100.37	-0.19
CH6/23	106.50	Orthopyroxenite	55.50	0.10	2.24	1.03	8.38	0.19	29.97	2.12	0.26	0.03	0.01	0.47	0.10	100.39	-0.23
CH6/24	111.15	Orthopyroxenite	55.30	0.09	2.37	1.02	8.25	0.19	29.88	2.17	0.16	0.02	0.01	0.47	0.08	100.02	-0.21
CH6/25	115.15	Orthopyroxenite	55.50	0.09	1.84	1.04	8.41	0.20	30.76	1.90	0.18	0.02	0.01	0.57	0.09	100.60	-0.2

Table C.1: Continued

Sample No.	Depth (m)	Lithology	SiO_2	TiO_2	Al_2O_3	Fe_2O_3	FeO	MnO	MgO	CaO	Na_2O	K_2O	P_2O_5	Cr_2O_3	NiO	TOTAL	L.O.I.
CH6/26	118.41	Orthopyroxenite	55.58	0.11	2.07	1.10	8.88	0.21	29.60	2.12	0.20	0.05	0.01	0.45	0.08	100.45	-0.28
CH6/27	121.57	Orthopyroxenite	55.43	0.10	2.11	1.15	9.30	0.21	29.30	2.13	0.17	0.05	0.01	0.46	0.08	100.50	-0.33
CH6/28	124.78	Orthopyroxenite	55.23	0.09	2.10	1.19	9.63	0.22	29.40	2.12	0.10	0.01	0.01	0.46	0.08	100.63	-0.34
CH6/29	128.34	Orthopyroxenite	55.00	0.09	2.02	1.19	9.66	0.22	29.22	2.09	0.16	0.02	0.01	0.46	0.08	100.23	-0.34
CH6/30	132.47	Orthopyroxenite	55.12	0.09	2.17	1.21	9.81	0.22	28.77	2.25	0.13	0.03	0.01	0.42	0.08	100.32	-0.39
CH6/31	136.60	Orthopyroxenite	54.91	0.09	2.07	1.21	9.77	0.22	28.87	2.21	0.24	0.02	0.01	0.42	0.08	100.13	-0.37
CH6/32	139.86	Orthopyroxenite	54.88	0.08	2.49	1.23	9.93	0.23	28.62	2.35	0.07	0.01	0.01	0.42	0.08	100.39	-0.4
CH6/33	143.19	Orthopyroxenite	54.84	0.08	1.93	1.24	10.06	0.23	28.89	2.15	0.10	0.01	0.01	0.42	0.09	100.05	-0.38
CH6/34	145.43	Pyroxenite	54.83	0.09	1.92	1.23	9.92	0.24	28.72	2.21	0.15	0.02	0.01	0.40	0.08	99.81	-0.41
CH6/35	149.16	Pyroxenite	55.01	0.10	2.34	1.23	9.98	0.24	28.33	2.45	0.37	0.05	0.01	0.30	0.08	100.49	-0.44
CH6/36	153.67	Pyroxenite	54.95	0.10	2.39	1.20	9.71	0.25	28.34	2.59	0.21	0.04	0.01	0.27	0.08	100.13	-0.17
CH6/37	157.15	Pyroxenite*	53.05	0.11	2.86	1.15	9.34	0.23	28.73	3.99	0.10	0.02	0.01	0.24	0.07	99.92	-0.13
CH6/38	159.48	Int. Norite/Pyroxenite	53.74	0.08	7.79	0.98	7.97	0.20	23.78	5.04	0.39	0.02	0.01	0.21	0.07	100.29	-0.3
CH6/39	161.45	Pyroxenite	53.98	0.08	5.40	1.05	8.50	0.22	25.91	4.02	0.38	0.03	0.01	0.22	0.07	99.87	-0.32
CH6/40	164.18	Melanorite	52.75	0.07	12.13	0.79	6.42	0.17	20.10	7.12	0.60	0.02	0.01	0.14	0.05	100.37	-0.17
CH6/41	167.51	Int. Norite/Pyroxenite	50.02	0.06	20.91	0.39	3.18	0.09	9.77	14.30	1.14	0.04	0.01	0.08	0.02	100.02	0.09
CH6/42	170.44	Interlayered norite	51.38	0.07	15.36	0.60	4.85	0.13	15.28	11.29	0.80	0.04	0.01	0.13	0.04	99.98	-0.06
CH6/43	172.57	Interlayered norite	52.42	0.07	13.19	0.70	5.64	0.15	18.02	9.48	0.72	0.03	0.01	0.15	0.05	100.63	-0.03
CH6/44	176.09	Interlayered norite	52.54	0.07	13.13	0.69	5.60	0.15	18.27	9.26	0.76	0.05	0.01	0.16	0.05	100.75	-0.13
CH6/45	179.66	Interlayered norite	53.32	0.09	8.94	0.89	7.18	0.18	22.98	5.72	0.43	0.03	0.01	0.24	0.11	100.11	-0.18
CH6/46	182.54	Melanorite	50.62	0.08	6.40	1.09	8.85	0.18	28.16	3.92	0.25	0.02	0.01	0.60	0.17	100.35	-0.14
CH6/47	186.26	Pyroxenite	55.56	0.11	1.91	1.16	9.42	0.22	29.67	1.99	0.16	0.05	0.01	0.44	0.09	100.79	-0.38
CH6/48	189.16	Pyroxenite	55.44	0.13	2.06	1.13	9.18	0.21	29.24	2.13	0.16	0.09	0.01	0.42	0.09	100.30	-0.33
CH6/49	191.74	Pyroxenite	55.33	0.12	2.15	1.09	8.87	0.20	29.62	2.06	0.16	0.03	0.01	0.44	0.09	100.16	-0.3
CH6/50	194.86	Pyroxenite	50.31	0.11	1.86	1.04	8.45	0.20	29.11	1.93	0.19	0.03	0.01	0.43	0.08	93.76	-0.21

Table C.1: Continued

Sample No.	Depth (m)	Lithology	SiO_2	TiO_2	Al_2O_3	Fe_2O_3	FeO	MnO	MgO	CaO	Na_2O	K_2O	P_2O_5	Cr_2O_3	NiO	TOTAL	L.O.I.
CH6/51	198.51	Pyroxenite	55.61	0.13	2.32	1.07	8.64	0.20	29.64	2.10	0.16	0.05	0.01	0.46	0.09	100.47	-0.1
CH6/52	200.61	Pyroxenite	55.33	0.12	2.12	1.06	8.59	0.20	30.06	1.99	0.17	0.05	0.02	0.47	0.09	100.25	-0.23
CH6/53	207.54	Pyroxenite	55.76	0.12	1.90	1.07	8.70	0.20	29.99	1.95	0.12	0.05	0.01	0.45	0.08	100.39	-0.17
CH6/54	211.44	Pyroxenite	55.58	0.12	2.11	1.06	8.58	0.20	29.64	2.03	0.14	0.06	0.01	0.45	0.08	100.07	-0.19
CH6/55	216.27	Pyroxenite	55.78	0.13	2.14	1.06	8.60	0.20	29.62	2.07	0.20	0.09	0.02	0.45	0.08	100.44	-0.15
CH6/56	218.62	Pyroxenite	56.11	0.12	2.57	1.04	8.42	0.19	28.89	2.08	0.22	0.17	0.02	0.44	0.08	100.35	-0.17
CH6/57	219.59	Pyroxenite	55.72	0.12	2.12	1.06	8.61	0.19	29.73	2.01	0.14	0.06	0.01	0.45	0.08	100.31	-0.15
CH6/58	221.66	Pyroxenite	55.69	0.12	2.11	1.07	8.68	0.20	29.84	2.06	0.27	0.07	0.02	0.45	0.09	100.67	-0.23
CH6/59	223.12	Pyroxenite	54.91	0.12	2.14	1.05	8.51	0.20	29.65	2.10	0.17	0.06	0.02	0.46	0.08	99.46	-0.16
CH6/60	227.51	Pyroxenite	54.56	0.13	2.12	1.03	8.32	0.19	29.25	2.02	0.15	0.07	0.01	0.43	0.09	98.37	-0.25
CH6/61	230.36	Pyroxenite	55.75	0.12	2.19	1.05	8.51	0.20	29.78	2.00	0.18	0.07	0.01	0.47	0.08	100.41	-0.3
CH6/62	235.85	Pyroxenite	55.56	0.12	2.35	1.06	8.55	0.20	29.56	2.11	0.20	0.06	0.01	0.45	0.09	100.31	-0.27
CH6/63	238.80	Pyroxenite	55.47	0.12	2.30	1.06	8.56	0.20	29.39	2.03	0.18	0.07	0.01	0.45	0.09	99.93	-0.23
CH6/64	242.59	Pyroxenite	55.12	0.12	2.46	1.07	8.68	0.20	29.10	2.15	0.24	0.07	0.02	0.46	0.08	99.79	-0.29
CH6/65	244.15	Pyroxenite	55.43	0.12	2.91	1.07	8.66	0.21	28.95	2.31	0.25	0.06	0.01	0.46	0.08	100.52	-0.29
CH6/66	249.17	Pyroxenite	55.57	0.14	2.46	1.07	8.64	0.20	28.72	2.17	0.28	0.16	0.02	0.43	0.08	99.94	-0.22
CH6/67	254.28	Pyroxenite	55.65	0.13	2.38	1.05	8.48	0.20	29.17	2.07	0.20	0.12	0.02	0.45	0.09	100.02	-0.18
CH6/68	257.67	Pyroxenite	54.40	0.11	1.98	1.10	8.88	0.19	31.04	1.86	0.09	0.03	0.01	0.42	0.09	100.20	-0.12
CH6/69	261.40	Pyroxenite	55.52	0.11	1.90	1.07	8.67	0.20	30.30	1.94	0.07	0.02	0.01	0.46	0.08	100.34	-0.06
CH6/70	263.17	Pyroxenite	55.55	0.12	1.89	1.08	8.74	0.20	30.28	1.95	0.11	0.02	0.01	0.46	0.09	100.49	-0.11
CH6/71	268.13	Pyroxenite	54.78	0.11	4.30	1.04	8.45	0.19	27.32	3.23	0.28	0.03	0.01	0.40	0.08	100.22	-0.31
CH6/72	272.15	Pyroxenite	54.30	0.10	4.69	1.03	8.35	0.19	26.80	3.31	0.32	0.04	0.01	0.40	0.07	99.62	-0.2
CH6/73	274.82	Pyroxenite	54.25	0.11	5.23	1.02	8.22	0.18	26.13	3.54	0.34	0.04	0.01	0.39	0.07	99.53	-0.05
CH6/74	277.87	Pyroxenite	55.18	0.15	2.14	1.16	9.41	0.21	28.77	2.17	0.23	0.07	0.01	0.45	0.08	100.03	-0.3
CH6/75	282.74	Pyroxenite	54.35	0.11	5.17	1.05	8.47	0.19	26.14	3.53	0.37	0.04	0.01	0.40	0.07	99.90	-0.34

Table C.1: Continued

Sample No.	Depth (m)	Lithology	SiO_2	TiO_2	Al_2O_3	Fe_2O_3	FeO	MnO	MgO	CaO	Na_2O	K_2O	P_2O_5	Cr_2O_3	NiO	TOTAL	L.O.I.
CH6/76	285.31	Pyroxenite	55.46	0.16	2.31	1.17	9.48	0.21	27.80	2.16	0.20	0.23	0.03	0.42	0.08	99.70	-0.34
CH6/77	288.39	Pyroxenite	55.28	0.15	2.29	1.16	9.39	0.21	28.19	2.35	0.21	0.11	0.02	0.39	0.08	99.82	-0.37
CH6/78	292.53	Melanorite	53.44	0.14	4.31	1.08	8.74	0.19	26.10	3.36	0.37	0.09	0.02	0.34	0.08	98.26	-0.31
CH6/79	295.42	Pyroxenite	55.09	0.15	3.35	1.14	9.23	0.20	27.19	2.79	0.27	0.10	0.01	0.36	0.08	99.97	-0.45
CH6/80	297.83	Interlayered norite	51.27	0.07	18.15	0.58	4.66	0.10	14.56	9.48	1.04	0.07	0.01	0.20	0.06	100.25	-0.1
CH6/81	305.43	Pyroxenite	54.70	0.16	2.18	1.15	9.28	0.20	27.71	2.21	0.19	0.17	0.02	0.39	0.08	98.44	-0.32
CH6/82	309.63	Pyroxenite	55.06	0.15	2.46	1.17	9.44	0.21	28.03	2.36	0.16	0.10	0.02	0.40	0.09	99.63	-0.35
CH6/83	311.68	Pyroxenite	54.95	0.14	2.70	1.17	9.47	0.20	27.78	2.47	0.21	0.11	0.02	0.39	0.08	99.70	-0.33
CH6/84	317.62	Pyroxenite	54.20	0.10	4.44	1.13	9.18	0.20	26.53	3.21	0.25	0.03	0.01	0.39	0.08	99.75	-0.38
CH6/85	319.54	Pyroxenite	55.28	0.14	1.95	1.23	9.94	0.23	28.71	2.08	0.15	0.07	0.02	0.40	0.08	100.26	-0.42
CH6/86	323.17	Pyroxenite	55.18	0.12	2.21	1.19	9.65	0.22	28.52	2.26	0.20	0.07	0.01	0.34	0.08	100.06	-0.39
CH6/87	325.58	Pyroxenite	54.71	0.13	2.09	1.19	9.62	0.21	28.22	2.11	0.14	0.10	0.01	0.35	0.08	98.99	-0.37
CH6/88	329.46	Pyroxenite	55.03	0.12	1.72	1.20	9.73	0.22	29.25	1.94	0.08	0.03	0.01	0.37	0.09	99.78	-0.42
CH6/89	331.16	Pyroxenite	54.72	0.12	1.61	1.18	9.56	0.22	29.52	1.83	0.08	0.02	0.01	0.38	0.09	99.34	-0.28
CH6/90	333.54	Pyroxenite	55.20	0.16	3.73	1.06	8.60	0.19	27.15	2.90	0.37	0.10	0.02	0.42	0.08	99.99	-0.33
CH6/91	339.23	Pyroxenite	55.63	0.19	3.28	1.07	8.67	0.18	27.16	2.72	0.36	0.19	0.03	0.42	0.08	99.98	-0.24
CH6/92	343.72	Pyroxenite	54.81	0.15	5.22	1.04	8.41	0.18	25.42	3.54	0.51	0.12	0.02	0.38	0.08	99.88	-0.27
CH6/93	350.44	Pyroxenite	55.43	0.17	3.47	1.10	8.91	0.20	26.95	2.88	0.33	0.16	0.02	0.37	0.08	100.08	-0.17
CH6/94	353.73	Pyroxenite	55.62	0.18	3.09	1.10	8.94	0.19	26.89	2.70	0.34	0.24	0.03	0.39	0.08	99.79	-0.28
CH6/95	358.17	Pyroxenite	54.01	0.15	4.73	1.06	8.62	0.19	25.65	3.38	0.46	0.11	0.02	0.39	0.08	98.85	-0.34
CH6/96	362.21	Pyroxenite	55.15	0.15	3.66	1.13	9.17	0.20	26.80	2.88	0.35	0.12	0.02	0.38	0.08	100.09	0
CH6/97	369.40	Pyroxenite	55.11	0.13	2.55	1.19	9.66	0.22	28.43	2.50	0.15	0.02	0.01	0.36	0.09	100.42	-0.55
CH6/98	374.27	Pyroxenite	55.02	0.14	2.23	1.21	9.77	0.22	28.89	2.32	0.15	0.03	0.01	0.37	0.09	100.43	-0.56
CH6/99	376.58	Pyroxenite	54.63	0.12	4.06	1.11	9.03	0.20	27.22	2.99	0.26	0.02	0.01	0.35	0.08	100.08	-0.46
CH6/100	384.15	Pyroxenite	55.64	0.17	2.40	1.14	9.19	0.21	28.23	2.26	0.24	0.13	0.02	0.41	0.09	100.13	-0.38

Table C.1: Continued

Sample No.	Depth (m)	Lithology	SiO_2	TiO_2	Al_2O_3	Fe_2O_3	FeO	MnO	MgO	CaO	Na_2O	K_2O	P_2O_5	Cr_2O_3	NiO	TOTAL	L.O.I.
CH6/101	388.35	Pyroxenite	55.47	0.16	2.90	1.12	9.06	0.20	27.79	2.46	0.43	0.15	0.02	0.40	0.09	100.24	-0.4
CH6/102	391.90	Pyroxenite	55.93	0.18	2.39	1.15	9.31	0.21	27.95	2.31	0.22	0.20	0.02	0.34	0.09	100.28	-0.5
CH6/103	394.22	Pyroxenite	55.57	0.17	2.42	1.17	9.45	0.21	27.81	2.33	0.24	0.16	0.02	0.37	0.09	100.01	-0.53
CH6/104	396.37	Pyroxenite	55.70	0.16	2.53	1.17	9.46	0.21	28.08	2.38	0.26	0.10	0.02	0.39	0.09	100.56	-0.57
CH6/105	399.26	Pyroxenite	55.60	0.15	2.67	1.16	9.36	0.21	27.74	2.48	0.26	0.10	0.02	0.41	0.09	100.24	-0.5
CH6/106	404.14	Pyroxenite	55.63	0.16	2.04	1.15	9.34	0.20	28.59	2.27	0.17	0.16	0.02	0.47	0.09	100.30	-0.47
CH6/107	408.62	Pyroxenite	55.35	0.14	1.65	1.17	9.44	0.21	29.76	2.06	0.07	0.03	0.01	0.45	0.10	100.43	-0.17
CH6/108	412.54	Pyroxenite	55.50	0.16	1.94	1.14	9.25	0.21	28.80	1.99	0.14	0.13	0.02	0.48	0.10	99.87	-0.42
CH6/109	417.09	Pyroxenite	55.11	0.17	3.70	1.09	8.83	0.20	26.86	2.96	0.35	0.12	0.01	0.41	0.09	99.90	-0.47
CH6/110	419.87	Pyroxenite	55.56	0.17	2.67	1.14	9.25	0.21	27.77	2.53	0.25	0.12	0.02	0.44	0.09	100.21	-0.51
CH6/111	425.43	Pyroxenite	55.77	0.19	2.27	1.16	9.38	0.21	28.02	2.26	0.22	0.18	0.02	0.43	0.09	100.21	-0.46
CH6/112	430.25	Pyroxenite	55.68	0.18	2.36	1.16	9.40	0.21	28.10	2.31	0.28	0.14	0.02	0.45	0.10	100.39	1.51
CH6/113	434.19	Pyroxenite	54.77	0.15	4.83	1.07	8.68	0.19	26.16	3.63	0.35	0.07	0.02	0.44	0.10	100.45	-0.28
CH6/114	438.33	Pyroxenite	55.22	0.15	2.54	1.16	9.36	0.21	28.33	2.53	0.12	0.05	0.01	0.46	0.10	100.23	-0.44
CH6/115	440.32	Pyroxenite	55.20	0.15	2.43	1.16	9.43	0.21	28.37	2.49	0.11	0.06	0.02	0.46	0.10	100.19	-0.38
CH6/116	444.41	Pyroxenite	55.42	0.17	2.08	1.20	9.73	0.22	28.22	2.23	0.10	0.14	0.02	0.41	0.10	100.04	-0.3
CH6/117	447.76	Pyroxenite	54.91	0.16	3.26	1.22	9.86	0.21	27.18	2.90	0.21	0.05	0.02	0.42	0.09	100.49	-0.31
CH6/118	450.31	Pyroxenite	54.34	0.15	5.65	1.22	9.89	0.21	24.22	3.99	0.41	0.07	0.01	0.40	0.08	100.63	-0.41
CH6/119	454.69	Patchy pyroxenite	51.80	0.10	15.79	0.85	6.85	0.14	14.74	8.63	1.08	0.08	0.01	0.15	0.06	100.27	-0.13
CH6/120	457.63	Patchy pyroxenite	53.64	0.14	6.18	1.43	11.56	0.24	22.28	4.21	0.41	0.07	0.01	0.30	0.07	100.55	-0.45
CH6/121	459.15	Patchy pyroxenite	53.85	0.15	4.32	1.52	12.31	0.26	23.98	3.36	0.28	0.05	0.01	0.31	0.07	100.46	-0.51
CH6/122	462.72	Patchy pyroxenite	51.73	0.10	18.52	0.75	6.04	0.12	10.96	10.53	1.51	0.11	0.02	0.09	0.04	100.51	-0.13
CH6/123	466.85	Patchy pyroxenite	52.82	0.12	10.50	1.14	9.24	0.20	18.57	6.42	0.76	0.06	0.01	0.15	0.06	100.07	-0.31
CH6/124	471.15	Patchy pyroxenite	52.33	0.11	15.03	0.91	7.39	0.16	14.98	8.07	1.17	0.09	0.01	0.14	0.04	100.44	-0.27
CH6/125	473.65	Patchy pyroxenite	53.43	0.13	13.61	0.96	7.75	0.17	15.24	8.69	1.19	0.10	0.01	0.14	0.05	101.47	-0.18

Table C.1: Continued

Sample No.	Depth (m)	Lithology	SiO_2	TiO_2	Al_2O_3	Fe_2O_3	FeO	MnO	MgO	CaO	Na_2O	K_2O	P_2O_5	Cr_2O_3	NiO	TOTAL	L.O.I.
CH6/126	477.49	Norite	52.83	0.13	12.04	1.11	9.03	0.19	16.33	7.68	1.00	0.09	0.01	0.16	0.05	100.66	-0.3
CH6/127	480.58	Norite	52.79	0.12	11.34	1.17	9.51	0.20	16.76	7.40	0.92	0.08	0.01	0.17	0.05	100.53	-0.4
CH6/128	482.88	Norite	52.71	0.12	11.26	1.18	9.54	0.21	16.61	7.52	0.95	0.08	0.01	0.19	0.06	100.44	-0.33
CH6/129	487.20	Norite	52.07	0.11	15.52	0.94	7.63	0.17	12.84	9.34	1.43	0.13	0.01	0.08	0.04	100.32	0.1
CH6/130	489.50	Norite	51.71	0.10	16.38	0.87	7.07	0.15	11.33	10.53	1.55	0.10	0.01	0.08	0.03	99.93	-0.18
CH6/131	492.65	Norite	51.94	0.12	14.59	0.97	7.84	0.19	12.10	10.50	1.46	0.09	0.01	0.05	0.03	99.89	-0.19
CH6/132	495.30	Norite	51.86	0.12	17.74	0.71	5.73	0.13	9.65	11.50	1.89	0.12	0.01	0.05	0.02	99.53	-0.11
CH6/133	500.50	Norite	52.72	0.13	16.18	0.81	6.55	0.15	11.46	10.54	1.70	0.13	0.01	0.08	0.03	100.49	-0.19
CH6/134	502.86	Norite	52.79	0.14	15.70	0.83	6.76	0.15	11.59	10.47	1.72	0.15	0.02	0.09	0.03	100.44	-0.13
CH6/135	507.47	Norite	52.81	0.15	15.89	0.81	6.53	0.15	11.36	10.52	1.78	0.16	0.02	0.08	0.03	100.28	-0.23
CH6/136	510.22	Norite	52.77	0.15	16.20	0.78	6.35	0.14	11.09	10.45	1.81	0.19	0.02	0.08	0.03	100.07	-0.19
CH6/137	513.62	Norite	53.12	0.15	16.51	0.78	6.28	0.14	10.72	10.72	1.92	0.21	0.02	0.07	0.03	100.66	-0.11
CH6/138	516.77	Norite	53.21	0.16	16.73	0.78	6.29	0.14	10.51	10.81	1.87	0.21	0.02	0.07	0.03	100.81	-0.23
CH6/139	520.45	Norite	53.08	0.16	17.16	0.72	5.84	0.13	9.72	11.33	1.97	0.23	0.02	0.06	0.03	100.46	-0.06
CH6/140	523.59	Norite	52.90	0.15	17.50	0.72	5.80	0.13	9.52	11.20	2.01	0.22	0.02	0.06	0.02	100.23	-0.05
CH6/141	526.19	Norite	52.95	0.15	17.33	0.73	5.94	0.13	9.98	10.83	1.98	0.20	0.02	0.07	0.03	100.33	-0.2
CH6/142	529.56	Norite	53.15	0.15	15.94	0.83	6.71	0.14	11.37	9.87	1.85	0.20	0.02	0.10	0.03	100.36	-0.24
CH6/143	533.18	Norite	53.14	0.15	15.87	0.85	6.92	0.15	11.55	9.36	1.80	0.22	0.02	0.11	0.03	100.15	-0.3
CH6/144	537.48	Norite	53.25	0.14	15.60	0.87	7.03	0.15	11.76	9.69	1.83	0.19	0.02	0.10	0.03	100.65	-0.26
CH6/145	539.42	Norite	53.17	0.16	15.40	0.87	7.05	0.15	11.71	9.76	1.85	0.13	0.02	0.08	0.02	100.38	-0.27
CH6/146	542.67	Norite	52.89	0.14	16.13	0.84	6.78	0.15	11.24	9.73	1.88	0.17	0.02	0.09	0.02	100.09	-0.21
CH6/147	547.64	Norite	52.96	0.15	14.01	0.91	7.35	0.15	13.99	7.96	1.60	0.18	0.02	0.14	0.03	99.46	-0.19
CH6/148	550.62	Norite	53.30	0.13	18.01	0.61	4.91	0.12	8.62	12.42	2.27	0.20	0.01	0.05	0.02	100.66	-0.14
CH6/149	552.46	Norite	53.08	0.14	16.36	0.76	6.14	0.13	10.68	10.75	1.98	0.17	0.02	0.08	0.02	100.30	-0.18
CH6/150	555.49	Norite	53.13	0.13	16.78	0.75	6.05	0.13	10.71	10.52	2.03	0.17	0.01	0.10	0.02	100.53	-0.24

Table C.1: Continued

Sample No.	Depth (m)	Lithology	SiO_2	TiO_2	Al_2O_3	Fe_2O_3	FeO	MnO	MgO	CaO	Na_2O	K_2O	P_2O_5	Cr_2O_3	NiO	TOTAL	L.O.I.
CH6/151	559.16	Melanorite	53.04	0.14	16.10	0.75	6.09	0.13	11.23	10.66	1.90	0.17	0.01	0.12	0.03	100.38	-0.05
CH6/152	563.35	Melanorite	53.31	0.14	15.33	0.86	6.97	0.14	12.79	8.64	1.79	0.19	0.02	0.13	0.03	100.33	-0.33
CH6/153	566.60	Melanorite	53.99	0.16	13.24	0.99	8.03	0.16	14.81	7.79	1.54	0.19	0.02	0.15	0.04	101.12	-0.3
CH6/154	569.42	Melanorite	53.64	0.16	12.41	1.03	8.31	0.17	15.49	7.59	1.43	0.16	0.02	0.16	0.04	100.61	-0.37
CH6/155	573.65	Melanorite	54.03	0.17	12.32	1.02	8.25	0.17	15.82	7.45	1.43	0.18	0.02	0.16	0.04	101.05	-0.31
CH6/156	576.13	Melanorite	53.62	0.18	11.36	1.05	8.49	0.17	16.42	7.01	1.29	0.19	0.02	0.18	0.04	100.03	-0.39
CH6/157	580.63	Melanorite	53.85	0.18	11.47	1.05	8.50	0.17	16.46	7.09	1.31	0.19	0.02	0.18	0.04	100.52	-0.34
CH6/158	583.59	Melanorite	54.62	0.17	11.22	1.06	8.57	0.17	16.73	6.74	1.28	0.20	0.02	0.18	0.04	101.00	-0.37
CH6/159	587.45	Melanorite	53.92	0.17	11.22	1.04	8.45	0.18	16.80	6.70	1.28	0.19	0.02	0.18	0.04	100.20	-0.36
CH6/160	590.36	Melanorite	53.99	0.18	12.10	1.02	8.23	0.17	16.03	7.00	1.38	0.20	0.02	0.17	0.04	100.53	-0.33
CH6/161	595.16	Melanorite	54.26	0.19	10.83	1.06	8.56	0.18	17.14	6.69	1.25	0.24	0.02	0.19	0.05	100.65	-0.35
CH6/162	597.86	Melanorite	53.94	0.18	10.65	1.06	8.56	0.18	17.51	6.24	1.23	0.21	0.02	0.19	0.05	100.00	-0.35
CH6/163	600.34	Melanorite	53.96	0.19	10.42	1.06	8.60	0.17	17.70	6.33	1.18	0.22	0.02	0.19	0.05	100.10	-0.36
CH6/164	603.16	Melanorite	54.11	0.19	9.59	1.10	8.90	0.18	18.41	6.00	1.07	0.21	0.02	0.20	0.05	100.03	-0.38
CH6/165	605.63	Melanorite	54.23	0.18	12.20	1.00	8.09	0.16	15.90	6.90	1.43	0.29	0.02	0.18	0.04	100.63	-0.31
CH6/166	609.58	Melanorite	54.15	0.20	9.93	1.11	8.97	0.18	18.00	6.04	1.14	0.25	0.02	0.20	0.05	100.23	-0.33
CH6/167	616.31	Melanorite	54.49	0.20	9.04	1.15	9.30	0.19	19.12	5.54	1.00	0.24	0.02	0.21	0.06	100.56	-0.38
CH6/168	616.76	Melanorite	54.54	0.20	9.52	1.10	8.94	0.18	18.67	5.86	1.10	0.23	0.02	0.21	0.05	100.63	-0.21
CH6/169	624.65	Melanorite	54.40	0.20	8.20	1.17	9.45	0.19	20.04	5.56	0.92	0.18	0.02	0.23	0.05	100.62	-0.29
CH6/170	630.48	Melanorite	54.79	0.19	8.29	1.17	9.51	0.19	20.19	5.59	0.89	0.18	0.02	0.23	0.05	101.31	-0.28
CH6/171	633.41	Melanorite	53.86	0.19	8.36	1.17	9.45	0.19	19.67	5.52	0.91	0.18	0.02	0.22	0.05	99.80	-0.34
CH6/172	636.36	Melanorite	54.63	0.19	8.06	1.18	9.60	0.19	20.44	5.24	0.89	0.18	0.02	0.23	0.05	100.91	0
CH6/173	639.57	Melanorite	53.77	0.19	7.11	1.18	9.57	0.19	20.80	5.06	0.75	0.17	0.02	0.24	0.05	99.11	-0.31
CH6/174	643.44	Melanorite	55.25	0.20	7.43	1.20	9.75	0.20	21.32	5.12	0.80	0.18	0.02	0.24	0.06	101.77	-0.34
CH6/175	646.71	Melanorite	54.03	0.19	7.17	1.16	9.43	0.20	21.15	5.00	0.82	0.16	0.02	0.24	0.06	99.63	-0.05

Table C.1: Continued

Sample No.	Depth (m)	Lithology	SiO_2	TiO_2	Al_2O_3	Fe_2O_3	FeO	MnO	MgO	CaO	Na_2O	K_2O	P_2O_5	Cr_2O_3	NiO	TOTAL	L.O.I.
CH6/176	649.25	Feldspathic pyroxenite	54.73	0.20	6.40	1.20	9.76	0.20	22.34	4.54	0.69	0.15	0.02	0.26	0.06	100.54	-0.08
CH6/177	652.59	Feldspathic pyroxenite	55.01	0.22	5.42	1.24	10.06	0.21	22.73	4.25	0.61	0.22	0.02	0.26	0.06	100.32	-0.03
CH6/178	662.51	Feldspathic pyroxenite	55.31	0.22	5.61	1.23	9.98	0.21	22.40	4.18	0.66	0.25	0.03	0.26	0.06	100.40	0.13
CH6/179	667.48	Feldspathic pyroxenite	54.98	0.21	6.19	1.20	9.70	0.20	22.05	4.47	0.73	0.21	0.02	0.26	0.06	100.28	0.04
CH6/180	672.53	Feldspathic pyroxenite	54.77	0.20	6.17	1.21	9.82	0.20	22.23	4.51	0.68	0.17	0.02	0.26	0.06	100.31	0.06
CH6/181	677.75	Feldspathic pyroxenite	54.77	0.21	5.71	1.24	10.04	0.22	22.50	4.35	0.66	0.22	0.02	0.27	0.06	100.25	0.06
CH6/182	679.42	Feldspathic pyroxenite	54.03	0.18	10.27	1.04	8.43	0.19	18.23	6.27	1.24	0.18	0.02	0.24	0.06	100.37	-0.17
CH6/183	683.39	Feldspathic pyroxenite	55.17	0.21	6.36	1.19	9.63	0.21	22.26	4.63	0.80	0.21	0.02	0.27	0.06	101.00	-0.3
CH6/184	686.16	Feldspathic pyroxenite	55.51	0.21	6.06	1.20	9.74	0.21	22.83	4.25	0.73	0.19	0.03	0.27	0.06	101.29	-0.22
CH6/185	688.31	Feldspathic pyroxenite	55.48	0.21	6.18	1.18	9.55	0.20	22.53	4.50	0.75	0.21	0.03	0.28	0.06	101.17	-0.27

Table C.2: Trace elements geochemistry of the CH6 Drill Core (ppm, XRF data).

Sample No	Depth (m)	Lithology	Sc (ppm)	V (ppm)	Cr (ppm)	Co (ppm)	Ni (ppm)	Cu (ppm)	Zn (ppm)	Ga (ppm)	Rb (ppm)	Sr (ppm)	Y (ppm)	Zr (ppm)	Nb (ppm)	Mo (ppm)	Ba (ppm)	Pb (ppm)
CH6/1	30.59	Dunite	4.30	34.82	5042.99	164.59	2101.11	2.03	79.55	b.d*	2.41	4.62	b.d	2.88	2.32	0.59	20.09	1.72
CH6/2	31.93	Dunite	4.13	25.54	4809.06	174.11	2256.34	b.d	89.25	0.90	2.53	2.65	b.d	1.75	1.98	1.17	10.74	0.01
CH6/3	42.60	Orthopyroxenite	18.28	67.95	4012.74	110.76	931.64	2.38	68.59	2.39	2.12	2.36	b.d	1.94	1.50	0.53	25.10	b.d
CH6/4	46.23	Orthopyroxenite	18.42	72.20	2842.23	99.83	762.91	7.40	68.92	3.40	2.37	10.51	0.39	6.07	2.54	1.09	35.02	1.42
CH6/5	50.26	Orthopyroxenite	22.96	66.03	3153.09	101.42	725.84	4.95	70.50	3.04	2.19	6.39	0.12	4.10	1.95	0.34	15.87	1.48
CH6/6	52.75	Orthopyroxenite	18.41	70.48	3303.06	97.51	824.60	12.72	73.52	1.89	1.50	6.38	0.31	3.70	2.01	0.98	17.24	2.02
CH6/7	55.18	Orthopyroxenite	20.48	68.70	2988.74	100.73	721.60	7.36	68.79	3.57	7.36	11.01	b.d	3.42	2.44	1.24	35.79	2.22
CH6/8	59.10	Orthopyroxenite	19.69	66.48	2935.79	100.70	736.06	1.42	73.81	3.32	1.57	5.87	0.00	1.79	1.35	b.d	9.87	0.98
CH6/9	62.53	Orthopyroxenite	21.35	78.15	3026.72	93.22	705.71	11.20	75.34	3.09	2.22	18.09	b.d	6.51	1.26	0.22	38.56	0.35
CH6/10	64.19	Orthopyroxenite	24.27	81.08	3247.32	94.95	725.40	7.20	77.12	3.53	0.67	11.67	b.d	4.11	1.53	0.64	16.60	0.02
CH6/11	68.23	Orthopyroxenite	20.01	70.69	3163.70	96.14	771.94	3.22	73.34	2.54	2.50	15.56	b.d	6.43	2.11	1.25	28.62	2.65
CH6/12	70.15	Orthopyroxenite	22.04	69.39	3315.10	101.80	823.10	3.88	73.92	2.16	b.d	4.49	b.d	3.01	1.32	0.69	9.94	2.28
CH6/13	76.27	Harzburgite	10.10	44.33	3235.54	166.85	1725.71	2.00	85.17	1.46	1.83	8.99	b.d	4.42	1.50	0.94	24.71	1.34
CH6/14	78.71	Harzburgite	8.16	28.78	1557.98	166.31	1857.94	0.46	81.04	1.91	2.55	10.26	b.d	3.89	2.25	0.35	26.43	1.11
CH6/15	81.49	Orthopyroxenite	18.88	73.22	3116.25	97.43	679.16	5.16	69.29	3.21	2.65	12.20	1.52	5.65	2.02	0.67	19.84	2.95
CH6/16	85.53	Orthopyroxenite	19.76	74.25	3158.05	101.15	689.13	8.78	72.81	1.82	3.59	10.31	0.94	5.20	1.78	0.88	21.14	0.28
CH6/17	88.25	Orthopyroxenite	18.76	72.24	3193.15	90.98	689.77	2.93	65.12	2.26	3.26	5.64	0.41	3.35	1.48	1.12	18.47	1.46
CH6/18	91.55	Orthopyroxenite	20.88	73.41	3209.78	96.69	685.56	4.31	71.53	3.15	1.93	10.01	1.33	4.22	1.32	b.d	23.76	b.d
CH6/19	94.42	Orthopyroxenite	20.15	74.71	3223.07	97.17	695.58	2.96	68.65	2.68	0.65	7.87	2.26	3.38	0.26	0.84	17.69	1.11
CH6/20	99.88	Orthopyroxenite	24.75	82.48	3056.86	95.07	655.00	5.85	75.51	2.43	5.92	15.06	3.20	11.13	0.13	b.d	70.84	3.42
CH6/21	102.89	Orthopyroxenite	22.23	81.02	3153.10	95.70	685.76	9.71	76.61	2.81	b.d	17.85	2.07	3.68	0.45	1.12	15.51	3.85
CH6/22	103.86	Orthopyroxenite	22.87	81.01	3183.66	101.52	690.93	9.29	72.82	3.37	1.53	16.19	1.42	3.68	0.83	1.03	21.17	0.43
CH6/23	106.50	Orthopyroxenite	22.44	78.29	3062.64	98.20	747.01	4.11	72.84	4.22	1.27	16.12	2.01	3.76	0.64	0.18	19.39	1.18
CH6/24	111.15	Orthopyroxenite	23.20	77.33	3091.33	92.48	652.14	10.41	75.57	3.90	2.23	16.27	0.46	2.65	1.61	b.d	6.15	1.91
CH6/25	115.15	Orthopyroxenite	25.75	82.59	3828.12	93.64	679.20	26.79	66.97	3.13	2.27	3.94	0.61	1.71	2.11	1.09	5.74	1.55

* b.d = below detection limit.

Table C.2: Continued

Sample No	Depth (m)	Lithology	Sc (ppm)	V (ppm)	Cr (ppm)	Co (ppm)	Ni (ppm)	Cu (ppm)	Zn (ppm)	Ga (ppm)	Rb (ppm)	Sr (ppm)	Y (ppm)	Zr (ppm)	Nb (ppm)	Mo (ppm)	Ba (ppm)	Pb (ppm)
CH6/26	118.41	Orthopyroxenite	23.87	79.91	2994.13	94.89	646.76	19.64	79.84	4.00	3.80	11.62	0.78	4.95	2.27	0.33	16.55	b.d
CH6/27	121.57	Orthopyroxenite	27.31	86.45	3044.61	97.57	632.83	18.62	84.31	2.03	3.34	12.91	0.58	4.84	3.37	1.44	29.38	1.96
CH6/28	124.78	Orthopyroxenite	28.86	85.61	3092.82	100.39	647.24	9.71	84.41	1.55	0.52	9.56	0.69	1.77	2.76	1.17	5.45	0.18
CH6/29	128.34	Orthopyroxenite	29.72	84.27	3141.64	98.03	654.28	7.81	81.92	2.50	1.18	9.35	b.d	1.69	2.77	0.56	3.33	1.17
CH6/30	132.47	Orthopyroxenite	32.39	101.76	2791.03	98.63	650.18	11.90	89.32	2.65	2.88	13.57	b.d	4.35	3.44	0.42	10.17	0.44
CH6/31	136.60	Orthopyroxenite	29.73	87.05	2756.17	103.27	647.85	9.12	83.35	2.34	0.76	10.57	b.d	2.24	2.65	0.13	2.64	1.43
CH6/32	139.86	Orthopyroxenite	31.04	86.22	2792.32	99.82	666.87	6.05	88.17	3.28	2.10	17.11	b.d	2.27	2.58	0.42	b.d	1.85
CH6/33	143.19	Orthopyroxenite	29.34	95.80	2819.14	104.13	676.10	12.61	77.60	2.75	0.24	6.93	b.d	1.34	2.39	-0.01	3.30	b.d
CH6/34	145.43	Pyroxenite	33.79	95.17	2766.12	108.57	647.66	11.90	77.66	3.62	1.66	7.44	0.75	2.61	1.51	0.26	6.95	1.63
CH6/35	149.16	Pyroxenite	32.01	94.82	2076.77	111.83	613.83	13.81	81.52	2.39	2.26	15.55	b.d	2.99	1.60	1.39	14.41	0.94
CH6/36	153.67	Pyroxenite	33.65	104.98	1859.63	107.94	603.13	14.83	78.92	2.70	2.03	16.29	b.d	2.63	1.01	b.d	18.85	5.29
CH6/37	157.15	Pyroxenite*	32.42	96.19	1622.89	103.29	560.10	21.13	76.91	3.97	2.35	25.90	1.15	6.13	1.59	1.12	21.93	3.71
CH6/38	159.48	Int. Norite	29.70	84.19	1427.36	97.02	534.78	53.21	62.08	6.03	1.62	85.83	b.d	1.39	1.27	1.16	8.88	1.02
CH6/39	161.45	Pyroxenite	28.26	89.46	1503.43	107.23	526.22	12.10	71.33	3.94	2.81	54.72	b.d	1.04	1.57	b.d	6.94	0.68
CH6/40	164.18	Melanorite	27.98	62.90	926.12	76.56	379.18	9.67	56.55	9.39	2.00	142.31	b.d	0.96	1.76	b.d	4.53	2.23
CH6/41	167.51	Int. Norite	27.67	65.87	486.19	36.49	205.85	4.15	26.76	12.60	2.49	250.83	b.d	2.26	1.26	0.57	23.22	b.d
CH6/42	170.44	Interlayered norite	31.57	67.93	803.90	59.57	314.60	3.28	43.56	10.56	2.53	176.46	b.d	2.38	1.38	0.83	24.42	1.75
CH6/43	172.57	Interlayered norite	29.10	71.77	901.81	71.38	361.87	4.16	48.95	8.82	2.44	143.56	b.d	1.92	1.52	b.d	14.35	1.48
CH6/44	176.09	Interlayered norite	27.97	69.76	1032.96	69.40	385.27	3.42	41.02	8.48	2.28	140.27	0.75	2.29	0.60	0.53	9.69	0.77
CH6/45	179.66	Interlayered norite	26.06	70.40	1542.46	94.76	862.53	270.53	56.03	7.19	2.40	87.29	0.70	2.67	0.71	0.66	15.63	0.79
CH6/46	182.54	Melanorite	23.62	72.68	3698.17	109.63	1336.47	15.27	68.62	5.84	2.27	61.45	0.92	2.02	1.64	1.76	15.63	0.35
CH6/47	186.26	Pyroxenite	26.33	85.63	2960.49	101.37	678.69	10.54	84.91	2.42	3.36	5.61	0.84	3.82	0.78	0.01	9.94	2.62
CH6/48	189.16	Pyroxenite	25.46	94.09	2873.52	96.34	678.44	10.34	74.68	3.51	5.80	10.26	1.43	6.55	0.65	0.57	36.06	1.82
CH6/49	191.74	Pyroxenite	24.98	90.64	2975.38	97.07	686.57	9.31	77.00	3.59	2.28	13.02	2.13	3.62	b.d	b.d	20.88	0.75
CH6/50	194.86	Pyroxenite	22.96	86.57	3050.41	91.55	699.68	10.32	75.55	2.17	3.01	10.10	2.21	5.23	b.d	0.89	11.80	1.99

Table C.2: Continued

Sample No	Depth (m)	Lithology	Sc (ppm)	V (ppm)	Cr (ppm)	Co (ppm)	Ni (ppm)	Cu (ppm)	Zn (ppm)	Ga (ppm)	Rb (ppm)	Sr (ppm)	Y (ppm)	Zr (ppm)	Nb (ppm)	Mo (ppm)	Ba (ppm)	Pb (ppm)
CH6/51	198.51	Pyroxenite	24.46	93.39	3035.42	93.01	694.82	15.07	74.32	2.19	3.88	15.93	2.06	6.83	0.02	0.83	24.47	1.93
CH6/52	200.61	Pyroxenite	21.64	87.30	3089.32	96.72	730.93	8.71	74.50	3.07	4.22	11.83	2.24	5.69	b.d	0.02	33.17	2.82
CH6/53	207.54	Pyroxenite	21.40	81.78	3075.37	98.77	665.83	11.87	74.50	3.61	2.58	7.18	2.36	5.53	0.30	1.29	15.97	1.70
CH6/54	211.44	Pyroxenite	20.70	80.48	2999.13	94.63	648.23	10.73	75.95	2.55	3.43	11.97	1.23	6.47	1.93	0.51	37.29	0.36
CH6/55	216.27	Pyroxenite	21.16	85.30	3067.36	99.96	650.47	12.16	74.92	2.70	3.66	13.40	0.97	6.30	1.89	0.78	38.64	b.d
CH6/56	218.62	Pyroxenite	20.59	82.12	2909.17	87.39	624.60	10.27	76.90	3.15	7.58	20.40	0.72	15.84	3.11	1.41	91.84	0.49
CH6/57	219.59	Pyroxenite	24.21	89.21	3057.71	98.76	642.20	6.59	74.35	4.02	3.57	13.12	0.43	5.11	1.68	b.d	27.66	1.77
CH6/58	221.66	Pyroxenite	22.50	84.75	3096.18	94.58	657.77	8.77	70.28	3.26	2.51	10.76	1.08	6.45	1.77	b.d	19.67	0.30
CH6/59	223.12	Pyroxenite	20.79	78.33	3075.06	92.15	636.44	9.99	70.07	3.43	3.95	13.93	1.54	6.59	2.62	0.56	37.75	3.11
CH6/60	227.51	Pyroxenite	23.92	88.67	3021.45	93.35	648.16	9.16	69.52	2.07	4.45	13.89	3.03	7.59	2.85	1.33	27.15	2.88
CH6/61	230.36	Pyroxenite	19.93	81.88	3064.58	93.12	655.36	5.76	72.24	3.12	4.16	14.68	2.50	5.66	2.04	0.17	31.89	2.04
CH6/62	235.85	Pyroxenite	24.11	83.69	3051.31	92.23	659.09	7.72	77.87	2.22	4.63	15.75	2.35	6.49	2.04	b.d	34.47	b.d
CH6/63	238.80	Pyroxenite	24.25	85.84	3054.61	91.38	665.51	8.54	71.44	2.77	3.33	15.00	2.96	7.11	2.91	b.d	30.25	1.92
CH6/64	242.59	Pyroxenite	25.30	89.06	3153.06	89.87	655.09	18.30	75.90	2.56	3.76	18.53	1.86	5.51	1.62	0.88	26.43	2.30
CH6/65	244.15	Pyroxenite	27.29	83.07	3069.94	94.87	635.61	15.12	71.48	2.70	3.04	28.45	2.49	4.96	0.97	0.54	21.38	2.89
CH6/66	249.17	Pyroxenite	25.21	98.55	2925.14	93.48	619.52	11.62	73.72	4.81	6.03	19.36	3.56	11.81	1.52	0.49	46.75	2.47
CH6/67	254.28	Pyroxenite	24.55	94.79	3029.63	95.23	665.58	11.65	70.75	3.05	5.12	15.92	3.50	11.18	1.73	0.69	42.56	2.99
CH6/68	257.67	Pyroxenite	21.38	78.06	2758.50	98.86	752.14	1.46	71.28	3.28	3.10	10.45	2.45	4.87	1.93	1.18	19.22	2.18
CH6/69	261.40	Pyroxenite	26.76	85.82	3047.39	94.49	680.84	10.02	70.69	3.85	0.95	4.65	0.80	3.52	1.40	0.04	8.17	b.d
CH6/70	263.17	Pyroxenite	21.60	94.73	3100.22	98.68	731.88	12.05	70.35	4.13	0.44	5.95	1.28	4.09	0.99	b.d	7.37	0.35
CH6/71	268.13	Pyroxenite	27.43	85.42	2641.54	87.04	604.24	8.24	70.32	4.49	1.30	49.90	0.85	2.85	1.18	0.83	15.27	b.d
CH6/72	272.15	Pyroxenite	27.04	84.99	2644.27	92.14	587.82	10.20	80.07	4.91	2.47	54.67	1.74	4.59	1.94	0.33	19.44	0.94
CH6/73	274.82	Pyroxenite	27.04	84.43	2637.35	92.28	569.78	10.45	70.08	6.64	2.57	62.91	1.22	3.33	1.67	0.62	28.93	0.41
CH6/74	277.87	Pyroxenite	26.43	107.20	3048.77	95.82	643.27	18.64	79.94	2.49	1.89	13.85	1.89	7.20	0.34	0.13	40.03	2.80
CH6/75	282.74	Pyroxenite	24.94	85.00	2659.59	93.57	572.32	10.32	72.65	5.01	0.72	60.49	0.38	4.35	0.50	0.35	26.94	2.19

Table C.2: Continued

Sample No	Depth (m)	Lithology	Sc (ppm)	V (ppm)	Cr (ppm)	Co (ppm)	Ni (ppm)	Cu (ppm)	Zn (ppm)	Ga (ppm)	Rb (ppm)	Sr (ppm)	Y (ppm)	Zr (ppm)	Nb (ppm)	Mo (ppm)	Ba (ppm)	Pb (ppm)
CH6/76	285.31	Pyroxenite	28.14	104.11	2806.36	98.35	626.45	10.72	83.20	3.28	8.92	15.64	2.20	18.05	2.00	0.19	69.21	3.19
CH6/77	288.39	Pyroxenite	29.16	107.54	2592.63	98.91	624.94	13.90	86.20	3.59	3.67	15.70	1.73	10.82	1.19	0.15	44.32	1.37
CH6/78	292.53	Melanorite	29.90	116.24	2292.42	91.69	653.23	11.92	72.72	5.39	3.72	47.40	1.25	10.79	0.02	0.21	30.03	b.d
CH6/79	295.42	Pyroxenite	29.78	140.19	2432.32	96.60	674.68	10.84	88.15	4.43	6.13	35.09	3.56	9.91	2.32	1.48	42.40	2.21
CH6/80	297.83	Interlayered norite	22.62	59.93	1241.39	53.11	416.67	13.70	44.17	12.66	3.34	237.16	0.39	1.34	0.53	b.d	26.47	b.d
CH6/81	305.43	Pyroxenite	28.49	125.12	2656.09	93.07	655.99	10.11	87.49	2.91	8.03	14.39	3.42	11.60	2.91	0.21	58.15	0.71
CH6/82	309.63	Pyroxenite	27.68	112.80	2703.92	97.37	670.46	3.01	86.31	2.58	7.39	19.78	2.77	10.30	2.37	0.84	45.30	1.01
CH6/83	311.68	Pyroxenite	27.59	112.73	2689.56	100.65	662.24	2.08	86.77	3.60	5.75	23.68	2.95	8.14	2.43	1.03	44.19	0.98
CH6/84	317.62	Pyroxenite	29.48	110.96	2615.77	90.15	630.49	6.32	76.61	4.00	1.98	48.50	2.23	2.87	0.89	0.42	24.87	0.82
CH6/85	319.54	Pyroxenite	30.74	128.54	2688.38	103.04	658.89	6.75	88.60	4.07	4.41	10.76	2.60	6.53	2.12	0.92	31.56	2.37
CH6/86	323.17	Pyroxenite	28.62	136.18	2237.65	100.30	657.71	6.38	80.04	3.33	2.46	14.63	2.37	6.92	1.58	1.02	34.87	1.73
CH6/87	325.58	Pyroxenite	27.99	136.02	2393.32	101.06	657.44	5.53	92.49	2.51	5.07	12.35	2.35	9.49	1.73	1.11	42.56	2.54
CH6/88	329.46	Pyroxenite	28.50	112.93	2518.99	105.11	692.47	6.39	89.35	1.81	1.77	5.39	1.90	4.99	1.36	0.80	3.80	0.51
CH6/89	331.16	Pyroxenite	25.96	104.43	2679.64	103.86	695.14	3.13	78.77	2.98	1.72	2.99	2.04	4.20	3.45	1.35	7.72	0.55
CH6/90	333.54	Pyroxenite	23.36	91.44	2792.28	90.12	639.33	22.04	81.81	5.41	4.18	42.56	2.49	11.05	3.06	0.99	50.62	1.05
CH6/91	339.23	Pyroxenite	24.57	96.11	2853.23	92.36	657.18	8.79	77.08	4.17	8.01	37.24	4.62	16.01	3.21	0.70	69.16	1.27
CH6/92	343.72	Pyroxenite	24.03	91.31	2514.25	84.00	583.96	15.84	71.39	4.24	5.69	67.38	2.85	12.59	3.41	0.07	55.27	1.67
CH6/93	350.44	Pyroxenite	27.57	106.19	2479.86	90.77	626.44	7.65	75.38	4.25	7.14	38.63	3.99	10.94	3.20	0.71	57.35	1.98
CH6/94	353.73	Pyroxenite	29.52	116.88	2610.10	88.85	632.25	7.35	78.58	4.44	11.03	32.48	3.92	19.55	2.71	0.69	97.30	1.77
CH6/95	358.17	Pyroxenite	24.66	96.64	2611.63	88.92	602.99	12.90	78.33	5.09	3.51	59.00	3.14	10.53	1.84	b.d	53.48	2.28
CH6/96	362.21	Pyroxenite	26.31	113.01	2538.24	92.94	642.44	7.38	96.68	4.80	6.09	40.00	2.69	8.55	2.31	b.d	45.35	2.82
CH6/97	369.40	Pyroxenite	26.56	114.21	2379.07	101.08	694.18	6.65	90.41	2.65	1.68	21.84	1.72	3.46	2.32	0.53	4.07	1.82
CH6/98	374.27	Pyroxenite	30.82	121.70	2441.05	98.98	703.80	9.13	81.00	3.58	0.98	16.08	1.66	4.37	1.94	0.70	14.01	0.85
CH6/99	376.58	Pyroxenite	23.04	111.88	2337.08	98.79	655.04	10.38	78.08	4.37	0.83	47.35	0.80	1.96	b.d	b.d	14.28	1.45
CH6/100	384.15	Pyroxenite	26.04	103.38	2776.76	96.27	703.63	15.53	86.38	1.67	7.31	21.28	2.77	14.57	1.12	0.15	51.50	3.72

Table C.2: Continued

Sample No	Depth (m)	Lithology	Sc (ppm)	V (ppm)	Cr (ppm)	Co (ppm)	Ni (ppm)	Cu (ppm)	Zn (ppm)	Ga (ppm)	Rb (ppm)	Sr (ppm)	Y (ppm)	Zr (ppm)	Nb (ppm)	Mo (ppm)	Ba (ppm)	Pb (ppm)
CH6/101	388.35	Pyroxenite	29.08	97.35	2656.03	95.63	704.65	15.25	96.52	3.29	6.21	28.59	4.12	12.27	1.05	0.59	56.12	1.39
CH6/102	391.90	Pyroxenite	27.84	105.96	2220.38	98.04	683.91	4.06	84.54	3.33	8.66	19.87	3.80	15.80	1.38	0.19	78.74	1.64
CH6/103	394.22	Pyroxenite	29.85	104.18	2456.65	100.15	701.21	9.24	90.83	4.33	7.84	19.98	1.85	21.74	1.37	0.66	60.24	1.55
CH6/104	396.37	Pyroxenite	29.95	102.22	2610.61	96.22	698.03	11.03	92.22	2.87	4.03	21.66	2.20	10.60	1.22	1.01	39.75	1.23
CH6/105	399.26	Pyroxenite	29.57	108.77	2744.40	89.02	694.32	9.69	86.94	2.95	3.20	22.55	1.83	9.80	0.30	0.62	36.96	3.19
CH6/106	404.14	Pyroxenite	29.91	107.78	3099.63	95.29	744.05	9.29	90.69	3.07	8.12	10.58	1.44	12.68	0.19	b.d	41.50	2.50
CH6/107	408.62	Pyroxenite	28.34	104.25	3072.43	93.75	814.81	-1.25	88.62	2.84	1.02	3.21	0.87	4.33	0.05	0.15	11.13	1.29
CH6/108	412.54	Pyroxenite	26.21	108.13	3194.76	96.96	775.79	9.90	84.85	4.40	6.36	8.44	2.28	11.38	2.59	1.26	53.98	0.61
CH6/109	417.09	Pyroxenite	28.42	102.31	2799.18	92.07	697.51	13.63	75.96	4.79	5.04	44.04	3.16	9.46	2.33	1.40	60.44	1.15
CH6/110	419.87	Pyroxenite	28.14	114.49	3041.15	101.21	768.62	18.92	87.03	5.03	7.19	19.45	1.73	13.54	2.60	1.52	50.01	2.03
CH6/111	425.43	Pyroxenite	27.10	116.00	2844.86	93.09	720.88	10.08	78.62	5.11	7.70	17.12	2.93	14.16	2.04	1.17	66.65	2.77
CH6/112	430.25	Pyroxenite	29.01	111.70	2937.38	94.97	743.75	15.97	84.91	2.57	5.09	23.15	1.97	11.59	1.75	0.86	54.94	2.75
CH6/113	434.19	Pyroxenite	28.64	100.06	2849.40	83.96	715.06	16.16	80.10	5.35	3.35	61.64	4.49	6.39	b.d	0.35	31.11	1.25
CH6/114	438.33	Pyroxenite	28.96	101.82	3087.69	89.00	741.08	9.14	94.39	3.45	1.77	22.01	4.34	6.46	b.d	b.d	28.32	b.d
CH6/115	440.32	Pyroxenite	27.08	110.19	3038.48	92.17	735.80	5.87	84.69	2.37	3.39	19.53	4.48	8.38	0.38	0.77	36.67	b.d
CH6/116	444.41	Pyroxenite	30.29	108.79	2755.00	94.68	751.44	11.60	86.52	2.97	5.53	15.23	5.44	13.72	0.44	0.49	57.10	2.63
CH6/117	447.76	Pyroxenite	29.67	105.09	2772.41	88.98	704.08	10.57	88.23	2.99	2.89	37.47	5.30	6.80	b.d	0.09	31.64	1.26
CH6/118	450.31	Pyroxenite	31.49	94.78	2624.49	84.12	643.58	42.59	96.43	5.98	1.28	76.66	5.02	4.90	b.d	b.d	36.75	2.58
CH6/119	454.69	Patchy pyroxenite	23.97	65.69	965.08	64.13	380.00	88.97	75.87	11.06	0.90	240.50	3.50	2.65	b.d	0.28	51.75	1.04
CH6/120	457.63	Patchy pyroxenite	32.83	117.92	1969.80	95.68	505.07	79.34	110.93	6.12	1.90	83.64	4.67	4.47	b.d	0.41	30.31	b.d
CH6/121	459.15	Patchy pyroxenite	33.65	126.75	2100.93	104.24	538.21	94.12	107.80	5.17	1.29	53.34	4.82	3.96	b.d	b.d	25.57	1.77
CH6/122	462.72	Patchy pyroxenite	25.21	82.01	528.57	50.30	278.75	115.08	51.79	14.32	0.78	276.91	3.91	3.45	b.d	0.10	50.72	2.56
CH6/123	466.85	Patchy pyroxenite	31.39	95.50	985.30	83.21	424.43	86.69	90.11	9.53	1.64	154.79	3.46	3.29	1.27	b.d	28.56	0.40
CH6/124	471.15	Patchy pyroxenite	24.97	69.35	872.72	63.81	280.66	-6.44	69.10	12.64	1.95	231.76	4.24	4.54	1.11	b.d	55.62	b.d
CH6/125	473.65	Patchy pyroxenite	31.95	96.83	879.10	66.79	376.64	89.78	76.57	11.26	1.13	211.04	4.69	3.24	1.08	0.48	51.48	0.77

Table C.2: Continued

Sample No	Depth (m)	Lithology	Sc (ppm)	V (ppm)	Cr (ppm)	Co (ppm)	Ni (ppm)	Cu (ppm)	Zn (ppm)	Ga (ppm)	Rb (ppm)	Sr (ppm)	Y (ppm)	Zr (ppm)	Nb (ppm)	Mo (ppm)	Ba (ppm)	Pb (ppm)
CH6/126	477.49	Norite	31.65	106.57	1059.08	70.21	397.73	81.66	113.66	10.38	1.93	180.27	4.50	3.99	1.16	b.d	52.00	b.d
CH6/127	480.58	Norite	32.37	106.74	1059.19	78.04	413.48	94.19	114.26	9.23	0.91	169.06	4.42	3.80	1.24	0.77	49.15	2.36
CH6/128	482.88	Norite	33.55	110.92	1077.60	82.04	406.23	122.22	102.70	11.04	1.16	174.75	5.33	2.44	0.80	0.39	50.42	1.66
CH6/129	487.20	Norite	33.54	90.95	495.34	64.40	273.05	114.52	68.21	13.07	0.45	244.27	4.15	2.96	0.35	0.21	63.07	0.43
CH6/130	489.50	Norite	34.16	102.10	493.41	64.64	208.88	118.68	57.85	13.34	b.d	273.21	5.29	3.20	0.60	0.33	56.49	1.86
CH6/131	492.65	Norite	41.30	109.63	288.33	70.02	206.16	85.61	67.44	13.47	0.10	242.48	5.15	3.34	0.72	0.66	47.94	0.65
CH6/132	495.30	Norite	37.20	115.12	263.04	47.84	147.65	82.91	73.76	17.15	1.38	290.82	4.94	2.89	0.07	0.33	66.26	0.69
CH6/133	500.50	Norite	33.65	129.26	483.80	60.55	209.38	65.14	60.02	13.44	0.81	260.42	5.23	3.63	0.18	0.30	67.44	0.50
CH6/134	502.86	Norite	32.57	134.28	495.62	56.23	213.35	61.12	66.29	12.39	2.39	249.52	5.34	6.60	0.75	0.51	73.40	0.35
CH6/135	507.47	Norite	28.90	135.92	480.93	54.22	212.36	63.80	58.96	13.32	2.88	248.89	5.64	8.11	0.11	0.16	79.01	b.d
CH6/136	510.22	Norite	32.36	130.44	431.95	58.04	196.43	57.05	61.99	14.54	2.46	253.15	5.94	9.64	0.61	0.10	85.01	1.47
CH6/137	513.62	Norite	33.39	128.83	374.44	50.81	199.44	70.32	48.34	14.93	3.81	255.62	6.71	11.40	0.46	0.40	84.17	1.19
CH6/138	516.77	Norite	35.96	133.02	376.25	50.69	195.57	74.87	55.15	13.15	3.94	257.84	4.55	10.29	b.d	0.52	96.03	0.30
CH6/139	520.45	Norite	35.05	130.53	326.25	48.70	188.12	71.90	57.51	14.53	4.34	271.31	5.11	12.58	0.06	1.29	109.24	1.28
CH6/140	523.59	Norite	29.87	136.69	313.56	47.23	184.85	75.90	43.85	15.16	5.30	274.86	4.30	12.76	b.d	0.60	95.92	0.77
CH6/141	526.19	Norite	29.78	119.15	376.97	52.26	199.58	96.54	49.46	14.72	4.03	273.02	4.53	10.27	b.d	b.d	107.11	1.95
CH6/142	529.56	Norite	31.71	121.75	522.80	58.47	207.92	54.23	57.63	12.52	3.57	250.93	4.76	10.73	b.d	b.d	89.96	0.73
CH6/143	533.18	Norite	30.00	122.54	582.56	60.10	203.50	25.67	60.51	15.10	5.54	245.29	4.57	12.24	0.44	0.65	92.38	1.74
CH6/144	537.48	Norite	30.50	131.66	588.51	57.31	200.91	25.39	62.59	14.14	3.83	241.72	4.84	11.46	b.d	b.d	88.01	0.74
CH6/145	539.42	Norite	31.64	141.76	583.80	53.82	200.84	33.31	73.12	14.41	6.18	237.60	4.60	13.54	0.11	0.82	92.12	0.59
CH6/146	542.67	Norite	31.01	129.81	536.61	54.20	188.80	22.95	59.69	13.63	2.82	251.75	4.06	7.79	b.d	b.d	71.80	0.05
CH6/147	547.64	Norite	29.15	131.41	461.47	47.00	159.89	14.23	55.42	15.39	1.97	270.72	3.80	6.25	b.d	0.44	97.76	0.04
CH6/148	550.62	Norite	33.56	158.00	261.09	42.81	143.12	4.79	43.22	14.83	2.04	285.85	4.91	8.57	0.35	b.d	98.84	b.d
CH6/149	552.46	Norite	33.75	153.99	480.83	46.59	175.61	11.51	47.75	14.29	1.53	260.77	4.29	6.84	0.84	0.64	69.23	b.d
CH6/150	555.49	Norite	31.14	148.08	555.71	50.74	176.45	15.04	51.59	14.41	2.71	261.82	3.24	5.92	1.22	1.51	83.49	0.69

Table C.2: Continued

Sample No	Depth (m)	Lithology	Sc (ppm)	V (ppm)	Cr (ppm)	Co (ppm)	Ni (ppm)	Cu (ppm)	Zn (ppm)	Ga (ppm)	Rb (ppm)	Sr (ppm)	Y (ppm)	Zr (ppm)	Nb (ppm)	Mo (ppm)	Ba (ppm)	Pb (ppm)
CH6/151	559.16	Melanorite	29.53	146.73	682.09	53.92	193.74	18.65	55.98	13.18	1.81	250.75	5.11	7.31	0.17	b.d	84.48	b.d
CH6/152	563.35	Melanorite	25.20	129.26	761.55	56.98	229.09	23.37	63.83	13.07	2.73	237.28	3.46	8.76	1.52	0.50	96.64	2.60
CH6/153	566.60	Melanorite	32.07	142.71	905.84	63.55	272.30	20.16	70.62	10.33	4.42	200.69	4.33	10.19	2.84	b.d	84.20	1.93
CH6/154	569.42	Melanorite	30.35	146.22	974.91	66.64	287.53	26.13	83.75	11.61	2.73	186.81	4.63	9.86	2.43	b.d	79.32	0.81
CH6/155	573.65	Melanorite	26.98	131.95	871.50	57.42	259.39	23.89	75.00	12.81	1.47	213.07	3.94	8.16	2.51	0.93	81.90	2.51
CH6/156	576.13	Melanorite	29.19	147.29	1071.70	68.68	277.37	25.35	79.48	9.66	3.23	178.59	3.72	10.03	3.34	b.d	88.86	0.13
CH6/157	580.63	Melanorite	27.32	156.73	1114.18	71.28	318.54	27.15	84.44	11.01	3.80	171.36	5.54	13.33	3.12	0.97	91.40	0.82
CH6/158	583.59	Melanorite	30.00	153.10	1133.31	71.34	317.40	31.34	92.32	10.03	3.40	166.65	5.80	12.18	2.14	0.55	92.33	0.27
CH6/159	587.45	Melanorite	28.95	155.31	1145.72	68.55	324.15	27.95	79.04	10.17	3.89	167.72	5.14	12.22	0.36	0.23	81.43	1.07
CH6/160	590.36	Melanorite	25.94	149.26	1087.88	63.38	299.66	25.27	82.90	10.89	4.59	180.14	6.02	14.02	2.06	b.d	84.06	1.61
CH6/161	595.16	Melanorite	31.14	159.97	1224.41	68.59	334.20	27.34	73.19	9.53	5.85	160.00	6.37	16.99	1.79	b.d	111.87	b.d
CH6/162	597.86	Melanorite	29.37	142.28	1205.07	67.40	336.27	24.63	90.79	10.24	5.73	159.60	4.56	12.94	1.64	b.d	88.58	2.15
CH6/163	600.34	Melanorite	29.58	157.88	1214.11	71.00	330.22	23.15	93.82	10.49	6.78	153.86	6.41	13.44	0.35	b.d	95.78	2.18
CH6/164	603.16	Melanorite	31.12	165.07	1299.86	74.16	357.82	27.73	85.51	8.52	8.11	138.80	6.61	14.10	b.d	0.33	82.18	1.55
CH6/165	605.63	Melanorite	29.18	142.93	1072.35	62.70	302.98	26.59	92.37	11.32	9.44	181.29	6.29	17.29	b.d	b.d	111.87	2.36
CH6/166	609.58	Melanorite	35.62	152.13	1246.58	78.23	351.68	25.77	90.72	9.03	9.04	147.12	5.78	16.27	0.04	b.d	102.73	b.d
CH6/167	616.31	Melanorite	29.63	157.92	1315.20	79.10	378.96	25.77	101.49	9.10	7.64	130.12	6.64	17.68	0.29	b.d	89.80	2.97
CH6/168	616.76	Melanorite	30.61	149.93	1314.57	74.44	374.23	29.33	94.31	8.79	5.81	136.10	6.61	15.74	b.d	b.d	88.35	0.83
CH6/169	624.65	Melanorite	33.82	180.10	1440.97	72.90	402.60	22.16	86.68	8.45	6.44	117.26	5.76	13.98	0.04	b.d	73.29	1.65
CH6/170	630.48	Melanorite	33.13	159.01	1409.22	76.89	390.91	32.01	79.64	7.59	5.10	123.43	6.12	13.28	b.d	b.d	83.12	0.96
CH6/171	633.41	Melanorite	34.01	171.23	1468.65	80.79	406.94	24.72	88.91	7.96	5.99	116.17	5.38	13.83	0.19	0.90	84.49	3.05
CH6/172	636.36	Melanorite	31.97	182.11	1541.53	77.80	421.07	14.38	78.71	7.43	5.06	102.89	6.69	12.67	b.d	b.d	71.66	0.23
CH6/173	639.57	Melanorite	33.02	174.77	1553.13	83.07	425.23	23.74	92.91	6.66	4.63	106.65	7.06	13.14	0.09	b.d	80.35	0.82
CH6/174	643.44	Melanorite	31.91	165.65	1581.44	78.36	426.04	24.83	103.03	8.54	4.82	104.87	5.45	11.62	0.46	0.47	81.22	b.d
CH6/175	646.71	Melanorite	31.18	166.44	1652.62	80.60	450.88	17.91	106.72	6.36	4.57	90.59	6.87	10.29	1.68	0.75	75.04	1.62

Table C.2: Continued

Sample No	Depth (m)	Lithology	Sc (ppm)	V (ppm)	Cr (ppm)	Co (ppm)	Ni (ppm)	Cu (ppm)	Zn (ppm)	Ga (ppm)	Rb (ppm)	Sr (ppm)	Y (ppm)	Zr (ppm)	Nb (ppm)	Mo (ppm)	Ba (ppm)	Pb (ppm)
CH6/176	649.25	Feldspathic pyroxenite	32.82	182.58	1759.19	89.84	469.49	20.93	93.86	5.94	7.47	73.25	7.39	14.63	0.92	0.26	81.68	b.d
CH6/177	652.59	Feldspathic pyroxenite	36.49	181.98	1711.41	86.82	460.65	21.93	101.28	6.38	8.59	76.27	6.92	18.21	0.52	b.d	88.11	2.60
CH6/178	662.51	Feldspathic pyroxenite	34.23	161.13	1700.44	84.86	447.32	11.64	106.22	4.57	10.54	79.85	7.00	21.09	1.69	b.d	97.37	3.64
CH6/179	667.48	Feldspathic pyroxenite	31.47	173.50	1655.76	84.01	450.85	2.53	131.82	5.74	6.52	89.84	8.04	15.06	1.99	1.41	85.73	1.22
CH6/180	672.53	Feldspathic pyroxenite	31.95	164.28	1676.24	83.64	456.66	6.68	100.39	6.26	4.39	88.61	7.69	12.26	1.25	0.33	68.05	3.64
CH6/181	677.75	Feldspathic pyroxenite	32.37	168.47	1731.97	83.08	453.93	3.22	187.74	6.48	7.70	81.76	7.30	15.39	0.67	b.d	106.19	2.86
CH6/182	679.42	Feldspathic pyroxenite	30.52	143.82	1537.68	71.87	421.05	9.16	92.37	10.00	3.94	158.20	6.14	9.64	0.78	0.19	94.10	2.61
CH6/183	683.39	Feldspathic pyroxenite	32.26	166.28	1720.55	84.61	441.71	25.72	104.94	6.86	7.98	92.49	6.51	14.31	0.49	0.94	104.13	2.87
CH6/184	686.16	Feldspathic pyroxenite	31.20	156.96	1782.93	87.70	461.73	16.25	102.97	6.47	7.77	86.27	7.42	14.77	0.48	-0.16	90.66	1.28
CH6/185	688.31	Feldspathic pyroxenite	30.53	150.32	1796.15	85.09	445.84	25.83	91.22	6.76	8.24	90.06	7.54	14.60	-0.09	0.34	102.95	0.82

Table C.3: Whole-rocks trace elements and REE data (ppm, combined LA-ICP-MS and ICP-MS).

Sample No	CH6 2	CH6	CH6 3	CH6 7	CH6 14	CH6 19	CH6 22	CH6 25	CH6 28	CH6 32
Depth (m)	31.93	38.84	42.60	55.18	78.71	94.42	103.86	115.15	124.63	139.86
Li	1.51	0.68	0.58	0.51	2.31	0.44	0.24	0.72	0.24	0.12
P	59.88	22.25	21.49	41.02	84.12	45.00	93.00	30.78	9.64	27.01
Sc	5.44	10.39	8.09	12.71	8.56	12.04	8.81	16.81	13.60	16.54
Ti	135.46	341.83	780.11	583.39	279.84	621.91	907.61	543.52	423.20	483.90
V	38.39	44.01	44.29	51.57	30.91	59.87	58.50	64.48	55.63	71.28
Cr	7944.75	2918.68	2135.42	2631.85	1667.39	2719.70	1506.04	3486.52	2123.51	2441.81
Co	190.10	100.95	73.40	100.54	193.48	103.61	60.73	106.40	85.99	114.83
Ni	2252.31	775.08	663.45	775.40	2099.59	744.20	458.48	759.18	586.93	720.81
Cu	14.93	6.90	16.66	10.41	12.55	9.16	14.51	28.61	13.54	13.90
Zn	112.03	66.44	43.08	67.39	85.67	68.04	49.56	68.49	59.89	84.06
Ga	1.88	1.46	0.93	1.74	1.43	1.61	1.70	1.95	1.24	1.97
As	0.70	0.51	0.39	0.46	1.37	0.26	0.23	0.44	0.14	0.11
Rb	0.62	0.41	0.32	7.70	1.35	1.10	2.31	0.64	0.33	0.31
Sr	2.40	2.74	2.55	13.46	12.17	9.94	16.99	5.00	9.91	21.81
Y	0.24	0.63	0.46	1.22	0.81	1.11	1.39	1.06	0.69	0.80
Zr	1.34	1.35	8.07	4.62	2.97	3.50	13.37	1.64	1.36	1.48
Nb	0.13	0.05	0.53	0.37	0.21	0.16	1.55	0.05	0.06	0.05
Ba	3.99	1.99	2.95	10.48	8.70	5.28	7.65	2.12	1.88	2.10
Sn	0.38	0.09	0.35	0.44	0.61	0.35	0.75	0.34	0.14	0.30
Cs	0.21	0.03	0.03	0.49	0.09	0.07	0.11	0.05	0.03	0.02
La	0.38	0.23	0.21	0.80	0.65	0.46	0.78	0.27	0.24	0.67
Ce	0.64	0.29	0.74	1.37	1.37	0.87	1.97	0.45	0.34	0.35
Pr	0.07	0.03	0.04	0.16	0.15	0.11	0.17	0.05	0.04	0.04
Nd	0.26	0.15	0.18	0.62	0.59	0.45	0.71	0.21	0.19	0.18
Sm	0.04	0.04	0.04	0.13	0.12	0.10	0.15	0.06	0.05	0.05
Eu	0.01	0.01	0.01	0.04	0.03	0.03	0.04	0.02	0.02	0.02
Gd	0.04	0.06	0.05	0.15	0.13	0.13	0.18	0.08	0.05	0.07
Tb	0.01	0.01	0.01	0.02	0.02	0.02	0.03	0.02	0.01	0.01
Dy	0.02	0.08	0.06	0.16	0.12	0.15	0.20	0.14	0.08	0.09
Ho	0.01	0.02	0.01	0.04	0.02	0.03	0.04	0.03	0.02	0.02
Er	0.02	0.06	0.05	0.12	0.07	0.10	0.13	0.11	0.07	0.08
Tm	b.d	0.01	0.01	0.02	0.01	0.02	0.02	0.02	0.01	0.01
Yb	0.04	0.09	0.06	0.13	0.09	0.13	0.15	0.15	0.10	0.11
Lu	0.01	0.01	0.01	0.02	0.02	0.02	0.03	0.03	0.02	0.02
Hf	0.03	0.04	0.25	0.14	0.08	0.10	0.35	0.06	0.05	0.05
Ta	b.d	b.d	0.04	0.03	0.03	b.d	0.09	b.d	0.01	b.d
W	0.31	b.d	0.10	0.12	0.06	0.03	0.15	0.05	0.10	0.03
Pb	0.90	0.39	0.78	1.91	1.14	1.06	1.60	1.15	0.55	0.72
Th	0.07	0.02	0.02	0.17	0.10	0.06	0.12	0.01	0.03	0.01
U	0.05	0.01	0.05	0.35	0.05	0.04	0.69	0.01	0.01	0.01

Table C.3: Continued

Sample No	CH6 34	CH6 36	CH6 40	CH6 44	CH6 45	CH6 46	CH6 47	CH6 51	CH6 56	CH6 62
Depth (m)	145.29	153.67	164.18	176.09	179.66	182.39	186.26	198.51	218.62	235.85
Li	0.19	0.15	0.32	0.56	0.82	0.22	0.40	1.28	0.26	0.22
P	11.83	31.03	36.77	31.80	52.75	14.32	40.69	72.64	67.98	74.54
Sc	16.73	19.10	18.80	22.02	11.09	12.41	15.14	11.13	11.93	11.02
Ti	444.00	583.87	418.89	457.34	382.04	377.75	615.61	537.27	695.62	832.87
V	68.31	84.51	60.33	70.17	51.05	50.14	61.58	48.43	62.94	64.22
Cr	1920.00	1617.49	954.72	1178.82	4457.08	2930.05	2639.37	2194.36	2654.35	2143.38
Co	96.80	121.52	89.04	77.39	127.02	95.78	105.11	147.94	104.08	82.83
Ni	575.40	654.32	445.13	456.11	1458.27	1217.24	764.46	1451.16	728.89	605.55
Cu	13.13	22.39	15.32	6.35	119.94	19.07	16.29	15.59	11.00	16.75
Zn	57.70	76.35	60.59	49.21	74.19	49.82	73.45	80.24	69.75	63.83
Ga	1.33	2.01	8.58	9.45	3.26	3.31	1.86	1.77	1.83	1.89
As	0.20	0.16	0.25	0.21	0.40	0.36	0.40	0.65	0.25	0.17
Rb	0.63	1.22	0.58	0.49	0.72	0.63	4.71	2.08	4.54	2.60
Sr	7.57	22.14	170.38	151.28	51.40	59.68	10.32	16.23	17.89	18.65
Y	0.82	1.09	0.71	1.41	0.66	0.70	1.25	1.38	1.49	1.57
Zr	1.95	3.43	1.31	1.86	2.72	1.71	4.89	4.61	7.27	10.29
Nb	0.09	0.11	0.06	0.06	0.31	0.10	0.30	0.27	0.86	0.96
Ba	2.89	8.97	10.33	16.57	6.06	7.30	8.95	8.88	19.49	8.24
Sn	0.13	0.33	0.33	0.31	0.46	0.15	0.41	0.55	0.41	0.59
Cs	0.06	0.24	0.02	0.02	0.12	0.04	0.29	0.15	0.27	0.14
La	0.27	1.80	0.47	0.69	0.52	0.40	1.26	0.96	1.36	0.92
Ce	0.52	2.28	0.72	1.30	0.85	0.61	2.00	1.93	2.56	2.06
Pr	0.06	0.20	0.08	0.15	0.10	0.08	0.20	0.22	0.28	0.21
Nd	0.27	0.70	0.32	0.66	0.41	0.34	0.79	0.84	1.05	0.82
Sm	0.07	0.10	0.07	0.17	0.08	0.08	0.14	0.18	0.20	0.17
Eu	0.02	0.04	0.08	0.11	0.05	0.05	0.04	0.05	0.06	0.05
Gd	0.08	0.15	0.08	0.19	0.09	0.08	0.17	0.20	0.22	0.20
Tb	0.01	0.02	0.01	0.03	0.02	0.01	0.03	0.03	0.03	0.03
Dy	0.10	0.15	0.10	0.22	0.10	0.09	0.18	0.20	0.21	0.22
Ho	0.02	0.03	0.02	0.05	0.02	0.02	0.04	0.04	0.04	0.05
Er	0.08	0.10	0.07	0.13	0.06	0.07	0.12	0.12	0.14	0.14
Tm	0.01	0.02	0.01	0.02	0.01	0.01	0.02	0.02	0.02	0.02
Yb	0.10	0.13	0.08	0.14	0.08	0.08	0.14	0.14	0.16	0.16
Lu	0.02	0.02	0.02	0.02	0.01	0.01	0.03	0.03	0.03	0.03
Hf	0.06	0.10	0.04	0.07	0.08	0.05	0.15	0.13	0.19	0.27
Ta	0.01	b.d	b.d	b.d	0.01	0.01	0.02	0.02	0.05	0.05
W	0.05	0.09	0.03	0.03	0.17	0.04	0.10	0.07	0.10	0.10
Pb	0.47	7.82	0.87	0.92	1.06	0.46	1.51	1.75	1.64	1.51
Th	0.04	0.06	0.03	0.04	0.06	0.06	0.15	0.13	0.27	0.14
U	0.02	0.07	0.02	0.02	0.63	0.02	0.21	0.08	0.11	0.39

Table C.3: Continued

Sample No	CH6 67	CH6 71	CH6 78	CH6 80	CH6 81	CH6 85	CH6 93	CH6 101	CH6 106	CH6 109
Depth (m)	254.28	268.13	292.53	297.83	305.43	319.39	350.44	388.35	404.14	417.09
Li	0.40	0.22	0.22	1.43	0.52	0.24	0.31	0.28	0.63	0.31
P	61.52	36.65	50.14	49.84	61.06	27.50	104.37	27.15	84.84	50.53
Sc	14.65	15.37	18.20	15.47	20.90	14.04	10.67	12.39	16.59	14.96
Ti	683.19	961.40	739.20	428.44	739.38	690.65	984.67	895.23	897.50	942.85
V	67.28	70.04	89.50	61.04	86.04	86.50	77.50	72.42	82.84	77.08
Cr	3033.93	2005.18	1851.34	1201.67	1893.19	1798.52	1220.41	2468.47	3226.03	2899.55
Co	104.37	87.58	115.50	75.27	92.57	90.66	39.90	87.33	88.47	85.23
Ni	751.86	574.54	696.00	496.72	598.88	588.77	241.93	513.54	552.15	548.82
Cu	23.09	17.84	20.63	16.59	8.20	6.76	10.77	16.63	11.53	15.29
Zn	67.31	64.56	75.41	56.36	68.62	63.55	33.30	72.64	78.29	63.77
Ga	1.98	2.28	2.79	10.83	6.04	1.40	1.74	2.24	2.18	3.14
As	0.30	0.16	0.20	0.25	0.33	0.16	0.20	0.11	0.43	0.24
Rb	3.48	0.71	2.50	0.65	4.82	2.55	3.79	4.97	7.43	4.61
Sr	13.44	39.51	42.15	204.16	83.37	9.62	28.78	26.60	11.02	44.48
Y	1.65	1.27	1.74	0.83	2.44	1.41	2.34	2.29	2.52	3.36
Zr	5.70	5.34	7.86	1.77	5.61	4.80	27.51	8.08	19.32	9.34
Nb	0.43	1.29	0.31	0.06	0.48	0.37	1.23	0.53	0.76	0.52
Ba	9.95	3.92	10.32	21.54	20.53	7.19	19.99	11.89	19.09	19.32
Sn	0.41	0.72	0.32	0.43	0.45	0.21	0.66	0.40	0.32	0.32
Cs	0.22	0.04	0.24	0.02	0.28	0.14	0.20	0.26	0.36	0.20
La	1.08	0.66	1.88	0.73	1.46	0.81	2.80	1.64	1.82	2.23
Ce	2.08	0.76	3.20	1.23	2.83	1.60	4.25	3.53	3.86	4.12
Pr	0.23	0.10	0.30	0.13	0.32	0.18	0.53	0.39	0.45	0.45
Nd	0.87	0.41	1.13	0.51	1.21	0.72	1.97	1.59	1.77	1.72
Sm	0.18	0.10	0.21	0.10	0.27	0.14	0.37	0.32	0.34	0.36
Eu	0.05	0.05	0.08	0.12	0.10	0.04	0.10	0.08	0.08	0.11
Gd	0.21	0.13	0.26	0.11	0.31	0.16	0.41	0.34	0.38	0.42
Tb	0.04	0.02	0.04	0.02	0.05	0.03	0.06	0.06	0.06	0.07
Dy	0.23	0.17	0.26	0.11	0.34	0.19	0.38	0.35	0.35	0.46
Ho	0.05	0.04	0.06	0.03	0.07	0.04	0.08	0.08	0.08	0.10
Er	0.15	0.12	0.16	0.08	0.22	0.13	0.22	0.22	0.23	0.29
Tm	0.03	0.02	0.03	0.01	0.04	0.02	0.03	0.03	0.03	0.04
Yb	0.18	0.15	0.18	0.10	0.25	0.16	0.22	0.22	0.26	0.33
Lu	0.03	0.03	0.03	0.02	0.04	0.03	0.04	0.03	0.04	0.05
Hf	0.16	0.16	0.21	0.05	0.17	0.15	0.68	0.25	0.47	0.26
Ta	0.02	0.08	0.01	b.d	0.02	0.03	0.10	0.05	0.05	0.04
W	0.09	0.04	0.08	0.04	0.06	0.17	0.39	0.17	0.13	0.11
Pb	1.37	0.92	4.60	1.24	1.55	0.85	1.31	1.61	1.45	1.73
Th	0.25	0.04	0.16	0.03	0.30	0.15	0.45	0.28	0.43	0.35
U	0.08	0.72	0.10	0.02	0.11	0.07	0.16	0.10	0.15	0.17

Table C.3: Continued

Sample No	CH6 112	CH6 113	CH6 116	CH6 119	CH6 122	CH6 126	CH6 128	CH6 131	CH6 133	CH6 134
Depth (m)	430.25	434.19	444.41	454.69	462.72	477.49	482.75	492.65	500.35	502.86
Li	0.37	0.42	0.37	1.43	2.22	0.89	1.43	4.07	2.19	3.02
P	73.13	20.23	51.90	21.98	17.14	19.13	8.06	10.92	21.29	24.80
Sc	15.93	17.71	16.83	19.63	19.52	28.62	30.98	36.18	21.71	28.86
Ti	954.59	895.03	1178.27	619.41	537.67	782.52	653.78	642.19	980.65	810.17
V	83.94	84.57	100.91	73.07	83.60	109.18	104.10	115.73	125.35	142.44
Cr	3009.85	2667.60	1536.53	1092.95	593.80	752.03	995.16	325.71	274.84	549.21
Co	89.84	94.80	56.13	67.91	58.14	46.64	80.78	74.42	32.12	64.49
Ni	575.02	815.57	472.67	522.84	323.11	276.89	403.14	232.14	133.23	248.77
Cu	18.58	25.20	17.78	96.81	125.66	50.36	99.40	85.75	47.11	58.21
Zn	68.64	83.05	45.96	77.80	56.71	63.82	77.39	65.24	27.92	68.67
Ga	2.42	4.13	1.74	13.39	14.47	6.56	7.81	12.49	6.03	13.08
As	0.17	0.21	0.29	0.29	0.34	0.31	0.20	0.26	0.21	0.34
Rb	4.91	2.72	3.19	0.89	1.05	1.21	1.11	0.59	0.74	1.83
Sr	23.70	66.34	10.96	228.77	243.69	165.86	155.44	231.73	159.98	226.20
Y	2.80	2.78	2.53	1.91	1.87	2.94	2.94	3.33	2.80	4.06
Zr	10.46	5.41	12.58	2.71	3.12	5.92	2.73	2.83	11.42	6.71
Nb	0.52	0.25	0.79	0.16	0.12	0.32	0.07	0.05	0.58	0.26
Ba	13.65	10.23	12.82	43.80	49.63	21.82	36.17	44.77	34.94	57.89
Sn	0.30	0.30	0.46	0.53	0.30	0.35	0.15	0.20	0.28	0.33
Cs	0.21	0.14	0.12	0.04	0.04	0.04	0.03	0.02	0.03	0.07
La	1.56	1.11	1.33	1.22	1.29	1.19	1.03	0.96	1.21	1.86
Ce	3.24	2.28	2.15	2.04	2.38	1.70	1.65	1.95	1.73	3.83
Pr	0.37	0.28	0.28	0.23	0.28	0.27	0.24	0.29	0.31	0.50
Nd	1.45	1.16	1.09	0.88	1.09	1.15	1.05	1.35	1.38	2.14
Sm	0.30	0.28	0.25	0.20	0.26	0.30	0.30	0.40	0.37	0.56
Eu	0.08	0.11	0.06	0.25	0.31	0.22	0.22	0.25	0.26	0.35
Gd	0.36	0.32	0.29	0.21	0.27	0.32	0.33	0.44	0.39	0.59
Tb	0.06	0.06	0.05	0.04	0.04	0.06	0.06	0.08	0.07	0.10
Dy	0.38	0.38	0.33	0.25	0.28	0.40	0.43	0.52	0.45	0.64
Ho	0.08	0.08	0.07	0.06	0.06	0.09	0.10	0.11	0.09	0.13
Er	0.24	0.24	0.21	0.18	0.18	0.27	0.30	0.32	0.28	0.39
Tm	0.04	0.04	0.03	0.03	0.03	0.04	0.05	0.05	0.04	0.06
Yb	0.27	0.27	0.25	0.24	0.22	0.34	0.35	0.34	0.30	0.40
Lu	0.04	0.04	0.04	0.04	0.03	0.05	0.06	0.05	0.05	0.06
Hf	0.28	0.16	0.33	0.08	0.10	0.17	0.10	0.12	0.38	0.20
Ta	0.03	0.01	0.06	0.01	0.01	0.02	0.01	b.d	0.05	0.01
W	0.11	0.04	0.13	0.08	0.06	0.05	0.02	0.03	0.03	0.10
Pb	1.64	1.65	1.42	2.23	1.85	1.43	1.48	2.40	0.86	1.83
Th	0.39	0.13	0.34	0.06	0.07	0.09	0.05	0.03	0.04	0.15
U	0.13	0.06	0.11	0.02	0.03	0.03	0.02	0.01	0.03	0.05

Table C.3: Continued

Sample No	CH6 139	CH6 142	CH6 146	CH6 148	CH6 150	CH6 155	CH6 165	CH6 169
Depth (m)	520.45	529.42	542.67	550.46	555.49	573.65	605.63	624.50
Li	5.23	4.75	4.51	4.74	5.81	1.74	2.24	1.21
P	44.02	36.80	29.98	30.88	23.17	28.84	67.42	46.46
Sc	27.94	26.55	22.69	22.22	24.94	21.82	25.40	29.59
Ti	896.71	859.42	746.23	794.69	749.28	987.32	1096.31	1092.75
V	141.31	125.94	132.40	160.78	144.11	133.06	138.34	150.40
Cr	368.00	526.59	578.38	283.79	629.37	537.95	1148.80	1348.47
Co	49.93	55.72	56.70	41.62	53.83	31.80	69.83	78.16
Ni	212.49	220.18	212.03	156.62	208.44	177.74	350.24	391.52
Cu	75.67	48.92	23.12	9.83	15.55	21.36	27.13	23.05
Zn	59.78	50.04	56.68	38.16	52.23	39.51	92.74	65.77
Ga	14.34	11.69	12.95	11.82	13.37	6.14	10.95	6.22
As	0.33	0.28	0.30	0.23	0.30	0.21	0.37	0.27
Rb	3.86	2.67	1.86	1.81	1.40	1.67	8.83	4.90
Sr	248.52	216.13	219.07	202.49	245.72	171.61	186.21	112.94
Y	5.12	4.32	3.50	4.06	4.24	4.04	5.35	5.38
Zr	12.82	9.08	7.41	6.97	5.69	9.71	19.82	12.37
Nb	0.58	0.40	0.30	0.21	0.14	0.48	1.10	0.68
Ba	80.78	76.62	70.79	64.38	78.37	43.54	86.69	50.14
Sn	0.34	0.50	0.22	0.18	0.22	0.42	0.47	0.26
Cs	0.20	0.14	0.07	0.05	0.04	0.08	0.33	0.48
La	2.84	2.41	2.22	1.70	2.22	2.64	4.32	3.15
Ce	6.18	4.53	4.27	4.15	4.56	3.06	7.75	5.31
Pr	0.75	0.60	0.50	0.48	0.55	0.56	0.95	0.76
Nd	3.14	2.52	2.04	2.17	2.29	2.18	3.62	2.97
Sm	0.78	0.61	0.50	0.59	0.59	0.49	0.78	0.70
Eu	0.44	0.36	0.40	0.33	0.44	0.37	0.42	0.30
Gd	0.81	0.63	0.53	0.61	0.61	0.51	0.81	0.76
Tb	0.13	0.10	0.09	0.10	0.10	0.09	0.13	0.13
Dy	0.83	0.66	0.55	0.65	0.66	0.58	0.79	0.84
Ho	0.16	0.14	0.12	0.14	0.14	0.13	0.17	0.18
Er	0.49	0.41	0.35	0.38	0.41	0.38	0.51	0.52
Tm	0.07	0.07	0.05	0.06	0.06	0.06	0.07	0.09
Yb	0.50	0.45	0.39	0.38	0.44	0.44	0.54	0.59
Lu	0.08	0.07	0.06	0.06	0.07	0.07	0.09	0.09
Hf	0.36	0.26	0.22	0.22	0.18	0.27	0.50	0.35
Ta	0.04	0.03	0.02	0.02	0.01	0.03	0.07	0.05
W	0.07	0.06	0.06	0.03	0.05	0.06	0.14	0.09
Pb	2.57	4.33	1.66	1.51	1.79	1.67	2.54	1.19
Th	0.38	0.26	0.19	0.13	0.10	0.20	0.69	0.47
U	0.15	0.08	0.07	0.05	0.03	0.04	0.24	0.14

Table C.3: Continued

Sample No	CH6 173	CH6 176	CH6 178	CH6 180	CH6 182	CH6 183	CH6 185
Depth (m)	639.57	649.25	662.36	672.53	679.25	683.39	688.17
Li	1.07	1.02	1.01	0.88	1.59	1.08	0.93
P	58.13	66.76	70.46	65.41	44.09	98.06	76.76
Sc	31.03	31.30	26.63	30.62	30.29	33.19	20.67
Ti	1240.69	1454.52	1252.49	1348.58	1027.04	1382.76	1553.80
V	166.53	183.16	136.27	165.18	130.05	175.68	128.49
Cr	1747.94	1994.45	1499.75	1917.61	1489.30	2053.49	980.65
Co	96.24	108.79	83.21	105.48	73.76	105.96	50.21
Ni	484.70	571.59	436.34	537.08	424.58	535.66	281.70
Cu	28.21	28.84	14.48	11.41	14.04	30.51	24.45
Zn	93.08	98.57	82.97	110.41	73.83	122.88	45.18
Ga	7.65	6.17	4.63	6.89	8.16	7.28	3.26
As	0.35	0.46	0.36	0.37	0.29	0.42	0.33
Rb	6.55	8.45	9.85	7.34	4.57	8.42	4.80
Sr	124.30	86.73	80.44	104.82	162.15	112.65	75.88
Y	5.50	6.15	5.71	5.55	5.72	6.05	4.83
Zr	13.33	13.11	12.42	11.54	9.41	16.83	19.63
Nb	0.68	0.71	1.07	0.78	0.51	0.71	1.39
Ba	44.04	37.32	43.89	31.50	74.00	51.28	31.15
Sn	0.29	0.52	0.31	0.31	0.22	0.36	0.52
Cs	0.36	0.54	0.53	0.41	0.27	0.33	0.26
La	2.79	2.61	3.78	2.77	3.70	3.54	3.13
Ce	5.16	5.03	6.33	4.87	5.64	6.12	4.47
Pr	0.66	0.64	0.88	0.60	0.81	0.76	0.74
Nd	2.62	2.57	3.34	2.38	3.13	3.02	2.90
Sm	0.59	0.61	0.75	0.54	0.71	0.71	0.64
Eu	0.26	0.22	0.25	0.23	0.40	0.26	0.23
Gd	0.66	0.69	0.82	0.62	0.75	0.78	0.70
Tb	0.11	0.12	0.13	0.11	0.12	0.13	0.12
Dy	0.73	0.77	0.86	0.70	0.83	0.82	0.75
Ho	0.16	0.17	0.18	0.15	0.17	0.17	0.16
Er	0.47	0.49	0.55	0.45	0.53	0.48	0.45
Tm	0.08	0.08	0.09	0.07	0.09	0.08	0.08
Yb	0.56	0.56	0.59	0.51	0.60	0.55	0.48
Lu	0.09	0.09	0.09	0.08	0.09	0.09	0.07
Hf	0.38	0.35	0.37	0.31	0.27	0.42	0.59
Ta	0.04	0.04	0.07	0.05	0.03	0.05	0.11
W	0.09	0.09	0.09	0.11	0.07	0.13	0.10
Pb	1.88	1.71	2.66	4.08	2.17	3.59	1.59
Th	0.45	0.54	0.83	0.52	0.41	0.67	0.47
U	0.15	0.19	0.20	0.24	0.11	0.25	0.15

Table C. 4: CIPW Norm (*Volume %) of the CH6 Drill Core

Sample No.	Depth (m)	Lithology	Hypersthene	Plagioclase	Diopside	Olivine	Quartz	Orthoclase	Chromite	Magnetite	Ilmenite	Total
CH6/1	30.59	Dunite	5.56	3.93	0.40	87.63	0.00	0.23	0.72	1.43	0.05	99.95
CH6/2	31.925	Dunite	2.29	1.77	0.00	93.20	0.00	0.08	0.68	1.53	0.04	99.59
CH6/3	42.6	Orthopyroxenite	78.74	5.59	2.38	11.59	0.00	0.00	0.56	1.01	0.11	99.98
CH6/4	46.23	Orthopyroxenite	86.41	7.36	3.13	1.31	0.00	0.30	0.40	0.95	0.13	99.99
CH6/5	50.26	Orthopyroxenite	87.12	6.93	3.19	0.93	0.00	0.30	0.44	0.94	0.13	99.98
CH6/6	52.745	Orthopyroxenite	86.40	7.01	3.07	1.76	0.00	0.23	0.45	0.94	0.12	99.98
CH6/7	55.18	Orthopyroxenite	86.89	7.47	2.97	0.00	0.20	0.98	0.42	0.92	0.13	99.98
CH6/8	59.1	Orthopyroxenite	87.29	6.70	3.16	1.21	0.00	0.15	0.41	0.93	0.13	99.98
CH6/9	62.525	Orthopyroxenite	85.09	8.96	3.35	0.58	0.00	0.53	0.41	0.92	0.14	99.98
CH6/10	64.19	Orthopyroxenite	86.82	7.91	3.18	0.42	0.00	0.15	0.44	0.92	0.13	99.97
CH6/11	68.225	Orthopyroxenite	84.66	8.62	2.94	1.75	0.00	0.53	0.43	0.92	0.13	99.98
CH6/12	70.145	Orthopyroxenite	84.05	6.94	2.42	4.96	0.00	0.08	0.45	0.96	0.12	99.98
CH6/13	76.265	Harzburgite	31.61	5.46	1.56	59.17	0.00	0.38	0.45	1.27	0.08	99.98
CH6/14	78.705	Harzburgite	30.17	4.60	1.38	62.09	0.00	0.15	0.22	1.26	0.07	99.94
CH6/15	81.485	Orthopyroxenite	86.53	7.99	2.88	0.78	0.00	0.30	0.43	0.92	0.14	99.97
CH6/16	85.525	Orthopyroxenite	87.66	7.43	2.98	0.05	0.00	0.38	0.43	0.92	0.13	99.98
CH6/17	88.245	Orthopyroxenite	86.12	7.15	3.13	1.69	0.00	0.38	0.44	0.92	0.13	99.96
CH6/18	91.545	Orthopyroxenite	87.48	7.30	3.05	0.50	0.00	0.15	0.44	0.92	0.13	99.97
CH6/19	94.415	Orthopyroxenite	85.67	7.14	3.70	1.68	0.00	0.30	0.44	0.91	0.13	99.97
CH6/20	99.88	Orthopyroxenite	84.48	7.34	4.07	0.00	1.31	1.20	0.42	`	0.20	99.02
CH6/21	102.885	Orthopyroxenite	83.13	9.29	4.01	1.80	0.00	0.23	0.43	0.93	0.13	99.95
CH6/22	103.855	Orthopyroxenite	84.33	8.58	4.16	1.17	0.00	0.23	0.44	0.93	0.14	99.98
CH6/23	106.5	Orthopyroxenite	83.63	8.48	4.44	1.71	0.00	0.23	0.42	0.94	0.13	99.98
CH6/24	111.145	Orthopyroxenite	85.26	8.45	3.99	0.65	0.00	0.15	0.43	0.94	0.12	99.99
CH6/25	115.145	Orthopyroxenite	84.88	6.82	4.14	2.38	0.00	0.15	0.53	0.95	0.12	99.97

***Density corrections applied during the calculation process.**

Table C. 4: Continued

Sample No.	Depth (m)	Lithology	Hypersthene	Plagioclase	Diopside	Olivine	Quartz	Orthoclase	Chromite	Magnetite	Ilmenite	Total
CH6/26	118.405	Orthopyroxenite	85.44	7.58	4.66	0.36	0.00	0.38	0.42	1.00	0.14	99.98
CH6/27	121.565	Orthopyroxenite	85.74	7.56	4.51	0.18	0.00	0.38	0.43	1.05	0.13	99.98
CH6/28	124.78	Orthopyroxenite	86.26	7.32	4.16	0.53	0.00	0.08	0.43	1.09	0.12	99.99
CH6/29	128.335	Orthopyroxenite	85.27	7.37	4.47	1.07	0.00	0.15	0.44	1.09	0.12	99.98
CH6/30	132.47	Orthopyroxenite	85.74	7.63	4.68	0.00	0.08	0.23	0.39	1.11	0.12	99.98
CH6/31	136.595	Orthopyroxenite	83.98	7.90	5.10	0.23	0.00	0.15	0.38	1.11	1.12	99.97
CH6/32	139.855	Orthopyroxenite	84.89	8.21	4.25	0.47	0.00	0.53	0.39	1.13	0.11	99.98
CH6/33	143.185	Orthopyroxenite	86.36	6.82	4.68	0.39	0.00	0.08	0.39	1.15	0.11	99.98
CH6/34	145.43	Pyroxenite	85.74	7.01	5.14	0.29	0.00	0.15	0.38	1.14	0.12	99.97
CH6/35	149.155	Pyroxenite	79.97	9.36	6.00	2.73	0.00	0.38	0.28	1.13	0.13	99.98
CH6/36	153.67	Pyroxenite	82.65	8.76	5.87	0.92	0.00	0.30	0.26	1.10	0.13	99.99
CH6/37	157.15	Pyroxenite*	69.62	9.76	9.98	9.04	0.00	0.15	0.23	1.05	0.14	99.97
CH6/38	159.475	Int. Norite	67.94	26.40	4.27	0.06	0.00	0.15	0.19	0.87	0.10	99.98
CH6/39	161.445	Pyroxenite	71.83	19.11	5.49	2.07	0.00	0.22	0.20	0.94	0.10	99.96
CH6/40	164.175	Melanorite	54.99	39.96	3.74	0.25	0.00	0.14	0.13	0.68	0.09	99.98
CH6/41	167.51	Interlayered norite	18.90	65.91	13.64	0.80	0.00	0.27	0.06	0.32	0.07	99.97
CH6/42	170.44	Interlayered norite	35.12	49.84	13.12	0.92	0.00	0.28	0.11	0.51	0.08	99.98
CH6/43	172.565	Interlayered norite	43.93	43.28	10.68	1.08	0.00	0.21	0.12	0.60	0.09	99.99
CH6/44	176.09	Interlayered norite	43.95	43.17	10.14	1.55	0.00	0.35	0.13	0.59	0.09	99.97
CH6/45	179.655	Interlayered norite	63.55	29.98	4.56	0.56	0.00	0.22	0.21	0.78	0.11	99.97
CH6/46	182.54	Melanorite	56.12	21.62	2.45	18.05	0.00	0.15	0.50	0.98	0.10	99.97
CH6/47	186.255	Pyroxenite	86.09	6.87	4.32	0.70	0.00	0.38	0.41	1.06	0.14	99.97
CH6/48	189.16	Pyroxenite	85.71	7.20	4.67	0.00	0.10	0.68	0.40	1.03	0.17	99.96
CH6/49	191.735	Pyroxenite	86.02	7.73	4.07	0.36	0.00	0.23	0.42	1.00	0.16	99.99
CH6/50	194.855	Pyroxenite	76.09	7.40	4.59	10.04	0.00	0.23	0.43	1.02	0.17	99.97

Table C. 4: Continued

Sample No.	Depth (m)	Lithology	Hypersthene	Plagioclase	Diopside	Olivine	Quartz	Orthoclase	Chromite	Magnetite	Ilmenite	Total
CH6/51	198.51	Pyroxenite	85.88	8.16	3.88	0.00	0.12	0.38	0.42	0.98	0.17	99.99
CH6/52	200.61	Pyroxenite	85.11	7.60	3.89	1.43	0.00	0.38	0.43	0.97	0.16	99.97
CH6/53	207.535	Pyroxenite	87.00	6.61	4.07	0.00	0.36	0.38	0.43	0.98	0.16	99.99
CH6/54	211.44	Pyroxenite	86.11	7.38	4.03	0.00	0.46	0.45	0.42	0.97	0.16	99.98
CH6/55	216.265	Pyroxenite	85.53	7.64	4.34	0.00	0.20	0.68	0.43	0.97	0.17	99.96
CH6/56	218.62	Pyroxenite	83.31	8.81	3.70	0.00	1.36	1.28	0.40	0.94	0.16	99.96
CH6/57	219.585	Pyroxenite	86.20	7.38	3.91	0.00	0.48	0.45	0.43	0.97	0.16	99.98
CH6/58	221.655	Pyroxenite	83.94	7.99	4.57	1.38	0.00	0.53	0.43	0.97	0.16	99.97
CH6/59	223.12	Pyroxenite	84.84	7.67	4.32	1.13	0.00	0.45	0.43	0.97	0.16	99.97
CH6/60	227.505	Pyroxenite	86.15	7.55	4.06	0.00	0.14	0.53	0.42	0.96	0.17	99.98
CH6/61	230.36	Pyroxenite	86.05	7.77	3.89	0.00	0.20	0.53	0.43	0.96	0.16	99.99
CH6/62	235.85	Pyroxenite	85.50	8.46	4.00	0.02	0.00	0.45	0.43	0.97	0.16	99.99
CH6/63	238.795	Pyroxenite	85.54	8.15	3.78	0.00	0.41	0.53	0.43	0.97	0.16	99.97
CH6/64	242.585	Pyroxenite	84.33	9.01	4.09	0.42	0.00	0.53	0.43	0.98	0.16	99.95
CH6/65	244.15	Pyroxenite	83.45	10.47	3.76	0.30	0.00	0.45	0.42	0.97	0.16	99.98
CH6/66	249.165	Pyroxenite	83.35	8.86	4.51	0.00	0.47	1.20	0.41	0.98	0.18	99.96
CH6/67	254.28	Pyroxenite	84.56	8.33	3.90	0.00	0.72	0.90	0.41	0.96	0.17	99.95
CH6/68	257.665	Pyroxenite	81.75	6.83	3.41	6.23	0.00	0.23	0.38	1.01	0.14	99.98
CH6/69	261.395	Pyroxenite	87.87	6.46	3.78	0.16	0.00	0.15	0.43	0.98	0.14	99.97
CH6/70	263.165	Pyroxenite	87.09	6.64	3.95	0.58	0.00	0.15	0.43	0.99	0.16	99.99
CH6/71	268.125	Pyroxenite	78.64	15.13	4.42	0.11	0.00	0.22	0.37	0.94	0.14	99.97
CH6/72	272.15	Pyroxenite	77.11	16.60	4.06	0.47	0.00	0.30	0.36	0.94	0.13	99.97
CH6/73	274.815	Pyroxenite	75.77	18.39	3.84	0.00	0.25	0.30	0.36	0.92	0.14	99.97
CH6/74	277.87	Pyroxenite	84.94	7.93	4.88	0.01	0.00	0.53	0.43	1.07	0.20	99.99
CH6/75	282.735	Pyroxenite	75.82	18.32	4.04	0.05	0.00	0.30	0.36	0.95	0.14	99.98

Table C. 4: Continued

Sample No.	Depth (m)	Lithology	Hypersthene	Plagioclase	Diopside	Olivine	Quartz	Orthoclase	Chromite	Magnetite	Ilmenite	Total
CH6/76	285.31	Pyroxenite	82.58	7.76	4.65	0.00	1.53	1.73	0.39	1.07	0.21	99.92
CH6/77	288.385	Pyroxenite	83.24	8.16	5.27	0.00	0.83	0.83	0.36	1.07	0.20	99.96
CH6/78	292.53	Melanorite	75.27	15.76	5.39	1.37	0.00	0.67	0.32	0.99	0.18	99.95
CH6/79	295.42	Pyroxenite	80.00	11.90	4.85	0.00	0.89	0.75	0.34	1.04	0.21	99.98
CH6/80	297.83	Interlayered norite	38.28	58.24	1.74	0.52	0.00	0.48	0.16	0.48	0.08	99.98
CH6/81	305.425	Pyroxenite	83.04	7.61	5.07	0.00	1.31	1.28	0.37	1.07	0.21	99.96
CH6/82	309.63	Pyroxenite	83.31	8.51	4.73	0.00	1.00	0.76	0.38	1.08	0.20	99.97
CH6/83	311.68	Pyroxenite	82.53	9.51	4.82	0.00	0.64	0.83	0.37	1.08	0.18	99.96
CH6/84	317.615	Pyroxenite	78.70	15.53	3.94	0.00	0.06	0.22	0.36	1.03	0.13	99.97
CH6/85	319.54	Pyroxenite	85.83	6.89	4.60	0.00	0.42	0.53	0.37	1.13	0.18	99.95
CH6/86	323.165	Pyroxenite	84.77	8.01	4.99	0.00	0.12	0.53	0.31	1.09	0.16	99.98
CH6/87	325.58	Pyroxenite	85.05	7.27	4.54	0.00	0.74	0.76	0.33	1.11	0.18	99.98
CH6/88	329.455	Pyroxenite	87.70	5.96	4.28	0.00	0.19	0.23	0.35	1.11	0.16	99.98
CH6/89	331.155	Pyroxenite	87.98	5.67	4.08	0.48	0.00	0.15	0.37	1.09	0.16	99.98
CH6/90	333.54	Pyroxenite	78.54	13.56	4.82	0.00	0.73	0.75	0.38	0.97	0.21	99.96
CH6/91	339.225	Pyroxenite	78.47	11.77	5.14	0.00	1.52	1.42	0.39	0.97	0.25	99.93
CH6/92	343.715	Pyroxenite	73.38	18.85	4.59	0.00	0.77	0.89	0.34	0.94	0.19	99.95
CH6/93	350.435	Pyroxenite	78.34	12.31	5.27	0.00	1.29	1.20	0.34	0.99	0.22	99.96
CH6/94	353.73	Pyroxenite	78.28	10.90	5.57	0.00	1.80	1.80	0.36	1.00	0.23	99.94
CH6/95	358.165	Pyroxenite	75.30	17.37	4.93	0.00	0.03	0.82	0.35	0.97	0.19	99.96
CH6/96	362.21	Pyroxenite	80.59	11.05	4.88	0.00	0.70	0.71	0.54	1.64	0.28	100.39
CH6/97	369.4	Pyroxenite	84.22	8.99	4.88	0.00	0.15	0.15	0.33	1.09	0.17	99.98
CH6/98	374.27	Pyroxenite	84.38	7.93	4.89	0.90	0.00	0.23	0.34	1.11	0.18	99.96
CH6/99	376.58	Pyroxenite	80.06	14.35	3.92	0.01	0.00	0.15	0.32	1.01	0.16	99.98
CH6/100	384.145	Pyroxenite	82.78	8.58	4.79	0.00	1.18	0.98	0.39	1.04	0.22	99.96

Table C. 4: Continued

Sample No.	Depth (m)	Lithology	Hypersthene	Plagioclase	Diopside	Olivine	Quartz	Orthoclase	Chromite	Magnetite	Ilmenite	Total
CH6/101	388.35	Pyroxenite	80.92	11.08	5.20	0.00	0.03	1.13	0.37	1.02	0.21	99.96
CH6/102	391.9	Pyroxenite	81.94	8.16	5.08	0.00	1.67	1.51	0.30	1.05	0.23	99.94
CH6/103	394.215	Pyroxenite	82.11	8.54	5.10	0.00	1.36	1.21	0.34	1.07	0.22	99.95
CH6/104	396.37	Pyroxenite	82.45	9.18	4.95	0.00	0.98	0.75	0.36	1.07	0.21	99.95
CH6/105	399.26	Pyroxenite	81.52	9.65	5.05	0.00	1.35	0.75	0.38	1.05	0.20	99.95
CH6/106	404.14	Pyroxenite	83.75	6.96	5.43	0.00	0.92	1.21	0.43	1.05	0.21	99.96
CH6/107	408.615	Pyroxenite	87.48	5.64	4.85	0.09	0.00	0.23	0.43	1.07	0.18	99.97
CH6/108	412.535	Pyroxenite	85.09	6.59	4.38	0.00	1.21	0.98	0.45	1.05	0.21	99.96
CH6/109	417.09	Pyroxenite	78.11	13.31	5.15	0.00	0.91	0.90	0.38	0.99	0.23	99.98
CH6/110	419.87	Pyroxenite	81.31	9.52	5.27	0.00	1.28	0.90	0.41	1.04	0.22	99.95
CH6/111	425.425	Pyroxenite	82.32	7.88	5.12	0.00	1.58	1.36	0.40	1.06	0.25	99.97
CH6/112	430.25	Pyroxenite	82.39	8.60	5.22	0.00	0.98	1.06	0.41	1.06	0.24	99.96
CH6/113	434.19	Pyroxenite	75.41	16.97	5.10	0.00	0.40	0.52	0.39	0.96	0.19	99.94
CH6/114	438.33	Pyroxenite	83.36	8.70	4.98	0.00	0.87	0.38	0.43	1.06	0.20	99.98
CH6/115	440.32	Pyroxenite	83.68	8.26	5.01	0.00	0.87	0.46	0.42	1.06	0.20	99.96
CH6/116	444.41	Pyroxenite	84.00	6.81	4.92	0.00	1.46	1.06	0.38	1.10	0.22	99.95
CH6/117	447.76	Pyroxenite	80.72	11.46	5.13	0.00	0.57	0.38	0.39	1.11	0.21	99.97
CH6/118	450.31	Pyroxenite	72.19	19.85	5.00	0.00	0.77	0.52	0.35	1.09	0.19	99.96
CH6/119	454.69	Patchy pyroxenite	42.21	52.28	3.58	0.00	0.39	0.56	0.12	0.72	0.12	99.98
CH6/120	457.63	Patchy pyroxenite	70.23	21.63	4.75	0.00	1.11	0.52	0.27	1.29	0.18	99.98
CH6/121	459.15	Patchy pyroxenite	76.59	15.29	4.99	0.00	0.85	0.38	0.29	1.39	0.20	99.98
CH6/122	462.72	Patchy pyroxenite	34.44	56.21	7.06	0.00	0.74	0.65	0.12	1.09	0.19	100.50
CH6/123	466.85	Patchy pyroxenite	55.83	36.26	5.19	0.00	0.99	0.44	0.13	1.00	0.15	99.99
CH6/124	471.15	Patchy pyroxenite	43.69	50.51	3.38	0.00	0.75	0.63	0.11	0.77	0.13	99.97
CH6/125	473.65	Patchy pyroxenite	42.19	46.15	8.57	0.00	1.30	0.70	0.11	0.81	0.16	99.99

Table C. 4: Continued

Sample No.	Depth (m)	Lithology	Hypersthene	Plagioclase	Diopside	Olivine	Quartz	Orthoclase	Chromite	Magnetite	Ilmenite	Total
CH6/126	477.49	Norite	48.08	41.47	7.55	0.00	0.99	0.64	0.13	0.96	0.16	99.98
CH6/127	480.58	Norite	50.10	39.24	7.70	0.00	1.06	0.58	0.14	1.02	0.15	99.99
CH6/128	482.88	Norite	49.51	39.20	8.44	0.00	0.94	0.58	0.14	1.03	0.15	99.99
CH6/129	487.20	Norite	36.73	52.97	8.00	0.00	0.39	0.91	0.06	0.79	0.13	99.98
CH6/130	489.50	Norite	30.93	56.05	10.93	0.00	0.47	0.70	0.06	0.73	0.12	99.99
CH6/131	492.65	Norite	32.70	50.90	14.27	0.00	0.48	0.63	0.04	0.83	0.15	100.00
CH6/132	495.30	Norite	23.96	60.99	12.75	0.00	0.68	0.83	0.03	0.59	0.14	99.97
CH6/133	500.50	Norite	29.76	55.56	11.81	0.00	1.07	0.90	0.06	0.68	0.16	100.00
CH6/134	502.86	Norite	30.06	54.34	12.61	0.00	0.99	1.04	0.06	0.69	0.17	99.96
CH6/135	507.47	Norite	29.16	55.09	12.62	0.00	1.06	1.11	0.06	0.68	0.18	99.96
CH6/136	510.22	Norite	28.60	56.02	11.90	0.00	1.24	1.31	0.05	0.65	0.18	99.95
CH6/137	513.62	Norite	27.06	56.92	12.56	0.00	1.10	1.44	0.04	0.65	0.18	99.95
CH6/138	516.77	Norite	26.62	57.18	12.25	0.00	1.58	1.44	0.05	0.64	0.19	99.95
CH6/139	520.45	Norite	23.53	58.78	13.62	0.00	1.63	1.57	0.04	0.59	0.19	99.95
CH6/140	523.59	Norite	23.51	59.99	12.59	0.00	1.55	1.50	0.04	0.59	0.18	99.95
CH6/141	526.19	Norite	25.32	59.47	11.47	0.00	1.49	1.37	0.05	0.60	0.18	99.95
CH6/142	529.56	Norite	30.34	55.33	10.45	0.00	1.51	1.38	0.07	0.69	0.18	99.95
CH6/143	533.18	Norite	31.98	54.96	8.65	0.00	1.87	1.52	0.08	0.71	0.18	99.95
CH6/144	537.48	Norite	31.73	54.29	10.40	0.00	1.26	1.31	0.08	0.73	0.17	99.97
CH6/145	539.42	Norite	31.45	54.18	11.03	0.00	1.41	0.90	0.08	0.73	0.19	99.97
CH6/146	542.67	Norite	30.61	56.26	9.63	0.00	1.35	1.18	0.07	0.70	0.17	99.97
CH6/147	547.64	Norite	40.02	49.61	6.67	0.00	1.37	1.27	0.06	0.78	0.18	99.96
CH6/148	550.62	Norite	18.13	62.10	16.61	0.00	1.10	1.35	0.03	0.50	0.15	99.97
CH6/149	552.46	Norite	26.60	57.07	13.11	0.00	1.15	1.17	0.06	0.63	0.17	99.96
CH6/150	555.49	Norite	27.13	58.30	11.61	0.00	0.94	1.16	0.07	0.62	0.15	99.98

Table C. 4: Continued

Sample No.	Depth (m)	Lithology	Hypersthene	Plagioclase	Diopside	Olivine	Quartz	Orthoclase	Chromite	Magnetite	Ilmenite	Total
CH6/151	559.16	Melanorite	27.86	56.02	13.11	0.00	0.94	1.17	0.09	0.62	0.17	99.98
CH6/152	563.35	Melanorite	35.77	53.53	7.03	0.00	1.33	1.32	0.10	0.72	0.17	99.97
CH6/153	566.60	Melanorite	42.09	46.49	7.33	0.00	1.57	1.33	0.11	0.84	0.19	99.95
CH6/154	569.42	Melanorite	44.34	44.06	7.93	0.00	1.28	1.13	0.12	0.88	0.20	99.94
CH6/155	573.65	Melanorite	44.96	43.53	7.63	0.00	1.38	1.27	0.11	0.87	0.21	99.96
CH6/156	576.13	Melanorite	47.50	40.57	7.61	0.00	1.65	1.36	0.14	0.91	0.22	99.96
CH6/157	580.63	Melanorite	47.30	40.79	7.71	0.00	1.54	1.35	0.14	0.90	0.22	99.95
CH6/158	583.59	Melanorite	48.21	39.64	6.80	0.00	2.62	1.42	0.15	0.91	0.21	99.96
CH6/159	587.45	Melanorite	48.73	40.02	6.69	0.00	1.89	1.36	0.15	0.90	0.21	99.95
CH6/160	590.36	Melanorite	46.29	42.78	6.30	0.00	1.93	1.41	0.14	0.87	0.22	99.94
CH6/161	595.16	Melanorite	49.19	38.43	7.44	0.00	1.88	1.71	0.16	0.91	0.23	99.95
CH6/162	597.86	Melanorite	51.15	38.17	6.05	0.00	1.78	1.51	0.16	0.92	0.22	99.96
CH6/163	600.34	Melanorite	51.38	37.21	6.72	0.00	1.75	1.58	0.16	0.92	0.24	99.96
CH6/164	603.16	Melanorite	53.82	34.36	6.84	0.00	2.05	1.52	0.17	0.96	0.24	99.96
CH6/165	605.63	Melanorite	45.72	42.89	6.07	0.00	2.01	2.04	0.14	0.85	0.22	99.94
CH6/166	609.58	Melanorite	52.79	35.48	6.59	0.00	1.93	1.80	0.16	0.97	0.25	99.97
CH6/167	616.31	Melanorite	56.42	32.18	6.07	0.00	2.13	1.73	0.17	1.00	0.25	99.95
CH6/168	616.76	Melanorite	54.30	34.03	6.56	0.00	2.04	1.65	0.17	0.95	0.25	99.95
CH6/169	624.65	Melanorite	58.57	29.57	7.51	0.00	1.53	1.31	0.19	1.03	0.25	99.96
CH6/170	630.48	Melanorite	58.71	29.49	7.28	0.00	1.72	1.30	0.19	1.02	0.24	99.95
CH6/171	633.41	Melanorite	58.35	30.24	7.04	0.00	1.55	1.32	0.19	1.03	0.24	99.96
CH6/172	636.36	Melanorite	60.14	28.93	6.47	0.00	1.63	1.31	0.21	1.03	0.24	99.96
CH6/173	639.57	Melanorite	62.05	25.91	7.44	0.00	1.78	1.26	0.21	1.06	0.24	99.95
CH6/174	643.44	Melanorite	61.98	26.41	6.99	0.00	1.77	1.30	0.21	1.05	0.25	99.96
CH6/175	646.71	Melanorite	62.44	26.34	7.25	0.00	1.23	1.18	0.22	1.03	0.24	99.93

Table C. 4: Continued

Sample No.	Depth (m)	Lithology	Hypersthene	Plagioclase	Diopside	Olivine	Quartz	Orthoclase	Chromite	Magnetite	Ilmenite	Total
CH6/176	649.25	Feldspathic pyroxenite	65.91	23.19	6.61	0.00	1.58	1.10	0.24	1.07	0.26	99.96
CH6/177	652.59	Feldspathic pyroxenite	67.38	19.60	7.51	0.00	2.22	1.63	0.23	1.11	0.28	99.96
CH6/178	662.51	Feldspathic pyroxenite	66.40	20.27	7.00	0.00	2.80	1.85	0.23	1.10	0.28	99.93
CH6/179	667.48	Feldspathic pyroxenite	64.97	22.56	7.07	0.00	2.24	1.55	0.22	1.07	0.27	99.95
CH6/180	672.53	Feldspathic pyroxenite	65.75	22.42	7.02	0.00	1.95	1.26	0.23	1.08	0.26	99.97
CH6/181	677.75	Feldspathic pyroxenite	66.79	20.76	7.45	0.00	1.71	1.63	0.23	1.11	0.27	99.95
CH6/182	679.42	Feldspathic pyroxenite	52.28	37.13	6.90	0.00	1.03	1.29	0.20	0.90	0.22	99.95
CH6/183	683.39	Feldspathic pyroxenite	64.67	23.28	7.52	0.00	1.40	1.54	0.23	1.05	0.27	99.96
CH6/184	686.16	Feldspathic pyroxenite	66.71	22.03	6.35	0.00	1.89	1.39	0.24	1.06	0.27	99.94
CH6/185	688.31	Feldspathic pyroxenite	65.28	22.43	7.16	0.00	1.98	1.53	0.24	1.04	0.27	99.93

Table C.5: Orthopyroxene Geochemistry (Major Elements) in wt. %

Sample No.	Depth (m)	Na_2O	MgO	Al_2O_3	SiO_2	K_2O	CaO	TiO_2	Cr_2O_3	MnO	FeO	NiO	Total	Mg#
CH6/2	31.93	0.00	30.57	0.78	56.10	b.d	0.77	0.09	0.25	0.25	10.78	0.08	99.69	83
CH6/3	42.60	0.06	31.39	1.70	55.46	0.01	1.25	0.09	0.47	0.19	8.20	0.08	98.90	87
CH6/7	55.18	0.02	29.91	1.01	55.97	b.d	0.96	0.09	0.30	0.26	11.61	0.08	100.21	82
CH6/14	78.71	0.03	31.40	1.52	55.61	b.d	1.06	0.12	0.46	0.21	9.06	0.07	99.53	86
CH6/22	103.86	0.03	31.10	1.10	56.07	b.d	1.40	0.11	0.49	0.20	9.81	0.09	100.40	85
CH6/25	115.15	0.02	31.44	1.24	56.29	b.d	1.30	0.09	0.49	0.20	9.42	0.10	100.59	86
CH6/28	124.78	0.01	30.26	1.36	55.40	0.01	1.38	0.09	0.47	0.22	9.64	0.08	100.11	85
CH6/32	139.86	0.03	29.52	1.25	55.12	b.d	1.63	0.08	0.46	0.24	11.38	0.09	99.81	82
CH6/34	145.43	0.02	29.70	1.35	55.18	0.01	1.41	0.09	0.41	0.24	10.20	0.08	99.96	84
CH6/36	153.67	0.02	31.65	1.14	56.52	b.d	0.83	0.08	0.45	0.19	9.05	0.07	100.00	86
CH6/40	164.18	0.01	30.60	0.95	56.19	b.d	1.40	0.09	0.22	0.27	10.88	0.07	100.68	83
CH6/44	176.09	0.02	30.64	0.92	56.08	0.01	1.20	0.09	0.24	0.25	10.39	0.09	99.93	84
CH6/45	179.66	0.01	30.63	1.10	55.84	0.01	1.02	0.10	0.31	0.25	10.34	0.08	99.69	84
CH6/46	182.54	0.02	30.95	1.68	55.12	0.01	1.26	0.10	0.40	0.22	9.07	0.11	100.06	86
CH6/47	186.26	0.02	30.49	1.27	55.99	b.d	1.13	0.11	0.47	0.22	10.85	0.09	100.62	83
CH6/50	194.86	0.03	30.93	1.25	55.60	b.d	1.14	0.12	0.45	0.21	8.96	0.09	98.79	86
CH6/56	218.62	0.02	31.21	1.08	56.10	0.01	1.11	0.09	0.48	0.22	9.95	0.08	100.35	85
CH6/62	235.85	0.02	31.16	1.12	56.02	b.d	0.78	0.11	0.47	0.21	10.16	0.09	100.16	85
CH6/67	254.28	0.04	30.60	1.15	55.73	b.d	1.59	0.12	0.50	0.22	9.92	0.09	99.94	85
CH6/71	268.13	0.02	30.31	1.07	55.23	b.d	1.16	0.11	0.41	0.22	10.87	0.09	99.49	83
CH6/78	292.53	0.04	30.37	1.00	55.66	b.d	0.99	0.14	0.38	0.24	11.08	0.10	100.00	83
CH6/80	297.83	0.01	30.67	1.35	55.64	0.01	1.05	0.13	0.40	0.21	9.51	0.12	100.29	85
CH6/85	319.54	0.03	30.04	1.14	55.25	0.01	1.14	0.13	0.39	0.24	10.22	0.08	98.69	84
CH6/93	350.44	0.03	30.25	1.06	55.56	0.01	1.14	0.16	0.37	0.23	9.95	0.09	98.86	84
CH6/101	388.35	0.02	29.71	0.99	56.22	b.d	1.21	0.14	0.40	0.22	10.99	0.09	100.00	83

Table C.5: Continued

Sample No.	Depth (m)	Na_2O	MgO	Al_2O_3	SiO_2	K_2O	CaO	TiO_2	Cr_2O_3	MnO	FeO	NiO	Total	Mg#
CH6/106	404.14	0.04	30.20	1.15	55.42	0.01	1.18	0.14	0.43	0.23	9.83	0.09	98.74	85
CH6/112	430.25	0.12	29.03	0.85	55.28	b.d	2.12	0.17	0.49	0.23	11.04	0.09	99.44	82
CH6/113	434.19	0.03	29.87	0.91	55.24	b.d	1.29	0.13	0.49	0.23	11.17	0.10	99.45	83
CH6/116	444.41	b.d	29.76	1.16	55.29	0.03	0.23	0.16	0.41	0.23	10.26	0.10	99.91	84
CH6/118	450.31	0.03	28.72	1.19	54.67	0.01	1.17	0.15	0.42	0.25	11.75	0.09	98.46	81
CH6/119	454.69	0.02	28.11	0.61	55.20	b.d	1.39	0.16	0.25	0.30	15.05	0.07	101.16	77
CH6/122	462.72	0.02	27.26	0.50	54.50	0.01	0.99	0.16	0.19	0.32	16.31	0.07	100.33	75
CH6/124	471.15	b.d	27.54	1.06	54.68	0.01	0.87	0.16	0.22	0.30	13.51	0.07	98.41	78
CH6/126	477.49	b.d	26.41	1.09	54.21	0.01	1.26	0.16	0.23	0.31	14.66	0.07	98.43	76
CH6/128	482.88	b.d	25.82	1.12	53.97	0.01	1.30	0.16	0.23	0.32	15.26	0.07	100.26	75
CH6/131	492.65	0.03	24.57	0.81	54.14	b.d	1.36	0.15	0.06	0.42	18.68	0.05	100.27	70
CH6/133	500.50	0.02	25.78	0.91	53.69	0.02	1.39	0.18	0.13	0.34	15.33	0.07	99.72	75
CH6/139	520.45	0.09	25.20	0.73	54.66	0.01	1.36	0.19	0.08	0.35	18.17	0.05	100.88	71
CH6/142	529.56	b.d	25.71	0.88	54.06	0.02	1.18	0.22	0.14	0.33	15.72	0.06	100.28	74
CH6/146	542.67	0.08	24.86	0.82	54.22	b.d	1.56	0.17	0.15	0.33	18.03	0.06	100.27	71
CH6/148	550.62	0.02	25.57	0.78	54.08	0.02	1.31	0.20	0.08	0.35	15.98	0.06	100.39	74
CH6/150	555.49	0.01	26.35	0.71	55.01	b.d	0.84	0.18	0.16	0.34	17.39	0.07	101.02	73
CH6/155	573.65	0.02	26.81	0.80	54.87	b.d	0.97	0.19	0.21	0.31	16.15	0.06	100.39	75
CH6/161	595.16	0.02	27.40	0.81	54.82	b.d	0.85	0.20	0.25	0.29	15.81	0.07	100.53	76
CH6/165	605.63	0.02	27.48	0.82	55.23	0.01	0.82	0.19	0.26	0.29	15.53	0.07	100.72	76
CH6/178	662.51	b.d	28.30	0.92	55.12	0.04	0.95	0.19	0.26	0.26	12.56	0.07	100.24	80
CH6/180	672.53	0.09	28.40	0.76	55.21	b.d	0.72	0.15	0.24	0.27	14.22	0.07	100.13	78
CH6/183	683.39	b.d	28.37	0.96	54.84	0.02	1.01	0.20	0.29	0.27	12.37	0.07	98.41	80

Table C6: Orthopyroxene trace elements geochemistry in ppm (combined LA-ICP-MS and ICP-MS).

Sample	CH6 38.23 OPX	CH6 38.84 OPX	CH6 3 OPX	CH6 4	CH6 7	CH6 14	CH6 22	CH6 26	CH6 28 OPX
Depth	38.23	38.84	42.60	46.23	55.18	78.71	103.86	118.41	124.78
Li	2.654	1.693	0.851	2.471	2.007	1.548	2.905	2.506	0.955
P	16.321	6.495	3.885						0.078
Sc	30.136	21.627	20.934	25.419	26.646	26.248	23.703	28.656	26.615
Ti	460.158	403.042	455.752	505.367	525.203	628.018	590.162	588.432	483.484
V	59.035	53.257	49.450	70.277	68.418	72.486	76.839	80.623	77.145
Cr	3407.223	2424.018	3300.667	3219.423	3338.296	3471.778	3331.476	3173.902	3788.017
Co	81.486	75.143	86.597	98.111	98.755	86.305	102.003	99.183	106.993
Ni	509.940	439.500	624.807	709.968	715.979	592.311	679.663	690.683	704.530
Cu	4.374	0.778	1.817						4.283
Zn	183.156	95.942	50.847						80.123
Ga	2.223	2.084	1.817	2.974	3.033	3.508	3.449	3.348	2.376
As	0.058	0.064	0.212						0.142
Rb	0.096	0.139	0.112	0.003	0.003	0.002	0.001	0.004	0.140
Sr	1.240	1.004	1.042	0.285	0.307	0.348	0.227	0.216	0.587
Y	1.608	1.269	1.033	2.076	1.904	3.111	1.909	2.181	0.930
Zr	1.792	1.763	1.349	5.840	3.562	11.236	3.507	6.033	1.351
Nb	0.028	0.036	0.030	0.219	0.090	0.050	0.059	0.106	0.058
Ba	1.544	1.013	0.848	0.013	0.019	0.012	0.033	0.015	0.685
Sn	0.062	0.100	0.099						0.087
Cs	0.004	0.009	0.011	0.001	0.001	0.001	0.001	0.001	0.006
La	0.137	0.083	0.071	0.259	0.205	0.300	0.149	0.251	0.116
Ce	0.203	0.160	0.119	0.913	0.692	1.196	0.489	0.849	0.139
Pr	0.024	0.022	0.016	0.131	0.089	0.184	0.074	0.120	0.018
Nd	0.160	0.134	0.098	0.624	0.431	0.920	0.377	0.570	0.101
Sm	0.056	0.058	0.037	0.170	0.136	0.256	0.116	0.161	0.034
Eu	0.013	0.016	0.011	0.037	0.032	0.052	0.028	0.030	0.007
Gd	0.089	0.080	0.058	0.195	0.157	0.309	0.142	0.196	0.051
Tb	0.019	0.018	0.013	0.036	0.029	0.054	0.029	0.037	0.010
Dy	0.179	0.155	0.117	0.269	0.242	0.388	0.228	0.256	0.101
Ho	0.046	0.041	0.029	0.061	0.057	0.088	0.055	0.064	0.026
Er	0.167	0.138	0.109	0.195	0.186	0.284	0.195	0.210	0.098
Tm	0.029	0.026	0.019	0.031	0.030	0.045	0.035	0.036	0.017
Yb	0.245	0.201	0.162	0.251	0.243	0.350	0.282	0.304	0.158
Lu	0.038	0.036	0.025	0.041	0.041	0.053	0.048	0.048	0.025
Hf	0.064	0.061	0.046	0.112	0.072	0.186	0.155	0.137	0.048
Ta	b.d	b.d	b.d	0.008	0.002	0.004	0.003	0.003	0.004
W	b.d	b.d	0.020						0.014
Pb	0.392	0.218	1.956	0.125	0.064	0.127	0.102	0.061	0.658
Th	0.030	0.023	0.019	0.368	0.124	0.357	0.249	0.399	0.027
U	0.009	0.008	0.006	0.085	0.041	0.076	0.059	0.035	0.010

Table C6: Continued

Sample	CH6 32	CH6 34 OPX	CH6 41	CH6 43 OPX	CH6 177.01	CH6 46 OPX	CH6 48 OPX	CH6 50 OPX	CH6 51
Depth	**139.86**	**145.43**	**167.51**	**172.57**	**177.01**	**182.54**	**189.16**	**194.86**	**198.51**
Li	1.300	0.694	0.638	1.257	1.684	0.322	3.492	1.045	2.339
P		6.571		14.526		10.184	4.101	4.863	
Sc	33.943	34.146	33.863	42.303	51.195	30.847	40.134	26.051	25.638
Ti	468.389	552.942	514.183	518.418	683.035	630.285	850.143	676.690	674.329
V	93.714	96.996	89.706	86.417	133.539	79.311	95.829	68.751	76.879
Cr	2996.884	3522.769	1200.011	1429.194	2103.114	3385.682	3038.967	3257.483	2925.181
Co	107.666	126.722	118.625	107.798	91.621	107.534	99.778	93.888	98.211
Ni	658.713	714.468	706.673	544.410	590.653	965.811	690.686	679.452	684.734
Cu		3.558		8.934		8.630	8.087	2.992	
Zn		83.477		240.283		66.202	89.984	62.341	
Ga	3.141	2.470	2.709	2.125	3.016	2.653	3.138	2.167	3.311
As		0.141		0.062		0.194	0.325	0.195	
Rb	0.105	0.306	0.001	0.061	0.035	0.240	0.399	0.369	0.043
Sr	0.929	0.592	0.187	1.151	5.170	1.286	0.882	0.544	0.471
Y	1.463	0.894	0.979	1.170	3.738	0.947	3.609	1.657	2.402
Zr	2.279	2.007	0.739	0.928	3.797	2.058	3.624	3.417	3.638
Nb	0.054	0.075	0.025	0.028	0.073	0.062	0.050	0.094	0.059
Ba	0.042	1.166	0.007	1.152	0.164	0.624	1.559	0.929	0.252
Sn		0.330		0.088		0.085	0.148	0.126	
Cs	0.017	0.031	0.001	0.003	0.001	0.018	0.048	0.047	0.008
La	0.087	0.136	0.017	0.142	0.224	0.128	0.223	0.302	0.189
Ce	0.384	0.217	0.051	0.090	1.040	0.109	0.519	0.407	0.670
Pr	0.051	0.027	0.008	0.010	0.193	0.018	0.079	0.057	0.085
Nd	0.247	0.140	0.059	0.085	1.146	0.107	0.386	0.259	0.423
Sm	0.087	0.042	0.029	0.027	0.389	0.037	0.132	0.077	0.134
Eu	0.027	0.008	0.007	0.003	0.091	0.008	0.027	0.015	0.032
Gd	0.114	0.060	0.049	0.048	0.469	0.052	0.190	0.111	0.181
Tb	0.022	0.011	0.011	0.010	0.079	0.011	0.046	0.022	0.034
Dy	0.174	0.109	0.099	0.123	0.549	0.112	0.391	0.194	0.286
Ho	0.044	0.026	0.029	0.032	0.114	0.029	0.106	0.048	0.070
Er	0.142	0.096	0.103	0.132	0.346	0.105	0.385	0.166	0.235
Tm	0.026	0.015	0.019	0.023	0.048	0.019	0.076	0.030	0.039
Yb	0.215	0.142	0.167	0.208	0.361	0.166	0.597	0.238	0.323
Lu	0.036	0.023	0.029	0.032	0.053	0.028	0.100	0.038	0.051
Hf	0.071	0.116	0.030	0.040	0.116	0.074	0.123	0.103	0.096
Ta	0.002	0.006	0.002	b.d	0.006	0.004	0.001	0.002	0.005
W		0.013		b.d		0.019	0.019	0.026	
Pb	0.024	0.468	0.056	0.657	0.049	0.296	0.067	0.197	0.247
Th	0.018	0.049	0.024	0.032	0.076	0.047	0.152	0.128	0.155
U	0.010	0.016	0.007	0.009	0.024	0.013	0.019	0.291	0.035

Table C6: Continued

Sample	CH6 60	CH6 67	CH6 74	CH6 78 OPX	CH6 80 OPX	CH6 85 OPX	CH6 93 OPX	CH6 106 OPX	CH6 410.13
Depth	**227.505**	**254.28**	**277.87**		**297.83**	**319.54**	**350.435**	**404.14**	**410.13**
Li	2.198	3.203	2.781	4.075	1.224	0.837	1.237	2.318	2.702
P				15.675	9.693	6.686	4.772	4.312	
Sc	24.813	28.234	31.458	42.031	24.709	31.904	29.657	32.228	26.008
Ti	734.042	463.743	754.686	729.716	666.649	733.839	934.865	833.970	894.656
V	78.470	79.801	95.444	121.975	101.202	97.051	86.880	85.150	98.584
Cr	3239.335	3365.498	3205.298	2654.119	3052.978	2836.983	2759.112	3157.625	3066.524
Co	96.125	98.719	98.665	99.715	105.813	101.904	99.131	96.805	105.780
Ni	667.214	687.729	627.831	558.753	982.118	635.836	655.258	709.395	768.341
Cu				4.692	2.571	1.710	2.552	1.919	
Zn				265.598	70.768	78.607	74.515	84.066	
Ga	3.202	3.309	3.489	2.609	2.618	2.244	2.527	2.758	3.843
As				0.059	0.156	0.182	0.180	0.292	
Rb	0.015	0.009	0.008	0.248	0.144	0.296	0.453	0.715	0.004
Sr	0.411	0.314	0.303	0.517	2.432	0.481	0.554	0.595	0.292
Y	2.362	2.987	3.183	3.081	1.311	1.665	2.603	3.072	2.670
Zr	3.849	3.093	6.642	5.240	2.025	3.586	3.235	3.710	3.178
Nb	0.085	0.066	0.071	0.097	0.054	0.085	0.068	0.091	0.043
Ba	0.214	0.061	0.019	1.861	0.570	0.632	0.942	1.295	0.066
Sn				0.145	0.093	0.192	0.199	0.213	
Cs	0.009	0.002	0.001	0.033	0.005	0.046	0.068	0.090	0.001
La	0.181	0.289	0.263	0.459	0.052	0.223	0.292	0.530	0.123
Ce	0.582	0.957	1.055	1.118	0.080	0.521	0.681	1.124	0.473
Pr	0.079	0.142	0.147	0.163	0.015	0.072	0.104	0.162	0.070
Nd	0.381	0.663	0.653	0.765	0.100	0.317	0.473	0.713	0.363
Sm	0.129	0.211	0.210	0.195	0.038	0.083	0.142	0.185	0.124
Eu	0.024	0.041	0.043	0.025	0.006	0.015	0.022	0.030	0.029
Gd	0.162	0.242	0.255	0.245	0.064	0.114	0.182	0.226	0.170
Tb	0.035	0.045	0.049	0.044	0.014	0.023	0.037	0.045	0.037
Dy	0.272	0.371	0.388	0.382	0.143	0.198	0.316	0.359	0.281
Ho	0.068	0.086	0.092	0.094	0.037	0.048	0.078	0.089	0.075
Er	0.240	0.284	0.304	0.326	0.140	0.164	0.255	0.301	0.277
Tm	0.040	0.045	0.050	0.054	0.024	0.032	0.048	0.057	0.049
Yb	0.325	0.368	0.390	0.447	0.220	0.244	0.363	0.436	0.412
Lu	0.050	0.059	0.062	0.070	0.035	0.042	0.061	0.071	0.071
Hf	0.115	0.056	0.154	0.174	0.069	0.119	0.128	0.139	0.091
Ta	0.002	0.003	0.008	b.d	0.002	0.001	b.d	0.001	0.001
W				0.001	0.007	0.039	0.035	0.035	
Pb	0.209	0.316	0.168	0.512	0.292	0.109	1.868	0.521	0.032
Th	0.256	0.109	0.284	0.352	0.040	0.162	0.193	0.396	0.091
U	0.041	0.030	0.046	0.067	0.013	0.044	0.033	0.070	0.013

Table C6: Continued

Sample	CH6 113	CH6 116 OPX	CH6 121	CH6 124 OPX	CH6 126 OPX	CH6 128 OPX	CH6 131	CH6 133 OPX
Depth	434.19	444.41	459.15	471.15	477.49	482.88	492.65	500.50
Li	3.800	2.528	3.334	3.895	3.876	3.670	1.772	4.574
P		-0.070		3.868	6.420	1.993		16.106
Sc	32.563	32.142	37.712	44.276	55.987	53.192	42.736	33.621
Ti	711.694	957.686	720.561	891.108	913.221	947.143	778.621	1087.262
V	108.041	102.522	126.999	111.111	133.493	153.472	128.831	173.525
Cr	3474.021	3321.622	2342.815	1683.844	1682.187	1868.168	284.601	1923.568
Co	100.571	110.546	120.511	123.371	116.038	142.060	145.125	107.736
Ni	772.058	803.189	536.149	539.452	553.571	600.824	381.582	513.127
Cu		4.641		1.580	8.056	7.990		4.321
Zn		87.218		106.135	112.507	137.023		40.357
Ga	4.603	3.120	3.404	2.987	2.825	3.133	3.098	3.134
As		0.246		0.256	0.283	0.291		0.155
Rb	0.006	0.644	0.089	0.504	0.636	0.437	0.018	0.613
Sr	8.708	0.691	0.656	2.016	2.332	1.781	0.330	0.742
Y	3.817	2.995	2.696	2.724	3.421	2.481	2.078	4.308
Zr	4.593	4.863	2.246	1.941	2.686	1.864	0.931	4.262
Nb	0.078	0.111	0.063	0.028	0.068	0.056	0.016	0.026
Ba	2.684	2.289	0.399	1.362	1.674	1.541	0.048	2.585
Sn		0.149		0.153	0.147	0.094		0.643
Cs	0.001	0.056	0.008	0.059	0.043	0.030	0.001	0.126
La	0.266	0.339	0.047	0.155	0.124	0.081	0.015	0.234
Ce	1.184	0.738	0.186	0.261	0.262	0.156	0.059	0.445
Pr	0.165	0.115	0.034	0.030	0.043	0.025	0.012	0.067
Nd	0.762	0.543	0.173	0.151	0.229	0.143	0.080	0.372
Sm	0.235	0.154	0.074	0.051	0.087	0.060	0.046	0.135
Eu	0.061	0.026	0.022	0.015	0.025	0.017	0.013	0.021
Gd	0.300	0.209	0.135	0.094	0.149	0.106	0.091	0.212
Tb	0.062	0.044	0.032	0.025	0.037	0.025	0.022	0.048
Dy	0.462	0.362	0.280	0.258	0.352	0.263	0.206	0.486
Ho	0.108	0.088	0.077	0.076	0.100	0.074	0.056	0.134
Er	0.361	0.294	0.297	0.304	0.369	0.269	0.224	0.459
Tm	0.060	0.051	0.055	0.065	0.076	0.057	0.042	0.092
Yb	0.488	0.402	0.474	0.532	0.606	0.457	0.367	0.733
Lu	0.081	0.066	0.078	0.098	0.108	0.080	0.065	0.125
Hf	0.100	0.169	0.067	0.071	0.099	0.076	0.037	0.191
Ta	0.005	0.014	0.003	b.d	b.d	0.004	0.002	b.d
W		0.033		0.022	0.021	0.013		0.009
Pb	0.138	0.604	0.113	0.923	0.350	0.421	0.020	2.048
Th	0.297	0.246	0.047	0.073	0.098	0.043	0.023	0.101
U	0.057	0.036	0.013	0.011	0.020	0.013	0.005	0.005

Table C6: Continued

Sample	CH6 138 OPX	CH6 142 OPX	CH6 148 OPX	CH6 155	CH6 174	CH6 178 OPX	CH6 180	CH6 183 OPX
Depth	516.77	529.56	550.62	573.65	643.44	662.51	672.53	683.39
Li	4.475	3.105	2.168	3.000	4.048	4.287	4.785	3.727
P	21.277	-1.443	4.799			3.881		5.546
Sc	49.858	38.539	42.677	35.439	32.589	33.541	34.852	39.914
Ti	1353.524	1078.615	1001.678	1075.407	1203.827	1041.968	1021.307	1119.592
V	181.245	156.239	208.595	191.276	168.310	149.221	174.701	163.427
Cr	774.569	957.970	504.797	1488.107	1858.992	1964.492	1991.820	2100.711
Co	131.071	120.209	126.162	116.148	110.627	110.437	107.626	110.142
Ni	425.524	430.734	426.511	483.835	547.309	512.025	549.135	547.446
Cu	30.250	19.360	1.858			5.087		4.274
Zn	152.795	114.034	130.589			108.721		88.055
Ga	2.928	2.823	2.478	3.343	3.624	3.200	3.686	3.115
As	0.109	0.257	0.165			0.201		0.261
Rb	0.543	0.444	0.289	0.008	0.028	1.149	0.042	0.788
Sr	0.923	0.902	0.739	0.651	0.244	1.218	1.777	0.821
Y	3.846	3.244	3.144	4.489	4.388	4.671	5.282	4.559
Zr	5.178	4.020	2.179	6.033	4.392	3.637	5.618	3.370
Nb	0.660	0.078	0.049	0.017	0.022	0.194	0.030	0.042
Ba	2.210	1.759	1.077	0.085	0.018	3.807	0.104	3.050
Sn	0.180	0.100	0.107			0.175		0.206
Cs	0.107	0.110	0.010	0.002	0.007	0.129	0.021	0.090
La	0.239	0.156	0.162	0.092	0.029	1.140	0.241	0.263
Ce	0.379	0.327	0.290	0.378	0.159	1.605	1.125	0.563
Pr	0.054	0.052	0.046	0.069	0.034	0.175	0.211	0.087
Nd	0.272	0.270	0.239	0.387	0.237	0.704	1.115	0.432
Sm	0.105	0.097	0.097	0.161	0.107	0.201	0.379	0.165
Eu	0.020	0.020	0.021	0.031	0.022	0.029	0.055	0.026
Gd	0.161	0.155	0.151	0.259	0.197	0.290	0.451	0.241
Tb	0.039	0.038	0.037	0.056	0.047	0.064	0.081	0.057
Dy	0.401	0.349	0.341	0.488	0.440	0.546	0.649	0.494
Ho	0.107	0.099	0.095	0.127	0.118	0.142	0.153	0.128
Er	0.433	0.382	0.362	0.451	0.446	0.496	0.512	0.450
Tm	0.085	0.079	0.076	0.081	0.080	0.093	0.085	0.089
Yb	0.726	0.629	0.600	0.692	0.650	0.702	0.678	0.687
Lu	0.127	0.110	0.106	0.107	0.104	0.119	0.102	0.118
Hf	0.197	0.169	0.090	0.180	0.166	0.150	0.155	0.145
Ta	0.030	0.005	0.002	0.001	0.001	0.016	0.002	b.d
W	0.046	0.020	0.007			0.030		0.043
Pb	1.197	0.499	0.408	0.068	0.018	0.799	0.054	1.150
Th	0.231	0.134	0.074	0.134	0.087	0.467	0.195	0.164
U	0.052	0.014	0.012	0.004	0.001	0.146	0.012	0.005

Table C.7: Plagioclase Major elements geochemistry in the CH6 section in wt. % (XRF data).

Sample No.	Depth (m)	Na_2O	MgO	Al_2O_3	SiO_2	K_2O	CaO	TiO_2	Cr_2O_3	MnO	FeO	NiO	Total	An
CH6/2	31.93	1.94	0.02	32.64	48.05	0.08	16.96	0.01	0.02	b.d	0.27	0.01	100.00	83
CH6 76.87	76.87	4.38	1.33	29.71	51.87	0.15	11.89	0.04	b.d	0.02	0.38	b.d	99.85	60
CH6/22	103.86	4.48	0.01	28.04	54.91	0.24	11.07	0.02	0.01	0.01	0.28	b.d	99.06	58
CH6/25	115.15	4.00	0.02	29.72	52.09	0.20	13.76	0.01	b.d	0.01	0.19	b.d	100.00	66
CH6/28	124.78	2.52	0.38	32.21	48.74	0.21	15.28	0.02	b.d	0.01	0.22	b.d	99.64	77
CH6/32	139.86	2.56	0.01	32.07	48.61	0.13	16.32	0.01	0.01	0.01	0.27	b.d	100.00	78
CH6/34	145.43	3.34	0.56	31.54	50.01	0.18	14.03	0.01	b.d	b.d	0.26	b.d	99.98	70
CH6/40	164.18	2.09	0.02	32.41	47.61	0.12	16.89	0.01	0.01	b.d	0.22	b.d	99.38	82
CH6/44	176.09	2.03	0.03	32.91	47.21	0.10	17.06	0.01	b.d	0.01	0.27	b.d	99.62	82
CH6/45	179.66	1.70	4.44	28.31	48.37	0.11	14.78	0.02	0.05	0.04	1.71	0.01	99.54	83
CH6/46	182.54	1.68	0.37	34.16	47.28	0.09	16.94	0.02	0.01	0.01	0.26	b.d	100.87	85
CH6/47	186.26	4.49	0.02	29.11	52.82	0.23	12.63	0.02	0.01	b.d	0.26	b.d	99.58	61
CH6/56	218.62	4.07	0.02	29.46	51.81	0.24	13.37	0.03	0.02	b.d	0.16	0.01	99.15	65
CH6/62	235.85	4.01	0.02	29.74	52.13	0.23	13.66	0.01	0.01	0.01	0.16	b.d	100.00	65
CH6/67	254.28	4.58	0.01	29.24	52.99	0.24	12.75	0.03	0.02	0.01	0.12	0.01	100.00	61
CH6/71	268.13	3.09	0.01	31.00	50.18	0.17	15.31	0.02	b.d	0.01	0.22	b.d	100.00	73
CH6 291	291.00	1.94	0.13	33.58	47.46	0.09	16.67	0.02	b.d	b.d	0.18	b.d	100.10	83
CH6/78	292.53	2.01	0.03	32.65	47.58	0.12	17.40	0.01	b.d	b.d	0.21	b.d	100.00	83
CH6/80	297.83	2.01	0.15	33.82	47.19	0.12	16.51	0.02	b.d	b.d	0.15	b.d	100.01	82
CH6/101	388.35	5.01	0.01	28.34	54.64	0.32	11.48	0.03	0.01	b.d	0.14	b.d	100.00	56
CH6/112	430.25	5.20	0.01	27.92	54.56	0.30	11.10	0.02	0.01	0.01	0.19	b.d	99.33	54
CH6/113	434.19	2.62	0.01	31.59	49.66	0.17	15.73	0.02	0.01	b.d	0.19	b.d	100.00	77
CH6/116	444.41	3.09	0.27	21.87	64.58	1.72	8.17	0.05	0.01	b.d	0.24	b.d	100.04	59
CH6/118	450.31	3.19	0.19	30.94	51.19	0.30	13.95	0.02	b.d	0.01	0.21	b.d	100.06	71
CH6/119	454.69	2.74	0.06	31.11	49.86	0.23	15.48	0.02	b.d	0.01	0.48	b.d	100.00	76

Table C.7: Continued

Sample No.	Depth (m)	Na_2O	MgO	Al_2O_3	SiO_2	K_2O	CaO	TiO_2	Cr_2O_3	MnO	FeO	NiO	Total	An
CH6/122	462.72	2.72	0.03	30.65	50.75	0.22	15.29	0.01	0.01	0.01	0.31	b.d	100.00	76
CH6/126	477.49	2.97	0.20	31.34	50.35	0.22	14.53	0.03	b.d	b.d	0.35	b.d	100.04	73
CH6/128	482.88	2.97	0.18	30.92	50.39	0.21	14.28	0.03	b.d	b.d	0.35	b.d	99.39	73
CH6/131	492.65	3.45	0.02	30.54	50.65	0.17	14.63	0.02	0.01	0.01	0.40	0.01	99.90	70
CH6/133	500.50	3.88	0.23	28.99	54.11	0.47	12.19	0.04	b.d	b.d	0.35	b.d	100.04	63
CH6/139	520.45	3.90	0.01	29.91	51.71	0.25	13.84	0.04	0.01	b.d	0.34	0.01	100.00	66
CH6/142	529.56	3.78	0.14	30.11	52.17	0.36	12.92	0.04	b.d	b.d	0.24	b.d	99.81	65
CH6/146	542.67	4.13	0.02	29.56	52.61	0.30	13.10	0.03	0.01	0.01	0.28	b.d	100.02	64
CH6/150	555.49	3.74	0.02	30.00	52.28	0.29	13.53	0.02	b.d	b.d	0.23	b.d	100.12	67
CH6/155	573.65	3.58	0.02	30.41	51.57	0.23	14.19	0.01	0.01	b.d	0.25	0.01	100.28	69
CH6/165	605.63	3.84	0.03	30.31	51.66	0.21	13.80	0.02	b.d	0.01	0.22	b.d	100.09	66
CH6/173	639.57	3.87	0.33	29.06	53.65	0.43	12.18	0.04	0.01	b.d	0.28	0.01	99.91	63
CH6/178	662.51	3.94	0.28	26.24	57.95	0.68	10.36	0.05	b.d	0.01	0.32	b.d	99.89	59
CH6/180	672.53	3.80	0.01	30.22	51.13	0.20	13.95	0.04	b.d	b.d	0.17	b.d	99.52	67
CH6/183	683.39	4.11	0.17	27.91	55.75	0.61	11.28	0.04	b.d	0.01	0.19	b.d	100.12	60

Table C.8: Trace Elements in Plagioclase at the CH6 section in ppm (combined LA-ICP-MS and ICP-MS).

Sample	CH6 38.23	CH6 38.84 OPX	CH6 3	CH6 4	CH6 7	CH6 14	CH6 22	CH6 26	CH6 32
Depth	**38.23**	**38.84**	**42.6**	**46.23**	**55.18**	**78.705**	**103.855**	**118.405**	**139.855**
Li	21.292	60.920	15.570	2.085	2.010	b.d	1.465	3.133	2.450
P									
Sc	1.904	1.527	2.385	1.113	1.062	1.031	1.036	1.836	0.897
Ti	179.430	107.704	85.840	111.675	79.505	213.360	103.493	135.070	56.683
V	1.434	0.418	2.654	0.458	0.351	0.460	0.364	2.973	0.542
Cr	35.764	3.932	88.780	3.305	4.530	3.727	4.223	105.113	2.773
Co	1.524	0.447	5.569	1.300	0.163	0.049	0.085	4.115	0.101
Ni	10.535	1.546	45.490	10.162	0.238	0.229	0.328	27.777	0.242
Cu									
Zn									
Ga	194.332	97.420	40.605	45.035	33.605	62.083	45.530	41.080	49.933
As									
Rb	1.567	0.848	0.461	8.303	0.185	0.032	0.275	0.404	0.099
Sr	386.046	1261.628	541.760	354.385	410.770	534.270	331.590	338.047	386.720
Y	0.249	0.092	0.114	0.134	0.133	0.208	0.124	0.174	0.081
Zr	0.372	0.100	0.060	0.065	0.018	0.037	0.012	0.125	0.007
Nb	0.101	0.011	0.008	0.018	0.001	0.001	0.004	0.008	0.001
Ba	782.102	386.570	148.455	145.280	94.425	214.247	137.347	113.523	149.953
Sn									
Cs	0.573	0.075	0.070	0.364	0.004	0.003	0.006	0.011	0.003
La	13.284	12.996	6.575	17.765	14.295	30.997	11.173	13.780	3.017
Ce	13.744	10.328	3.680	20.185	16.105	41.230	12.593	16.220	3.523
Pr	0.938	0.526	0.185	1.275	1.027	2.930	0.798	1.039	0.246
Nd	2.445	1.167	0.451	3.010	2.390	7.050	1.870	2.497	0.920
Sm	0.207	0.080	0.048	0.221	0.166	0.428	0.144	0.178	0.077
Eu	0.410	0.362	0.330	0.686	0.647	0.811	0.379	0.619	0.304
Gd	0.131	0.069	0.040	0.126	0.109	0.258	0.083	0.116	0.064
Tb	0.013	0.005	0.005	0.009	0.007	0.013	0.007	0.010	0.005
Dy	0.043	0.027	0.022	0.042	0.043	0.057	0.034	0.051	0.016
Ho	0.011	0.003	0.004	0.005	0.004	0.007	0.005	0.007	0.002
Er	0.016	0.007	0.008	0.007	0.007	0.016	0.009	0.014	0.008
Tm	0.002	b.d	0.004	0.002	0.001	0.001	0.002	0.003	0.001
Yb	0.016	0.008	0.009	0.005	0.004	0.007	0.009	0.030	0.006
Lu	0.002	0.001	0.003	0.001	b.d	0.001	0.001	0.003	b.d
Hf	0.029	0.009	0.006	0.003	0.003	0.004	0.002	0.011	0.006
Ta	0.030	0.004	0.002	0.003	b.d	0.001	0.001	0.001	0.001
W									
Pb	7.078	9.026	19.385	6.145	5.495	8.227	7.303	5.093	2.074
Th	0.955	0.003	0.015	0.003	0.001	0.009	0.002	0.006	b.d
U	0.147	b.d	0.003	0.102	0.001	0.002	0.004	0.002	b.d

Table C.8: Continued

Sample	CH6 41	CH6 177.01	CH6 46	CH6 51	CH6 56	CH6 60	CH6 74	CH6 80	CH6 93
Depth	167.51	177.01	182.54	198.51	218.62	227.505	277.87	297.83	350.435
Li	2.330	2.420	0.553	1.890	3.733	1.690	1.525	3.841	3.587
P			29.805					18.682	47.384
Sc	1.004	1.072	0.103	0.999	1.007	0.963	0.939	0.183	0.138
Ti	61.345	75.580	55.902	101.283	171.890	136.585	137.025	53.203	118.279
V	1.416	1.485	1.069	0.451	1.448	0.624	0.465	1.297	1.087
Cr	3.630	3.060	14.633	11.003	3.187	3.580	3.665	9.749	10.296
Co	0.270	0.249	6.227	0.478	0.245	0.074	0.112	1.313	2.843
Ni	1.398	0.698	31.819	2.470	1.237	0.208	0.217	22.156	11.710
Cu			6.757					16.645	5.140
Zn			8.860					72.194	4.223
Ga	27.405	26.375	20.460	31.830	75.137	38.665	34.770	18.089	16.538
As			0.039					0.046	0.037
Rb	1.217	1.026	0.962	0.207	0.479	0.166	0.228	0.689	13.647
Sr	388.580	358.260	532.026	353.620	418.813	362.285	304.390	405.828	422.134
Y	0.064	0.079	0.164	0.166	0.181	0.180	0.177	0.098	0.279
Zr	0.166	0.366	0.272	0.019	0.025	0.016	0.011	0.202	25.218
Nb	0.003	0.020	0.026	0.001	0.005	0.002	0.001	0.031	0.047
Ba	42.985	38.570	62.713	74.283	257.013	100.500	79.600	62.078	314.133
Sn			0.100					0.070	0.040
Cs	0.362	0.048	0.005	0.019	0.076	0.004	0.004	0.014	0.322
La	0.940	0.934	2.617	16.193	9.437	16.560	15.285	1.345	8.225
Ce	1.457	1.496	3.615	19.053	14.273	21.260	17.620	2.099	11.830
Pr	0.129	0.141	0.333	1.243	1.248	1.482	1.170	0.233	0.981
Nd	0.439	0.461	0.982	2.890	3.680	3.735	2.895	0.799	2.614
Sm	0.063	0.063	0.124	0.205	0.329	0.260	0.231	0.139	0.449
Eu	0.197	0.180	0.299	0.715	0.861	0.769	0.750	0.288	0.809
Gd	0.043	0.038	0.110	0.120	0.161	0.149	0.126	0.102	0.309
Tb	0.003	0.005	0.006	0.011	0.013	0.012	0.011	0.003	0.019
Dy	0.012	0.032	0.031	0.055	0.053	0.053	0.060	0.028	0.066
Ho	0.002	0.004	0.005	0.008	0.005	0.006	0.010	0.003	0.010
Er	0.009	0.007	0.009	0.010	0.015	0.017	0.017	0.007	0.029
Tm	b.d	0.001	0.001	0.001	0.001	0.001	0.001	0.001	0.003
Yb	0.004	0.003	0.004	0.006	0.007	0.006	0.004	0.003	0.015
Lu	b.d	0.001	b.d	0.001	0.001	0.001	0.001	b.d	0.001
Hf	0.005	0.008	0.006	0.002	0.004	0.001	0.001	0.004	0.605
Ta	0.001	0.003	b.d	0.001	0.002	0.001	0.022	b.d	-0.003
W			0.011					b.d	-0.003
Pb	0.702	0.582	1.162	6.377	13.547	3.625	5.005	1.679	5.723
Th	0.048	0.057	0.009	0.003	0.004	0.001	b.d	b.d	0.060
U	0.003	0.007	0.007	0.005	0.006	0.001	0.003	0.006	0.069

Table C.8: Continued

Sample	CH6 410.13	CH6 113	CH6 116	CH6 118	CH6 121	CH6 126	CH6 128	CH6 131	CH6 133
Depth	410.13	434.19	444.41	450.31	459.15	477.49	482.88	492.65	500.50
Li	2.063	9.160	2.466	2.743	4.073	4.459	3.567	8.270	5.185
P			10.521	41.000		38.854	19.030		23.189
Sc	1.017	7.921	0.162	0.291	0.992	0.438	0.291	1.066	0.235
Ti	171.630	330.550	192.431	99.028	126.278	122.577	122.811	155.074	164.991
V	0.878	24.414	1.763	1.043	1.455	2.325	2.381	2.174	2.925
Cr	3.547	996.720	34.249	6.252	3.573	52.059	6.239	4.038	2.955
Co	8.017	34.250	5.963	3.980	0.237	6.500	9.136	0.431	4.980
Ni	0.534	261.422	62.420	14.509	0.261	36.887	37.430	0.466	15.537
Cu			36.046	17.155		58.975	108.629		30.772
Zn			86.006	5.640		11.297	24.486		11.063
Ga	55.573	35.587	12.143	20.526	45.045	21.717	25.302	40.736	25.472
As			0.047	0.035		0.048	0.048		0.042
Rb	0.167	0.184	20.094	1.467	0.634	1.952	1.260	1.051	1.150
Sr	372.367	316.100	208.093	520.038	442.718	516.650	619.663	461.016	596.612
Y	0.210	0.584	0.154	0.189	0.170	0.211	0.234	0.125	0.269
Zr	0.013	0.449	32.457	0.413	0.011	0.543	0.311	0.141	0.402
Nb	0.002	0.015	1.436	0.014	0.005	0.059	0.026	0.039	0.046
Ba	163.437	97.293	818.833	111.204	108.820	111.709	106.131	91.560	97.070
Sn			0.134	0.057		0.047	0.045		0.384
Cs	0.047	0.015	0.605	0.020	0.006	0.052	0.012	0.007	0.017
La	11.913	3.413	3.054	4.853	3.288	2.914	3.019	1.575	3.363
Ce	14.570	5.708	4.586	6.231	4.868	4.148	4.303	2.418	4.955
Pr	0.992	0.525	0.458	0.536	0.409	0.389	0.410	0.225	0.485
Nd	2.560	1.641	1.198	1.545	1.247	1.247	1.285	0.745	1.532
Sm	0.228	0.170	0.436	0.222	0.128	0.211	0.197	0.091	0.226
Eu	0.713	0.403	0.720	0.555	0.510	0.558	0.660	0.372	0.738
Gd	0.125	0.117	0.142	0.198	0.094	0.151	0.142	0.067	0.167
Tb	0.010	0.016	0.006	0.011	0.009	0.009	0.011	0.007	0.014
Dy	0.064	0.109	0.041	0.042	0.039	0.046	0.047	0.034	0.058
Ho	0.009	0.021	0.005	0.008	0.007	0.004	0.008	0.005	0.011
Er	0.013	0.085	0.019	0.017	0.012	0.018	0.018	0.010	0.020
Tm	0.003	0.013	0.002	0.001	0.022	0.002	0.002	0.002	0.002
Yb	0.007	0.106	0.010	0.006	0.010	0.007	0.008	0.006	0.010
Lu	0.001	0.026	0.001	b.d	0.001	0.001	b.d	0.002	0.001
Hf	0.002	0.012	0.658	0.007	0.002	0.014	0.007	0.007	0.009
Ta	0.017	0.002	0.112	b.d	0.001	b.d	b.d	0.008	b.d
W			0.093	b.d		b.d	0.017		0.030
Pb	6.400	2.606	3.860	6.212	5.718	3.809	2.085	2.131	1.458
Th	b.d	0.002	0.102	0.014	b.d	0.029	0.008	0.007	0.019
U	0.002	0.001	0.068	0.013	0.001	0.014	0.006	0.001	0.009

Table C.8: Continued

Sample	CH6 142	CH6 146	CH6 546.37	CH6 148	CH6 155	CH6 165	CH6 174	CH6 178	CH6 180	CH6 183
Depth	529.56	542.670	546.370	550.62	573.65	605.63	643.44	662.51	672.53	683.39
Li	5.369	9.143	9.823	4.179	8.560	11.075	11.910	3.575	4.098	6.545
P	36.394			30.243				26.364		48.398
Sc	0.245	0.976	0.951	0.240	0.988	0.899	0.889	0.197	0.897	0.304
Ti	164.111	196.417	192.967	172.361	165.115	173.685	206.200	268.180	179.045	180.789
V	1.923	2.968	2.253	2.768	2.294	1.854	1.898	2.483	1.560	1.925
Cr	2.324	3.633	3.407	1.654	4.010	3.182	3.565	11.519	6.923	6.089
Co	4.510	0.254	0.198	3.561	0.231	0.167	0.188	10.134	0.518	4.187
Ni	15.632	0.298	0.195	8.010	0.605	0.425	0.277	58.482	2.347	13.350
Cu	34.753			3.670				20.430		14.629
Zn	26.671			9.785				66.077		1866.259
Ga	24.478	48.760	49.577	23.743	89.365	37.095	43.650	18.366	48.355	19.172
As	0.046			0.040				0.050		0.066
Rb	2.122	1.651	0.596	1.670	10.962	0.446	0.564	3.709	0.416	8.431
Sr	551.870	431.113	426.040	553.949	412.717	405.943	417.300	311.085	428.745	460.002
Y	0.309	0.190	0.187	0.287	0.270	0.310	0.328	0.254	0.349	0.372
Zr	0.593	0.013	0.009	0.359	0.070	0.019	0.015	34.621	0.012	1.005
Nb	0.043	0.008	0.001	0.043	0.002	0.009	0.001	2.978	0.001	0.052
Ba	118.900	125.783	129.937	107.582	283.488	78.325	100.510	206.391	124.165	214.559
Sn	0.088			0.060				0.098		0.052
Cs	0.044	0.095	0.004	0.020	0.197	0.010	0.027	0.136	0.011	0.221
La	5.685	3.100	3.603	4.800	3.467	4.692	5.685	2.804	6.570	5.486
Ce	8.515	4.853	5.623	6.999	6.442	8.850	10.015	5.261	11.355	9.380
Pr	0.811	0.443	0.491	0.672	0.626	0.927	0.972	0.668	1.101	1.004
Nd	2.388	1.440	1.542	2.038	2.012	3.183	3.170	2.226	3.553	3.310
Sm	0.303	0.175	0.157	0.271	0.220	0.347	0.365	0.406	0.362	0.486
Eu	0.826	0.685	0.678	0.968	0.726	0.766	0.829	0.646	0.902	0.901
Gd	0.248	0.101	0.115	0.228	0.151	0.214	0.198	0.253	0.241	0.361
Tb	0.018	0.011	0.011	0.017	0.014	0.019	0.017	0.016	0.023	0.028
Dy	0.069	0.054	0.047	0.067	0.070	0.090	0.081	0.079	0.089	0.093
Ho	0.012	0.009	0.007	0.011	0.010	0.011	0.012	0.011	0.014	0.013
Er	0.028	0.020	0.016	0.025	0.022	0.019	0.026	0.041	0.025	0.037
Tm	0.002	0.001	0.002	0.002	0.001	0.003	0.003	0.004	0.003	0.002
Yb	0.011	0.010	0.010	0.010	0.010	0.012	0.011	0.029	0.009	0.013
Lu	b.d	0.001	0.002	b.d	0.001	0.002	0.002	0.002	0.002	0.001
Hf	0.011	0.003	0.005	0.008	0.007	0.004	0.004	0.724	0.003	0.023
Ta	b.d	0.002	0.001	b.d	0.002	0.009	0.001	0.208	0.002	b.d
W	0.039			0.026				0.277		0.003
Pb	2.595	1.975	1.676	1.006	1.815	2.151	2.470	1.970	2.460	4.092
Th	0.048	0.002	b.d	0.031	0.006	0.001	0.001	0.031	0.001	0.024
U	0.015	0.004	0.001	0.009	0.001	0.002	b.d	0.027	b.d	0.005

Table C.9: Clinopyroxene trace elements geochemistry in CH6 (ppm, combined LA-ICP-MS and ICP-MS).

Sample	CH6 38.23	CH6 38.84	CH6 3	CH6 14	CH6 22	CH6 26	CH6 28	CH6 32	CH6 41
Depth	38.23	38.84	42.60	78.71	103.86	118.41	124.78	139.86	167.51
Li	6.991	7.002	4.314	14.559	8.713	6.895	7.623	3.246	2.538
P	23.366	20.194		27.692			33.368		
Sc	78.455	78.394	84.896	136.721	76.422	105.687	112.528	90.748	84.558
Ti	904.615	896.460	984.607	1710.094	1291.282	1520.021	854.387	917.709	816.072
V	145.179	143.335	145.748	268.961	202.582	219.058	182.787	221.660	251.211
Cr	4198.464	4081.216	4091.225	6060.573	6567.269	5893.791	5969.956	5363.558	2084.265
Co	39.850	35.429	44.410	41.144	41.561	43.056	41.416	48.954	60.451
Ni	387.975	304.060	371.132	433.317	405.274	420.116	363.741	411.378	459.399
Cu	21.667	25.486		57.920			29.019		
Zn	200.610	75.344		123.460			97.617		
Ga	2.623	2.585	3.202	3.845	4.130	4.068	2.749	3.641	3.303
As	0.033	0.038		0.119			0.134		
Rb	0.630	0.899	0.054	2.046	0.074	4.612	0.289	0.093	0.008
Sr	124.904	112.417	44.821	13.964	13.021	11.383	15.686	16.595	13.992
Y	11.362	11.485	10.165	34.470	18.801	20.748	11.358	9.987	7.260
Zr	25.194	25.807	22.630	57.429	37.299	89.231	17.481	20.952	6.581
Nb	0.218	0.258	0.345	2.067	0.295	0.864	0.223	0.167	0.140
Ba	5.656	7.807	1.284	13.047	1.144	2.623	2.596	0.074	0.040
Sn	0.243	0.216		0.828			0.321		
Cs	0.036	0.047	0.007	0.164	0.007	0.899	0.034	0.014	0.001
La	8.745	8.395	4.605	7.273	5.753	8.888	3.106	1.924	0.575
Ce	19.070	18.979	9.426	26.075	24.220	36.020	8.945	7.992	2.614
Pr	2.543	2.516	1.067	5.270	3.847	5.243	1.602	1.313	0.466
Nd	10.243	10.124	4.767	24.902	18.947	23.810	7.194	6.785	2.669
Sm	2.258	2.226	1.393	6.215	4.267	4.983	1.735	1.773	0.859
Eu	0.595	0.595	0.423	0.978	0.818	0.779	0.388	0.441	0.210
Gd	2.433	2.430	1.579	6.422	3.785	4.407	1.894	1.768	1.037
Tb	0.369	0.368	0.252	1.047	0.527	0.597	0.311	0.255	0.168
Dy	2.081	2.108	1.613	6.060	3.146	3.488	1.906	1.656	1.132
Ho	0.410	0.419	0.312	1.130	0.595	0.639	0.371	0.310	0.228
Er	1.044	1.046	0.832	2.858	1.532	1.593	1.008	0.842	0.633
Tm	0.143	0.142	0.107	0.381	0.199	0.210	0.141	0.108	0.088
Yb	0.876	0.868	0.697	2.171	1.235	1.215	0.867	0.736	0.595
Lu	0.129	0.131	0.098	0.299	0.171	0.172	0.122	0.103	0.079
Hf	0.874	0.881	0.578	1.916	0.962	2.173	0.567	0.616	0.199
Ta	0.036	0.040	0.045	0.173	0.023	0.095	0.027	0.025	0.010
W	b.d	b.d		0.061			0.015		
Pb	0.776	1.000	0.385	3.914	0.512	0.467	1.377	0.141	0.081
Th	0.271	0.264	0.280	0.865	0.600	0.530	0.063	0.031	0.142
U	0.072	0.077	0.078	0.114	0.189	0.056	0.031	0.017	0.055

Table C.9: Continued

Sample	CH6 43	CH6 177.01	CH6 46	CH6 51	CH6 56	CH6 60	CH6 67	CH6 74	CH6 78
Depth	**172.57**	**177.01**	**182.54**	**198.51**	**218.62**	**227.51**	**254.28**	**277.87**	
Li	4.371	2.767	1.642	7.363	7.360	6.528	6.754	7.704	10.251
P	17.532		32.829						38.967
Sc	107.808	83.141	101.378	90.944	78.622	78.669	106.369	109.308	133.596
Ti	876.174	924.240	978.528	1600.479	1436.200	1411.072	1313.034	1506.067	1341.369
V	215.022	232.792	158.988	218.958	210.962	209.187	226.281	246.421	303.448
Cr	2482.875	2677.383	4435.083	6189.328	6125.370	6262.268	4858.466	5624.019	4504.423
Co	49.880	55.050	37.775	40.286	41.092	41.063	41.307	40.951	41.490
Ni	328.777	413.351	489.137	404.065	390.287	385.352	396.276	379.057	334.300
Cu	6.095		20.856						8.198
Zn	174.478		21.579						210.928
Ga	2.620	4.198	2.899	3.770	3.663	3.978	6.764	3.618	3.136
As	0.027		0.048						0.083
Rb	0.062	0.032	0.404	0.109	0.024	0.164	1.357	0.052	1.640
Sr	15.329	18.534	26.475	14.549	16.689	16.055	14.235	10.793	11.897
Y	8.986	8.243	12.346	21.521	21.502	21.876	23.316	27.368	25.566
Zr	8.501	7.864	21.134	55.915	37.055	35.250	50.853	72.384	57.139
Nb	0.121	0.142	0.358	0.206	0.209	0.245	0.108	0.155	0.526
Ba	0.967	1.926	6.254	0.588	0.326	1.165	18.748	0.251	6.355
Sn	0.127		0.234						0.642
Cs	0.001	0.003	0.047	0.015	0.002	0.026	0.713	0.013	0.196
La	0.785	0.621	2.708	8.004	10.285	8.639	9.064	7.135	11.654
Ce	3.280	2.848	9.541	33.656	40.442	35.386	35.901	29.868	45.355
Pr	0.630	0.521	1.780	5.333	6.024	5.413	5.643	4.808	7.393
Nd	3.505	2.996	8.778	26.065	28.264	26.075	27.175	24.244	33.147
Sm	1.110	0.981	2.389	5.784	6.021	5.724	6.076	6.086	6.594
Eu	0.234	0.245	0.530	1.012	1.019	0.999	0.952	0.977	0.949
Gd	1.223	1.179	2.510	4.960	4.999	4.867	5.391	5.724	6.034
Tb	0.224	0.191	0.427	0.670	0.660	0.658	0.726	0.804	0.875
Dy	1.489	1.282	2.563	3.826	3.782	3.742	4.163	4.710	4.742
Ho	0.300	0.255	0.512	0.664	0.675	0.681	0.728	0.839	0.864
Er	0.796	0.720	1.349	1.652	1.662	1.702	1.762	2.080	2.205
Tm	0.110	0.095	0.189	0.202	0.208	0.216	0.211	0.256	0.271
Yb	0.727	0.650	1.104	1.199	1.271	1.300	1.238	1.529	1.655
Lu	0.100	0.088	0.152	0.153	0.165	0.173	0.163	0.192	0.225
Hf	0.299	0.238	0.743	1.692	0.989	0.960	1.715	2.004	1.904
Ta	b.d	0.009	0.041	0.026	0.014	0.015	0.008	0.027	0.042
W	0.001		0.032						0.053
Pb	0.497	0.123	1.274	1.024	0.529	0.786	10.926	0.527	1.124
Th	0.114	0.182	0.356	0.584	0.711	0.482	0.163	0.507	0.706
U	0.032	0.056	0.095	0.154	0.198	0.115	0.134	0.097	0.191

Table C.9: Continued

Sample	CH6 80	CH6 93	CH6 410.13	CH6 113	CH6 121	CH6 128	CH6 133	CH6 138
Depth	297.83	350.44	410.13	434.19	459.15	482.88	500.50	516.77
Li	5.021	8.159	6.951	8.575	9.731	7.610	6.873	13.398
P						26.145	23.580	26.690
Sc	67.505	121.958	86.577	86.820	120.626	155.549	151.101	143.602
Ti	949.873	2217.582	1827.370	1335.137	1459.958	1416.688	1576.962	2005.492
V	196.710	312.039	265.120	208.295	320.842	312.364	422.650	488.040
Cr	3161.681	4992.308	6267.666	4447.750	4193.651	2791.913	1536.495	1498.969
Co	62.405	43.125	46.975	30.851	56.088	61.233	62.991	67.859
Ni	590.589	400.640	482.335	348.225	351.746	359.924	297.602	285.658
Cu						44.944	24.191	29.323
Zn						38.819	39.632	118.464
Ga	3.053	3.736	4.867	13.657	4.147	3.106	2.809	3.819
As						0.074	0.106	0.125
Rb	0.042	0.156	0.354	0.082	0.252	0.264	0.242	1.060
Sr	11.289	13.087	18.112	137.646	16.413	20.673	16.153	14.717
Y	10.773	34.039	26.347	23.671	24.102	20.158	22.420	27.909
Zr	20.287	76.996	30.266	38.818	28.906	16.434	16.281	47.088
Nb	0.162	0.142	0.331	0.138	0.243	0.184	0.128	0.293
Ba	0.127	0.438	1.186	32.392	1.038	4.199	2.083	4.851
Sn						0.254	0.254	0.492
Cs	0.015	0.049	0.061	0.012	0.031	0.028	0.029	0.104
La	0.648	10.617	6.832	3.829	1.756	2.114	2.262	2.498
Ce	3.305	46.969	26.101	14.809	8.943	8.556	9.430	9.601
Pr	0.668	7.920	3.972	2.486	1.656	1.719	1.930	2.195
Nd	4.066	40.028	19.976	13.166	9.282	9.312	10.471	11.608
Sm	1.412	9.432	5.179	3.688	2.927	3.056	3.447	3.417
Eu	0.251	1.280	1.084	0.762	0.623	0.690	0.608	0.548
Gd	1.580	8.050	4.999	3.976	3.403	3.514	3.959	3.801
Tb	0.267	1.077	0.729	0.611	0.551	0.643	0.719	0.683
Dy	1.732	6.088	4.368	3.806	3.664	4.190	4.594	4.402
Ho	0.331	1.075	0.827	0.724	0.733	0.858	0.950	0.911
Er	0.876	2.568	2.145	1.856	2.040	2.306	2.571	2.481
Tm	0.112	0.309	0.282	0.227	0.266	0.343	0.385	0.373
Yb	0.731	1.824	1.775	1.382	1.740	2.067	2.321	2.303
Lu	0.100	0.238	0.228	0.176	0.237	0.298	0.334	0.334
Hf	0.483	2.503	0.899	0.856	0.732	0.608	0.648	1.249
Ta	0.036	0.010	0.023	0.017	0.023	0.015	0.012	0.047
W						0.025	0.028	0.031
Pb	0.385	0.766	0.446	0.805	1.037	0.327	0.537	1.379
Th	0.136	0.080	0.224	0.063	0.124	0.169	0.165	0.767
U	0.058	0.017	0.051	0.027	0.025	0.032	0.022	0.098

Table C.9: Continued

Sample	CH6 142	CH6 146	CH6 546.37	CH6 148	CH6 155	CH6 174	CH6 180
Depth	529.56	542.67	546.37	550.62	573.65	643.44	672.53
Li	8.245	7.213	7.376	7.610	10.043	10.406	12.178
P	23.453			24.169			
Sc	148.261	101.770	98.973	150.063	130.807	107.796	90.447
Ti	1759.701	1522.447	1334.060	1760.018	2091.049	2223.694	1530.862
V	423.412	432.742	433.071	499.271	530.434	443.973	387.328
Cr	1660.798	1732.048	1547.883	951.265	3039.812	2372.584	4048.951
Co	58.918	71.342	71.264	55.597	51.187	49.721	56.122
Ni	288.366	309.895	300.205	266.241	305.818	333.374	369.246
Cu	16.021			3.556			
Zn	39.844			50.173			
Ga	3.049	3.888	3.810	2.761	3.990	4.226	4.541
As	0.117			0.090			
Rb	1.111	0.038	0.077	0.427	0.125	0.377	0.201
Sr	13.608	12.343	13.545	13.206	13.214	14.968	16.617
Y	29.230	21.395	19.074	27.487	38.312	40.221	21.395
Zr	42.186	28.882	18.689	25.262	84.919	72.262	15.182
Nb	0.118	0.180	0.380	0.090	0.039	0.058	0.135
Ba	6.391	0.170	0.515	2.641	0.624	1.959	1.332
Sn	0.547			0.302			
Cs	0.159	0.010	0.007	0.034	0.028	0.105	0.049
La	3.505	1.783	1.870	2.937	1.567	2.852	3.145
Ce	15.239	8.569	8.418	12.788	10.564	17.943	12.798
Pr	3.114	1.522	1.401	2.664	2.396	3.822	1.976
Nd	15.947	8.228	7.340	14.276	14.745	21.969	9.953
Sm	4.841	2.474	2.146	4.506	5.018	6.535	2.826
Eu	0.725	0.456	0.429	0.804	0.738	0.828	0.556
Gd	5.272	2.766	2.433	5.009	5.606	6.551	2.972
Tb	0.940	0.454	0.391	0.900	0.909	1.011	0.472
Dy	5.874	3.112	2.731	5.653	5.936	6.376	3.156
Ho	1.210	0.636	0.562	1.169	1.159	1.208	0.622
Er	3.297	1.807	1.607	3.208	3.100	3.105	1.757
Tm	0.490	0.249	0.225	0.477	0.408	0.393	0.236
Yb	3.004	1.657	1.544	2.896	2.488	2.414	1.603
Lu	0.435	0.239	0.216	0.418	0.342	0.316	0.223
Hf	1.202	0.484	0.373	0.956	2.233	1.981	0.436
Ta	0.032	0.051	0.037	0.013	0.005	0.007	0.005
W	0.044			0.034			
Pb	0.441	0.124	0.247	0.417	0.605	0.645	0.280
Th	0.771	0.463	0.604	0.241	0.116	0.089	0.629
U	0.048	0.022	0.046	0.027	0.007	0.003	0.022

Table C.10: Major element geochemistry of the CH1 Drill Core (wt. %, XRF data).

Sample No.	Depth (m)	SiO_2	Al_2O_3	Fe_2O_3	FeO	MnO	MgO	CaO	Na_2O	K_2O	TiO_2	P_2O_5	Cr_2O_3	NiO	TOTAL	L.O.I.
CH1/12/1	385.50	56.04	1.93	0.99	7.98	0.19	30.65	1.72	0.13	0.07	0.12	0.02	0.46	0.10	100.38	-0.30
CH1/12/2	387.35	55.81	1.91	0.99	8.01	0.19	30.70	1.72	0.10	0.04	0.12	0.02	0.47	0.10	100.17	-0.37
CH1/12/3	389.20	55.96	1.86	0.99	8.04	0.20	30.98	1.67	0.07	0.03	0.11	0.01	0.49	0.10	100.51	-0.38
CH1/12/4	392.22	55.85	1.94	0.98	7.91	0.19	30.82	1.71	0.11	0.04	0.11	0.02	0.48	0.10	100.27	-0.36
CH1/12/5	394.24	55.92	1.96	0.98	7.94	0.19	30.90	1.73	0.10	0.05	0.11	0.01	0.47	0.10	100.48	-0.24
CH1/12/6	396.60	56.20	2.12	0.96	7.79	0.19	30.53	1.76	0.16	0.11	0.12	0.02	0.45	0.10	100.52	-0.08
CH1/12/7	398.79	56.02	1.88	0.96	7.78	0.19	31.10	1.69	0.10	0.05	0.11	0.02	0.46	0.10	100.46	-0.03
CH1/12/8	401.83	55.61	1.89	0.97	7.88	0.19	30.90	1.70	0.08	0.03	0.12	0.02	0.47	0.10	99.95	-0.29
CH1/12/9	403.60	55.79	2.07	0.99	8.01	0.19	30.78	1.78	0.07	0.03	0.12	0.01	0.46	0.11	100.40	-0.27
CH1/12/10	405.67	55.67	1.98	0.99	8.00	0.19	30.86	1.77	0.08	0.03	0.12	0.01	0.49	0.10	100.28	-0.32
CH1/12/11	408.97	54.32	2.29	1.00	8.12	0.18	30.87	2.09	0.09	0.38	0.13	0.02	0.47	0.11	100.06	-0.16
CH1/12/12	410.47	41.57	0.76	1.45	11.75	0.19	43.05	0.61	0.05	0.05	0.04	0.03	0.17	0.31	100.04	-0.89
CH1/12/13	412.52	42.61	0.89	1.44	11.66	0.19	42.17	0.69	0.07	0.03	0.04	0.02	0.18	0.29	100.29	-0.82
CH1/12/14	414.35	55.42	3.00	0.98	7.97	0.19	29.54	2.26	0.23	0.06	0.12	0.01	0.68	0.09	100.56	-0.33
CH1/12/15	414.71	48.01	1.96	1.25	10.15	0.19	36.28	1.37	0.15	0.06	0.09	0.02	0.84	0.20	100.56	-0.51
CH1/12/16	415.82	40.02	0.84	1.52	12.34	0.20	43.96	0.40	0.02	0.06	0.04	0.02	0.68	0.31	100.40	-0.34
CH1/12/17	418.42	50.48	1.55	1.17	9.46	0.20	35.13	1.34	0.04	0.04	0.09	0.02	0.53	0.17	100.22	-0.08
CH1/12/18	419.09	39.88	0.75	1.53	12.40	0.20	44.41	0.36	0.03	0.08	0.04	0.02	0.52	0.33	100.54	-0.80
CH1/12/19	420.60	54.71	1.73	1.04	8.40	0.21	31.54	1.68	0.04	0.04	0.12	0.01	0.49	0.13	100.14	0.74
CH1/12/20	421.89	55.66	2.21	1.00	8.09	0.19	30.37	1.93	0.10	0.03	0.12	0.01	0.47	0.09	100.27	-0.41

Table C.11: Trace element geochemistry in the CH1 Drill Core (ppm, XRF data).

Sample No.	Depth (m)	Sc	V	Cr	Co	Ni	Cu	Zn	Ga	Rb	Sr	Y	Zr	Nb	Mo	Ba	Pb
CH1/12/1	385.50	25.65	85.99	3164.80	93.28	740.46	3.34	67.98	3.00	2.19	10.95	1.55	5.77	b.d	1.00	22.24	1.91
CH1/12/2	387.35	23.35	77.11	3210.98	95.03	738.45	5.19	68.66	2.66	1.30	10.81	1.36	5.75	b.d	0.61	22.59	1.45
CH1/12/3	389.20	24.81	78.16	3300.94	99.06	744.54	4.90	66.44	2.35	0.71	7.42	1.39	4.45	b.d	0.15	26.99	1.38
CH1/12/4	392.22	22.77	78.24	3296.46	97.05	761.85	8.32	67.89	3.37	0.87	10.50	0.57	5.57	0.02	0.74	21.76	0.32
CH1/12/5	394.24	22.00	78.26	3193.84	95.41	754.81	6.26	67.65	3.29	1.24	10.64	0.58	5.39	b.d	0.30	29.43	0.68
CH1/12/6	396.60	22.52	71.82	3062.47	92.54	751.52	7.08	66.89	2.12	4.55	14.50	0.23	11.35	0.57	0.14	34.31	0.10
CH1/12/7	398.79	23.71	69.96	3144.16	88.44	758.41	10.68	70.18	1.83	2.09	9.88	b.d	5.80	0.84	0.68	25.61	0.25
CH1/12/8	401.83	23.01	74.15	3163.28	92.01	754.40	3.17	70.20	1.67	1.34	9.15	0.06	6.94	0.55	1.71	23.36	0.70
CH1/12/9	403.60	22.59	75.56	3082.28	90.47	792.90	3.95	66.46	2.79	0.56	11.49	2.03	5.37	b.d	0.66	18.97	b.d
CH1/12/10	405.67	24.25	76.88	3272.73	83.94	731.65	4.74	65.50	3.54	1.48	8.82	2.56	4.59	b.d	0.96	19.50	0.60
CH1/12/11	408.97	20.69	80.69	3192.13	92.22	848.21	b.d	87.34	3.86	19.07	6.43	3.13	18.86	1.03	1.16	75.73	3.49
CH1/12/12	410.47	6.22	19.67	996.35	169.01	2488.42	5.45	93.51	0.70	1.67	11.40	1.21	3.35	b.d	0.61	27.73	3.40
CH1/12/13	412.52	6.15	22.93	1133.23	180.22	2231.34	0.95	83.16	1.89	1.89	12.65	1.22	2.84	b.d	1.02	16.79	1.39
CH1/12/14	414.35	23.08	76.79	4496.82	86.84	682.45	9.33	67.83	4.20	0.77	29.72	3.44	6.35	0.42	0.73	33.89	1.70
CH1/12/15	414.71	18.04	58.30	5187.72	143.38	1524.11	4.25	79.16	2.00	2.49	17.95	3.13	6.05	0.28	0.46	40.68	0.78
CH1/12/16	415.82	5.67	28.15	4018.14	191.44	2364.80	b.d	92.52	0.71	1.11	3.26	1.44	4.10	b.d	0.29	35.28	3.52
CH1/12/17	418.42	18.52	58.27	3366.64	132.69	1286.67	5.06	76.87	2.16	1.03	7.86	3.05	6.46	b.d	0.18	32.87	5.00
CH1/12/18	419.09	7.58	21.12	3097.49	192.85	2577.79	b.d	89.81	1.43	1.87	3.55	1.84	4.46	b.d	0.97	15.98	0.65
CH1/12/19	420.60	20.37	65.66	3200.73	95.92	985.38	10.82	86.95	1.61	1.52	6.12	2.15	5.53	b.d	0.87	28.72	14.85
CH1/12/20	421.89	22.04	73.20	3168.66	88.56	715.10	4.55	70.29	3.41	0.99	14.00	1.93	3.80	b.d	-0.38	20.12	0.35

Appendix D: Petrolog Modelling- Data Output

Tabled D.1: Marginal Zone parental magma derived from fractionation of B1-magma

% crystallization	0%	5%	10%	15%	20%	25%	30%	31%	32%			35%
	Recalculated B1-Magma of Wilson (2012)						Proposed Marginal Zone Parental magma					
SiO_2	56.18	56.19	56.21	56.25	56.31	56.41	56.62	56.70	56.77	56.85	56.93	57.01
TiO_2	0.28	0.30	0.31	0.33	0.35	0.37	0.40	0.41	0.41	0.42	0.42	0.43
Al_2O_3	11.33	11.74	12.20	12.70	13.26	13.88	14.21	14.13	14.04	13.96	13.87	13.79
Fe_2O_3	1.25	1.21	1.18	1.15	1.12	1.10	1.11	1.13	1.15	1.17	1.19	1.20
FeO	8.06	8.24	8.40	8.54	8.63	8.65	8.69	8.73	8.78	8.83	8.87	8.92
MnO	0.17	0.18	0.19	0.20	0.21	0.23	0.24	0.25	0.25	0.25	0.26	0.26
MgO	13.60	12.54	11.39	10.15	8.80	7.34	6.15	6.05	5.96	5.86	5.76	5.65
CaO	6.36	6.67	7.02	7.39	7.81	8.26	8.59	8.58	8.57	8.57	8.57	8.56
Na_2O	1.43	1.51	1.59	1.69	1.79	1.91	2.01	2.01	2.02	2.02	2.03	2.03
K_2O	1.05	1.11	1.17	1.24	1.31	1.40	1.50	1.52	1.55	1.57	1.59	1.62
P_2O_5	0.07	0.07	0.08	0.08	0.09	0.09	0.10	0.10	0.10	0.10	0.11	0.11
Cr_2O_3	0.22	0.23	0.24	0.26	0.28	0.29	0.31	0.32	0.32	0.33	0.33	0.34
Temp.	1366.16	1346.31	1323.30	1296.31	1264.24	1225.40	1191.32	1189.47	1187.58	1185.57	1183.45	1181.19
Olv_Fo	-1	-1	-1	-1	-1	-1	-1	-1	-1	-1	-1	-1
Olv_Kd	-1	-1	-1	-1	-1	-1	-1	-1	-1	-1	-1	-1
Plg_An	-1	-1	-1	-1	-1	-1	73.83	73.51	73.18	72.86	72.53	72.19
Cpx_Mg#	-1	-1	-1	-1	-1	-1	-1	-1	-1	-1	-1	-1
Opx_Mg#	90.85	90.01	88.99	87.73	86.11	83.96	81.56	81.25	80.94	80.61	80.26	79.9
Pressure(kbar)	2	2	2	2	2	2	2	2	2	2	2	2
Lg(fO_2)	-6.62	-6.8	-7.02	-7.28	-7.61	-8.02	-8.4	-8.42	-8.44	-8.47	-8.49	-8.52
density	2.619	2.619	2.619	2.618	2.616	2.614	2.612	2.612	2.612	2.612	2.611	2.611
Ln(viscosity)	4.67	4.97	5.32	5.74	6.23	6.83	7.35	7.38	7.41	7.44	7.47	7.51
Melt_%	99.99	95.00	90.00	84.99	79.99	75.00	70.00	69.00	68.00	67.00	66.00	65.00
Olv_%_cumulate	0.00	0.00	0.00	0.00	0.00	0.00	0.00	0.00	0.00	0.00	0.00	0.00
Plg_%_cumulate	0.00	0.00	0.00	0.00	0.00	0.00	0.92	1.48	2.05	2.61	3.17	3.73
Cpx_%_cumulate	0.00	0.00	0.00	0.00	0.00	0.00	0.00	0.00	0.00	0.00	0.00	0.00
Opx_%_cumulate	0.01	5.00	10.00	15.01	20.01	25.00	29.08	29.52	29.95	30.39	30.83	31.28

Table D.1: Continued

% crystallization					***40%***						***45%***
SiO_2	57.10	57.18	57.27	57.36	***57.45***	57.54	57.55	57.67	57.78	57.91	***58.04***
TiO_2	0.44	0.45	0.45	0.46	***0.47***	0.47	0.47	0.48	0.48	0.48	***0.48***
Al_2O_3	13.70	13.61	13.52	13.43	***13.35***	13.27	13.26	13.21	13.15	13.09	***13.04***
Fe_2O_3	1.22	1.24	1.26	1.29	***1.31***	1.33	1.33	1.35	1.37	1.39	***1.42***
FeO	8.96	9.01	9.05	9.09	***9.13***	9.17	9.18	9.23	9.29	9.34	***9.40***
MnO	0.27	0.27	0.27	0.28	***0.28***	0.29	0.29	0.29	0.30	0.30	***0.30***
MgO	5.54	5.43	5.31	5.19	***5.07***	4.95	4.94	4.85	4.76	4.66	***4.56***
CaO	8.56	8.56	8.56	8.56	***8.57***	8.57	8.56	8.46	8.36	8.25	***8.14***
Na_2O	2.04	2.04	2.05	2.05	***2.06***	2.06	2.06	2.07	2.08	2.09	***2.10***
K_2O	1.64	1.67	1.70	1.72	***1.75***	1.78	1.78	1.81	1.85	1.88	***1.91***
P_2O_5	0.11	0.11	0.11	0.11	***0.12***	0.12	0.12	0.12	0.12	0.13	***0.13***
Cr_2O_3	0.34	0.35	0.36	0.36	***0.37***	0.37	0.37	0.38	0.39	0.39	***0.40***
Temp.	1178.82	1176.28	1173.54	1170.74	***1167.67***	1164.75	1164.60	1163.00	1161.36	1159.64	***1157.85***
Olv_Fo	-1	-1	-1	-1	***-1***	-1	-1	-1	-1	-1	***-1***
Olv_Kd	-1	-1	-1	-1	***-1***	-1	-1	-1	-1	-1	***-1***
Plg_An	71.85	71.51	71.17	70.81	***70.46***	70.15	70.12	69.85	69.58	69.3	***69.02***
Cpx_Mg#	-1	-1	-1	-1	***-1***	75.67	75.62	75.09	74.54	73.96	***73.36***
Opx_Mg#	79.52	79.12	78.7	78.26	***77.78***	77.34	77.31	76.88	76.43	75.96	***75.46***
Pressure(kbar)	2	2	2	2	***2***	2	2	2	2	2	***2***
Lg(fO_2)	-8.54	-8.57	-8.61	-8.64	***-8.67***	-8.71	-8.71	-8.73	-8.75	-8.77	***-8.79***
density	2.611	2.611	2.61	2.61	***2.61***	2.61	2.609	2.609	2.608	2.607	***2.606***
Ln(viscosity)	7.54	7.58	7.63	7.67	***7.72***	7.76	7.76	7.8	7.84	7.89	***7.93***
Melt_%	64.00	62.99	61.99	61.00	***59.99***	59.09	58.99	58.00	57.00	56.00	***54.99***
Olv_%_cumulate	0.00	0.00	0.00	0.00	***0.00***	0.00	0.00	0.00	0.00	0.00	***0.00***
Plg_%_cumulate	4.28	4.83	5.38	5.93	***6.46***	6.95	6.99	7.43	7.87	8.31	***8.75***
Cpx_%_cumulate	0.00	0.00	0.00	0.00	***0.00***	0.01	0.05	0.47	0.91	1.34	***1.78***
Opx_%_cumulate	31.72	32.17	32.63	33.08	***33.54***	33.96	33.97	34.10	34.23	34.35	***34.47***

Table D.1: Continued

% crystallization					*50%*				*54%*
									*Residual Magma**
SiO_2	58.17	58.31	58.45	58.60	***58.76***	58.92	59.09	59.27	***59.45***
TiO_2	0.48	0.48	0.48	0.48	***0.48***	0.48	0.48	0.47	***0.47***
Al_2O_3	12.98	12.92	12.86	12.80	***12.74***	12.68	12.62	12.56	***12.49***
Fe_2O_3	1.44	1.46	1.49	1.51	***1.53***	1.56	1.59	1.61	***1.64***
FeO	9.46	9.51	9.57	9.62	***9.67***	9.72	9.78	9.82	***9.87***
MnO	0.31	0.31	0.31	0.32	***0.32***	0.33	0.33	0.33	***0.34***
MgO	4.46	4.36	4.26	4.15	***4.04***	3.93	3.82	3.71	***3.59***
CaO	8.03	7.91	7.79	7.66	***7.53***	7.39	7.24	7.10	***6.94***
Na_2O	2.11	2.12	2.13	2.14	***2.14***	2.15	2.16	2.17	***2.18***
K_2O	1.95	1.98	2.02	2.06	***2.10***	2.15	2.19	2.24	***2.29***
P_2O_5	0.13	0.13	0.13	0.14	***0.14***	0.14	0.15	0.15	***0.15***
Cr_2O_3	0.41	0.41	0.42	0.43	***0.44***	0.44	0.45	0.46	***0.47***
Temp.	1156.07	1154.20	1152.26	1150.23	***1148.19***	1146.04	1143.88	1141.63	***1139.32***
Olv_Fo	-1	-1	-1	-1	***-1***	-1	-1	-1	***-1***
Olv_Kd	-1	-1	-1	-1	***-1***	-1	-1	-1	***-1***
Plg_An	68.73	68.44	68.14	67.84	***67.54***	67.23	66.91	66.59	***66.26***
Cpx_Mg#	72.72	72.05	71.37	70.64	***69.86***	69.06	68.21	67.32	***66.39***
Opx_Mg#	74.96	74.44	73.87	73.29	***72.68***	72.03	71.37	70.67	***69.94***
Pressure(kbar)	2	2	2	2	***2***	2	2	2	***2***
Lg(fO_2)	-8.81	-8.83	-8.86	-8.88	***-8.91***	-8.93	-8.96	-8.99	***-9.02***
density	2.605	2.603	2.602	2.601	***2.6***	2.598	2.597	2.595	***2.593***
Ln(viscosity)	7.98	8.03	8.08	8.13	***8.18***	8.24	8.3	8.36	***8.42***
Melt_%	54.00	53.00	52.00	51.00	***50.00***	49.00	48.00	47.00	***46.00***
Olv_%_cumulate	0.00	0.00	0.00	0.00	***0.00***	0.00	0.00	0.00	***0.00***
Plg_%_cumulate	9.18	9.62	10.05	10.49	***10.92***	11.35	11.77	12.20	***12.63***
Cpx_%_cumulate	2.23	2.69	3.14	3.60	***4.07***	4.54	5.02	5.50	***5.99***
Opx_%_cumulate	34.59	34.70	34.81	34.92	***35.02***	35.12	35.21	35.30	***35.38***

Table D.2: Parental Magma of the Lower Orthopyroxenite Subzone (LZa) at Clapham Trough

	#Compositions similar to BB* and ORT**							Compositions similar to CH6			
SiO2_magma	57.1855	57.2018	57.2192	57.2373	57.2565	57.2766	57.2979	57.3204	57.3441	57.3693	57.3956
TiO2_magma	0.3406	0.344	0.3475	0.3511	0.3547	0.3584	0.3623	0.3662	0.3701	0.3742	0.3784
Al2O3_magma	11.6827	11.765	11.8497	11.935	12.0226	12.111	12.2018	12.2941	12.3881	12.4847	12.582
Fe2O3_magma	1.2773	1.2717	1.2662	1.2609	1.2556	1.2505	1.2455	1.2406	1.236	1.2314	1.2271
FeO_magma	8.6863	8.7096	8.7319	8.7527	8.7722	8.7899	8.8062	8.8205	8.8329	8.8432	8.8511
MnO_magma	0.2214	0.2236	0.2259	0.2282	0.2306	0.233	0.2355	0.238	0.2406	0.2433	0.2459
MgO_magma	10.597	10.3781	10.1539	9.9288	9.6985	9.4673	9.2309	8.9914	8.7491	8.5015	8.2533
CaO_magma	6.5376	6.5978	6.6595	6.7217	6.7856	6.8498	6.9157	6.9826	7.0506	7.1202	7.1901
Na2O_magma	1.6577	1.6744	1.6915	1.7089	1.7267	1.7448	1.7634	1.7824	1.8017	1.8216	1.8418
K2O_magma	1.4243	1.4386	1.4534	1.4683	1.4836	1.4991	1.5151	1.5314	1.5481	1.5652	1.5825
P2O5_magma	0.0942	0.0951	0.0961	0.0971	0.0981	0.0991	0.1002	0.1012	0.1023	0.1035	0.1046
Cr2O3_magma	0.2955	0.2985	0.3015	0.3046	0.3078	0.311	0.3143	0.3177	0.3212	0.3247	0.3283
Temperature	1319.266	1314.544	1309.63	1304.614	1299.392	1294.059	1288.504	1282.771	1276.851	1270.681	1264.363
Olv_Fo _magma	-1	-1	-1	-1	-1	-1	-1	-1	-1	-1	-1
Olv_Kd	-1	-1	-1	-1	-1	-1	-1	-1	-1	-1	-1
Plg_An _cumulate	-1	-1	-1	-1	-1	-1	-1	-1	-1	-1	-1
Cpx_Mg#Cpx_cumulate	-1	-1	-1	-1	-1	-1	-1	-1	-1	-1	-1
Opx_Mg#Opx_cumulate	87.93	87.81	87.69	87.56	87.44	87.31	87.17	87.03	86.89	86.74	86.58
Pressure(kbar)	2	2	2	2	2	2	2	2	2	2	2
Lg(fO2)	-7.06	-7.11	-7.15	-7.2	-7.25	-7.31	-7.36	-7.42	-7.48	-7.54	-7.61
density	2.609	2.609	2.609	2.609	2.608	2.608	2.607	2.607	2.607	2.606	2.606
Ln(viscosity)	5.52	5.59	5.67	5.75	5.83	5.91	6	6.09	6.18	6.28	6.38
Melt_%_magma	99.99	98.995	97.9904	96.9959	95.9923	94.9991	93.9974	92.9969	91.9979	90.9914	89.996
Olv_%_cumulate	0	0	0	0	0	0	0	0	0	0	0
Plg_%_cumulate	0	0	0	0	0	0	0	0	0	0	0
Cpx_%_cumulate	0	0	0	0	0	0	0	0	0	0	0
Opx_%_cumulate	0.01	1.005	2.0096	3.0041	4.0077	5.0009	6.0026	7.0031	8.0021	9.0086	10.004

 # Compositions derived through mixing 0.3 of the residual magma in Table D.1 and B1-magma of Wilson (2012). *Burgersfort Bulge, ** Olifants River Trough

Table D.2: Continued

											Compositions observed in LZ norite, Plag. discrepancy	
SiO2_magma	57.4235	57.453	57.484	57.517	57.5518	57.5885	57.6276	57.6688	57.7127	57.759	***57.7811***	***57.8237***
TiO2_magma	0.3826	0.387	0.3914	0.396	0.4006	0.4054	0.4103	0.4153	0.4204	0.4257	***0.4281***	***0.4311***
Al2O3_magma	12.6819	12.7836	12.887	12.9931	13.1011	13.211	13.3237	13.4384	13.5561	13.6757	***13.7274***	***13.6876***
Fe2O3_magma	1.223	1.219	1.2152	1.2117	1.2083	1.2051	1.202	1.1992	1.1964	1.1938	***1.1929***	***1.2014***
FeO_magma	8.8565	8.8592	8.859	8.8556	8.8487	8.8381	8.8235	8.8045	8.7806	8.7518	***8.7381***	***8.7572***
MnO_magma	0.2487	0.2515	0.2544	0.2574	0.2604	0.2635	0.2667	0.2699	0.2733	0.2767	***0.2782***	***0.2802***
MgO_magma	8.0001	7.7441	7.4855	7.222	6.9562	6.688	6.4155	6.1411	5.8627	5.5828	***5.4596***	***5.4101***
CaO_magma	7.2618	7.3344	7.4079	7.4831	7.5591	7.636	7.7143	7.7934	7.8737	7.9546	***7.9898***	***7.9853***
Na2O_magma	1.8625	1.8837	1.9053	1.9275	1.9502	1.9734	1.9972	2.0215	2.0465	2.0721	***2.0834***	***2.0856***
K2O_magma	1.6003	1.6185	1.6371	1.6562	1.6757	1.6955	1.716	1.7369	1.7584	1.7803	***1.7903***	***1.8029***
P2O5_magma	0.1058	0.107	0.1082	0.1095	0.1108	0.1121	0.1134	0.1148	0.1162	0.1177	***0.1183***	***0.1192***
Cr2O3_magma	0.332	0.3358	0.3396	0.3436	0.3476	0.3517	0.356	0.3603	0.3648	0.3693	***0.3714***	***0.374***
Temperature	1257.774	1250.96	1243.91	1236.551	1228.93	1221.035	1212.785	1204.23	1195.284	1186.002	***1181.839***	***1180.758***
Olv_Fo _magma	-1	-1	-1	-1	-1	-1	-1	-1	-1	-1	***-1***	***-1***
Olv_Kd	-1	-1	-1	-1	-1	-1	-1	-1	-1	-1	***-1***	***-1***
Plg_An _cumulate	-1	-1	-1	-1	-1	-1	-1	-1	-1	-1	***71.49***	***71.41***
Cpx_Mg#Cpx_cumulate	-1	-1	-1	-1	-1	-1	-1	-1	-1	-1	***-1***	***-1***
Opx_Mg#Opx_cumulate	86.43	86.26	86.09	85.91	85.73	85.54	85.34	85.14	84.92	84.7	***84.6***	***84.54***
Pressure(kbar)	2	2	2	2	2	2	2	2	2	2	***2***	***2***
Lg(fO2)	-7.68	-7.75	-7.82	-7.9	-7.98	-8.07	-8.16	-8.25	-8.36	-8.46	***-8.51***	***-8.52***
density	2.605	2.605	2.604	2.604	2.603	2.603	2.602	2.601	2.6	2.6	***2.599***	***2.599***
Ln(viscosity)	6.48	6.59	6.7	6.81	6.93	7.05	7.18	7.31	7.45	7.6	***7.66***	***7.68***
Melt_%_magma	88.9936	87.9936	86.9961	85.9927	84.9924	83.9954	82.9934	81.9952	80.9928	79.9946	***79.5479***	***78.9929***
Olv_%_cumulate	0	0	0	0	0	0	0	0	0	0	***0***	***0***
Plg_%_cumulate	0	0	0	0	0	0	0	0	0	0	***0.008***	***0.3171***
Cpx_%_cumulate	0	0	0	0	0	0	0	0	0	0	***0***	***0***
Opx_%_cumulate	11.0064	12.0064	13.0039	14.0073	15.0076	16.0046	17.0066	18.0048	19.0072	20.0054	***20.4442***	***20.6899***